APPENDIX F – DECOMP PHYSICAL MODEL 2016 ANNUAL REPORT: PRE-FLOW (BASELINE) AND HIGH-FLOW MONITORING OF THE WATER CONSERVATION AREA 3 DECOMPARTMENTALIZATION AND SHEETFLOW ENHANCEMENT PROJECT

This page intentionally left blank

The Decomp Physical Model (DPM) 2016 Annual Report: Pre-Flow (Baseline) and High-Flow Monitoring of the Water Conservation Area (WCA) 3 Decompartmentalization and Sheet Flow Enhancement Project.

This document contains details associated with annual report and data deliverables associated with Task 2: Hydrologic monitoring and associated sedimentological and ecological measurements and Task 3: Biological monitoring.

Period covered: 2009 to May 2016
Submitted: Sep 2016
Revised: n/a

Project: CERP: WCA 3 Decomp Physical Model
Project Number: 114558
Agency: US Geological Survey
Principal Technical POC: Barry H. Rosen; brosen@usgs.gov; 407-803-5508
Point of Contact: Tim Gysan; Earl.T.Gysan@usace.army.mil; 904-232-3272
Agreement: W32CS501185613

Editors:
Colin J. Saunders
Barry Rosen

The DPM Science Team
Jay Choi
Carlos Coronado-Molina
Eric Cline
Judson Harvey
David Ho
Laurel Larsen
Sue Newman
Barry H. Rosen
Colin J. Saunders
Kristin Seitz
Fred H. Sklar
Katie Skalak
Erik Tate-Boldt
Joel Trexler
Christa Zweig

DRAFT

EXECUTIVE SUMMARY

In this report, the DPM science team documents data collected during baseline, low-flow conditions (June 2010 – October 2013) and before, during and after three high-flow events (November 5 to December 30, 2013; November 4 to January 29, 2015; and November 16, 2015 to May 3, 2016). In this executive summary, we highlight the key findings and remaining uncertainties associated with the effects of high-flow on hydrology, particle characteristics and fluxes, and biogeochemical processes; and the effects of canal backfill treatments and levee removal on fauna and canal environmental conditions. This section is divided into two parts: (1) key findings during baseline and high-flow conditions; and (2) a summary of implications for water management. In this report, we also provide, as an appendix, a detailed list of the major findings and remaining uncertainties that were discussed during a 1-day DPM Synthesis Workshop (April 24, 2015) attended by the full DPM science team. The workshop aimed at both educating the team and taking a forward-looking approach to future field tests and monitoring needed to resolve remaining uncertainties.

Key findings from baseline and high-flow conditions

As expected, environmental conditions in the baseline period were characterized by:

- Water column velocities typically <1 cm s^{-1}, i.e., below the theoretical limit required to entrain benthic sediments
- Wet season water column total phosphorus (TP) typically <10 µg/L, indicating oligotrophic conditions
- Gradients in benthic floc chemistry associated with distance from canal/levee structures (higher nutrient content at sites downstream of levees)

Key results from the first high-flow period included the following:

- During the high flow period, sustained water column velocities >3 cm s^{-1}) were achieved at the RS1 sentinel site approximately 400-m downstream of the S-152. These velocities were above measured Critical Entrainment Threshold (CET) velocities, i.e., velocities required to entrain benthic sediments.
- The levee gap may have greater influence on overall flow in the pocket than the S-152. During S-152 operations, velocities > 1 cm s^{-1} were mainly restricted to a 500-m radius of the S-152 culvert structure.

- High velocities continued to increase over time, such that higher velocities were observed in December. In contrast, head difference and discharge at the S-152 remained the same or decreased slightly over this period.
- The CET velocities of sediment changed before and after the flow event. Benthic flumes demonstrated less variability in the entrainment of sediments after the flow event. Relative to pre-flow particles, post-high flow particles were entrained as more homogeneous, fine material. Although post-high flow CET tended to be lower (more easily entrained), CET ranges in both pre- and high-flow periods were still relatively low 1-2 cm s^{-1}.
- Sediment transport, measured by horizontal traps, increased at sites with velocities > 3 cm s^{-1}. At RS1 (the sentinel site nearest the S-152), sediment transport increased approximately 20-fold above pre-flow levels. In addition, transport at the site increased with flow duration, consistent with increasing velocities with flow duration.
- While it is theoretically possible that erosion of benthic floc contributed to higher transport, changes in size distributions of suspended sediments during flow indicated an increase in fine particles, suggesting SAV- or periphyton-derived sources of these particles.
- With the exception of the initial pulse on the first day of high-flow, water TP remained low (< 10 $\mu g\ L^{-1}$) throughout the site, including in the pocket and marshes downstream of the L67C canal/levee-gap.
- The sources and stocks of fine sediments in the water column deplete quickly after the initial high-flow pulse. This finding suggests that entrained particles quickly settled in the benthos or were trapped by water column vegetation. Water clarity was clean enough to decrease the signal:noise ratio in the ADVs.
- Canal partial and full backfill treatments exhibited increased densities (catch per unit effort, CPUE) of large fish, including largemouth bass. Fish densities in backfilled areas essentially resembled those of canal edge habitat, where fish are concentrated (by contrast, fish densities are very low in the open portions of canals). Understanding the effects of flow on fish densities and movement is ongoing.
- Some changes in fish community were observed between pre- & post-levee breach. Understanding the underlying factors is ongoing.
- In the canal, vertical sediment accumulation increased in the open canal treatment during the high-flow period, but minimal changes were observed in the partial or full backfill treatments.
- A clear influence of canal construction was evident, however, in the canal sediment traps. The density of sediments accumulating in partial and full backfill treatments increased 5-10-fold, reflecting fill material. This change was observed immediately after construction was completed.

DRAFT

Findings from the second and third high-flow events largely corroborated the above observations. The latter flow events achieved similarly high slough velocities, increased sediment transport, and differential transport between ridge and slough. The longer durations of flow in these events and closer examination of chemical and physical sediment properties from the both flow events have since indicated the following:

- At sites near the S-152, temporary increases in suspended sediments and TP occurred during the first few hours of the initial pulse flow. This was likely a result of slough periphyton breaking up and entering the water column, as suggested by sediment size analysis and high resolution aerial imagery of sloughs;

- Transport of sediments (per day) was larger during the initial pulse than typical steady state flow conditions; however, steady-state transport increased with duration of culvert operations such that the highest transport rates were observed (from traps) in the January through May period.

- Aerial imagery showed that at RS1, most of the slough periphyton broke up and sank within hours to days after S-152 openning. This process likely reduced vegetation resistance in sloughs, explaining increased velocities and transport with flow duration.

- Repeated measurements of floc height in the slough showed floc height initially increased (within 3 weeks of flow) but decreased monotonically with flow duration.

- Analysis of floc biomarkers and synthetic floc experiments showed evidence of slough-sediments moving through sloughs and settling in ridges under high flow. In contrast, synthetic floc deployed in ridges showed minimal or undetectable movement under high flow

- Biomarker data showed widespread sediment sources changes in the L67C canal with flow, suggesting sediments are entrained in or near the L67C. Budget models and synthesis efforts are ongoing to determine the likely source of these sediments and implications for sediment and nutrient movement through the L67C backfill area and gap.

- Active management of vegetation, achieved by creating a linear open slough within a sawgrass-dominated area was effective in enhancing flow velocities and sediment redistribution, warranting larger-scale field tests, to be initiated during the fourth flow event.

DRAFT

With the completion of three flow events, DPM presents a growing body of evidence that sheetflow both impacts and is altered by biogeochemical changes in slough periphyton and algal communities. For flow 3, a pilot study was initiated to characterize periphyton productivity, biomass, and species responses to flow. We hypothesized that accelerated flows increase local total phosphorus (TP) loads, attenuating with distance from inflow. Because the native periphyton community is P limited, we hypothesize that increased loads will increase periphyton biomass and productivity due to their sensitivity to P enrichment (Gaiser et al., 2008; Gaiser et al., 2004; Hagerthey et al., 2011; McCormick et al., 1996; McCormick et al., 2002), and if their threshold P load is exceeded, there will be a loss of native periphyton species. Thus flow was expected to alter algal communities of periphyton. Additionally, during the third flow event, we focused high-resolution aerial imagery to capture relatively rapid, large-scale changes in the periphyton community which had been visually observed in previous years.

Relevance to Water Management

The third DPM flow event continued to support previous findings that sustained flow operations of 8-10 weeks, rather than multiple pulses, are needed to maximize slough velocities, sediment transport and sediment redistribution, critical steps for landscape restoration. The pulse study indicated that although the initial flow increases suspended sediments 10-fold within the first few hours, successive pulse events do not have large-scale or sustainable effects on sediment transport. In contrast, the advantage of maintaining continuous sheetflow is that structural changes to sloughs (loss of periphyton) lead to changes in the physical and biological properties of floc (i.e., more erodible, possibly more labile sources), which further accelerate flow and sediment redistribution.

The effectiveness of the S152 in restoring large areas still remains a key unknown. At this time, our results suggest three potential trajectories for restoration within the DPM study area: (1) sheetflow generated by the S152 will only restore small areas (500-m radius of the S152), therefore active management is needed; (2) sheetflow impacts may eventually "spread" across the landscape, likely involving feedbacks between sheetflow and biogeochemical responses; or (3) some combination of 1 and 2. Whether high velocities can be extended beyond 500-m appears to be linked to biogeochemical responses of slough SAV and periphyton to both water column TP and velocity (P loading).

Results from the created slough indicated that active management of vegetation, combined with high flow conditions, can be successful in generating high slough velocities. Such an approach is likely needed to accelerate ridge-and-slough landscape restoration given the limited spatial extent of high velocities observed thus far. An important next step in DPM will be to increase the areal expanse of sloughs that have been invaded by sawgrass as a result of drainage. Given evidence showing the importance of vegetation in shaping the direction and speed of flows, we anticipate larger-scale active management of sloughs could be used to

redirect more flow toward the natural (north-south) orientation of the landscape, and to increase the areal extent of sheetflow and sediment redistribution (i.e., to kilometers rather than a few hundred meters).

Canal velocities roughly doubled under high flow, reaching 7-8 cm s^{-1}, above critical erosion thresholds for Everglades sediments. Therefore, the widespread changes in canal sediment sources, as evidenced by molecular biomarker, may be caused by velocity changes in or around the canal. Given the high TP of canal sediments, this process could potentially alter P cycling in the canal. Additional sampling and biomarker analyses of canal benthic sediments will be conducted in the third flow in order to assess the extent to which high flows, or alternate mechanisms, are causing the widespread changes in canal sediment sources.

DRAFT

1. INTRODUCTION AND BACKGROUND

Over the last century, hydrologic impoundment of Everglades wetlands into isolated basins with minimal flow has led to the degradation of prominent features of the landscape. Historically characterized by sheetflow up to ten times faster, the Everglades developed with linear sawgrass ridges and deep sloughs oriented parallel to flow. Sawgrass ridges were typically 100 to 300-m wide with sloughs about 25% wider, with ground-surface elevations of ridges standing >30 cm higher than sloughs (McVoy et al., 2011). This patterning is completely lost in about 50% of the historic area of ridge and slough and pattern degradation has occurred in most of the remaining areas due to loss of flow and overdrainage in some areas and drowning by excessively high water levels in others. Further, even in the apparent "pristine" areas, historical accounts indicate that the current microtopographic variation (usually less than 20 cm) is a fraction of what it was historically (McVoy et al., 2011; Watts et al., 2011). Modeling studies have identified complex feedbacks between flow hydraulics and sediment redistribution and variable rates of peat accretion affecting microtopography and vegetation communities (Larsen and Harvey, 2010). Loss of flow and modification of water levels over the past century have contributed to loss of 50% of historic, high-functioning ridge and slough and degradation of the remaining areas (Larsen et al., 2011). The loss of microtopography and the filling in of the long, deep water sloughs equates to a reduction in aquatic productivity and ecological connectivity, key ecosystem functions that sustain consumer populations (Hoffman et al., 1994; Green et al., 2006).

It is widely recognized that restoring sheetflow is critical in rebuilding the patterned, flow-parallel landscape pattern. Modeling studies indicate that water velocities greater than 2 cm s^{-1}, several-fold higher than measured in the current system, may be needed to sufficiently entrain and redistribute sediment to build landscape patterning and topography (Larsen et al., 2011). However, these important advances in our understanding of the mechanisms of landscape formation and degradation have been made using small-scale experiments and large-scale modeling. Scientific and engineering uncertainties remain over how rapidly the ridge and slough landscape will respond to restored sheetflow. In addition, even with restored sheetflow and levee removal, it is unknown to what extent the existing canals will hinder the restoration of the ridge and slough landscape. In this regard, key restoration uncertainties for decompartmentalizing the current impounded system include (1) the extent to which canals must be backfilled to ensure the restoration of sheetflow and sediment redistribution and (2) the extent to which restored sheetflow conditions may facilitate the transport of high-nutrient canal sediments to areas downstream.

DRAFT

A Brief History of the DECOMP Physical Model

On 21 October 2004, the PDT (Project Delivery Team) for the Decompartmentalization (DECOMP) CERP Project developed an issue paper proposing that demonstration tests be created for the DECOMP project "as a means to reduce uncertainties, narrow objectives of the project scope, build confidence in the predicted benefits and potentially reduce overall project costs." Under this project-level adaptive management approach, the PMP was revised to include the DECOMP Adaptive Management Plan (DAMP). At the time, DECOMP was struggling with conflicts of interests and disagreements on how to proceed across a broad spectrum of agencies, Tribal Nations, fisherman, hunters, and Conservation NGO's. The PDT decided that DAMP would focus on the some of the biggest issues, including: 1) What are the effects of hydrologic structures (canals, levees, weirs, and roads) on landscape structure & function? 2) What are the differential effects of partial versus complete backfilling of canals on landscape structure & function? 3) What are the effects of sheetflow and water table fluctuations on Ridge & Slough ecosystem processes? 4) What are the effects of sheetflow and water table fluctuations on tree island population dynamics? 5) How can the variance and uncertainties of the hydraulic models, needed to develop restoration scenarios, be reduced?

DAMP made it clear to the USACOE and the SFWMD that Adaptive Management is: 1) a scientific, systematic approach for finding answers to ecosystem management questions; 2) a study that can be implemented at any point within the planning, design, construction and operation of a restoration project; 3) a process of "learning by doing" – using the scientific method to evaluate natural resources and environmental impacts of large-scale restoration or management plans; 4) an organized and inclusive means for identifying and addressing key uncertainties (often an alternative to numerical models), allowing managers to move forward in the face of inadequate knowledge and finally; 5) a directive of Section 601(h)(3) of WRDA 2000.

After four years of planning and designing, the scope and cost of DAMP was found to be too great to implement, especially when the infrastructures proposed along the L-67A were no longer elements of the Modified Water Deliveries Project; a Park and USACOE project to increase conveyance of water across Tamiami Trail. Everyone wanted the "heart of Everglades restoration" to move forward however, none of the DECOMP uncertainties had yet been addressed. The solution was the DECOMP Physical Model (DPM), the first active Adaptive Management program in USACOE and SFWMD history. It is considered active because it used CERP planning funds to build a small water control structure, remove 3000 ft. of levee and fill part of a canal, within the footprint of CERP restoration, as a way to address hypotheses and questions associated with uncertainties #1, #2 and #3 listed above. This report presents the cutting edge science and technology needed to understand the complex movement and creation of Everglades organic matter.

DRAFT

2. OBJECTIVES

Located in the area between the L-67A and L-67C structures known as "the pocket" (**Fig. i-A**), the DPM is a multi-agency, multidisciplinary, landscape-scale project designed to address uncertainties associated with the effects of sheetflow and canal backfilling options on structure and function of the ridge-and-slough landscape. The central research questions addressed by the DPM are summarized as follows:

> Sheetflow Questions: To what extent do entrainment, transport, and settling of sediments differ in ridge and slough habitats under high and low flow conditions? Does high flow cause changes in water chemistry and consequently changes in sediment and periphyton metabolism and organic matter decomposition?
>
> Canal Backfill Questions: Will canal backfill treatments act as sediment traps, reducing overland transport of sediment? Will high flows entrain nutrient-rich canal sediments and carry them into the water column downstream? To what extent are these functions altered by the various canal backfill options, including partial and full backfills?

Twenty-three specific physical and biological hypotheses are addressed by the experiment and are detailed in the DPM Science Plan (DPM Science Team, 2010).

To reproduce pre-drainage flow conditions, new structures were built for the experiment, including ten gated culverts on the L-67A levee (the S-152, shown in **Fig. i-A**), a 3000-foot gap in the L-67C levee, and three 1000-foot canal backfill treatments in the adjacent canal (**Fig. i-A**). With a combined discharge capacity of 750 cfs, the culverts were expected to generate water velocities of 2-5 cm s^{-1} in the flow-way. The DPM utilizes a Before-After-Control-Intervention (BACI) experimental design, consisting of field monitoring of hydrologic and biological parameters under no-flow (baseline) and high-flow (impact) conditions in both impacted and non-impacted marsh and canal "control" sites. Due to water quality and flooding constraints, the operational window of the S-152 is limited to the months of November, December and January. The first high-flow event was initiated on November 5, 2013.

In a BACI experimental design, it is necessary to explain the baseline variability in the response variables, so that impact effects can be teased apart from existing sources of variability in the data (e.g., weather or fire events, local variation among habitats and sites). Here we report on the data collected in the DPM under the baseline, low-flow conditions and two high-flow events, the first occurring from November 5 to December 30, 2013, second from November 4 to January 29, 2015. We highlight the extent of the temporal and spatial variability of the diverse array of hydrological and ecological data sets, and to the extent possible, the factors explaining that variability. Data presented include hydrologic parameters (water levels; water surface slopes; water flow velocity and direction; vegetation effects on flow); particle characteristics and

processes (size distributions, particle biogeochemistry, elemental cycling rates, and transport rates); faunal communities in the L-67C canal and the surrounding marshes; and environmental characteristics and particle dynamics in the L-67C canal. Finally, this report provides initial findings of a pilot study aimed at increasing flow and sediment transport using an active management approach (**Fig. i-A**, bottom panel). The latter was motivated by the limited spatial extent of high velocities observed in the first flow event.

3. METHODS

3.1 Hydrology

3.1.1 Water Levels (J. Harvey, L. Larsen)

Water levels have been measured continuously at eight wetland sites and discontinuously at one canal at sites in the DPM experimental footprint (**Table 3-1**). Water level is measured by pressure transducers (KPSI water-level sensors) that were emplaced in fixed-elevation 1.5-inch PVC wells and that have operated continuously (except for a few unavoidable data gaps) since October 2010. The pressure transducers have an accuracy of +/- 0.15 cm and record water level at 15-minute intervals. KPSI transducer sites are serviced approximately monthly during the wet season at which times data are downloaded. Data are currently being QA/QC'ed and corrected for drift according to common practices and procedures used by the USGS Office of Surface Water and the USGS Hydrologic Instrumentation facility (Kenney 2010). We are also in the process of referencing the elevation of pressure transducer ports to a common horizontal (1983 NAD) and vertical datum (1988 NGVD) using high-precision, ground-based GPS surveying. Data will be initially analyzed by calculating the slope of the water surface across the DPM flow-way by fitting a best-fit plane through measured water levels. Transducers will remain operational for the duration of the project.

3.1.2 Local Scale Flow Patterns (J. Harvey, L. Larsen)

Water velocity is being measured at eight "sentinel" sites and at nine temporary sites selected to overlap with other measurements (**Table 3-1**). Velocity-gaging methods utilize 10 megahertz (MHz) down-looking acoustic Doppler velocimeters (ADV) manufactured by SonTek/YSI® and Nortek®. We follow the operating procedure outlined in Harvey et al. (2009). At each site flow speed and direction will be measured at a fixed depth in the water column. The ADV approach can measure flow velocity to a resolution of 0.01 cm s^{-1} with an accuracy of 1% of measured velocity (SonTek, 2001). Velocities will be sampled at a frequency of 10 Hz in one minute bursts collected every 30 min. Velocity datasets will be filtered and edited according to standard criteria suggested by the instrument manufacturer (SonTek, 2001) as well as specific criteria that were developed and refined in a prior Everglades study (Riscassi and Schaffranek, 2002). A minimum statistical correlation of 70% per sample and a minimum of 200 valid samples per

burst will be used as quantitative filters. Data with an acoustic signal-to-noise ratio (SNR) of 5 dB or less will be discarded. The resulting quality assured data set of 30-min point velocities will be averaged to produce daily values. Criteria for editing the velocity profile data are an extension of those used in the editing of the continuous point velocity data. In addition to using the same minimum 70% correlation filter used previously for point velocity data, a phase space threshold despiking process will also be applied to the profile data (Goring and Nikora, 2002;Wahl, 2003). Signal-to-noise-ratios are monitored continuously during collection of the vertical velocity profiles to determine if the ADV sample volume was obstructed by vegetation and as an indicator of the vertical location of the top of the floc. The large number of samples averaged for each burst and the filtering and quality assurance procedures used to edit and process the data provide confidence that the maximum possible resolution (0.01 cm s^{-1}) reported for this instrumentation (SonTek, 2001) is achieved in these measurements.

ADVs have been serviced during monthly site visits, during which data has been downloaded, batteries replaced, and compass calibration and diagnostics performed on the instrument. Between site visits, the height of the ADV sensor was adjusted based on the need to keep the sensor submerged until the next site visit. The height of each ADV sensor was adjusted to keep the sampling volume approximately at or slightly below the middle depth of the water column anticipated for the deployment period. ADVs were deployed on average for sixth months in 2010-2011 and 2011-2012 water years, centered on the anticipated operational window for flow releases (November –to December, 2013 and November, 2014 to January, 2015).

Two times during each deployment period, velocity profiles were obtained as described in Harvey et al. (2009), using the same ADV sensors deployed for continuous monitoring. For the profiles, velocities were measured at 10 Hz in 1 or 2 min bursts yielding 600 or 1200 samples, respectively, at each depth increment. Flow velocities were measured at 1.5, 3, or 6 cm depth increments throughout the water column, depending on total water depth, apparent vertical variability in vegetation architecture, and overall favorability of measurement conditions and time constraints.

For all three flow events, a spatial survey of flow was conducted at select sites near (<500-m) and far (>1000-m) from the S-152. These additional measurements were made using a SonTek Handheld FlowTracker-ADV® co-located to the extent possible with spatial surveys, sediment trap and fauna sampling sites. FlowTrackers were configured to measure velocities over a 120-second sampling period.

We are in the process of determining water discharge through the DPM experimental footprint determined using water depths and flow velocities. A step that still needs to be accomplished is relating instantaneously measured velocity profiles to long-term data collected at a single point in the water column. Essentially, point velocities need to be converted to depth-

averaged velocities using velocity profile shape factors using the procedure documented in Lightbody and Nepf (2006) and in Harvey et al. (2009).

In the canal treatments, acoustic Doppler profilers (Sontek phase-coherent acoustic Doppler profilers and an Argonaut-SW) were deployed to provide continuous records of velocity profiles. Profilers were deployed in an up-looking configuration and sampled vertical profiles of flow velocity and direction in one-minute bursts collected every 30 minutes. Post-processing QA/QC followed the procedures described above for the ADVs. Depth-averaged flow velocities were computed directly from the profiles.

3.1.3 Vegetation Effects on Flow (J. Harvey, L. Larsen, K. Skalak)

Vegetation community composition, biomass (biovolume, including separate analysis of periphyton mass per unit area), and stem densities has been determined by harvesting of vegetation in 0.25-m^2 clip plots followed by physiognomic analysis to determine the distribution of stem diameters and frontal areas (Harvey et al., 2009). The vegetation quadrats have been sampled using a stratified random sampling scheme at ridge, slough, and transition zones at all sites within the hydrologic monitoring network. These measurements have been repeated several times during the past years to quantify seasonal and interannual variations in vegetation architecture. Additionally, these measurements will be used in ongoing efforts to verify empirical predictive relationships between biomass and flow resistance parameters following Harvey et al. (2009). In the future we are planning to test simpler surrogate measures of plant architecture based on sampling only whole-quadrat biomass and dominant species. With that data we can calculate frontal area and average stem diameter based on statistical relationships that relate biomass of prior samples to physiognomic characteristics such as frontal area and diameter. If successful this approach will vastly speed vegetation data collection and analysis.

3.1.4 Large Scale Flow Patterns using SF_6 and Fluorescein dye (D. Ho, E. Cline)

Sulfur Hexafluoride (SF_6) tracer

SF_6 tracer release experiments were conducted within the DPM footprint to define large-scale sheet flow patterns before and after the operation of the L-67A culverts (S-152) (**Fig. i-A**). In these experiments, an airboat was used to access the study sites and perform the SF_6 tracer release. For each experiment, 5 L of water saturated with SF_6 was released into the Everglades as a point source. After injection, the tracer distribution was sampled each day using a high-resolution SF_6 analysis system mounted on an airboat. Briefly, SF_6 was measured by pumping water to a gas extraction unit, followed by analysis with a gas chromatograph equipped with an electron capture detector (Ho et al., 2002; 2009). The detection limit for SF_6 was 10 fmol L^{-1}. Navigation was accomplished using high-resolution aerial images (USGS Digital Orthophoto Quarter Quadrangle; http://edc.usgs.gov/) on a portable personal computer equipped with a GPS.

As in some previous experiments (e.g., EverTREx 6), because of the high density of periphyton and sawgrass ridges in the study areas, the tracer was sampled in a stop and go manner, where the airboat was stopped at one location and the pump intake lowered into the water. A predefined number of measurements were made before raising the pump intake and moving to the next location. This sampling scheme ensured that the airboat did not break up periphyton mats and stir up sediments while the pumping unit was active.

To date, synoptic releases of pre-flow conditions (i.e., before the operation of the S152 culverts) have been made at four sites. From November 4 to 12, 2010, SF_6 tracer release experiments were conducted at RS2 (EverTREx7) and C2 (EverTREx8), and from October 10 to November 4, 2011, tracer release experiments were performed at RS1 (EverTREx9), C1 (EverTREx10), and RS2 (EverTREx11) (**Table 4-5**). In 2013 and 2014, SF6 deployments were conducted at sites RS1 and C1. In 2015, SF6 deployments were conducted during the high flow event at a site south of RS2 (referred to here as injection 1) and a site east of the tree island near RS1 (referred to here as injection 2).

All data analysis and quality assurance have been completed for all experiments. Since SF_6 measurements were taken in a stop-and-go mode, only the SF_6 data obtained after the analytical system had stabilized (i.e., 3 consecutive samples of the same value were obtained) were used. After the experiment, measured SF_6 concentration was calibrated using a concurrently measured SF_6 standard. SF_6 concentrations in the water were calculated by applying a relationship between oxygen extraction efficiency and SF_6 extraction efficiency determined in the lab, ensuring that dissolved oxygen data did not contain any anomalous excursions, and accounting for water and gas flow rates through the membrane contractor used to extract gases out of the water.

The tracer patch boundaries and center of mass were identified in each survey from the tracer distribution. Analysis of the spatially explicit, time-series data provided estimates of tracer heading (flow direction) and advection rate (cm s^{-1}) for each site. Advection was calculated from the movement of the center of the patch obtained by fitting the SF_6 distributions with two-dimensional Gaussians (Ho et al., 2009, Variano et al. 2009).

Fluorescein dye tracer

To characterize initial high-flow conditions downstream of the S-152 structure, a water tracing experiment was conducted using a visible dye tracer, sodium fluorescein. The dye study was conducted on the day the S-152 culverts were opened for the first two flow events (November 5, 2013 and November 4, 2014). Widely used in hydrologic monitoring (Hubbard et al., 1982), the dye has a shorter half-life relative to the commonly used rhodamine (Hubbard et al. 1982) and low eco-toxicity (Field et al., 1995). After S-152 discharges stabilized, 100 liters (L) of dye was mixed with site water (1:4 ratio) and injected upstream of S-152 at 10:15 am.

The plume of dye was photographed from a helicopter over the course of the next four hours, and later in the week field personnel noted dye locations by airboat and helicopter.

3.2 Water Quality

3.2.1 Water Chemistry (S. Newman)

Water column samples were collected monthly at DPM marsh sentinel sites, July–March, during the 2011-2016 sampling periods. Samples were collected mid-water column using a peristaltic pump, preserved and analyzed following standard District protocols. To obtain more detailed information on particle chemistry, water column total particulate phosphorus (TPP), labile (i.e., bicarbonate extractable) P and microbial (chloroform extractable minus bicarbonate extractable) P were obtained from water samples collected in November 2010, 2011, 2012, 2013, 2014, and 2015. Samples were collected mid-water column at all sites, and at sites DB2, C1 and RS1-S, samples were also collected at 5 cm above the sediment bed. At sites C1, RS1 and RS2, samples were collected from both the ridge and slough areas. Samples collected for water column suspended sediments were passed through 500 µm Nitex mesh prior to being stored on ice and brought to the laboratory for processing. Immediately upon return to the laboratory, samples were filtered through a 0.2 µm Pall membrane filter. The filters were extracted, digested and analyzed for TPP, microbial and labile P. Particulate mass was recorded on two filters per sample. In addition, to examine the effect of flow effects on particle chemistry, TPP was obtained from samples collected pre-flow, Oct 28th 2013 and compared to those collected during flow in November, 2013. Samples from structures S152 and S151 were collected weekly.

The dye study conducted in November 2013 demonstrated that the flow path was greater to the east than to the south (SFER 2015, Chapter 6), therefore additional grab samples were collected from sites east of the S152 during the Nov 2014 flow event. Sites along this new easterly transect ranged ~250 to 870 m from the structure, similar distances to those measured routinely along the southern transect. Concurrent flow (Sontek Flowtracker® and turbidity measurements were collected along with water samples.

To gain greater insight into the link between flow and surface water TP, an autosampler was deployed at site Z5-1 for the second flow event. For the first two days of flow the autosampler collected water samples hourly and composited them every three hours. From 11/6-11/9 samples were collected every three hours, composited daily and analyzed for total phosphorus (TP). The autosampler was redeployed prior to closing the structure and samples were collected every 6 hours. In addition to TP, continuous measurements of water level (Onset HOBO® water depth data logger), turbidity (Campbell Scientific OBS-500®) and flow (Sontek Argonaut-ADV®) were recorded at site Z5-1.

In the second flow event, we examined how flow affected water quality along the preferential, eastern flow path from the S152. Sites ranged 250 to 870 m from inflow, and flow effects were most evident within 500 m. In the third flow event, we continued the examination of this flow path, collecting samples during the start of two flow releases at sites 250, 300, 400 and 500 m from the S152. Concurrent flow (Sontek Flowtracker® measurements were collected along with water samples, and water level (Onset HOBO® water depth data logger) and specific conductivity (Hydrolab ®) were logged at 2 and 30 minute intervals, respectively.

3.2.2 Turbidity Monitoring Network (Erik Tate-Boldt)

To provide more information about flow effects (particularly the initial pulse event) on water turbidity, a proxy for suspended sediments, four Campbell Scientific turbidity sensors were deployed at sites varying in location relative to the S-152: Z5-1, RS-1, and site NE-S152 (ca. 180-m east-northeast of S-152). Turbidity was measured at 30-second (s) intervals. In addition to providing long-term data, it was expected these sites would capture sediment pulses associated with the initial flow release. The timing of observed peaks was used to quantify velocities of sediments transported from the S-152 to each monitoring site.

3.2.3 Dissolved Organic Carbon (L.Larsen, S. Newman, C. Saunders)

During the monthly water column sampling from November 2010 through January 2014 (section 3.2.1), 40mL samples were collected for dissolved organic carbon (DOC) analyses. Samples were collected using the protocol described in section 3.2.1 and stored in amber glass vials on ice until analysis, which occurred within 2 weeks of sample collection. DOC concentrations in the filtered samples were measured on an OI Model 700 Total Carbon analyzer with a mean standard error of 0.3 mg L^{-1} and a detection limit of 0.2 mg L^{-1}. UV absorption spectra were measured between 190 and 1100 nm at 1 nm resolution on an HP Chem spectrophotometer with a standard error of 6 x 10^{-4} AU. From the UV absorbance at 254 nm, specific UV absorbance (SUVA) was computed as the absorbance divided by the DOC concentration (Weishaar et al., 2003).

3.3 Particle Characteristics

3.3.1 Suspended sediment concentrations and size distributions (L. Larsen, J. Harvey)

During the DPM flow release of November 2013 and November 2014 suspended sediment and phosphorus samples were collected at sites RS1U, UB1, UB2, S1, DB1, DB2 and DB3. At site RS1U a 2 m interval sampling transect was developed to analyze upper, mid-depth, and near bed (5cm above the floc surface) variation of suspended sediment along a ridge to slough transect

(**Fig. i-A**). At the ridge and slough endpoints of the RS1U transect the sampling was conducted at three depths including lower (5cm above floc surface), middle of the water column, and upper (5cm below water surface at time of installation). Between those points were four additional points across the transition between ridge and slough where only the "lower" sample was collected. At sites UB1, UB2, S1, DB1, DB2 and DB3 samples were collected at a single location from two different water column depths; low (5cm above floc surface) and in the middle of the water column. Samples of surface water were collected with peristaltic pumps at a rate of 60 ml/min and filtered through a 500 µm Nitex screen. One liter samples were collected for SSC analysis and 250mL samples were collected for phosphorus analysis. Phosphorus samples were preserved with H_2SO_4 at pH of 2 and placed on ice before shipment to the South Florida Water Management District Lab.

Continuous records of suspended sediment size distributions were obtained from two sites (**Table 3-1**) using a laser diffraction particle size analyzer (LISST-FLOC, Sequoia Scientific) according to the method of Noe et al. (2010). Because the instrument is subject to biofouling, it was deployed for several days during fall intensive sampling period (fall intensives). The LISST-FLOC measures diffraction of a laser to estimate the in situ volume concentration and size distribution of suspended sediment. The particle size measurement range is 7.5-1500 µm, divided into 32 logarithmically spaced size-class bins. The instrument was suspended horizontally so that the optical path is located 5 cm above the floc layer and programmed to collect data in 5-second bursts every 10 minutes.

The LISST-FLOC (see above) provided continuous measurements of volumetric suspended sediment concentrations that will be converted to mass concentrations using the floc density vs. floc size relationship provided in Larsen et al. (2009a), which was developed for the Everglades and used in other studies such as Harvey et al. (2011). In addition, we have measured several suspended sediment concentration surrogates as a relative measure of differences in suspended sediment concentrations between sites. One surrogate is turbidity, determined with an optical probe on a sonde (YSI 600-OMS V2). During the high- flow event, a transect of three turbidity sondes was deployed 5 cm above the bed at station RS1 across the ridge-to-slough transition to determine the extent to which floc transport is attenuated with distance into the ridge.

A second surrogate is the signal-to-noise ratio obtained from the ADVs. ADVs operate by the Doppler shift of sound waves caused by particles in the flow, and the signal-to-noise ratio of the instrument increases in flows with more particles. The ADV's signal-to-noise ratio was related to suspended sediment concentration using regression that takes differences in water temperature and particle size into account, as described in Elçi et al. (2009).

DRAFT

3.3.2 Particle Biogeochemistry (J. Harvey, L. Larsen, S. Newman)

November sampling: periphyton and floc

Total particulate phosphorus and phosphorus fractionation (into microbial and labile P fractions) were obtained from water column, bed floc and epiphyton samples for all ridge and slough sites during each of the November intensive sampling efforts including the pre-S-152 flow release period and after the flow release during 2013 and 2014. Samples of bed floc and metaphyton particles were collected for biogeochemical characteristics (TPP, microbially-bound P, labile P, loss on ignition (LOI), and total nitrogen (TN)). Bed floc was collected by inserting a 20-cm acrylic core tube into the peat, capping, and withdrawing the intact core. After the floc settles, the clear overlying surface water is poured off, and the floc is then poured off and collected in 1-L plastic Nalgene bottles. Epiphyton was collected with a wet-dry vacuum as described in Larsen et al. (2009b). After collection, large biota are removed from the vacuum reservoir, and the well mixed remnants are collected in a 1-L Nalgene and concentrated by settling (for 10 min) and decanting until just before the point of entrainment of the settles material. Samples are stored in the dark on ice prior to analysis. Samples were shipped overnight from the field to the lab and are refrigerated upon receipt. Analyses were performed by the University of Florida Wetland Biogeochemistry laboratory (Gainesville, FL) within 1-2 days of sample collection. Analysis for TN and LOI is done in accordance with standard procedures within one week of receipt. Immediately upon receipt, TPP and phosphorus fractionation (into microbial and labile P fractions) were performed on bed floc and epiphyton samples for all ridge and slough sites using a modified Hedley procedure (Hedley and Stewart 1982). Each fractionation is performed in duplicate. The labile P fraction is extracted by the addition of 0.5 M $NaHCO_3$, followed by shaking, centrifugation, and digestion of the supernatant. The microbial+labile fraction is extracted by the addition of $CHCl_3$ followed by overnight incubation and then by the addition of $NaHCO_3$ as described above. The microbial fraction is estimated by differencing the microbial+labile fraction and the labile fraction.

3.3.3 Spatial Survey of floc and soil chemistry (C. Saunders, S. Newman)

Observations of floc and periphyton chemistry observed in the 2010-2011 sampling indicated substantial variation among sites and suggested large-scale gradients in nutrient standing stocks, bioavailability, sediment type (peat or marl) and vegetation type with distance from canals or landscape features such as tree islands. Understanding these gradients was deemed critical due to their potential interactive effects with the high-flow and canal backfill treatments on ecosystem response variables such as biogeochemical cycling and sediment entrainment and transport, among others. Therefore, a spatially explicit sampling design was generated to quantify and understand these spatial gradients across the entire DPM footprint.

Sampling sites for the spatial survey (**Fig. i-B**) were generated as part of the MAP-RECOVER system-wide landscape sampling and mapping project (PI: Dr. Michael Ross, Florida International Univ.). The sampling design entailed stratifying the DPM footprint (a 3-km x 7.5-km area, oriented parallel to the L-67A and C levees) into a grid of 18 1-km x 1.25-km zones. Within each zone one random location was selected. This location represents the center of a cluster of four additional points, or nodes, randomly selected within a given distance from the center of each cluster. At each node, three subplots are generated for a total 216 subplots. One of the subplots is the center node and the other two are at a random distance (3-23 m) north and east of the center node. Vegetation was surveyed by Dr. Ross and colleagues at all 216 subplots in October 2012

A spatial survey of floc and soil was conducted in pre-flow period (typically August-September) in 2012 - 2015. For this survey, only 14 of the 18 zones were used, as 4 zones were deemed outside of the relevant experimental footprint. In each of these 14 zones, one of the subplots was randomly chosen to be sampled. Because a primary objective of the DPM spatial survey was to quantify gradients in chemistry specifically as a function of distance from canal/levee structures, therefore one additional subplot located within 500-m of the structure was also sampled. For some zones, the sampling design failed to include any points within 500-m of a structure. In the latter case, one additional point was randomly generated to meet this criterion. In summary, a total of 28 points (2 per zone, of 14 zones) were sampled for the floc and soil survey. All samples were collected in slough habitats. In cases when subplots were not located exactly in sloughs, sampling occurred in the nearest slough. Follow-up measurements ("Phase-2" of the survey) of sediment entrainment, sediment chemistry, and sediment transport were made at a subset of the 28 sites and are described in individual sections below. Samples of bed floc were collected by inserting a 10-cm diameter x ca. 100-cm long aluminum core tube into the peat, capping, and withdrawing the intact core. After the floc settles, the clear overlying surface water is poured off, and the floc is then poured off and collected in pre-weighed, 1-gallon Ziploc ® bags. All floc and soil samples were analyzed for total moisture, dry weight, bulk density, LOI, and nutrient content (CNP) by the Wetland Biogeochemistry Laboratory, University of Florida.

3.4 Particle Fluxes

3.4.1 Critical Entrainment Threshold (CET) of sediments (PI: S. Newman, M. Manna):

Critical Entrainment Threshold (CET) describes the flow velocity at which sediment particles are first suspended in the flow field, thus, analogous to when erosion begins. CET of sediments within the DPM footprint are determined in situ using an annular benthic flume constructed of two cylinders that form a 0.1 m annular channel (Partrac 2005, 2006, 2008). Benthic annular flumes have a history of use extending back to the mid-1980's and have been chiefly used previously on intertidal and shallow sub-tidal cohesive sedimentary environments (Black and

Paterson 1997). The inner cylinder (radius 0.35 m), outer cylinder (radius 0.55m), and watertight lid are constructed of Perspex™. Bed shear stress is created via a rotating lid affixed to the channel top. Lid rotation is by a geared direct current motor controlled directly via software on a portable laptop computer with a specialized interface box. The software allows for control of the operational variables, start velocity, end velocity, step-wise rotation frequency increments, increment duration, and ramping rate between increments. An optical backscatter turbidity sensor (OBS) is fixed at 5 cm above the sediment water interface such that the sensing zone is directed across the channel. The flume was calibrated to derive the relationship between lid rotation and flow velocity at 0.05m above the sediment-water interface. CET is obtained by the relationship between flow velocity and turbidity. Upon completion of a CET experiment, estimates of particle settling velocities will be made by continuing to log turbidity after rotation of the lid has stopped.

Flume deployments are made among the sediment types (minimum n=5) located with the DPM footprint. In 2010, CET measurements were made in slough habitats at sites RS1, C1, S1, and C2 on 12/15/10, and at sites UB-1, -2, -3 and RS2 on 12/20/10. Due to issues with equipment, all tests were performed with step increases of 1.0 cm/s, instead of 0.5 cm s^{-1}. In 2011, the benthic flume equipment was shipped to manufacturer (PARTRAC, Scotland) for repairs and no measurements made in the DPM. In 2012, 2013, 2014, and 2015, CET was measured at sentinel site RS1, and at a subset of the spatial survey sites, Z5-1, Z6-1, Z5-3, Z4-1, Z10-2 and Z15-2. The latter were selected from the initial 28 survey points, which were stratified according to floc chemistry (% organic matter) and log-distance from the S-152 structure. To test the hypothesis that flow could redistribute surficial sediments and change the CET at a given site, sampling was conducted at these sites in the weeks prior to and immediately after the operational window (i.e., before November and after December) in 2012, 2013 and 2014.

3.4.2 Particle Transport - *Natural particle mobilization* (L. Larsen, J. Harvey):

Particle transport was studied by tracking mobilization of natural particles, using a combination of LISST and direct sampling by pumping (Harvey et al., 2011) and a combination of natural biomarkers on standing and sediment captured in traps (see below, section 3.4.3). Natural particle mobilization experiments were used to determine the bulk entrainment threshold and particulate phosphorus fluxes of natural particles of different sizes and from different source areas (e.g., epiphyton on rooted aquatics versus floating periphyton versus bed floc) through physical and chemical characteristics of sediment (Harvey et al., 2011). Through the natural particle mobilization experiment, mass fluxes of material from various sources areas will be quantified as will the standing stock of entrainable particles using the methods of Harvey et al. (2011),

The natural particle mobilization experiment is unique in automating particle size detection using the LISST and also quantifies source areas (epiphyton vs. floating periphyton vs. bed floc). Complementary dual synthetic tracer (DST) deployments (see section 3.4.3), are likely more accurate tracers of particle transport over defined flow paths, but synthetic tracers lack information about source of sediment and fluxes of particulate nutrients. However, DST tracers may provide the best information for quantifying floc transport distances and timescales. Thus, combining the two approaches provides the most comprehensive information about particulate material sources, fluxes, and transport distances.

One question addressed by the combination of DST tracers and natural particle mobilization experiments is the distance that slough particles are transported into the ridge—an important quantity to which ridge spreading rates are expected to be sensitive. Furthermore the combination of natural particle mobilization and DST tracing may reveal the extent to which enhanced settling of particles within vegetation canopies serves as a permanent sink for sediment and associated particulate phosphorus within ridges and sloughs. Present-day sloughs are more densely populated by emergent vegetation than under historic conditions (Bernhardt and Willard, 2009), but the role of that vegetation in enhancing sedimentation (possibly leading to loss of sloughs) is not well understood. In this way the natural particle mobilization experiment operating in parallel with the DST tracing addressed two critical uncertainties in understanding how the ridge and slough landscape evolved, has degraded, and may be restored. These data can be compared with results of ongoing modeling work (Larsen and Harvey, 2010), which suggests that redistribution of floc from sloughs to ridges is essential to maintaining distinct ridges and sloughs.

3.4.3 Particle Transport - *In situ* natural particle tracers (C. Saunders, C. Coronado-Molina, R. Jaffé, B. Rosen)

A second suite of natural tracer studies aims to quantify the origin, transport, and deposition rate of floc particles among adjacent ridge-and-slough habitats under modern (no flow) versus pre-drainage (high flow) conditions and across the boundaries of canal backfill and levee removal areas (see section 3.6.2). Field measurements are to include (1) vertical deposition of floc; (2) horizontal transport of floc; (3) floc standing stocks; and (4) floc biomarker assays to quantify the biogenic contributions to floc deposition, transport, and standing stocks. Sediment traps were used to measure horizontal sediment transport in marsh sites and the vertical deposition of sediment in the canal treatments. To measure horizontal transport, sediment traps were constructed, adapted from a design used to quantify sediment exchange in estuarine systems (Phillips et al., 2000). These traps represent a novel application for measuring sediment transport in Everglades wetlands. Molecular organic markers, or “biomarkers”, derived from plant lipids were used to provide information on changes in the sources of organic matter in the standing floc and horizontally advected sediments. The n-alkane-derived proxy, (Paq), was previously shown to effectively distinguish sawgrass from deeper water slough sources (Mead et

al. 2005; Saunders et al., 2006). Other useful proxies include a group of diterpenoids termed kaurenes, biomarkers that are highly enriched in (although not exclusive to) sawgrass tissues in the Everglades. Other biomarkers have been identified as being indicative of green algae (botryococcenes) and to cyanobacteria (highly branched isoprenoid alkanes (C20 HBIs) (Saunders et al., 2006; Gao et al., 2007; Gao, 2007). As such, a combination of the Paq value, the C20 HBI, the kaurenes and the botryococcenes are used to assess changes in organic matter sources in floc and advected sediments.

Horizontal trap deployments

As part of the BACI design, horizontal traps are deployed in paired ridge and slough plots at three marsh sites (RS1, C1, and RS2, 6 traps total) and oriented parallel to flow. During each deployment or retrieval, standing floc was also collected in ridge or slough habitat within 10-m of the trap (see 3.3.3 for collection methods and post-processing). Starting in November 2011, traps have been deployed for three weeks from October through January and six weeks from February to April. Loading rates are estimated as grams per frontal area per time, where frontal area is calculated from the inner diameter of the inlet and outlet tubes (6.4-mm). Loading rates per frontal area are converted to loading per ground area based on measured depth to the top of the floc layer during each deployment and retrieval event.

As part of the spatial survey Phase-2 (**Fig. i-B**), additional traps were deployed in sloughs to capture transport along a gradient in sediment chemistry (based on spatial survey Phase-1 results and follow-up CET measurements) and to quantify transport versus log-distance from the S-152 structure. Starting in November 2012, each trap was deployed from late October to January (i.e., overlapping with the operational period for S-152) and twice during February through April (post-flow period). These traps were deployed with slightly larger inlet diameters (12-mm) in order to capture larger amounts of sediment sufficient for biomarker analyses.

Biomarker Analysis – laboratory procedures

Vegetation-specific molecular markers, or biomarkers, have been developed and applied as a useful approach to identify the sources, transport and ultimately the fate of organic matter in Everglades (Jaffé et al., 2001; Gao et al., 2007; Saunders et al., 2014). The n-alkane-derived proxy, Paq, effectively distinguishes sawgrass from deeper water slough sources such as *Eleocharis* spp., *Nymphaea odorata*, submerged aquatic vegetation (such as *Chara* spp.; Mead et al. 2005; Saunders et al., 2014). Other proxies include Kaurenes, diterpenoids that are highly enriched in (although not exclusive to) sawgrass tissues (particularly enriched in belowground biomass). Other biomarkers have been identified as being indicative of green algae (Botryococcenes) and cyanobacteria (highly branched isoprenoids; C20 HBIs) (Gao et al., 2007; Gao, 2007). As such, the combination of Paq, C20 HBIs, the Kaurenes and the Botryococcenes

were used to determine changes in the source of organic matter composition of floc and water column particulates.

Biomarker analyses were performed on plant biomass and floc from ridges and sloughs collected at BACI and spatial survey sites within the DPM during the pre-, during and post-flow periods around the first flow event. These analyses were conducted to address the following objectives: (1) to assess spatial gradients in sediment organic matter (OM) sources across the DPM study and determine baseline relationships between sediment OM and source vegetation; (2) assess changes in the contributions of ridge and slough OM sources to sediments accumulating in canal backfill treatments under high and low sheetflow; and (3) assess changes in the contributions of ridge and slough OM sources to sediments transported across the landscape (km-scale) under high and low sheetflow. Specifically, it was expected that redistribution of sediment from sloughs into ridges would be evidenced by more slough-like biomarker values in ridge floc. To some degree, it was also expected that biomarkers would support findings of increased sediment transport (e.g., from traps) by showing a "moving front" of sediment biomarker values along the north-to-south flow path during high flow conditions.

To assess plant-biomarker relationships, biomarker analyses were performed on 46 plant samples (9 species, including above- and below-ground biomass). Sediment-source was assessed for baseline (no-flow) conditions through biomarker analysis of 107 sediment samples, including standing floc associated with sampling at BACI-ridge/slough sediment trap sites, spatial survey sites, and canal sediment trap sites collected from October 2011 to January 2013. To assess changes in sediment source under high-flow (Nov-Dec 2013) and post-flow (January-April, 2014) conditions, biomarker analyses were conducted on 180 floc and canal sediment samples collected from October to April for the first and second flow events. Biomarker analyses samples collected for the third flow event (i.e., October 2015 to April 2016) are still ongoing.

Biomarker analyses were previously described in Xu (et al. 2006). Briefly, freeze-dried samples (ca. 150 mg organic carbon) were Soxhlet extracted, saponified and the isolated neutral fraction was further fractionated over silica gel. Aliphatic and aromatic hydrocarbon fractions were used for GC/MS identification and quantification of n-alkanes, C20 HBIs, kaurenes and botryococcenes. Quantification was performed through the internal standard (Squalane) method. N-alkane distributions were used to determine the aquatic proxy Paq (Mead et al. 2005) defined as the ratio of the sum of the mid-chain n-alkanes (C23+C25) to the sum of the long chain n-alkanes (C27+C29+C31). The thermochemolysis method was similar to that used by Hatcher et al. (1995). Sediment or plant tissues containing approximately 10 mg carbon were placed in a 5 mL pre-combusted ampoule and an internal standard of n-eicosane in hexane was added. Methanolic tetramethylammonium hydroxide (TMAH: 100 mg of reagent) was added to ensure excess reagent for reaction. The ampoule was evacuated on a vacuum line for 6 h, after which it was flame sealed. The ampoule was heated to 250°C in a convection oven for 30 minutes. The ampoule was allowed to cool to room temperature, frozen to condense methanol and gases, and

cracked open. Products were extracted from the ampoule with methylene chloride and added to a 2.5 mL vial through a glass wool column, used to filter out product residue. The organic fraction was blown down to near dryness under a gentle stream of N_2 gas. Methylene chloride was added to dissolve the reaction products, which were transferred to a 300 µl glass insert prior to analysis by gas chromatography–mass spectrometry (GC/MS).

Capillary GC/MS analyses were performed on a HP 6890 GC interfaced to a HP 5973 quadrupole scanning mass spectrometer. A 5% phenyl methylsilicon bonded phase (J & W DB-5MS) fused silica capillary column (30 m, 0.25 mm i.d., 0.25 µm film thickness) was used for the separation. The carrier gas (He) was set at 11.34 psi. The transfer line was heated to 250 °C and the injector to 280°C. The mass range (50-550 Da) was scanned at rate of 2.89 scans sec^{-1} under EI (70 eV) mode. Compounds were identified by comparing results with a commercial mass spectra library (Wiley 275) and/or published mass spectra. To assess plant-biomarker relationships, biomarker analyses were performed on 46 plant samples (9 species, including above- and below-ground biomass).

Algal Taxonomy Analysis of Advected Sediments – laboratory procedures

Changes in the algal component of horizontally transported sediments before, during and after the 2013 flow event were characterized using sediment traps along a ridge-slough transect. The species (algae and cyanobacteria) richness (total number of species) in 77 samples from the control site (C-1), RS-1 and three downstream of the backfill sites was determined. Samples were collected in Whirl-Pak® Sample Collection Bags and kept refrigerated until examined. The sample was gently homogenized and a subsample (approximately 0.1 mL) mounted on a glass slide and 22 mm^2 glass coverslip before microscopic examination at 400, 600 or 1000x. The organisms present were photographed and tabulated.

3.4.4 Particle Transport - *Dual Signature Tracer (DST) studies* (E. Tate-Boldt, C. Saunders)

One of the parameters used to determine if particle transport is essential for the development and maintenance of the ridge & slough landscape by redistributing entrained sediments is Dual Signature Tracer (DST), which is hydraulically matched (i.e., representative) of the mean particle size and settling velocity of particles collected from the study region. The DST particle is made of an inert fluorescent material in which magnetite inclusions are imbedded (Partrac 2005, 2006, 2008).

2010 Deployments

In December 2010, DST was deployed in interior slough locations at sentinel sites C1, C2, RS1, and RS2. At each site, the tracer was deployed as frozen blocks, suspended in a 1x1-

m^2 screen just below the water surface, to ensure minimal contamination. A "drop" typically consists of 20-40 kg of tracer with a unique fluorescent signature per treatment. Tracer will be retrieved using magnetic rods in a sentinel and synoptic design in order to provide adequate temporal and spatial resolution. Short-term (7-day) tracer movement was followed at C1 and RS1. Magnets were placed around the location of DST deployment along 8 transects radiating out at 1, 2 and 3 meters along eight principle compass points (N, NE, E, SE, S, SW, W, and NW). Seven days after the DST deployment, all magnets were retrieved and photographed, and DST sample retained on each magnet was removed, dried and weighed.

A second synoptic sampling of DST was conducted in August 2012 to quantify long-term and potentially longer-distance movement and settling of the DST drops at RS1, C1, RS2 and C2 in 2010. Using the location of the original DST deployment as "site-zero", the sediment was sampled along transects radiating out from site-zero along eight principle compass points (N, NE, E, SE, S, SW, W, and NW). The sample locations along transects were at 1, 3, 6, and 12 meter increments (compared to the 1-, 2-, and 3-m locations during the initial 7-day deployment in 2010). At each location one magnet was lowered into the flocculent layer until the end of the magnet rested on the consolidated soil surface and was then pushed into the soil layer to 5 cm. Duplicates were sampled at various locations along the transects.

2013 Deployments

In 2013, two experiments were designed to assess particle transport during the S-152 high-flow operational period: a spatial experiment and a temporal experiment. The spatial experiment, replicating and expanding the design used in 2010, was devised to assess the direction of DST particle movement, and a temporal experiment to assess DST particle transport velocity and differential movement across the ridge-slough boundary. The DST was deployed at RS1 and C1 sites on October 31 and November 1 2013, respectively. The DST was retrieved on November 13th and 14; the week after the initial flow began. RS1 was chosen as the site to receive the greatest flows from the S-152 structure, and C1 was chosen as the low-flow control.

For the spatial experiment, the location of the DST deployment was considered "site-zero", and sediment was sampled along transects radiating out from site-zero along eight principle compass points (N, S, E, W, NE, SE, NW, and SW) in a radial fashion. The sample locations along transects included distances of 1, 3, and 6 meter increments from "site zero." For both RS1 and C1 sites, the 1 and 3 meter positions were sampled along each transect; however, given the prior information of flow directionality under low flow, and anticipated under high flow, only the 6 meter points at the E, SE, S and SW transects were sampled at both sites. The 11-guass magnets (deployed approximately 10-cm above the floc surface) were used to collect the DST at the sampling points. DST collected on each magnet was then dried and weighed. Due to inadvertent capture of organic matter, DST weight could only be reasonably measured to within 0.005 g; therefore, for samples weighing less than 0.005 g, DST abundance was

approximated by visually counting particles under an ultraviolet lamp, the final count based on the average of two independent observations per sample.

On November 5, 2013, a separate sampling design was performed at RS1 to determine sediment transport velocities in the slough under high flow. The temporal experiment was conducted at site RS1 only, as velocities above the critical entrainment threshold (i.e., sufficient to maintain long-distance sediment transport) were not expected at the control site. Magnets were deployed at two boardwalks 25-m and 55-m downstream of the drop site. The boardwalks, oriented normal to flow, span slough-to-ridge transects, and magnets were deployed at 4 locations per boardwalk. On November 5, magnets were deployed at mid-water column and collected and rinsed every 15 minutes from 9:00 am until 12:00 pm and every 60 minutes after that. Capture rates (particles s^{-1}) were calculated per sample, and velocities calculated based on location and timing of peak capture rates.

2014 and 2015 Deployments

Prior to opening the S152 structure, 25 kilograms (kg) of DST was frozen and then deployed in slough habitat (2010 and 2013), a slough-ridge ecotone (2014), and ridge habitat (2015) at the high flow site (RS1) and the control (C1). To measure spatial movement, 20-24 magnets (11-gauss) were placed radially around the deployment location at high flow and low flow sites and retrieved the week after flow started. DST collected on each magnet was then dried and weighed. Due to inadvertent capture of organic matter, DST weight could only be reasonably measured to within 0.005 g; therefore, for samples weighing less than 0.005 g, DST abundance was approximated by visually counting particles under an ultraviolet lamp, the final count based on the average of two independent observations per sample.

Similar to 2013, DST was deployed to measure sediment movement and redistribution during the 2014/2015 DPM high flow events. Performed at RS1 and C1 sites, these deployments included sampling designs to assess both the direction and extent of DST particle movement and particle transport velocities. At both sites, DST was deployed approximately along a slough edge (approximately 1-m from the ridge-slough ecotone) with half of the magnets deployed in the slough and half of the magnets deployed in the ridge. DST collected on each magnet was then dried and weighed. To measure DST velocities under high flow (RS1 only), sequential magnet deployment/retrievals were conducted at 15- to 30-minute intervals, at two boardwalks 20-m (RS1u) and 50-downstream (RS1d) of the DST deployment location, both spanning slough-to-ridge transects.

In the third flow event (2015), an additional DST deployment was conducted to measure spatial movement of particles in ridge habitats at the high flow (RS1) and control (C1) sites.

3.4.5 Particle Transport in an Actively Managed Slough

In September 2014, an experimental slough was created in a sawgrass-dominated area by clipping and removing aboveground live and dead sawgrass biomass. The created slough, located approximately 300-m east of the S152 (**Fig. i-A**), spans 3 m x 100 m, oriented parallel to the predominant flow direction (east-west). Prior to and during the flow event, velocities were measured mid-water column at a number of sites within the created slough and in the adjacent sawgrass. Measurements were made using a Sontek Flowtracker®, a handheld Acoustic Doppler Velocimeter (ADV). Sediment movement was tracked using a dual signature tracer (DST), paramagnetic (due to embedded magnetite inclusions) and hydraulically matched to Everglades floc particle size and settling velocity. Two weeks after flow was initiated in November 2014, approximately 25 kg of DST was deployed at both upstream and mid-point locations in the slough. Prior to these deployments, 11 gauss magnets were placed along 5-m transects oriented perpendicular to flow. In January, near the end of the flow event, the DST was collected from magnets, dried, and weighed.

3.5 Biogeochemical Processes

3.5.1 Ecosystem Metabolism (E. Tate-Boldt, C. Saunders, S. Newman)

Increased flow is expected to increase nutrient loading to the downstream system, and it is important to assess whether low-level phosphorus loading may alter ecosystem structure and function. For instance, nutrient loading may alter habitat quality by changing oxygen availability and stimulating net carbon loss through increased net aquatic heterotrophy. To address these questions, Hydrolab multiparameter sondes are deployed in adjacent ridge and slough habitats at sites C1, C2, RS1, and RS2 and in slough habitats at sites UB1, UB2, UB3, DB1, DB2, DB3, and S1. These instruments record high-frequency measurements (30 min.) of dissolved oxygen, temperature, conductivity and pH over 5-day deployments. Data will be used to estimate ecosystem metabolism (aquatic gross primary production, ecosystem respiration, and net ecosystem production). Calculation of estimates was obtained following Hagerthey et al. (2010).

Deployments are conducted nominally monthly from October to January and once in April. In 2010, deployments were conducted in slough habitats at all sentinel sites (except DB1, DB2 and DB3) on the following dates: 11/1/10 to 11/5/10 and 11/29/10 to 12/3/10. In 2011, deployments were performed at all sentinel sites, including DB sites and both ridge and slough deployments at sites C1, C2, RS1 and RS2. Deployments included 9/26/11 to 9/30/11, 10/31/11 to 11/4/11, and 11/28/11 to 12/2/11. In 2012, the deployments were performed on the following dates: 1/23/12 to 1/27/12; 4/23/12 to 4/27/12; 9/10/12 to 9/14/12; 10/29/12 to 11/2/12; 12/3/12 to 12/7/12; and 12/14/12 to 12/18/12. The latter deployment was performed at the DB sites only, specifically to capture the effects of the initial L-67C levee breach (December 7, 2012). During the 2013 season, deployments occurred in January and February, and monthly from September

DRAFT

through December. In 2014, Hydrolabs were deployed monthly from January through April. Data QA/QC is in progress for input into model to estimate metabolism.

3.5.2 Decomposition (S. Newman, K. Seitz)

To compare decomposition rates between ridges and sloughs during low and high flow conditions, short-term decomposition studies are conducted using a standard cotton strip substrate (Newman et al. 2001). Two 12 cm (wide) by 31 cm (long) cotton strips are attached to a stainless steel frame (6 mm) that supports the strips vertically, and deployed into the soil encompassing the water, floc and soil interfaces. The locations of the two interfaces are recorded, and after the strips are retrieved, loss in tensile strength is determined at 2 cm increments using a Chatillon TCD-200 tensiometer, equipped with a digital force gauge (DFIS 200, Chatillon, Greensboro, North Carolina). All data will be linearized and presented as annual cotton rotting rates to correct for non-linear changes over time (Hill et al. 1985). Decomposition was assessed pre, during and post flow.

In November 2011, cotton strips were deployed in adjacent ridge and slough habitats at C1, RS1, and RS2, and were retrieved after 3, 6 and 9 weeks. In November 2012 cotton strips were deployed in adjacent ridge and slough habitats at RS1, RS2, C1, and C2, and all were retrieved after 4 weeks. In November 2013, cotton strips were deployed in the ridge and slough at representative sites within the DPM footprint (C1, C2, RS1, and RS2) during the inaugural flow event, as well, as three months post-flow.

3.5.3 Biological Response to Pulsed Water Flows: Phosphatase Enzyme Activity (S. Newman)

Phosphatase activity will be used to indicate the relative degree of phosphorus limitation of the floc, water, and periphyton community in the sloughs during low and high flow conditions. Phosphatase activity will be measured fluorometrically using a standardized substrate; methylumbelliferyl phosphate. To ensure that the periphyton community is of known age, periphyton phosphatase activity and biomass will be determined from periphyton that is allowed to colonize dowels suspended within the water column. Data will be expressed per unit area (Newman et al. 2003).

Periphyton structure and function (community assemblages, P cycling rates, and tissue P content) can be highly variable temporally, with substantial changes occurring on the order of days to weeks. Because of this variability, comparison of enzyme activities across years is less informative than understanding the variability on shorter, weekly to monthly, time scales. Therefore, it was determined that the optimal sampling schedule for phosphatase activity in the DPM would occur at control and flow sites during the high-flow event, rather than comparing Phosphatase activity measured within the operational window of pre- versus flow-impact years.

DRAFT

3.5.4. Algal Processes

Changes in algal community, biomass and productivity were monitored in open water sloughs along the flow gradient at 250, 300, 400, and 500 m from the S152. Artificial substrates consisting of 7.5 cm long x 0.12 cm diameter acrylic dowels and 0.75 cm^2 acrylic plates were deployed at each site. Periphyton colonization was examined monthly from January through May, 2016, spanning the two dry season openings in February and May (see Study Design, above). The May 25th sampling date occurred during non-flowing conditions. Each sample represents the accumulation of algae and cyanobacteria on an acrylic plate over three-weeks prior to sampling. Biomass and dissolved oxygen measurements were performed using the dowels, while the plates were used for species determination. Productivity was measured using light/dark bottles, following SFWMD standard operating procedure for determining periphyton primary production (SFWMD 2015c). Productivity is calculated as a function of photosynthetic active radiation (PAR); however, PAR measurements were not taken during the January sampling and these were excluded from analysis. Subsamples of known volume (determined gravimetrically) were enumerated at 400x microscopically and calculated as number of cells per unit area of acrylic plate. Statistical tests included ANOVA followed by Tukey HSD multiple comparison tests using JMP software (SAS corporation).

Because changes in periphyton cover were observed in high-flowing sloughs during previous years, in flow event 3 we photo-documented periphyton loss in the RS1 slough using the 'box on an aircraft' imaging system (BOA; Sklar and Dreschel, 2015) at 900 ft altitude, resulting in an image with 3.7 cm/pixel resolution. We also measured floc depths along a transect across RS1 over time, during sediment trap deployments, to document concomitant changes in floc along with the changes in periphyton.

3.6 Environmental Characteristics of Canal Backfill and Biological (Fauna) Monitoring

3.6.1 Fish (Fauna) Monitoring (J. Trexler)

We are evaluating three hypotheses about the impact of reintroducing flowing water to wetlands of the Everglades on aquatic animal communities and food web dynamics. These are:

1. Water flow may directly affect the distribution of species by sorting them based on current velocity;
2. Levees and canals affect aquatic community function by changing patterns of connectivity across the landscape, altering the movement of fish across the landscape as water levels rise and fall;
3. Flowing water increases phosphorous loading to periphyton communities, changing phosphorus dynamics in ways that stimulate consumer productivity.

Hypotheses 1 and 2 are addressed by sampling studies of small and large fish. We are estimating small fish (<8 cm standard length) and macroinvertebrate density by sampling with a 1-m^2 throw trap and complementing those data with collections by drift fences. Catch-per-unit-effort (CPUE) from the drift fences is proportional to the speed fish are moving and the fences are set in an x-arrangement with a trap at the base of each arm to make separate collections from each direction (Obaza et al. 2011). These data provide an indication of the direction and speed fish are moving across the landscape. We are examining large fish (>8cm standard length) by electrofishing in the marsh and canal littoral zone. Finally, we are tracking movement of the two most abundant large fish using surgically implanted radio transmitters to document how the DPM project affects habitat use. Hypothesis 3 is being addressed by placing selected consumers into the field to permit us to trace changes in the food web using stoichiometric and fatty acid (FA) data. We hypothesize that increased flow velocity will lead to greater P loading in algal and heterotrophic bacterial biofilms and mats that will, in turn, affect algal species composition and edibility that will, in turn, cascade up to the consumers. FA profiles have proven to be a useful tool to trace the origin of energy flow because selected FAs are only known to be produced by algae, heterotrophic bacteria, or vascular plants, and are incorporated unchanged in the tissues of consumers (Belicka et al. 2012).

Sampling and Data Types

Organismal sampling for DPM began in September, 2010, and has continued through the end of 2015 (**Fig. i-C**). Sampling has been structured to capture seasonal dynamics in the study area to improve interpretation of data the November through January flow experiments. We sampled 10 times prior to the DPM construction efforts (September 2010 – June 2012), 4 times after the L-67C levee was degraded and before the first flow event (August 2012 – September 2013), and 7 after (November 2013 – March 2015). Sampling areas were located at the three sites selected to represent different distances from the L67-C canal: the UB sites, with three plots ~150-300 meters from the L-67C canal; the CB sites, with three plots immediately adjacent to the canal with each along a different canal-fill treatment; and the DB sites, with three plots ~100 meters east of the L-67C levee (**Fig. i-D**). The three canal-fill treatments (fill to marsh level, partial fill, and no fill control) were located along a prospective flow path crossing plot 1, 2, and 3, respectively, at each site (**Fig. i-E**). Beginning in August, 2011, flow-treatment control plots were established to the north and south of the DPM footprint.

Density of small fishes, amphibians, and aquatic invertebrates was determined using a 1-m^2 throw trap (Jordan et al. 1997). Directionality of small fishes was determined using 12-m wide portable drift fences set up in an "X" configuration, with four minnow traps embedded in the center, each one facing a different cardinal direction (Obaza et al. 2011). Drift fences were deployed for 24 hours at a time. For every sampling event, three throw-trap samples and three drift-fence samples were taken for every plot. We determined the abundance of large fishes and amphibians, as well as the large fish community structure, using airboat-mounted

electroshocking transects (Chick et al. 1999). We conducted quarterly surveys from December, 2010, to the present. We sampled transects at the CB and UB sites, along with the northern and southern control sites, and we sampled transects in the L-67C canal along the littoral edge; we were unable to maneuver our airboat to sample at the DB sites.

We assessed the behavior of large fishes in response to the DPM by surgically implanting with VHF radio transmitters in specimen of the two most common species in the area, Bowfin (*Amia calva*) and Florida Largemouth Bass (*Micropterus salmoides floridanus*), and locating them on a weekly basis (Parkos et al. 2014; 2015). The battery life of transmitters used was approximately six months. Large fish tracking began in May, 2011, and is ongoing. As of March, 2015, 198 fishes (99 of each species) have been implanted with transmitters.

Data analysis

Analyses involving CPUE, density, directional movement, and community structure, were conducted on the mean of data collected at sample plots. Water depth was estimated using data from the Everglades Depth Estimation Network (EDEN) that were adjusted to reflect conditions the study sites by use of *in situ* field measurements. When continuous water depth was not used as a covariate, sampling periods were designated a category based on time of the year: *Wet* for samples collected in August or September sampling periods, *Transition* for samples collected in November sampling periods, *Early Dry* for samples collected in January sampling periods, and *Late Dry* for samples collected in March sampling periods. All data were log(x+1), sqrt(x+1), or reciprocal (x+1) transformed as needed to meet standard assumptions. All community analyses were square root transformed.

Field Experiment

We placed small aquatic animals, two species of fish and a grass shrimp, into field cages in the DPM flow way to evaluate the possible impact of water flow on phosphorus mobility and transfer into the food web. Our study was conducted in a slough immediately downstream from the DPM culverts (latitude 25º 52’ N, longitude 80º 36’ W) during the fall of 2014. We placed 20 1-m^3 cages in the study area for 21 days in October, prior to the flow experiment, and again in November, during the flow experiment. This permitted us to capture data for low-flow and high-flow periods. Each cage was open at the top and enclosed with 2-mm mesh on the sides and bottom. Ten of the cages were shielded by a “V-shaped” flow baffle that were pointed into the direction of water flow and surrounded each cage. These baffles were designed to block water flow from passing through the cage and are referred to as the control cages. The other half of the cages were equipped with flow enhancing wings to increase natural flow levels and will be referred to as the open cages.

Half of each of the control and open cages received a pre-determined biomass of animals. The stocked cages tracked the assimilation of algae by consumers. The consumer-free cages tracked the changes in algae and periphyton biomass and composition in each of the open and closed-flow treatments, free from consumer constraints. Thus, at both sampling events there were four treatments, each replicated with 5 cages (Open-Stocked, Open-Empty, Control-Stocked, and Control-Empty), randomly arranged within 5 blocks, perpendicular to the flow of water.

Three weeks prior to the start of the field study, target species were collected from the surrounding marsh and housed in the laboratory, where they were fed a diet of algae flakes until the beginning of the experiment. This created a base of the fatty acid composition of all specimens and improved our ability to detect change from the experimental treatments. The total length of each fish and shrimp were measured for length-to-weight regression and then they were transported to each cage in the field. A sample of the laboratory-held fish and shrimp were preserved for a baseline lipid and stoichiometric analysis. Each cage was be stocked with common species from the area, each representing a different trophic level and at densities equal to average marsh densities during the particular time of year. Five Sailfin Mollies (*Poecilia latipinna*), 9 Eastern Mosquitofish (*Gambusia holbrooki*), and 23 riverine grass shrimp (*Palaemonetes paludosus*) created a food-web fragment reflective of the ambient aquatic community. These average densities were calculated from community composition data previously collected from the study area from October to December.

To create a substrate for epiphytic algae and heterotrophic bacteria to form a biofilm, we added plastic strips in a density of 150 stems per meter square, consistent with ambient vascular plant stem densities (Chick et al. 2008). The short time span of the experiment allowed time for pioneer species of algae and bacteria to colonize, but not be long enough to allow dominance by cyanobacteria and development of periphyton calcareous matrix. Using an uncolonized substrate as a "periphytometer" also allowed for the age of the periphyton growth to be known (Sklar et al. 2010). A volume of 2000 ml of floating periphyton mat, taken from the surrounding marsh, was added to each cage to match the mean biomass in the marsh. This volume was calculated from periphyton volumes typical of the DPM footprint based on past samples. An aliquot of the periphyton was sampled from each cage at the inception of the experiment to determine total phosphorus, AFDM, fatty acid and stoichiometric analysis. The algal species composition and biovolume of these mats was obtained from an aliquot of these samples. Flow measurements were taken at the initiation of the experiment and then weekly, taken from the upstream side of each of the open cages and within the baffle of the closed cages.

After 3 weeks, the fish and shrimp were removed from the cages by lifting enclosure bags and allowing the water to drain out (Geddes and Trexler 2003; Dorn et al. 2006; Chick et al. 2008). Animals were picked out of the periphyton, euthanized in MS-222, and immediately placed on ice. Standard length was measured and stomach contents were collected from each

organism and identified to lowest taxonomic unit possible. Samples were stored at -80ºC until being freeze dried and homogenized for fatty acid and stoichiometric analysis. Stomachs and their contents will not be included in the samples for lipid analysis and stoichiometric analysis. This will eliminate bacterial fatty acids present in the digestive tract tissue from being analyzed in combination with dietary sources of bacteria (Budge et al 2006).

Thirty strips of the artificial vegetation were collected and frozen for later processing (Geddes and Trexler 2003; Dorn et al. 2006; Chick et al. 2008). In the laboratory, each was scraped clean of epiphytic algae, homogenized and enumerated with a compound scope as number of biological units (cells for unicellular taxa, 10-µm segments for filamentous taxa, and colonies for colonial taxa) (Eaton et al. 1995). Standards methods will used to determine AFDM of epiphytic algae from the remaining samples. Periphyton were sampled from each cage at the end of each experiment to determine periphyton TP, AFDM, and for lipid analysis and stoichiometric analysis.

3.6.2 Canal sediment dynamics (C. Coronado-Molina)

To capture vertical sediment deposition in the canals, sediment traps were deployed in 2 canal control sites (CC1N, CC2S) and the three backfill treatments (CB1, CB2, and CB3). Each trap consisting of three vertically oriented tubes with an aspect ratio (length:width) of 8:1 (Kerfoot et al. 2004), were kept vertical using floats, the top of each trap suspended approximately 1 m above the sediment-water interface. Samples collected from all sediment traps were transported to the lab for processing. Samples were passed through a 1-mm mesh sieve to separate large (>1 mm) and small (<1-mm) sediments. Small particles were then captured using a settling (Imhoff) funnel. Particles from one designated tube were dried at 80ºC for dry-weight determination, while particles from the remaining two tubes were immediately frozen for future biomarker analysis. Vertical mass flux (g $m^{-2}yr^{-1}$) was calculated based on the weight of recovered particles, the trap inlet area (calculated from the tube inner diameter) and deployment duration. As median sediment particle size in Everglades wetlands is less than 100 µm (Noe et al., 2007) only the small particles are reported.

To date, canal vertical trap deployments have included 25 sampling events between November 2010 and April 2016. In November 2010, vertical sediment traps were deployed at the two canal control sites (1 trap per site) and 3 canal backfill sites (2 traps per site) on November 3, 2010 (8 traps total). Of these, 4 traps were missing upon retrieval in June 2011. Adjustments were made to improve trap detectability and recovery for subsequent deployments. It was determined that deployment duration be shortened to 3-weeks during operational window (Nov-Dec) and 6-weeks prior to and after that period. Initial results from 2011 indicated very low within-site variability (1-11% difference); therefore only 1 trap per treatment was used for future deployments. Three 3-week deployments were conducted in the November–December pre-operational window of 2011 and one 3-week deployment occurred in November 2012.

Deployments were suspended after November 2012 during the L-67C construction period and resumed October 2013 after the completion of L-67C construction.

Starting in November 2012, horizontal sediment traps were deployed at sites downstream of the L-67C, to measure sediment transport effects of the levee degrade and canal backfill treatments. In particular, traps were deployed at this time to detect flow effects associated with the initial opening of the L-67C levee (breached December 7, 2012). Horizontal traps were deployed in slough habitats at DB1, DB2 and DB3 and one control site (DCC2S, near CC2S) (4 traps total). In all, 13 deployments have occurred from November 2012 to March 2014. Traps were deployed for 3-weeks during the November-December period and 6-weeks from January to March 2013 and from January to March 2014. Data analysis and QA/QC of mass transport rates at the DB sites are in progress. Starting in November 2012, floc collection was conducted during each horizontal trap retrieval/re-deployment in areas next to the deployed sediment traps. Floc has been frozen and archived for molecular biomarker analysis.

3.6.3 Physicochemical monitoring (C. Coronado-Molina, C. Saunders)

Since November 2010, water temperature has been monitored in the L-67C canal during canal sediment trap deployments. One temperature probe is attached to each trap (5 data loggers total). The temperature dataloggers have also been deployed with marsh traps to enable better comparisons of continuous marsh and canal temperatures (temperature probes were attached to traps deployed at RS1, RS2, and C1 ridge and slough sites and the DB1, DB2, DB3 and DCC2S downstream sites).

After the fire event in June 2011, canal water was noticeably darker than previous trips. Depth profiles of water turbidity were subsequently measured starting in earnest in August 2011 during canal trap deployment and retrieval events. Profiles are measured by lowering an Optical Backscatter Sensor (OBS) at 0.5-m intervals and recording OBS.

4. RESULTS AND DISCUSSION

4.1 Hydrologic and Topographic Setting (J. Harvey, L. Larsen, M. Dickman)

The DPM experimental flow-way is located in a 1,800 m wide opening between the L-67A and L-67C levees (**Fig. i-A**). The slope of the ground surface in the DPM contributes to gradients in water surface elevations that drive sheetflow. Surveying indicates that the ground surface has a slope on the order of 5×10^{-5}, which is typical of the Everglades. However, DPM surface water is not free to flow in the direction of the ground slope because of impoundment in in a basin enclosed by the L-67A levee upstream and the L-67C levee downstream. Due to impoundment, the water surface often has a lesser slope than the ground surface, which imparts less driving force for sheetflow, with velocities that are typically on the order of 0.2 – 0.4 cm s^{-1}. The small

amount of sheetflow is driven by water flow through a few minor gaps in the levees and by groundwater underflow beneath levees.

The landscape character in the DPM is largely sawgrass with discontinuous remnant sloughs scattered throughout. The maximum observed difference in peat surface elevation between ridge and slough was 20 cm with standard deviations of elevations within ridges or sloughs tending to range between 2 and 4 cm. These elevation distributions compare favorably with the best preserved areas of Everglades ridge and slough. However, in many areas of the DPM the difference in elevation between ridges and sloughs is 9 cm or less, which is more representative of degraded areas of the Everglades (Watts et al., 2010). As a result the DPM was chosen for flow enhancement experimentation. Pre-flow release measurements occurred in 2010, 2011, and 2012, and the first break in the L-67C levee occurred on approximately 12/11/2012. Two experimental flow enhancements occurred between November 5 to December 30, 2013; November 4, 2014 to January 29, 2015; and November 16, 2015 to May 3, 2016.

4.1.1 Water Depths (J. Harvey, L. Larsen, M. Dickman)

Baseline conditions: 2010-2012

Water surface elevations in DPM are intermediate between upstream areas in WCA-3A and downstream areas in WCA-3B. On the upstream side, WCA-3A water levels are higher than DPM by an amount ranging between 0 and 0.6 m. On the downstream side WCA-3B water levels are approximately 0.25 m lower than DPM (**Fig. H1**). Water level measurements in DPM during the pre-flow release period (July 2010 – March 2013) indicate maximums stages in the DPM are reached each year between November 1 and January 1 and minimum stages are reached between May 1 and July 1 (**Fig. H2-11**). Maximum water depths were 50 – 70 cm during the 2010-2011, 2011-2012 and 2012-2013 wet seasons. The minimum water depth during the summer of 2012 dry season ranged between 20 and 40 cm, which is probably typical of the DPM. During the 2011 dry season water levels were below ground surface throughout the DPM, at a maximum ranging between -10 and -40 cm during the severe drought that occurred that summer. The drought was accompanied by a major wildfire that began in WCA-3B passed through the DPM on June 8-9, 2011. Repeat measurements of peat elevation indicated that the thickness of floc above the peat was reduced from 10 cm during the prior wet season in some areas to approximately 2 cm or less during the subsequent wet season. There was also some indications that the peat surface may have burned and been reduced in elevation by 10 cm or more in some areas of the DPM.

DRAFT

4.1.2 Baseline, Local-Scale Flow Patterns (2010-2012) (J. Choi, J. Harvey, L. Larsen, K. Skalak)

Average sheetflow velocities were generally less than 0.5 cm s^{-1} across all sites, below the typical threshold velocities needed to entrain sediment (Larsen et al., 2009). Velocities tended to be higher in upstream areas of DPM during the 2010 wet season but were more uniform across the DPM in 2012 (**Fig. H12; Table 4-1**). Flow direction was in the ESE direction at most sites (**Fig. H12**), which is similar to the direction of the shortest path across the DPM between levees (**Fig. i-A**). A dominant flow in the ESE direction is consistent with flow observed previously in WCA-3B, and is generally thought to be the result of management of water levels in the L-30 canal which are maintained low for seepage control on the eastern margin of the Everglades. A notable exception was seen in flow direction at DPM site RS1D-S. There, water flow was guided by the slough direction which was oriented SSE. In contrast, just a few meters away at site RS1D-R on the ridge the flow was more variable over time but tended to trend to the ESE like most of the other sites (**Fig. H12**).

Velocity profiles indicate generally higher velocities in the center of the water column or near the surface (**Figs. HY13-20**). Higher velocities were not necessarily associated with deeper flows, and in fact the opposite (higher velocities in shallower water) occurred in the upstream slough site RS1D-S. The initial effects of construction are observable during the 2012 wet season data from UB1 and UB2 which responded by increasing by a factor of two, from background velocities of approximately 0.4 cm s^{-1} up to a maximum of 0.7 cm s^{-1} at UB1 (**Fig. H18**).

At the very low flow velocities often observed (0.1 – 0.3 cm s^{-1}) the direction of flow varies substantially within the water column (**Figs. HY21-28**). Flow direction at 2.5 cm depth increments can vary by as much as 180 degrees over the full depth of the water column (typically 30 – 80 cm). The direction of flow tends to be much more uniform (varying no more than 20 degrees) at relatively high velocities above 0.5 cm s^{-1} (**Figs. HY21-28**).

Vegetation Effects on Flow

Frontal area of vegetation is positively related to vegetation biomass, and the relationship is improved by including live and dead vegetation (**Fig. H29**). Including biomass of epiphyton on plant leaves had relatively little effect on the relationship. Frontal area of slough vegetation was approximately an order of magnitude less than in ridges (**Fig. H29**), which implies greater flow resistance in ridges compared with sloughs as has been observed before (e.g., Harvey et al., 2009).

Sheetflow within the slough is faster (up to 1 cm s^{-1}) (**Fig. H30)** and better aligned with the generally north-south orientation of DPM sloughs. Sheetflow on ridges generally is oriented

across the ridges and is slower (< 0.4 cm s^{-1}). These preliminary data are consistent with dominant flow through sloughs steered by ridges, with flow crossing ridges on strong angles to compensate for a water surface slope that is not perfectly aligned with the landscape orientation.

The wildfire that crossed the DPM on June 8-9, 2011 burned biomass over most of the DPM down to the peat surface. Significant regrowth of vegetation from roots occurred within several months. Repeat surveys of vegetation in the fall of 2011 indicated that frontal area remained lower than prior to the fire, and frontal area still had not fully recovered by fall 2012 (**Fig. H31**). In contrast to ridges, the pattern of change in frontal area within sloughs was variable and may not have been detectable by our methods. We continue in our attempt to reaffirm previous studies that vegetation architectural characteristics, e.g. Principally frontal area, strongly influences variability in water velocity with the main effect being to steer water flow through sloughs.

4.1.3 Baseline, Large-Scale Flow Patterns (2010-2012) (D. Ho, E. Cline)

SF_6 tracer release experiments conducted to date include both ridge-and-slough control sites (C1 and C2) and two ridge-and-slough sites in the predicted flow path (RS1 and RS2). In general, results show slow rates of water advection (<0.2 cm s-1) and an east to southeast heading, and the temporal and spatial variation is described here.

In November 2010, the SF_6 tracer releases were conducted at RS2 and C2 (**Fig. H32; Table 4-5**). At RS2, the tracer patch advected to the southeast along the slough and then crossed several sawgrass patches (**Fig. H33)** at an average heading of 123±8°, which is significantly different from EverTREx 6 conducted at the same location the previous year (141±6°). Average advection rate for EverTREx 7 was 0.09±0.02 cm s^{-1}, which is higher than observed during EverTREx 6 (0.05±0.01 cm s^{-1}). The water depth was greater during EverTREx 6 (**Table 4-5**).

At C2, the SF_6 tracer moved to the southeast following the orientation of the slough, with an initial heading of 137±2.3° (**Fig. H34**). However, the leading edge of the SF_6 tracer patch then reached a sawgrass patch and changed direction, thereafter followed a preferential flow pathway along the slough, which curved to the south. We speculate that this change of direction was driven by the wind, which was channeled by the sawgrass ridges on either side. Overall flow direction during the experiment was 156±11°, which is significantly different from the one measured in EverTREx 7.

In 2011, tracer releases were conducted at RS1, C1 and RS2. At RS1, the tracer advected in a southeast heading (148±2.5°) while at sites C1 and RS2, the tracer heading was mainly to the east (109±3.1° and 106±4.0°, respectively) ((**Table 4-5; Fig. H35**). Average advection rates in these tracer release experiments ranged from 0.11±0.01 cm s^{-1} (RS1) to 0.15±.08 cm s^{-1} (C1) (**Table 3-3**), slightly higher than the range observed in previous experiments (0.04 to 0.09 cm

s^{-1}). However, these advection rates still indicate slow velocities that are well below critical entrainment velocities of 2-5 cm s^{-1} required to entrain benthic floc (Harvey et al., 2011; Larsen et al., 2009a, b).

These results show the high spatial and temporal variability of km scale flow patterns in the region between L-67A and C levees. This variability needs to be taken into account when trying to obtain representative flow pattern measurements to evaluate the impact of the operation of the L-67A culverts.

4.1.4 S-152 Structure Discharges (M. Dickman)

Prior to the 2013 S-152 flow release, the USGS installed monitoring platforms and instrumentation to record and compute continuous water levels on the west side of S-152 (headwater) and on the east side of S-152 (tail water) and flows through S-152. Water levels, or gage height data, were referenced to North American Vertical Datum of 1988 (NAVD 1988) and National Geodetic Vertical Datum of 1929 (NGVD 1929); for this section of the report, elevation values are referenced to NAVD 1988. The west or headwater platform was installed in the L-67A Canal about 300 feet north of S-152, and the east or tail water platform was installed in the wetland about 300 feet north of S-152; the SFWMD installed an water quality autosampler on the headwater platform to sample from the L-67A Canal. A Sontek Argonaut® SW acoustic Doppler velocity meter (ADVM) was deployed inside of the downstream end of culvert pipe number 2, as counted from the north end of the structure, and a second SW ADVM was installed inside of the downstream end of pipe number 6. For the purpose of determining the source of water flowing through the S-152 structure, the USGS also measured continuous water temperature and specific conductance at the S-152 headwater and tail water platforms, EDEN 8, and the east and west monitoring platforms of Site 69. **Table 4-2** lists the USGS monitoring stations, **Table 4-4** shows the data collected. Instruments were installed, inspected, and calibrated according to USGS procedures.

To develop the rating to compute discharge for the first and second flow releases, 10 discharge measurements were made during the first flow release, and 14 measurements were made during the second flow release. Discharge measurements were made at the downstream end of each culvert using a Sontek Flowtracker® during the first and second flow releases, and an acoustic Doppler current profiler (ADCP) was used during the second flow release to measure discharge at a section 20 feet upstream of the inlet to the culverts. Measured discharges during both flow releases are listed in **Table 4-3**.

At this site, a submerged orifice flow rating and an index-velocity rating could be developed to compute a continuous record of discharge through the structure. To develop a submerged orifice rating, discharge measurements and concurrent water levels on the headwater and tail water sides of the structure are necessary (Collins, 1977). However, a submerged-orifice

flow rating was not developed because the water levels measured at the tail water station were found to be significantly lower than the water levels at the downstream face of the structure.

An index-velocity rating, a regression relationship between the mean channel velocity and the concurrent ADVM velocity, was used to compute the discharge record as described in Levesque and Oberg (2012). For the index-velocity ratings, the mean channel velocity from the 24 measurements made during the first and second flow release period were tested with data from each ADVM individually. The index-velocity rating developed from the data recorded by the ADVM in pipe 6 proved to have the best regression statistics, making it the best rating for computing continuous discharge record. The range of discharge computed during the first and second flow release periods are listed in **Table 4-3-ADD**.

S-152 Structure Flow Releases 2013-2015

Before and after the first flow release, differential levels were run to the headwater and tail water gages to ensure accurate datum. For the first flow release, the gates were opened on November 5, 2013, and closed on December 30, 2013. A complete record was collected, and ten discharge measurements were made. During the first flow release, the recorded headwater gage height ranged from a maximum of 8.79 feet on November 19, 2013, to a minimum of 8.40 feet on December 23, 2013. The maximum recorded tail water gage height was 8.38 feet on November 27 and 28, 2013, and the minimum gage height was 8.09 feet on December 23-26, 2013.

Before and after the second flow release, differential levels were run to the headwater and tail water gages to ensure accurate datum. For the second flow release, the gates were opened on November 4, 2014, and closed on January 29, 2015. Velocity data from ADVM 6 was missing from November 4-7, 2014; the discharge computed from the ADVM 2 velocity data and index velocity rating was used to fill in the gap. Fourteen discharge measurements were made. The recorded headwater stage ranged from a maximum of 8.68 feet on November 19, 2014, to a minimum of 8.35 feet on January 27 – 29, 2015. The recorded tail water stage ranged from 8.28 feet on November 19 and 20, 2014, to 8.04 feet on January 26 – 29, 2015.

S-152 Structure Flow Effects on Downstream Water Levels and Velocities

Measured discharges through S152 and velocities at RS1 slough (downstream boardwalk) during the 2013, 2014-2015, and 2015-2016 flow events are shown in **Figures H36 and H37**. Velocity profiles at RS1 and RS2 in 2013 are shown in **Figure H38.** The combined discharge capacity of approximately 250 cubic feet per second through the S152 structure generated water velocities at RS1 as high as 4-5 cm s-1. Water released during the 2013 flow event spread radially from the S152 across the north and eastern portions of the study area (**Figure H39**). Whereas water levels, flow speeds and flow directions reached steady conditions within hours at

stations within a few hundred meters from the S152, it took three days for steady conditions to be reached 3 kilometers away. The maximum rise in water depths caused by the flow event was 11 cm (RS1), 6 cm (RS2), 5 cm (S1), 3.5 cm (UB2), and 2.5 cm (DB2). Flow speeds increased from background values (<1 cm s-1) reaching speeds up to 4.5 cm s-1 at RS1 (**Figure H37**). The highest flow speeds were considerably less at RS2 (2 cm s-1), S1 (1 cm s-1), UB1-3 (1 cm s-1) and DB1-3 (3 cm s-1). In the 2014 flow event, the rise in water depth was 12 cm (RS1), 5.5 cm (RS2), 5 cm (S1), 3 cm (UB2), and 4 cm (DB2). Flow speeds increased by 3.0 cm s-1 at RS1, 1.2 cm s-1 at RS2, 1.1 cm s-1 at S1, 0.3 cm s-1 at UB sites, and 0.7 cm s-1 at DB1 and 2. Thus the effects of the S152 flows on water depth and flow velocity were concentrated near the S152 and those effects decayed substantially with distance away. Flow speeds at control site C2 remained below 1 cm s-1 during the S152 flow event. In the 2015 flow event, we installed a new monitoring station, Z51_USGS at the upstream of RS1U, and our monitoring efforts were more focused on the transect between Z51_USGS to RS1D. The maximum rise in water depths caused by the flow event was 20 cm at Z51_USGS and 10 cm at RS1D. Flow speeds increased by 4-5 cm s-1 and 13-1 cm s-1 at Z51_USGS ridge and slough respectively. At RS1D, the flow speed at the slough increased to 6 cm s-1 (**Figure H37**), but the ridge side increased by only 3-4 cm s-1.

Flow speeds in sloughs generally were 25-40% faster than in ridges, due to reduced biomass and flow resistance in sloughs. Also, flow directions in sloughs tended to align with slough direction and while flow on ridges was somewhat misaligned with sloughs (with direction indicating that flow jumps across ridges between sloughs), these patterns in flow speed and direction through sloughs and ridges corroborate previous observations in the Everglades ridge and slough landscape (Harvey et al., 2009). In the 2014 and 2015 flow events, it was possible to monitor the extended steady state flow condition, because we had a much longer period of the high flow condition than with the 2013 experiment. From both 2014 and 2015 flow events, there was a gradual increase in flow speed at RS1D between November and December, followed by a decrease in the flow speed in January (**Figures H36 and H37**). The decrease can be caused by the gradual decrease in the water surface slope, the main driver of increasing the flow speed, due to the filling up the DPM study area between L67A and L67C.

4.1.5 Sheetflow Dynamics During the S-152 Structure Flow Releases (J. Choi, E. Cline, J. Harvey, D. Ho, L. Larsen, C. Saunders, E. Tate-Boldt)

2013 Flow Release

During the first flow event, starting November 5, 2013, the combination of dye and SF_6 tracers together showed that water moved radially away from the S-152 structure (**Figure H39**). The dye indicated the centerline of flow was in a direction that was more easterly than the centerline of the DPM experimental flow way. Within minutes after injection at 9:30 am 11/5/13, fluorescein dye was visible downstream of the S-152 and quickly demonstrated preferential flow paths, moving in an east- southeasterly direction. Using aerial monitoring, travel velocity for the

leading edge of the dye in the first 95 minutes of flow was 5.4 cm s^{-1}. The dye front then moved into a tree island approximately 500 m from S-152. By the second day the plume had become more diffuse (600 m wide) but was clearly visible in the water. The dye front was easily identified, 800 m east of the tree island, providing a travel velocity from minute 95 to 1450 post-injection of 1 cm s^{-1}.

Movement of SF_6 tagged water was mapped for 4 days each at C1 and RS1 (**Fig. H39**). Net advection at C1 and RS1 over 4 days was 0.28 ± 0.01 cm s^{-1} and 0.42 ± 0.01 cm s^{-1}, respectively, which was double and quadruple the rates measured during the pre-flow year of 2011 (0.15 ± 0.08 and 0.11 ± 0.01, respectively). At C1, the initial water flow direction was 70° for 600 m and changed to 100° for 370 m. Finally, the water flowed at 120° for 645 m into the canal. At RS1, flow direction was 170° for 800 m, and changed to 155° for the final 1060 m before entering the canal. In contrast, flow directions measured at C1 and RS1 in 2011 during pre-flow conditions were 109° ± 3.1° and 148° ± 2.5°, respectively.

Much of the flow released by the S-152 reached the L-67C canal at a location to the northeast of the levee gap. That water was shunted in a southwesterly direction in the L-67C canal until the levee gap was reached where the released water then moved southeast into WCA3B (**Fig. H39**). Accordingly, flow speeds at DB sites were higher than at UB sites (**Fig. H40**), most likely because a greater proportion of the released water that reached the DB sites was transported there by bypassing the RS2, S1 and UB sites. The ADV measurements at DB sites indicated only a slight preference for flow at DB1 compared with DB2 and DB3. However those measurements were sporadic in 2013 and should be confirmed by more frequent measurements in a future flow release. ADV flow tracker measurements associated with sediment trap and fauna sampling at several points around the L-67C also appear to indicate preferential flow across the northern-most gap treatment adjacent to DB1 (**Fig. H40**).

2014 Flow Release

In 2014, the SF_6 tracer release experiments were conducted in the same locations as in 2013 to examine temporal variability in the flow characteristics. After injection, the movement of SF_6 tagged water was mapped for 4 days each at C1 and RS1. The flow speeds and paths were very similar to 2013. Net advection at C1 and RS1 over 4 days were 0.32 ± 0.02 cm s^{-1} and 0.43 ± 0.04 cm s^{-1}, respectively, whereas they were 0.28 ± 0.01 cm s^{-1} and 0.42 ± 0.01 cm s^{-1} at C1 and RS1, respectively, in 2013.

At RS1, longitudinal dispersion coefficients decreased from a pre-flow value of ca. 1,000 cm^2 s^{-1} at RS1 to ca. 200 cm^2 s^{-1} in 2013 and 2014 after opening of S-152. At C1, the longitudinal dispersion coefficients changed from a pre-flow value of ca. 1,100 cm^2 s^{-1}, to ca. 550 cm^2 s^{-1} and ca. 1,300 cm^2 s^{-1} in 2013 and 2014, respectively. Lateral dispersion coefficients were very low for both RS1 and C1 (1 to 5 cm^2 s^{-1}), causing the patches to remain very narrow (ca. 30 m) even as they reach the L67-C canal. Before opening of culverts, advection and dispersion were

equally important at both sites. However, after opening of the S-152 culverts, flow at RS1 became dominated by advection.

2015 Flow Release

Two SF_6 injections were followed after the 2015 flow release. Injection 1 and 2 took place on November 30 and December 5, 2015, respectively. Movement of SF6 tagged water was mapped for 5 days after injection 1 and 4 days after injection 2 (**Figure H41)**. For injection 1, the initial water flow direction was ca. 157° for 830 m. Then, the direction changed to 150° for 1280 m into and across the L67C canal into WCA3B. For injection 2, the flow direction was ca. 137° for 925 m into the canal. The net advection at injections 1 and 2 for the first 2 days after injection were 0.34 ± 0.04 cm s-1 and 0.49 ± 0.10 cm s-1, respectively.

Comparison of flow measurements – 2013 flow release

Flow speeds described by various methods indicate substantial temporal and spatial variation during the 2013 flow event (**Table 4-6**). ADV-based flow speeds tended to be faster than those measured with the SF_6 tracer due to sensitivity of SF_6 to all processes affecting bulk transport of water, including movement into and out of slowing flowing waters in thick periphyton mats and vegetation. It is likely that the higher velocities of the dye, relative to SF_6, reflects that the dye delineated the preferential flowpath of water, initially captured flows closer to the S-152, and incorporated some uncertainty given the qualitative approach taken. The dye did however demonstrate slower speeds on days 2 and 3 (**Fig. H39**). When judged at a larger scale the ADV-based flow directions agreed with measurements made based on movement of the SF_6 tracer from its point of release at RS1. ADV data indicated that although the transport of released water was very strongly detected at RS1 it was more weakly detected at RS2, S1, and the UB sites. One reason is that the released water, after first being transported in a SSE direction toward those sites, then veered off in an easterly direction to eventually be intercepted by the L-67C canal. ADV data and SF_6 data indicated that once reaching the L-67C canal, the released water flowed southwest in the L-67C canal until reaching the experimental levee gap at which point the released water flowed southeast across the gap into WCA-3B.

4.2 Water Quality

4.2.1. Water Chemistry (S. Newman)

Baseline conditions (2010 – 2012)

Geometric mean water column TP concentrations were low throughout the DPM footprint, ranging 4 to 7 µg L^{-1} (**Fig. WQ1**). There were minor spatial differences as DB sites tended to

have greater TP concentrations than interior marsh sites and concentrations at UB sites decreased from north to south. However, there were significant temporal variations in TP as TP concentrations spiked in July and August 2011. These short duration spikes in water column TP were attributed to pulses of nutrients from the underlying sediments upon reflooding, following the prior summer dryout and vegetative burn.

A considerable percentage of the TP was bound in particulate form, averaging 53 percent in 2010 and 63 percent in 2011. Sites within the pocket had greater TPP values in 2011 than 2010 (**Fig. WQ1).** In contrast, DB sites had significantly greater TPP concentrations in 2010, attributable to their greater mass of suspended sediments ranging 4.1 to 5.5 mg L^{-1} in 2010, compared to values of 0.4 to 0.7 mg L^{-1} in 2011. Sites within the pocket had typically lower suspended sediment concentrations, ranging from 0.1 to 1.2 mg L^{-1} in 2010 and 2011.

High Flow conditions: 2013 S-152 flow release

During the entire sampling year, all DPM samples in the pocket had TP concentrations considerably < 0.01 mg L^{-1} (**Fig. WQ2**). S-152 concentrations remained below 0.01 mg L^{-1}, when flowing and when closed. Thus, the flow event did not provide increased water column TP to the downstream system and also did not increase TP concentrations in surface waters over a widespread area within the flow. Prior to the flow release the suspended sediment concentration (SSC) was generally low (0.6 to 1 mg L^{-1}). In the first few hours following the flow release the measured SSC increased at RS1 by an order of magnitude from approximately 1 mg L^{-1} up to 10 mg L^{-1} (**Fig. PC1**) but within a few hours had declined to levels slightly above background. Over the next few days SSC declined to levels equal to or slightly lower than the initial background.

Comparing representative samples of the full pre and flow periods, TPP concentrations were relatively unaffected, with a few exceptions (**Fig. WQ2**). Both ridge and slough sites at RS1 and the ridge at C1 were slightly higher during the flow, while southern sites (S1, UB) and a canal site (CB3) were slightly lower. TP did increase at RS1 and UB2 by approximately a factor of 2 from 0.0045 to 0.009 mg L^{-1} at 24 hours after the flow release began but had declined to 0.007 mgL^{-1} or lower after five days (**Fig. PC2**). In contrast to RS1, many other sites experienced little or no change in concentration as a result of the flow release (New USGS Fig. B). The high value at Ub2 on the first day of flow may be an outlier, because at RS2 sites, S1 and UB1 had decreased mass during the flow event, with little to no difference observed due to flow. Given such small changes in concentration overall, it is unlikely these concentration differences alone have large significance. However, TP loads also must be examined to assess downstream loading. The S-152 appears to have increased TP loads in the vicinity of the S-152 structure but these increases did not extend a far distance downstream. For example the TP load at RS1 increased by a factor of 10 as a result of the S-152 flow release and the increase last at least 5 days after opening of the S-152 structure (**Fig. PC3**). However, the increased TP load at

RS1 did not appear to propagate to downstream sites where TP load either stayed the same, decreased slightly, or increased slightly, with changes being bounded either way by no more than a factor of 50% (**Fig. PC3**). There appears to have been no significant effect of the S-152 flow release on long distance transport of TP.

In general, under no or low flow conditions, the TPP content of the water column was not influenced by habitat and likely was only affected in close proximity to the S-152 structure in response to flow. However, the sources of P to the particulate pool appeared to vary during pre and flow conditions. Prior to the flow release, the median volume weighted size of suspended particulates (D50) was initially relatively large (330 μm) but during the flow release many finer particles also entered suspension as reflected in values of D50 that decreased to as small as 50 um (**Fig. PC4**). Initially before flow became elevated the variability in particle size was low as reflected by a small value of the particle size variability metric D60/D50). After flow increased there was greater variability of particle size as reflected by a decrease in the particle size variability metric D60/D10 (**Fig. PC5**).

High Flow conditions: 2014 S-152 flow release

To focus on the effects of flow, we focus on data associated with the November 2013 and 2014 flow events; pre, during and post flow, and our discussion emphasizes those sites closest to inflow. In general, water entering the DPM footprint through the S152 structure was 1-2 μg L^{-1} lower in TP concentration than that measured at the upstream S151 structure (**Fig. WQ2**).

As observed in previous years, there was a distinct seasonality in total phosphorus (TP) concentrations within the canal system and, to a lesser extent, in the marsh (**Fig. WQ3** and **WQ4**). Highest concentrations were observed during the transition from dry to wet season, typically May to June. Phosphorus concentrations at RS1, the BACI site closest to inflow, appeared closely tied with those of the adjacent canal, L67A. One possibility is there is a direct relationship between canal water chemistry and the marsh; however it is also possible this is due to a greater contribution of TP from suspended sediments.

During the 2014 flow, a series of surface water samples were split and analyzed for particle size using a LISST-Portable particle size analyzer (Sequoia Scientific), and TP content (Buskirk et al, 2015). TP content increased immediately following flow implementation was associated with a decrease in particle size (results are presented in greater detail in sections following). However, unless sufficiently concentrated, fine particles may not be reflected in changes in turbidity - which relies on optical backscatter for detection. This likely explains the lag in turbidity response, following the dramatic TP increase, from 5 to 26 μg/L, observed at E250 immediately upon opening the gate (**Fig. WQ5**). The decrease in particle size observed by Buskirk et al., 2015 was short-lived, lasting only a few hours thus likely explaining the increase in turbidity at sites E250 and E300, two to three hours after flow initiation. Flow also increased

TP and turbidity at site E500, which was the furthest east site that exhibited a distinct response to flow restoration to the DPM flow-way. However, the lag between increased TP and turbidity was not apparent at eastern transect sites > 250m from inflow.

Point measurements allow us to assess the broad scale effects of flow at multiple locations, however, given the observed short term nature of surface water TP and particles, assessment at a greater temporal resolution was essential, resulting in the intensive monitoring initiated at site Z5-1 during the 2014 flow event. The initial opening of the S152 caused a higher tailwater stage, from 7.26 to 8.1 m. Downstream the opening of the structure resulted in a flow pulse, from < 1 to > 5 cm s-1 (**Fig. WQ6**). The high head differential between the marsh and canal likely caused the flow to pulse along with the spike in turbidity, because flow continued to increase after the initial pulse, while turbidity decreased. Opening the structure also resulted in an increase in surface water TP from 5 to 8 µg /L- although the lag between TP and turbidity was not as evident as observed at E250; however, nor was the TP increase as dramatic, a 3 versus 21 µg /L change. There are several hypotheses that might explain the differences observed at the two sites including: (1) Site E250 was in the preferential flow path from the structure, experiencing greater flows and potentially greater sediment transport or local disturbance exemplified by the rapid break-up of periphyton in the E250 slough (**Fig. WQ5**, right panel); (2) aerial imagery using the BOA suggest that the location of the autosampler was not within the preferred flow path in the Z5-1 slough area, further damping any potential signal because of the inability to capture higher flow pulses and lower likelihood of capturing fine sediments; and (3) differences in local sediments impact their suspension and effect on TP concentrations. While fluctuating, surface water TP concentrations remained elevated for several hours before returning to background concentrations.

Similarly, the response to closing the structure was also an increase in surface water TP. It is not clear what caused the increase, it could be attributed to local disturbance following rapid decline in water levels (e.g., increased sediment suspension, displacement of particulate material from plants) and lack of flow to transport those suspended materials- which in turn may explain the highly variable turbidity even after flow cessation. However, at this point this is speculation, further data analysis looking at periodicity may shed some light on these observations.

High Flow conditions: 2014 S-152 flow release

Hydrologic changes generated by both the S152 flows and L67C levee gap were key drivers of both spatial and temporal patterns in water quality. In pre-flow months, flow vectors in the pocket oriented primarily toward the gap, such that the southern portion of the study area flowed east or northeast (toward the gap) and the northern portions nearer the gap flowed south to southeast (**Figure WQ7**). Thus the southern and northern areas likely received different water sources, explaining why southern (UB/DB, C2) and northern sites (Z5-1, RS1, RS2, C1) clustered separately during pre-flow months (**Figures WQ7 and 8**). Conductivity and TP

showed that high flows spread water relatively evenly across the study area after 1-2 months (**Figure WQ8**). This reflects greater overall site-to-site connectivity associated with elevated velocities. During high flow, water moved from S152 preferentially eastward toward the L67C canal, then southwest down the canal. As a result, UB1-2 and DB1-2 tended to resemble S152 source water faster than UB/DB3 (**Figure WQ8**).

The effects of flow were more complex for some nutrients. For example, over the duration of flow, southernmost sites (C2, UB3, DB3) significantly clustered based on similar Ca concentrations. Calcium in fact increased with flow duration at these sites, leading us to hypothesize that flow may generate local Ca sources around this portion of the study area, though the mechanism remains unclear. Water TP variation also suggested dependence on localized processes. While most sites displayed low TP (≤ 0.006 mg l^{-1}) as flow continued, near-inflow sites Z5-1 and RS1 grouped together with higher TP. Despite the rapid velocities at these sites transporting P downstream to RS2, C1 and UB/DB sites, the limited extent of high TP reflects the rapid uptake and immobilization of P. This is not unexpected, as P is the most limiting nutrient of primary production in ridges and sloughs (Noe et al., 2001).

Along the preferential, eastern flow path, water levels increased and decreased concomitantly with the opening and closing of the S152 structure (**Figure WQ9**). Z5-1, initially at the same level as E250, rose ~6 cm higher, suggesting a slight head build-up prior to discharge to the south. Similarly while initial water depths at E400 were a few cm deeper than E250, E400 was shallower than E250 during flowing conditions. As expected, a velocity gradient was created along the flow path. The highest velocities measured during sampling events on the first few days of this year's pulses were 15, 13, 5, 4 to 3 cm s^{-1} at sites Z5-1, E250, E300, E400 and E500, respectively.

The lag of water movement across the landscape, and its associated effect on water chemistry, was evident from the sequential increase in specific conductivity with increasing distance from inflow (**Figure WQ10**). The highest conductivity, 687 µS cm^{-1} was observed in the canal during the second pulse. With the exception of E250 which had the lowest peak conductivity (max=630 µS cm^{-1}), conductivity values exhibited a slight decrease with distance, showing the dilution effect of marsh water on the S152 input. The inflow water had a distinct diel conductivity pattern, with maxima occurring around midnight. This pattern, though muted, was also observed in the marsh sites.

Similar to previous years, there was an increase in surface water TP concentrations as flow influenced local site conditions (**Figure WQ9**). While a single value of 35 µg L^{-1} TP was recorded at one location (1 out of 5 subsamples within site E250, data not shown), in general, TP concentrations doubled from 6 µg L^{-1} to 13 µg L^{-1} at sites closest to inflow and experiencing the highest velocities (Z5-1 and E250) within 1 hr of the first opening the S152. These concentrations decreased to 10 µg L^{-1} within 2 hrs, but did not decline to initial conditions until flow ceased. Upon the second opening, TP values were elevated to 10 to 12 µg L^{-1}, again for a limited 2 hr time period,

before decreasing to background levels. Sites downstream also saw an increase in TP levels, and as expected based on lower observed velocities, and delayed changes in conductivity and water depth, this lagged behind changes observed upstream. TP concentrations at sites 300-500 m did not increase above 10 μg L^{-1} during our sampling timeframe. It is unknown whether TP concentrations increased at E500 in response to the first flow pulse, because an elevated concentration was measured during the following stagnant period.

4.2.2 Turbidity (E. Tate-Boldt)

2013 flow event: Evidence of an initial pulse of sediments after the S-152 opening was indicated by turbidity sensors situated at varying distances around the S-152. Sites nearest the S-152 demonstrated turbidity peaks followed by rapid declines to baseline values (**Fig. H33**). At Z5-1 and NE-S-152, turbidity peaked at 11:15 am and 11:20 am, respectively, while turbidity peaked at RS1 at 12:20 pm. Based on the timing of the turbidity peaks, water velocities at Z5-1, NE-S-152, and RS1 were 2.9, 3.0, and 4.2 cm s^{-1}, respectively. No turbidity peak was evident at RS2, likely reflecting reduced velocities between RS1 and RS2 (shown above).

4.2.3 Dissolved Organic Carbon (L. Larsen, S. Newman, C. Saunders)

DOC and SUVA values reflected the impacts of the region-wide fire in 2011 and the first flow release in 2013. Box plots showing the distribution of the data over all sites show the highest concentrations of DOC in surface water (up to about 35 mg L^{-1} C, values typically found in porewater) the first sampling event after the fire in 2011. The DOC mobilized by the fire and subsequent rewetting also had the lowest SUVA values of the period of record (2.3-2.4 L mg^{-1} m^{-1}), suggestive of an increase in the aliphatic character/decrease in the aromatic character of the carbon mobilized. Out of all the sample sets, the spatial variability in DOC concentration was highest in the first set of samples after the fire. (**Fig. WQ11**)

Within one month of the rewetting post-fire, DOC values across the study area decreased and became more uniform across the Pocket. However, DOC concentrations remained higher than the pre-fire period. SUVA increased during this period and remained uniformly high for the entire post-fire wet season, relative to the other years of the study. The decrease in SUVA immediately following the fire, followed by relatively high SUVA for the remainder of the wet season, suggest that the fire initially liberated large quantities of mobile DOC, but that after this initial mobilization, the DOC pool was dominated by more refractory plant- and peat-produced material, with less of a contribution from microbial material.

Microbial contributions to the DOC pool appear to have recovered one year after the fire, by the 2012 wet season, when monthly mean SUVA values were typically 2.6-2.8 L mg^{-1} m^{-1}

and DOC concentrations were around 15-20 mg L^{-1} C. A slight increase in DOC across the Pocket late in the wet season may reflect an evapoconcentration effect, as observed by Larsen et al. (JGR-Biogeosciences, 2010).

Unlike the fire, the flow release in 2013 did not change DOC concentrations outside their previous range of variability. Relative to early in the 2013 wet season, the flow release increased DOC concentrations by less than 5 mg L^{-1} C. More substantial was the effect of the flow release on SUVA. The highest SUVA values of the study (>3.2 L mg^{-1} m^{-1}) were recorded approximately one month after the gap in the L67C levee had been breached. SUVA remained high after the November 2013 flow release, declining to previous levels only in January 2014. The post-flow increase in SUVA is suggestive of a relatively higher contribution of plants or peat to the DOC pool and a relatively lower contribution from microbial activity. The elevation of SUVA after the L67C gap was opened but prior to the opening of the L67A culverts suggests that the higher SUVA concentrations were not attributable to construction materials from the L67A but rather to materials and processes within the marsh ecosystem. Interestingly, while the breaching of the gap appeared to have triggered the increase in SUVA, the flow release from the L67A culverts triggered a decline in the spatial variability of DOC and SUVA to the lowest levels observed over the period of record (**Fig. WQ12**).

DOC results were modeled using a General Linear Mixed Model, with site treated as a fixed effect and date as a random effect. Collectively, site and date explained 63% of the variance in the DOC dataset, with 59% attributable to date alone. Though site was significant at $p<0.0001$, only sites C2, DB1, DB3, and L67A had main effects significantly different from zero. Site and date collectively explained 78% of the total variance in the DOC dataset, with 64% attributable to date. Most sites, with the exception of the DB1-DB3 sites and site RS2, had main effects significantly different from zero. For models of DOC and SUVA differences between sequential sampling events, the fire and post-flow period emerged as the most significant time effects. DOC responded instantaneously to these events, whereas SUVA tended to respond with a 1-2 month lag (**Fig. WQ13**).

4.3 Particle Characteristics

4.3.1 Suspended sediment concentrations and size distributions (L. Larsen and J. Harvey)

LISST Portable size distributions

During each of the November intensive sampling efforts for the pre-release period, size distributions of suspended sediment, bed floc, and metaphyton particles were obtained using the LISST-Portable. In 2010, bed floc size distributions were typically bimodal (**Fig. PC6**), with modes at ~100 µm and ~30 µm. Metaphyton particle size distributions tended to have similar

modes, with the exception that the large-size-class tail was typically heavier, suggesting that bed floc may ultimately originate from metaphyton but represent a more degraded pool of particles (i.e., with fewer intact large particles). In contrast, particles suspended within the water column tend to share the smaller-size mode with bed floc and metaphyton but exhibit a sharp decline in concentration at particle sizes > 50-70 µm. Many of the suspended particle histograms, however, exhibited a concentration spike within the largest size bin, which typically indicates the presence of a single large particle (e.g., a floating piece of macrophyte) contained within a low-concentration sample.

Bimodal particle size distributions in bed floc were the exception rather than the rule in fall of 2011, which followed the fire (**Fig. PC7**). The location of the peak was variable by site, ranging from 30 µm at site DB1to 120 µm at site S1. As in 2010, peaks in the size distributions of bed floc and metaphyton roughly aligned at most sites, except for at UB2 and S1, where they were decoupled. When the distributions were not decoupled, the metaphyton distributions often—but not always—had heavier tails than the bed floc distributions. Relative to 2010, bed floc in 2011 was scarcer, required more attempts to collect, and often had the appearance of containing significant quantities of ash. Based on these observations, we attribute the greater degree of decoupling between the floc and metaphyton pool in 2011 and the higher spatial variability in particle size distribution characteristics in 2011 to depletion of the floc pool by the fire (with spatially varying effects) and incomplete rebuilding of that pool by metaphyton-derived OM and ash.

Relative to 2010, bed floc and metaphyton particles were smaller in 2011, with the exception of sites S1, UB2, and DB3 (**Fig. PC8 and PC9**). No consistent trends in how the mass-weighted mean equivalent diameter of suspended sediment changed across the two years were observed. Within each year, there were also no consistent trends in spatial variability of mean particle sizes across the pocket for suspended particles, bed floc, or metaphyton (**Fig. PC9 and 10**).

LISST Continuous size distributions: Instrument comparison to other particle-size measurements

Unlike the LISST-Portable, the LISST-100x and the LISST-Floc record particle size distributions continuously during an *in situ* deployment. The LISST-Floc and LISST-100x differ only in the length of their optics, with the longer focal length of the LISST-Floc enabling it to detect larger aggregates. In 2010, serial deployment of the LISST-100X, LISST-Floc, and LISST-portable was attempted at sites RS1S and RS1R to assess the intercomparability of results obtained from these instruments.

Both the LISST-Portable and LISST-100x exhibited large masses of particles in the largest size bins, which, given the abundance of particles in larger size classes observed by the

LISST-Floc, appears to be a saturation effect. All three instruments observed bimodal size distributions, but the abundance of large particles observed by the LISST-Floc suggested that the other two instruments may have been incapable of resolving the larger mode of the distribution (**Fig. PC11**). Peaks of the smaller mode of the probability density functions roughly coincided around 30-50 µm.

Discrepancies between particle size distributions measured with the different LISST instruments suggest that the instruments are not directly intercomparable, and that the LISST-Portable and LISST-100x may produce underestimates of mean particle size. However, datasets collected with a single instrument provide useful relative comparisons across sites or over time that can be used to address the hypothesis that flow releases will increase the abundance and size of suspended particles within the water column.

4.3.2 Particle biogeochemistry (L. Larsen, S. Newman, J. Harvey)

Particulate phosphorus

Total P in periphyton in 2010 ranged between 177 mg kg^{-1} periphyton at site S1 and 902 mg kg^{-1} periphyton at site DB1 (**Table 4-7**). These sites also bracketed the range of total particulate P in floc for that year: 101 mg kg^{-1} floc at site S1 and 1085 mg kg^{-1} floc at site DB1 (**Table 4-8**). With the exception of site DB3, the highest concentrations of P in floc and periphyton were found at the sites immediately south of the L-67C canal, though the RS2 slough site also exhibited one of the highest values of total particulate P in periphyton. Following the fire, in 2011, the highest concentrations of total particulate P in periphyton were found at sites DB2 (530 mg kg^{-1}) and the RS2 ridge site (500 mg kg^{-1}), and the lowest concentration was found at site UB3 (181 mg kg^{-1}). For floc, the highest TP concentration in 2011 occurred at site DB2 (978 mg kg^{-1}), which was nearly twice that found at the next-highest site, RS1 slough (531 mg kg^{-1}). The lowest concentration of TP in floc occurred at site S1 (170 mg kg^{-1}).

There were no consistent differences in total particulate P in floc or periphyton across years or spatially across the Pocket. However, total particulate P in floc was generally lowest at the interior sites (RS2 and S1) located farthest from the canals/levees. For the majority of paired ridge-slough sampling events, the ridge contained higher particulate P than the slough. This trend is consistent with relative ridge-slough differences in dissolved P that have been observed in porewater and particulate P in peat (Ross et al. 2006) and may be related to the greater degree of evapoconcentration of P on the shorter-hydroperiod ridges and the sequestration of P within sawgrass biomass. Exceptions to this trend occurred for the paired RS2 periphyton samples from 2010 and RS1 floc samples from 2011.

Analyses of periphyton and floc particles sampled for P biogeochemistry also distinguished between the labile ($NaHCO_3$-exctractable), microbial ($NaHCO_3$+$CHCl_2$-

extractable – labile), and refractory components of the particulate P pool. For periphyton, although the total concentrations of particulate P did not vary consistently in space (i.e., across the Pocket) or temporally, the distribution of P among these three categories exhibited a marked temporal shift. Following the fire in 2011, the periphyton P pool became significantly ($p = 0.025$) more refractory compared to 2010 (**Fig. PC12**). This trend, however, was not apparent in the floc particles (**Fig. PC13**).

Introduction of relatively high flow velocities to the Pocket will transport particulate P downstream if those velocities are sufficient to entrain floc and periphyton. Differential entrainment of these two classes of particles is expected to have different impacts; not surprisingly, periphyton contains substantially higher concentrations and proportions of labile and microbial P than floc. Thus, its redistribution may have less of a favorable impact on landscape evolution than that of floc (because of its presumed degradability), and it may have more of an adverse impact as a vector of reactive P. We propose that portions of the landscape with abundant periphyton coverage may be more resilient against restoration efforts because of 1) the physical difficulty of obtaining the bed shear stresses needed to entrain floc in these areas, 2) the relative decomposability of periphyton-derived sediment compared to bed floc, and 3) the P reactivity associated with periphyton-derived sediment.

Particulate nitrogen

Similar to trends in particulate P in floc, particulate N in periphyton and floc in 2010 was generally lowest at interior sites within the Pocket (RS2 and S1) farthest from the canals and levees (**Fig. PC14**). The highest values of total N were generally found at sites DB1 and DB2; as with particulate P, site DB3 exhibited lower particulate nutrient concentrations than DB1 or DB2. Total N in periphyton consistently and significantly ($p = 0.04$) declined across the Pocket following the 2011 fire but did not exhibit significant changes in the floc pool. In 2010 TN in periphyton ranged from a low value of 11.6 g kg^{-1} at site UB2 to 35.3 g kg^{-1} at site DB2. TN in floc ranged from 9.4 g kg^{-1} at site RS2S upwards to 42.2 g kg^{-1} at site DB2. In 2011 periphyton TN ranged from ~8.5 g kg^{-1} at sites RS1R and DB3, upwards to 16.1 g kg^{-1} at RS2R; floc TN ranged from 9.2 g kg^{-1} at site S1 to 37.9 g kg^{-1} at site DB2.

Particulate carbon

Spatial trends in ash-free dry weight across the Pocket were more pronounced than 2010-2011 temporal trends (**Fig. PC15**). As with particulate N and P, ash-free dry weight (representative of the organic fraction of the sediment) tended to be lowest at the interior sites farthest from levees (RS2 and S1) and highest at sites just downstream of canals (sites C1, RS1, DB1, and DB2). Exceptions were site DB3, which exhibited relatively low ash-free dry weight (20-40% over the two years) and site UB3, which exhibited relatively high ash-free dry weight (nearly 70% in 2011).

Challenges

The pre-release characterization of particulate biogeochemistry across the Pocket revealed that prior to any canal treatments, the biogeochemistry of site DB3 is substantially different from that of sites DB1 and DB2, with nutrient concentrations that are generally much lower. We hypothesize that there is less underflow affecting site DB3 compared to sites DB1 and DB2. Because of the hypothesized lower pre-release hydrologic connectivity between the canal and site DB3, we expect to see larger relative changes in particulate biogeochemistry at site DB3 during the flow release. Disentangling the effects of that enhanced hydrologic connectivity from the effects of the different canal treatments will pose a challenge in the analysis.

4.3.3 Spatial survey of floc and soil chemistry (C. Saunders, S. Newman)

Phase-1 of the floc and soil spatial survey, conducted in July 2012, indicated clear gradients in the OM and nutrient content of sediments across the DPM footprint (**Fig. PC16**). Most notably, highly organic floc and soil was more typical of the marshes near the L-67A levee and southeast of the largest tree island, whereas all other areas in the pocket and downstream of the L-67C levee were mineral-rich. Spatial variation in floc P content (TP) was strongly and positively correlated with floc OM ($R^2 = 0.88$, $F_{1,26}=10.64$, $P<0.001$). Floc P content was typically >500 mg kg^{-1} at sites near the L-67A, and <300 mg kg^{-1} in the pocket and in WCA-3B. Phase-2 of the spatial survey includes follow-up measurements of critical entrainment threshold (CET) and sediment transport at sites spanning the range of OM and TP observed in the Phase-1. These measurements will provide important information for understanding the extent to which sediment entrainment and mobilization of P can be expected during the experimental flow events.

4.4 Particle Fluxes

4.4.1 Critical Entrainment Threshold (CET) of sediments (S. Newman, C. Saunders):

Benthic annular flumes conducted indicated that sediment entrainment required sustained velocities of 1.5 cm s^{-1} or higher, though considerable variation in the amount and behavior of bed entrainment was noted among sites. As shown by the examples presented in **Fig. PF1**, entrainment behavior differed between mineral-rich and organic-rich sediments. Site Z6-1 (near C1), which is dominated by organic sediments, indicated some low-level entrainment might occur at even slow velocities (0.5 to 1.5 cm s^{-1}), while a clear step increase in entrainment was observed at 2 cm s^{-1}. A gradual but steady increase in sediment entrainment was observed as velocities were increased above 2 cm s^{-1}. In contrast, the mineral-dominated sediments at site Z10-2 (between RS2 and UB2) showed no low-level entrainment at low velocities (<1.5 cm s^{-1}). Compared to site Z6-1, site Z10-2 also demonstrated a larger magnitude of bed entrainment as

velocities increased to 5 cm s^{-1}. While preliminary, these results indicate the potential for nonlinear responses to pulsed events in mineral-dominated substrates.

The Nov-2013 flow event did appear to have an effect on sediments, despite a lack of dramatic and sustained changes in the water column. Critical entrainment threshold (CET) velocities were generally lower in the post-flow sampling events, most noticeable at sites closest to the S-152 (**Fig. PF2**). While this reflects the changes in sediment properties following flow, increases in NTUs at sites in close proximity to construction may also reflect movement of construction materials. Detailed analyses of these data in concert with other sediment characteristics (e.g., floc mass, chemistry and biomarkers) that identify floc sources will help us understand the relative contribution of construction debris to floc transport during flow

4.4.2 Particle Transport - Natural particle mobilization (L. Larsen, J. Harvey)

Baseline conditions (2010-2012)

Simultaneous deployment of the LISST-100x and LISST-Floc instruments in the ridge and slough at site RS1 revealed characteristic diel dynamics in particles suspended within the water column. During the first November 2010 deployment (**Fig. PF3**), both sites exhibited an increase in the smallest particle size class during the day (< 6.5 µm in the slough, < 12.3 µm in the ridge). In the ridge, the increase in this small size class of particles caused an increase in overall particle concentrations; in the slough, overall particle concentrations tended to increase during the day, but inconsistently so. For example, in **Fig. PF3**), there is a threshold-type drop in slough particle concentrations during the first day before concentrations increase above nighttime levels. During the daytime, overall particle concentrations increased less than would be expected based on the increase in mass concentrations in small size classes, as these increases were accompanied by a decrease in particle concentrations in intermediate size classes (15-20 µm in ridges, 6-10 µm in sloughs). The second period of deployment in 2010 (**Fig. PF4**) resulted in a noisier dataset but still reflected mobilization of particles in small size classes during the day, with a concomitant increase in overall mass concentrations of particles in the slough.

Simultaneous deployments from August 7 – 9, 2012 (**Fig. PF5 and 6**) exhibited clear increases in small particles during the day in both ridge and slough, accompanied by a pronounced increase in overall particle concentrations during the daytime in the slough. Small-particle concentrations and overall mass concentrations peaked during the day in the ridge for the November 2012 deployment (**Fig. PF7 and 8**); in the slough for that period of time, the data were noisy but reflected a slight increase in the concentration of small particles during the day but relatively steady overall particle concentrations.

Increases in small particle concentrations during daylight relative to nighttime has been observed previously, at WCA-3A, and has been attributed to the movement of phototropic bacteria within the water column (Noe et al., 2007). The nighttime increases in intermediate size classes may reflect the differential settling and flocculation of smaller particles at night (e.g., Larsen et al., 2009). Bioturbation by feeding fish—as has been observed in the field—may also explain these patterns of daytime breakup of aggregated particles, followed by reaggregation and differential settling at night.

Generally, diel trends in particle equivalent diameter were less clear than those in the particle size distributions. Mean equivalent diameters generally exhibited high temporal variability and appeared noisy. However, for one of the datasets (August 2012), mean equivalent diameters exhibited a clear daytime increase.

Overall mean mass-corrected concentrations of suspended sediment observed during the LISST-continuous deployments were on the order of <1 $\mu g\ L^{-1}$ to 10 $\mu g\ L^{-1}$. This range compares favorably with concentrations previously observed in WCA-3A using a digital floc camera (1 $\mu g\ L^{-1}$-300 $\mu g\ L^{-1}$; Larsen et al., 2009) and is lower than concentrations of fine suspended particles (0.2-100 μm) measured in a study that used sequential filtration to asses particle concentrations in samples collected from across the Everglades (0.7-2.7 mg L^{-1}; Noe et al., 2007) and over two wet seasons at site WCA-3A-5 (mean = 0.94 mg L^{-1}; Noe et al., 2007).

Overall, diel deployment of the continuous LISST instruments revealed that particle size distributions in this landscape are dynamic and are likely influenced by biological as well as physical processes. Before-after comparisons in particle size distributions and concentrations should be made at similar points throughout the diel cycle. However, we hypothesize that as larger concentrations of sediment are entrained into suspension during high-flow events, the physical processes of entrainment and deposition may overwhelm diel biological signals in particle characteristics in areas through which sediment is actively redistributing. Thus, we propose that the presence or absence of a diel signal in particle data may be diagnostic of whether redistribution of sediment by flow is occurring.

The high temporal variability in the mean equivalent diameter statistic suggested that this first-order statistic is often not sufficient to resolve important changes in suspended sediment dynamics, particularly when obtained at a single point in time. As with interpretations of the discrete LISST-Portable data, examination of the whole particle size distribution will be critical for detecting real differences in particle source or aggregation/disaggregation dynamics following the flow release.

Particle Dynamics during 2013and 2014 S-152 Flow Release

One of the primary science hypotheses is that elevated flow during the release period will entrain larger concentrations and sizes of particles into suspension. With higher flow, we expect to see a shift in the mode of suspended particle size distributions to larger size classes and diminishment of the prominence of the largest size bins (which at low concentrations are subject to single-particle noise). The fact that the size distributions of suspended particles within the water column are presently shifted to much lower values than the size distributions of bed floc particles suggests that bed floc is not presently entrained, which is consistent with our hypothesis.

The pre-release particle size distributions suggest that the shape of the distributions may be diagnostic of the origin of the particles. Heavier tails on the large-particle side of the distribution may, for instance, be indicative of metaphyton as the source of the particles, whereas thinner tails may be more consistent with the entrainment of bed floc. Flume experiments in WCA-3A (Harvey et al. 2011) suggested that prior to entrainment of bed floc, significant quantities of metaphyton particles are entrained as suspended sediment. We expect to observe a similar phenomenon during the DPM flow release period.

The mass-weighted particle size distributions of the water column samples at all study sites are compared for the pre- and post- flow release experiments, 2013 and 2014 (**Fig. PF9**). They showed significant increase in the mass of particles over the particle size range, greater than 100 μm. **Fig. PF10** compare the particle size distributions of water column, floc and epiphyton samples collected during the high flow conditions of 2013 and 2014 experiments. The water column samples displayed the bimodal size distributions at both experiments and floc and epiphyton samples had similar size distributions at most sites.

The comparisons of LISST data from both 2013 and 2014 experiments show the sudden increase in the suspended sediment concentration after couple hours from the flow release at S-152 and the decrease in mass-weighted particle size that occurred simultaneous with the arrival of the flood wave release at S-152 (**Fig. PF11 and PF12**).

4.4.3 Particle Transport – Natural particle tracer movement during flow releases (C. Saunders, S. Newman, R. Jaffé, B. Rosen)

Horizontal sediment traps were used to determine the extent to which sheetflow will alter sediment transport and redistribution between ridges and sloughs. To evaluate temporal changes, we deployed sediment traps in paired ridge and sloughs using the BACI design at the near-impact site RS1, far-impact site RS2 and control site C1. Results from trap deployments from November 2011 to April 2015 are presented in **Fig. PF13**. We expected that higher-velocity sloughs at RS1 would demonstrate greater sediment transport than ridges or sloughs at the control site. Horizontal traps showed that high flow significantly increased slough sediment transport at RS1 (**Fig. PF13**; BACI time x trt (treatment), $t=-3.54$, $n=40$, $p=0.0010$) relative to

the control site C1. Transport during the high flow period was 5.4-fold higher (5.9±0.7 standard error (SE) mg cm-2 d-1) than during the baseline period (1.1±0.9SE). At the control site, transport has declined since 2011, likely reflecting recovery from a fire in 2011; thus, flow effects are likely underestimated by the BACI analysis. Relative to transport measured during just prior to each flow event (October) of each flow year, transport increased 12- to 15-fold above those pre-flow values. Ridge transport also increased under high flow (t=-2.7, n=37, p=0.0366), but by a smaller proportion (58%) relative to the baseline. On a ground area basis, slough sediment transport at RS1 ranged from 3,600 to 29,000 g m-2 yr-1 under high flow, approximately 10 to 100 times the magnitude of both floc standing stocks (ca. 100-300 g m-2) and sediment accumulation (ca. 160-250 g m-2 yr-1; Craft and Richardson, 1998). If just 5% of transported slough sediments entered ridges, this could theoretically increase sediment accumulation by 100-1000%. These findings suggest flow-mediated transport could be critical factor affecting differential sediment accumulation in ridges and sloughs.

In all three flow events, RS1 slough transport increased over the duration of the flow event such that transport in December and January was greater than transport in early and mid-November. In 2013, for instance, RS1 slough transport approximately doubled every 3 weeks. Similarly, in 2014/15, transport in December and January was approximately 4- to 8-fold higher (ranged based on duplicate samples) from initial rates in November. Velocity measurements paired with these deployments also increased over the first two months of flow, suggesting transport was in part driven by velocity. This phenomenon of increasing velocity and increasing transport over the duration of flow was not expected, because S152 discharges decreased over the duration of both flow events, for instance, from 252 to 208 cfs in 2013 (**Table 4-3**).

In the second and third flow events, floc height in the RS1 slough also decreased over the duration of flow, the reduction most evident 8-10 weeks after flow started (**Figure PF13B)**. Two weeks after flow started in Nov 2015, floc at RS1 slough approximately doubled in height, but also varied spatially, in a sinusoidal pattern across the slough (**Figure PF13B**). This likely reflects the sinking and disintegration of floating periphyton mats into the floc layer; a process visually observed within days or weeks during all three flow events (see Algal Changes, below). Based on the gradual decrease in floc height during flow events 2 and 3 (10-15 cm per 8 weeks), the estimated turnover time of floc was approximately 70-80 days. This rate is consistent with, if slightly longer, than floc turnover estimated from *in situ* incubations (turnover time = 30-60 days; Wood, 2005).

To examine spatial patterns in sediment transport, traps were also deployed in sloughs along the southern flowpath, as a function of log-distance from the S-152. As shown in **Figure PF14**, sediment transport in the high-flow events of 2013 and 2014 was 10x to 100x greater than in baseline conditions (2012), but only for sites within 500-m of the S-152. This was consistent with expectations, as mid-water column velocities beyond 500-m radius were much lower (typically < 1.5 cm/s) than at the RS-1 and Z5-1 sites. It also mirrors results from the traps

deployed with the BACI design (above), showing transport greatly increased at the near-impact site, RS1, over the control site C-1 and the far-impact site RS2.

Biomarker analysis of plant biomass

The collection and analysis of ridge and slough vegetation was primarily performed to assess the applicability of the proposed biomarker conceptual model for the DPM site. Previous vegetation samples for biomarker studies were mainly performed at Everglades National Park, although the biomarker composition at DPM is likely to be very similar (Mead et al., 2005). Plant sample analyses were focused specifically on the n-alkane proxy Paq, which has been used to differentiate between aquatic and emergent plant-derived organic matter (OM) (Ficken et al., 2000; Mead et al., 2005; Pisani et al., 2013). It is usually observed that aquatic vegetation, including the typical species present in long hydroperiod environments of the Everglades (*Eleocharis*, Nymphaeceae, *Utricularia*), are characterized by elevated Paq values, while emergent vegetation and the species characteristic for short hydroperiod environments (*Cladium*, *Typha*) in the Everglades have lower Paq values. Shown in **Fig. PF15** is the Paq distribution for the plant samples determined in this study. It is clear that in general terms the abovementioned conceptual model for Paq as an OM source proxy for long vs. Short or slough vs. ridge environments applies well. Periphyton is included in this Fig., but planktonic organism do not generate significant amounts of mid to long chain n-alkanes, and as such the Paq reported for the periphyton represents other OM sources such as detritus of emergent vegetation, remains of *Utricularia* and others which are part of the algal mat sample. With the exception of the kaurenes, which have been observed in higher plants, specifically in *Cladium* (Saunders et al., 2006; Neto et al., 2006), the other biomarkers C20 HBI and the botryococcanes are exclusively produced by plankton and were not analyzed in the plant samples.

For further proof of concept, floc from two ridge-to-slough transects (Z5-1 and Z6-1) were sampled during 2012 and 2013 and the biomarkers determined (**Fig. PF16**). As expected in all cases the Paq increased along the ridge-to-slough gradient. For the other biomarkers, although the C20 HBI abundance for Z5-1 increased along the gradient, this trend was not obvious for the Z6-1 transect. C20 HBI is associated with cyanobacterial biomass in periphyton derived OM (Pisani et al., 2013), and thus expected to be enriched in slough environments compared to ridges. The higher C20 HBI concentrations for Z5-1 are likely the result of nutrient enrichments at this site compared to others in the pocket area (except RS-1). Lastly, the kaurene distribution along transects agreed with their main source from *Cladium*, as they were present in higher abundance in the ridge compared to the slough.

The average values of Paq for all sample types (ridges, sloughs and canal sediment traps) during the baseline (pre-flow) period, regardless of season, are shown in **Fig. PF17**. The Paq

values were found to be consistently and statistically significantly higher for the slough than for the ridge samples demonstrating the viability of the conceptual biomarker model with regards to OM source differentiation. Interestingly, the average Paq value for the 20 canal sediment trap samples was similar and not statistically different from that of the slough samples. This fact suggests that indeed, the bulk of the OM in the sediment traps is derived from a slough-like environment, where velocities typically are a little higher compared to ridge-like environments (Choi et al., 2013). Higher flow will enhance entrainment and consequently mobilization of slough-like OM compared to ridge-like OM leading to a preferential accumulation of high Paq material in the traps. While this observation seems to be in complete agreement with the conceptual biomarker model, it is important to consider that canal inputs may also influence the materials collected in the sediment traps.

Concentrations of the biomarkers C20 HBI, botryococcenes and kaurenes for all sites are also shown in **Fig. PF17**. For this limited pre-flow period data set, no statistically significant differences were observed between ridge and slough samples for the C20 HBI or the botryococcenes, suggesting that at least in at the DPM study site the dynamics of periphyton seem uncoupled from typical variation in periphyton cover among habitats. The kaurenes on the contrary were consistently and statistically significantly more abundant throughout the DPM site at the ridges compared to the sloughs. Very interestingly, kaurenes were consistently detected in all canal sediment trap samples. This is somewhat unexpected considering that these compounds were very low in abundance or even undetected in the slough samples. Their consistent presence in the traps suggests that some constant contribution of ridge-like OM is also mobilized in the DPM area. Simple two end-member mixing calculation using average kaurene concentrations from ridges and sloughs suggests that in excess of 80% of the OM in sediment traps is slough-like and below 20% ridge-like. This estimate is different from the 100% estimated slough-derived OM based on the Paq estimations. However, considering that at many stations in the DPM study site the water depth difference is very small (9 cm) it can be expected that some ridge-derived OM will also accumulate in the sloughs. Regardless, although these are very rough estimated based on a limited dataset, the sediment mobilization in the DPM study site under present pre-flow conditions seem primarily slough derived.

Biomarker analysis of floc – background variation and flow effects

Molecular biomarkers were analyzed in benthic floc of paired ridge and slough samples, in the pre-, during, and post-flow periods for the 2013 flow, spanning October 2012 to May 2014 (**Fig. PF18**). For the n-alkane proxy Paq, a statistically different average value was observed for both the ridge and slough floc in the post-flow period, in which greater Paq values reflected increased slough-derived organic matter (OM). Although Kaurenes were not statistically different during the 2014 sampling dates compared to 2013 (not shown), a much higher range of values for Kaurenes was observed during high flow conditions compared to pre-flow conditions (**Fig. PF18**). Using all available data from all sites, no significant differences were observed

among the pre-, during, and post-flow conditions in ridge and slough samples for the C20 HBI. Although Botryococcenes showed a high degree of variability, the slough values were significantly different (higher) in the post-flow period. We stress that these data are preliminary, as they encompass only the first flow event and as a result unbalanced (far fewer samples in the flow and post-flow periods). Nevertheless, changes do appear consistent with the hypothesis that flow increased the presence of slough-derived organic matter settling in ridges. That slough Paq values also increased suggests some changes occurred in the content of the slough floc itself.

Some uncertainty remains about the mechanism of sediment redistribution, since biomarker changes occurred primarily in the post-flow period rather than during the flow event. Substantial capture of sediments by vegetation in the water column was observed, qualitatively, during flow, especially at RS1. Therefore, we hypothesize the biomarker changes in floc post-flow reflects the slower process of vegetation litterfall (which would include settling of captured sediments) over several months. An alternative hypothesis is that biomarker changes reflect shifts in local algal communities that ultimately produce a lot of the floc material. However, the taxonomy of advected sediment showed flow-driven changes in the algal community were fast (within weeks, see "Algal taxonomy" below) and therefore less likely to explain the slower rate of change in benthic floc biomarkers.

While the algal biomarkers C20 HBI and Botryococcenes are highly variable, closer inspection of the spatio-temporal distribution of all biomarkers suggests changes were widespread but mostly near the S152 (**Fig. PF19**). At sites near the S152, the algal sources of floc OM changed within the first flow event. While this is driven by local algal community changes (see Algal Changes, below), the physical transport of OM also likely contributes to some of this change. During and shortly after the first flow event, concentrations of Botryococcenes (a green algal marker) in floc increased from very low concentrations (<0.1 µg gdw-1) to 15 and 22 µg gdw-1 at sites 150- and 350-m, respectively, from S152 (**Fig. PF19**). Concomitantly, concentrations of C20 HBI's, indicative of cyanobacteria (abundant in metaphyton), showed decreased concentrations at the same sites. For both compounds, advected sediments (from horizontal traps) contained concentrations similar to those in the floc. The similarity of biomarker concentrations in both floc and advected sediment, and the magnitude of sediment transport, suggest sediment movement downstream likely contributes to the chemical changes in floc.

Although slough velocities of ≥1 cm s-1 were limited to ~500 m of the S152, biomarker results from the second flow event indicate biogeochemical changes in floc are occurring over a larger and expanding area. Shortly after the second flow event, Botryococcene concentrations increased at sites 700-m south and 1000-m east of the S152. Thus, biomarkers are useful indicators of slower, but larger-scale, responses of sediment biogeochemistry to sheetflow.

Algal taxonomy of floc – background variation and flow effects (B. Rosen)

C-1 ridge had low species richness (dominated by diatoms) and no changes between before and the two weeks after flow. After 5 weeks of flow, the C-1 ridge site showed a marked increase in species richness, with a significant increase in the number of cyanobacteria and the appearance of green algae (Table xxx). C-1 slough was slightly greater in species richness compared to the C-1 ridge, dominated by diatoms, and no perceptible change as a result of flow.

RS-1 ridge and slough both had very low species richness of all 77 samples, with only the presence of diatoms prior to the flow event. The few species present are known to thrive in calcium-rich habitats. In the slough, species richness increased substantially 2 weeks after the flow event and increased to its highest 5 weeks after flow, with green algae & cyanobacteria (added) accounting for over 55% of new organisms in the species richness calculation. Diatoms species richness also increased during the first 2 week period in the slough and even greater by the 5th week, while the ridge at RS-1 did not show the increase in richness until the 5th week. The additional diatoms species responsible for this increase in richness were not from calcium-rich habitats and are like associated sediment resuspension from the slough. RS-2 and DCC2 did not show a response to flow.

The three backfill treatments had the greatest species richness, with approximately equal numbers of green and diatom species and slightly fewer cyanobacteria. None of these treatments showed changes in species richness in response to flow. The green alga, *Botryococcus*, a known source of the botryococcene biomarkers, was found in 6% of the samples of the 77 sediment trap samples.

4.4.4 Particle Transport - Dual Signature Tracer (DST) studies (E. Tate-Boldt, C. Saunders)

2010 deployments

In December 2010, short-term movement of DST was tracked over a 7-day period at sites C1 and RS1. At C1, the DST indicated flow was to the east and northeast (**Fig. PF20**). Magnets spaced 1-m E and NE from the deployment location contained over 5-fold more DST than the magnets at 2-m and 3-m in those directions, indicating settling occurred almost immediately after deployment. At RS1, DST flowed to the east and also settled primarily within 1-m of the drop. Photographs taken of the magnets indicated most of the tracer was intercepted in the upper half of the magnet (**Fig. PF20**), suggesting little movement of tracer occurred near the floc surface, where slower velocities have been observed.

Large-scale and long-term synoptic surveys conducted at C1 and RS1 in August 2012 indicated very little movement had occurred since the original drop (**Fig. PF21**). At both sites, tracer detection was primarily limited to the magnets spaced 1-3 m from the drop. At C1, DST was detected at 18 of the 32 sampling locations and in all 8 transects. The highest abundance of

DST was along the eastern and northeastern transects. The northern and western transects had the lowest detections. At site RS1, sampling indicated a north-easterly flow direction also (**Fig. 4-76**). DST was detected at a total of 19 locations with locations in all 8 transects. Both the western and northwestern transects had a single detection. The highest abundance of DST was found in the NE, E and SE transects, the NE transect having the highest abundance.

2013 deployments

Some tracer movement was visually observed at C1 within minutes following deployment on Nov-1 (**Fig. PF22**), despite the fact that the S-152 was still closed. It was observed that the tracer was moving in a southeasterly direction with some movement along the east and south transects. Along the southeast transect it was observed that 4 minutes after the deployment; tracer was halfway to the 3 meter mark. Tracer was also observed to be attaching to the magnets and beginning to form bands. DST was collected from the magnets the week following the S-152 opening. C1 had a high concentration of tracer along the SE transect, with the highest abundance at the 1m point (>1000 particles) and approximately 500 particles at both the 3-m and 6-m points. All of the points sampled at C1 had at least 100 or greater particles except the 3 meter point on the North transect.

The spatial DST deployment at RS1 was located 28.5 m north of the northern-most (RS1u) boardwalk (**Fig. PF22**). There was a high concentration along the south transect. The highest abundance (> 500 particles) of DST was captured at the 1, 3, and 6 meter points along the South transect. The 1-m point on the SW transect also had a high DST abundance (> 450 particles) but not at the 3- m point (36 particles) and 6-m point (55 particles). All of the sampling points on the north, northeast, east, and northwest transects had less than 100 particles. The 1-m point on the west transect had approximately 200 particles while the 3-m point had only 43 particles. The high abundance of particles along the south transect and the relatively low abundance at the remaining points demonstrates the primary direction of flow at RS1 was in the southerly direction. In addition, the number of particles around the 1m points at the southeast and west transects (100 and 200 particles respectively) may be from pre-flow dispersion, and the low abundance at the other points shows that the increased flows kept the tracer from expanding further, as opposed to C1, which had sampling points with 100 or greater particles at all but one sampling point.

For the temporal experiment at RS1, results are shown in **Fig. PF22 (top)**. The DST, entrained in the water flowing from the “drop” site, was sampled at the RS1u and RS1d boardwalks during the initial flow event in order to estimate sediment transport velocities. The S-152 gates were opened at 09:30 on November 5, 2014. There are two boardwalks at RS1 that were constructed parallel to each other and are 29m apart. Half of the RS1 boardwalks lie in the slough and half in the sawgrass ridge. They are aligned longitudinally east and west. DST was sampled at four locations along the boardwalk: slough, near slough, near ridge, and ridge. The

ridge and slough points were 7 m from the slough/ridge interface, and the near slough and near ridge points were 2m from the slough ridge interface. Beginning at 09:10, samples were collected more at the beginning of the flow in order to provide temporal resolution in case flows were flows were faster following the initial opening of the gates at S-152. Using the number of particles collected per sample, the rate particles/second, was calculated for each sample time. The temporal DST particle data was Krieged and plotted using Sigma Plot statistical graphing software. The rate coupled with the distance traveled from the initial drop and the distance between the boardwalks were then used to calculate particle transport rates.

The DST particles were detected first at the upstream boardwalk. The majority of the DST detections for both the upstream and downstream boardwalks were concentrated at the slough and near slough positions. While the near ridge and ridge positions were limited to one or two particle detections. Using the contour plots produced with the Sigma Plot software, it was found that a primary plume of DST was detected at approximately 9:50 and then a secondary plume was detected at approximately 10:48. Downstream at the second boardwalk, the first plume of DST was detected at approximately 10:50 while a weak secondary plum was detected at approximately 12:30.

The temporal aspect of the DST deployment experiment at site RS1 demonstrates that benthic sediment flocculent sized material was entrained in the water flow created by the opening of the S-152 structure, travelled in a south-easterly direction, and was primarily limited to the slough at the RS1 site. DST particle transport rates between the boardwalks were estimated at between 0.64 cm s^{-1} using the first DST plume detected and 0.40 cm s^{-1} using the second DST plume detected; however, the DST particle transport rates calculated between the drop site and the individual boardwalks was 2.39 cm s^{-1} for the transport rate between the drop site and the upstream boardwalk and 0.95 cm s^{-1} for the transport rate between the drop site and the downstream boardwalk. Findings were consistent with temporal variation in ADV-based velocities at RS1, reaching 10.9±2.0 (SE) cm s^{-1} by 11:00 am and declining to 6.7±2.1 by 3:00 pm. Similar temporal variation was observed at Z5-1 and NE-S-152.

2014 deployments

For the DST deployed at RS1 and C1 sites in 2014, the spatial component of the experiment demonstrated that at the high flow site (RS1), DST was entrained and travelled in a southerly direction, moving into the ridge up to 6 meters (**Fig. PF23**). At the low flow site (C1), DST travelled along the ridge-edge and moved into the ridge as far as 3 meters (**Fig.PF24**). At the temporal experiment, no significant DST was found in the slough; however, DST was found at ridge locations but only at the upstream boardwalk RS1u (**Fig. PF25**).

Overall, the experiments demonstrated that DST was entrained under high flows created by the S152 structure. While sediment movement into the ridge does occur, it only moved up to

6 meters into the ridge, although some small amount did travel to the RS1u boardwalk, 20-m downstream. Sediment movement occurs in both the slough and ridge, but it is moderated by flow velocity. Sediment moves preferentially through the slough while movement through the ridge is restricted. The fact that DST was not detected at RS1d indicates that DST travel distance was bounded between 20 and 50 m downstream (into the ridge). This contrasts with the DST deployed in the slough in the 2013 flow, which showed DST travelled to the RS1d boardwalk, 55-m down-slough.

2015/16 deployments

Using a dual signature tracer (DST), we tested the hypothesis that increased sheetflow would entrain and transport sediments in slough habitats, where velocities are highest, and deposit sediments in sawgrass ridges. DST was entrained under high flows created by the S152 structure. DST travelled mainly south at the high flow site (**Figure PF26**). Due to low DST mass captured at the 3 and 6 m from the deployment plot, count data are used to compare particle movement at those distances. The DST count and mass data show more particulate movement in the sloughs, while in the ridge DST did not move beyond 3 m (**Figure PF26**). These findings support the hypothesis that sediment movement is less impeded through sloughs while ridge movement is reduced, due to vegetative resistance and decreased velocities. Examinations of DST deployments just upstream of ridges showed sediment moved at most 10 meters into the ridge from the slough under high flow (data not shown). These results confirm the importance of sheet-flow in redistributing sediment from sloughs to ridges, a critical mechanism for rebuilding topography and patterning of the landscape.

4.4.5 Particle Transport and Flow in an Actively Managed Slough (C. Zweig, E. Tate-Boldt)

Sawgrass encroachment and loss of sloughs is evident throughout WCA-3B, including the DPM study. The active management pilot study was conducted to determine the extent to which velocities could be increased by actively creating sloughs in sawgrass-dominated areas. During the second flow event (November 2014 to January 2015), velocities measured in sawgrass communities, surrounding the created slough, ranged from 1 to 3 cm s^{-1} (**Fig. PF27**). In contrast, velocities in the upstream, middle and downstream portions of the created slough were several-fold higher, averaging 16 cm s^{-1}. This result strongly suggests that active management can be an effective tool to increase localized flows in sloughs, while maintaining lower velocities in sawgrass.

The degree to which these conditions increased transport and net movement of sediment into ridges was quantified by capturing the DST released in the slough interior. DST captured

along slough-to-ridge transects (normal to flow) showed sediment was transported down the entire 100-m extent of the slough. Importantly, the DST was also found to move out of the slough and into the ridge. Capture of DST in the ridge was greatest toward the downstream portion of the slough, where the adjacent sawgrass vegetation was less dense. While sediment movement into the ridge does occur, it was limited to areas near the ridge-slough ecotone. Analysis of benthic sediments collected at locations 10-, 20- and 30-m into the ridge are ongoing, but preliminary evidence suggests DST settles within 10-m of the ecotone (C. Zweig, pers. comm.), as would be expected where lower velocities allow for more particle settling.

4.5. Biogeochemical Processes

4.5.1 Ecosystem metabolism (E. Tate-Boldt, C. Saunders, S. Newman)

Substantial temporal variation and spatial variation (among sites) is observed in water O_2 concentrations (**Fig. BG1**). During the Nov-Dec operational window mean (5-day average) O_2 concentrations ranged from 0.36 to 4.97 mg O_2 L^{-1} in 2010, from 3.10 to 11.08 mg O_2 L^{-1} in 2011, and from 1.09 to 9.10 mg O_2 L^{-1} in 2012. Similar diurnal patterns are observed for both ridge and slough habitats (examples are shown in **Fig. BG2)** and are indicative of alternating dominance of photosynthetic production of O_2 and heterotrophic respiration during light and dark hours, respectively. In a system-wide survey of the Everglades freshwater marshes, Hagerthey et al. (2010) observed that lower mean O_2 values were associated with eutrophic conditions, reflecting the dominance of cattails and substantial detrital material in these habitats. Our spatial survey of soil and floc chemistry indicated areas downstream of levees (including sites RS1, C1, and DB1-3) were relatively more enriched in total phosphorus and predominantly organic, compared to interior pocket sites (**Fig. PC16**), though none of the sites are dominated by cattails. Future tasks will include using analysis of covariance tests to determine the degree to which vegetative biomass, water column and floc chemistry, temperature, irradiance, sediment transport and additional factors underlie the variability in O_2 concentrations observed in pre-flow years. These analyses will complement the BACI statistical tests that evaluate sheetflow and canal backfill treatment effects over the duration of the DPM experiment.

4.5.2 Decomposition

Cotton strip decomposition during and post-flow are shown in **Fig. BG3**. In C1 soil and floc layers decomposition rates in the slough remained the same between flow and post-flow periods, while the ridge samples showed a decrease in decomposition. The water column samples had decreased decomposition rates in both ridge and slough samples. C2 decomposition was reduced in all horizons within the slough from flow to post flow with the greatest decreases occurring

within the soil and water. Cotton strip decomposition rates within the ridge remained relatively stable during this time in all horizons.

In contrast to control sites, the slough at RS1 exhibited increased decomposition rates between flow and post-flow in the soil and floc with a decrease in decomposition in the water column. Decomposition in the ridge decreased in the water column, increased slightly within the floc, and stayed the same at the soil. In general, decomposition at RS2 decreased in both the ridge and the slough. Greater decomposition is an indicator of increased microbial activity which can be influenced by many factors including oxygen, light, temperature, and nutrient availability. While some of these effects are likely due to the introduction of increased water flow and or increased bioavailable nutrients, seasonal differences are also possible contributors. The relative importance of these variables will be investigated in future analyses.

4.5.3 Algal (Periphyton) Responses to Flow

Algal community responses to flow

Accelerated flows at the sites closest to the S152 may have increased local TP loads and in turn changed algal communities in sloughs. Changes in algal taxonomy were evaluated at the eastern transect sites (**Figure iA**) during periods of varying S152 discharges (**Figure BG4**). Across all sites, diatoms dominated, comprising 73% of organisms found, followed by Cyanobacteria, Green algae, Chrysophytes and other (sum of Dinoflagellates, Euglenoids and Cryptophytes). Diatoms had the highest abundance (number per mm^2) of all but one sample and were greatest at the E300 site. With the exception of E500, diatoms peaked in April, during the highest flows, before declining in late May, the only colonization period with no S152 discharges. All sites had less colonization in February (collected March 2), the phenomenon most pronounced at E250 and E300. Overall, these observations suggest reduced flow contributed to lower algal abundance. This supports findings described in the SFER 2016 (Saunders et al., 2016) of high flows associated with higher algal species richness, and additionally higher green algae abundance. Similarly, the greatest abundance of green algae occurred at E250 (**Figure BG5**), peaking during the March (highest S152 discharges) colonization period. At E400 and E500, green algae peaked in the April colonization period.

Seasonal temperature changes likely account for some changes in algal community. For instance, Chrysophytes, which prefer cold water, were most abundant in January (**Figure BG4**).

Green algae generally increased from January through April at all sites except E250, suggesting some temperature effect (**Figure BG5**). Cyanobacteria, a thermophilic community, increased in abundance from January through May. The overall greatest number of cyanobacteria occurred at E400, which peaked during the April colonization period for both E400 and E500. The decrease in late May could reflect a response to reduced flow, which is contrary to the expected change based on season. E250 had fewer cyanobacteria compared to the other sites, and after the January colonization period, was the only site that did not show a seasonal response.

Flow impacts on algal biogeochemistry

We hypothesized that periphyton biomass and productivity would increase in response to higher flow and in turn higher P loading. Periphyton biomass tended to be higher at sites nearest the S152 and during periods of higher water flow, however the monthly variability suggests the influence of other factors such as temperature. Samples from both March and April had higher biomasses at E250 compared to E500 ($p<0.0001$ and $p=0.0082$) (**Figure BG6**). In contrast, while the May 5 and May 25 sampling dates showed significant differences among sites ($p=0.0029$ and $p=0.0338$), neither showed a clear, monotonic relationship with distance from S152. One caveat is that site E400's low biomass in the May 25 sampling date was likely due to shading of dowels and plates by the submerged aquatic plant *Utricularia foliosa*.

Pre-flow productivity measurements on March 2, 2016 had significant differences in gross primary production (GPP) between sites ($p<0.001$); however, sites nearest to the S152 did not always exhibit the highest GPP (**Figure BG7**). On April 6, GPP showed a significant ($p<0.0015$) effect of distance, site E250 being lower than E300 and E500. On May 5, GPP was significantly different among sites ($p<0.0001$), but E250 and E300 had higher GPP than E400 and E500. On May 25, 2016, post-flow, there were no significant differences in GPP among sites ($p=0.2922$).

This study was a first attempt at linking flow effects on both biogeochemical processes and taxonomic shifts in algae. The hypothesis that periphyton biomass and productivity would increase

with flow was supported during some but not all deployments from January through May 2016. Mostly, biomass attenuated with increased distance from S152 (i.e., lower velocities) or was reduced under low- or non-flowing conditions. Higher biomass with higher flow also appears consistent with greater algal species abundance, particularly green algae, under high flow. Temperature or other seasonal variation may also play a role and potentially interact with flow. Productivity results, however, generally showed greater variation, and both positive and negative responses to flow. Though preliminary, the results suggest that even under low water TP conditions, P loading due to high velocities may be important in governing algal community type, biomass and the production and cycling of OM and P.

Large-scale changes in periphyton

The loss of periphyton in sloughs with elevated velocities, such as RS1, had been visually observed during previous flow events. Just prior to flow event 3, high resolution imagery showed that floating metaphyton (white material in **Figure BG8**) covered virtually the entire RS1 slough. Sinking periphyton (tan/orange material) was observed within 4 days after flow began (**Figure BG8**). In the pre-flow condition, open water areas (evident as black lines in the imagery) represent likely alligator or other wildlife trails through the slough. The addition of flow caused these trails to widen or the periphyton in those areas to sink. We hypothesize that such alligator and wildlife trails may provide a path of least resistance through a slough and serve as starting points for larger flow paths. Based on the imagery, over 90% of the periphyton at RS1 had settled or was in the process of sinking with 4 days of flow. Settling of periphyton is consistent with the initial increase in floc height at RS1 (**Figure PF13B).** Moreover, areas of minimal floc across the transect are apparently in line with the initial alligator or wildlife trails. The sinking and eventual near disappearance of both metaphyton and floc (**Figure PF13B**) would reduce vegetative (live and dead) resistance to flow, explaining why velocities and sediment transport tended to increase with flow duration at RS1 (**Figure PF13**).

4.6 Biological (Fauna) Monitoring

4.6.1 Fish and Fauna (J. Trexler, B. Rosen)

Density of Small Fishes

The density of small fish at the sites adjacent to the L-67C canal (CB 1-3) increased by over 2-fold in 2013-2015 (post-canal fill) compared to 2010-2012 (pre-canal fill). The DB sites had the most fish throughout the study and increased by 190% from before to after construction (before:

24.37 fish m^{-2} SE=3.42, after: 70.80 fish m^{-2} SE=7.29), the CB sites had fewer fish, but more than UB and also changed significantly (223% increase; before 14.6 fish m^{-2} SE=2.02, after 47.16 fish m^{-2} SE=4.62), and the UB sites changed the least (136% increase; before: 8.44 fish m^{-2} SE=1.00, after: 19.87 fish m^{-2} SE=1.80). While the density of small fish at control sites north and south of the DPM study area also increased in some months, it was much less than at the sites in the DPM footprint. We also noted heterogeneity in the plots at the CB sites (adjacent to the L-67C canal), but not at the UB or DB sites (**Fig. FA1**). The plots adjacent to the canal fill treatments (CB-3 adjacent to the marsh-level fill and CB-2 adjacent to the partial fill) displayed the greatest increase in the post-fill period, while the site adjacent to the canal-fill control area (CB-1 adjacent to the no-fill area) displayed little increase in months when the DPM culverts were closed and was indistinguishable from the northern and southern controls. Interestingly, CB-1 displayed a similar increase to the other plots in November, when water was being released to the DPM area, but not in other months; the controls did not display this change in November.

Directionality of Small Fishes

Directed movement of small fishes revealed complex patterns of dispersal behavior across the CB experimental and control plots. For example, directed movement in CB Plot 2 was different from CB Plot 3 ($z = 3.27$, $df = 43$, $p < 0.001$) and near-significantly different from CB Plot 1 ($z = 1.80$, $df = 43$, $p = 0.070$), but was not significantly different from the CB control plots ($z = 0.83$, $df = 43$, $p = 0.40$). The small fishes of both the CB control plots ($z = -2.238$, $df = 43$, $p = 0.025$) and CB Plot 3 ($z = 3.33$, $df = 43$, $p< 0.001$) altered their directed movement as a result of changing water depths, though the movement patterns were not the same. Fishes in the CB control plots moved towards the L67-C canal as marsh water depths decreased, but fishes in CB Plot 3 moved away from the canal as water depths fell.

The interaction of water depth change and Site was nearly significant different for small fish directed movement at the UB sites compared to the UB controls ($z = 1.68$, $df = 46$, $p = 0.092$), though both the UB plots and UB control plots did not show significant directed movement as a results of changing water depths.

The most striking result was at the DB sites, where fish movement direction changed after the levee separating the canal was removed. Prior to the levee removal, there was no significant directionality of fish movement in this area, but afterwards, small fish tended to move toward the newly accessible canal when water was dropping and away from it when water was rising. The change was primarily driven by Bluefin Killifish, which displayed a significant interaction in the slope of probability of moving toward the canal and the change in water depth before and after levee removal (**Fig. FA2**). After the levee was removed, there was significant directionality of fish movement adjacent to the L-67C canal, but not at the control sites that were still blocked from the canal by remaining levee.

DRAFT

Small Fish Community Structure

The relative abundance of fishes in throw trap and drift fence samples differed among the three study sites (UB, CB, and DB) before and after levee removal. A permutational ANOVA (PERMANOVA) examining the community structure in throw trap samples from January, 2013 to March, 2015, indicated that the interaction of Site and Period (before and after levee removal) was not significant (Pseudo-F = 0.755, df = 6, p = 0.75). However, community structures were significantly different when examining just Site (Pseudo-F = 15.88, df = 2, p = 0.001). A pairwise test between the CB, UB, and DB sites reveals significant differences between every site combination. The nMDS plot suggests that sites were more heterogeneous before levee removal than after (**Fig. FA3**; greater spread in open symbols than filled symbols). Similarity-of-percentage (SIMPER) analyses revealed that the abundance a few species contributed to these differences, notably Eastern Mosquitofish (*Gambusia holbrooki*), Least Killifish (*Heterandria formosa*), Sailfin Molly (*Poecilia latipinna*), and Bluefin Killifish. These four species contributed 54-64% of dissimilarity between the UB, CB, and DB sites.

An examination of fish community collected in drift-fence samples also revealed a significant interaction between Site and Period (Pseudo-F = 2.14, df = 6, p = 0.001) (**Fig. FA3**). Pairwise comparisons reveal significant or near-significant (p = 0.05 – 0.099) differences between every Site*Period interaction, with the exception of the community structures of the UB and CB sites during March sampling events (t = 1.20, df = 16, p = 0.21).

Large Fish CPUE

Large fish CPUE did not differ among the canal treatments (F = 2.62, df =2, p = 0.11), nor was there an interaction of canal treatment and period (F = 0.37, df = 6, p = 0.88). Restricting analyses to just Florida Largemouth Bass, a similar pattern was revealed, with no significant differences between just the canal treatment effect (F = 1.67, df = 2, p = 0.22) or the interaction of canal treatment and period (F = 0.93, df = 6, p = 0.49) (**Fig. FA4A**).

Because there were no differences in CPUE among the canal fill treatments, we grouped these sites together under the designation “DPM” and compared CPUE of all large fishes and Florida Largemouth Bass between DPM canal transects, canal transects immediately to the north and south of the DPM construction area – “Outside DPM”, and control canal transects several kilometers to the north and south of DPM – “Controls”. While the CPUE of Florida Largemouth Bass was not significantly different across either site (F = 2.25, df = 2, p = 0.11) or the interaction of site and period (F = 0.96, df = 6, p = 0.46), total large fish CPUE was significantly different between sites (F = 56.94, df = 2, p < 0.001) and near-significantly different with the site*period interaction (F = 1.98, df = 6, p = 0.083) (**Fig. FA4B**). A Tukey’s post-hoc analyses reveals significantly higher CPUE of large fishes in DPM transects compared to both Outside

DPM and Control transects. CPUE of the Outside DPM and Control transects were not significantly different.

Large fish community structure also failed to yield differences among canal treatments (Pseudo-F = 1.61, df = 2, p = 0.12) or the treatment*period interaction (Pseudo-F = 0.87, df = 6, p = 0.68). Examining the large fish community structure between the DPM, Outside DPM, and Control sites did reveal significant differences at the site level (Pseudo-F = 7.33, df = 2, p = 0.001), but not with the interaction term between site and period. Pairwise analyses revealed the significance in differences between community structure to be between the DPM sites and the other two sites. SIMPER analyses revealed these differences to be largely driven by the high abundance in the DPM sites of just a few species such Warmouth (*Lepomis gulosus*), Bluegill (*Lepomis macrochirus*), and Lake Chubsucker (*Erimyzon sucetta*).

Large Fish Behavior

We tracked Florida Largemouth Bass and Bowfin continuously from May, 2011, to the present. We calculated the average distance that a fish moved daily and determined that neither species demonstrated a change in daily distance moved before and after DPM construction (**Fig. FA5**). Several fish of both species were documented moving across the degraded levee from the GAP study area and into or out of WCA 3B. Prior to levee degradation, this had not been documented, even with the removed section of levee several kilometers to the north of the DPM footprint.

Flow effects on Food webs

A number of factors differed between the October and November replication of this experiment. In addition to enhanced water flow velocity, temperature (**Figure FA6**), and photoperiod changed seasonally. Measured water flow velocity in the marsh surrounding the cages was not significantly different in October and November (**Figure FA7**). However, the flow enhancers (wings) did increase flow velocity in those cages in November, particularly early in the study before algae grew on the cage walls. Lipid content and nutrient status (stoichiometric ratios) were different in the periphyton mats and epiphytic biofilm in the two months, with greater lipid mass and higher phosphorous in epiphytic biofilms in November than in October (**Figure FA8**). These monthly differences are reflected in the fatty acid profiles of the epiphytic biofilms (**Figure FA9**), which are primarily algal and bacterial. The relative FA sources changed between October and November, from approximately equal in October to heavily algal in November.

Epiphytic algal and periphyton mat species composition was readily distinguished between October and November (dissimilarity 62%), with *Mougeotia* sp. and *Lyngbya* sp, the dominant taxa. *Mougeotia* sp, a green alga, accounted for 21% of the dissimilarity and was 8%

more common in November than October; *Lyngbya* sp., a cyanobacteria, accounted for 10% of the dissimilarity and decreased by 5% in November compared to October. Periphyton mats displayed a similar compositional shift characterized by changes in the same direction by these two dominant taxa.

The lipid abundance increased in all consumers in November compared to October, and the stoichiometric ratios changed to reflect greater phosphorus. The FA composition also changed significantly, with a 20% dissimilarity in Sailfin Mollies and 26% in Eastern Mosquitofish. As noted in the epiphytic biofilms and periphyton, the algal FAs increased in frequency in Eastern Mosquitofish and Sailfin Mollies, while bacterial FAs decreased, though by a lesser percentage (**Figure FA10**). Interestingly, Riverine Grass Shrimp displayed little change in FA source between the two months. Analyses of these data is ongoing.

4.6.2 Summary of Fish and Fauna (J. Trexler)

We have made marked progress in evaluating our three hypotheses of the effects of re-introducing flowing water into Everglades marshes as part of restoration. There is little evidence that the velocity of flows obtained by DPM directly exclude fish. Small fish density increased in the DPM flow period compared to the period before. This is probably because the study area dried in 2011 and fish populations were in a recovery phase in 2012. Large fish CPUE in the L-67C canal littoral zone showed no consistent pattern of change before and after the start of flow treatments and radio-tagged fish displayed no change in movement when water velocities were at their peak. Adults of all of the small fish collected in the study area are able to swim to sustain themselves in currents exceeding those attained in the DPM flow experiments to date. It is possible that larval fish of these species will be adversely affected, but further work must be completed to make conclusions about this.

Research reported here supports Hypothesis 2 in highlighting the importance of changing habitat connectivity by removal of levees and introducing flowing water. Both Largemouth Bass and Bowfin moved into WCA 3B from the L-67C canal and Gap area after the L-67C levee was degraded. Some individuals traveled long distances into WCA 3B when access was provided, returning to the L-67C canal when water levels receded. We also noted that small fish movement in WCA 3B (site DB) changed their movement direction following degrading of the L-67C levee. Prior to levee removal, the net movement of all small fish, and especially Bluefin Killifish, was toward WCA 3B when water levels receded, but after the levee was removed, they moved toward the canal when water level receded.

The elevated increase in small fish density at sites adjacent to the canal fill treatments compared to canal-fill treatment control sites suggests that the canal fill areas affected small fish communities in the adjacent marsh. The observed elevation of fish density at the CB1 plot in

November, post-levee degradation, suggests a possible impact of water flow or levee removal adjacent because this site is adjacent to the canal-fill control (no fill treatment).

Our enclosure experiment is still being analyzed, but some preliminary results related to hypothesis 3 are already clear. First, there was a marked increase in green algae known to respond to nutrient enrichment in the November study period when water flow was elevated. A nutrient effect from elevated P in the periphyton and epiphytic biofilm was also documented in November, and the FA analysis demonstrated a bloom in algal production compared to heterotrophic bacteria. We also demonstrated that this shift cascaded up to consumers that were held in the cages in November. Interestingly, the two fish species demonstrated a shift from a more detrital to a more algal diet in November compared to October, but riverine grass shrimp did not. This illustrates that the feedback modes of individual consumers must be considered in predicting effects of water flow and may mediate which species respond favorably and which do not. We conclude that the 2014 experiment was successful in demonstrating potentially important food web implications from elevating water flow velocity in the Everglades and that more work is needed to fully explore this aspect of effects from DECOMP.

4.7 Environmental Characteristics of Canal Backfill (C. Coronado-Molina)

Canal sediment dynamics – Baseline conditions 2011-2012 plus High-Flow Conditions

To address canal backfill questions, our main objective is to determine the extent to which sediment transport from the marsh interior contributes to sediment accumulation in the canal during both the baseline period and during the operational window period (Nov-Dec). During the baseline period in 2011 and 2012 canal accumulation averaged 3.7, 4.2, 2.7, 2.6, and 4.7 g m^{-1} d^{-1} at the CC1, CB1, CB2, CB3, and CC2sites, respectively (**Fig. CB1**). In contrast, during the operational window (Nov-Dec 2013) canal sediment accumulation increased in all but the CC1 site (2.5, 9.7, 7.3, 7.7, and 11.6 g m^{-1} d^{-1}, respectively, **Fig. CB2**). During and after the operational window (Nov 2013-March 2014), accumulation rate values were very variable but significantly different at most sites, except at the CC1 site where accumulation rate was significantly similar ($p>0.05$). Another important goal was to determine the source of the particulate sediment collected in the canal traps. In this sense, particulate density was a good indicator to determine whether the material contain more organic (low density) or inorganic (high density) material. During the baseline period (April 2011-November 2012), density values were relatively similar and averaged 0.038, 0.036, 0.033, 0.038, and 0.039 g cm^{-3} at the CC1, CB1, CB2, CB3, and CC2 sites, respectively. Similarly, during and after the operational window, density values were significantly ($p<0.05$) higher at the CB2 and CB3 sites ($p<0.05$) (**Fig. CB3**). This temporal pattern observed at CB2 and CB3 can be mostly attributed to the work associated with filling of the canal and to some extent the degradation of the levee during the previous months. Thus, to better answer the canal backfill questions it is necessary to include

more years of data to discern the effect of flowing water (rather than construction effects) on canal sediment dynamics during the operational window.

Sediment trap samples have been analyzed for biomarkers, including Paq, C20 HBI, kaurenes, and botryococcenes. We hypothesize that material that is entrained could be transported to and deposited into the L-67C canal. In this sense, biomarkers are important component of this project because they indicate the source of the material that is transported throughout the ridge-slough and, potentially, deposited in the canal. Results from the biomarker study show that during the high flow event Paq and C20 HBI values were significant lowest relative to pre and post-flow event period (**Fig. CB4**). These low Paq values suggest that most of the material deposited into the sediment traps could be from ridge material. However, the source of this material is not yet clear. Kaurenes and botryococcenes pattern was very variable (**Fig. CB5**).

As shown in **Fig. CB6**, OBS profiles indicate very low turbidity (<1 NTU) over the top 2-m depth at each canal site, the exception occurring immediately after the June 2011 fire. A clear step increase is observed at the bottom-most depths, indicating the top of the benthic floc layer in the canal. Temperature profiles of the L-67C canal from Nov-2010 to Jun-2011 showed little or no evidence for thermal stratification during cold events (**Fig. CB7**).

4.8 Data Synthesis

Synthesis Example 1: Ridge-and-Slough Sediment Budget under Baseline Conditions – Comparison of Methods

Data synthesis is achieved by examining relationships of multiple types of data that address common objectives or hypotheses. DPM data were synthesized by (1) comparing magnitudes and rates measured or inferred from different data sources, (2) comparing the consistency of findings in addressing DPM hypotheses, and (3) building a holistic understanding of sediment dynamics, highlighting important uncertainties. For the ridge and slough, an overview of data synthesis is presented in **Fig. SYN1**, using site RS1 as an example.

While the spatial and temporal scales of SF_6 and ADV measurements are quite different, both consistently showed that water flow in the baseline years is slow (< 0.5 cm s^{-1}), consistent with other Everglades studies (e.g., Harvey et al., 2009; Leonard et al., 2006). The SF_6 tracer deployment at RS1 indicated an overall southeastern flow of 0.11 cm s^{-1} [±0.01, standard deviation (SD)], which was lower but within the range of the mean and error of velocities measured by ADVs in the RS1 slough (0.31 ±0.29, SD) and ridge (0.32 ±0.17, SD) (**Fig. SYN1**, panel b).

Sediment entrainment patterns were different during the two sampling events spanning 2012–2013 (**Fig. SYN1**, panels b, e, f). Preliminary analysis of the CET in October 2012 suggests entrainment occurred around 1.1–1.4 cm s^{-1} and then there was a gradual increase in turbidity values indicating continued entrainment and sediment suspension. In contrast, the CET determined in March 2013 appeared slightly lower, approximately 0.77 to 1.1 cm s^{-1}; however, the subsequent increase in turbidity was relatively rapid. A comparison of these data with additional information, such as total floc mass, chemistry, and biomarkers that identify floc sources, will help us understand the relative differences in floc characteristics and the potential for floc transport.

Sediment transport ranged from 0.4 to 44 grams per square meter per day (g m^{-2} d^{-1}), and in both years of sampling, sediment transport rates were highest in November and decreased nearly monotonically as water levels decreased (**Fig. SYN1**, panel c). These trends were observed when transport was calculated per frontal area (independent of water depth) as well as per ground area (a function of depth). Although the CET of sediments decreased over time (October 2012–March 2013), flow velocities during this period remained below the CET. Water column particulates and sediment transport rates therefore were unlikely to be influenced by sediment resuspension. Sediment transport did not appear to correlate with the amount of floc available (**Fig. SYN1**, panel c, d). That sediment transport mirrored water recession suggested a minor influence of resuspension and a stronger link to processes within the water column such as reduced periphyton and SAV biomass, productivity, and turnover during drydown.

Transport rates measured by sediment traps were expected to underestimate transport, as Phillips et al. (2000) observed 30–71 percent retention efficiency of these traps in estuarine systems. To quantify this potential bias, transport was calculated using site- and habitat-specific water column particulate concentrations and flow velocities. Mid-water column particulate concentrations within the RS1 slough were 0.61 and 0.45 mg L^{-1} in 2011 and 2012, respectively, and in the ridge, 0.49, and 0.02 mg L^{-1} in 2011 and 2012, respectively. A range in transport was calculated by using velocity estimates from both ADV and SF_6 sources (as SF_6 estimates were not habitat-specific, the same velocity was applied to both habitats). Transport calculated in this manner ranged from 18 to 98 g m^{-2} d^{-1} in November 2011 and 0 to 35 in November 2012 (**Fig. SYN1**, panel c). In comparison, trap-based estimates ranged from 21 to 44 g m^{-2} d^{-1} in November 2011 and 17 to 38 in November 2012. Large variation the transport rates estimated by velocity and water column particulates largely reflect differences in mean velocity estimated by SF_6 and the ADVs, and secondarily to differences in water velocity and particulate concentrations between ridge and slough habitats. Given the wide range in the calculated transport rates, we could not detect evidence that the sediment traps underestimate sediment transport.

Taken together, these independent estimates of transport provide an envelope of uncertainty, to which the high flow treatment will be compared. Although the uncertainty

appears substantial, the effect of high experimental flows is expected to be much greater. For example, given sediment stocks of 400 grams dry weight per square meter (DPM-wide average), even if only 1% of sediments were entrained under high flows, water particulate concentrations, and therefore sediment transport, would be expected to increase by at least one to two orders of magnitude.

Comparison of water and sediment velocities, and methodologies, measured under high-sheetflow conditions

In this study, several methods have been employed to estimate water movement, from large, landscape-scale flow of water (e.g., dyes and SF6) to small-scale velocities of water or sediment in specific vegetation types or arrangements. We provide a synthesis of these alternate methods by evaluating the similarities and differences of approaches. Transport velocities of sediments were assessed by two methods, including movements of plumes of the dual-signature tracer (DST) and turbidity generated at the start of flow. In general, transport velocities for sediments were lower than water velocities estimated from ADVs and dye estimates (**Table 4-6**). At sites within 400-m of S-152 (Z5-1, NE-S-152, RS-1), velocities of the initial sediment plume were 5- to 20-fold slower than ADV-based velocities at the same sites. At RS1, DST velocities were 4- to 50-fold lower than ADV-based velocities, and roughly 2- to 10-fold slower than the initial sediment plume. To some degree, these differences among water and sediment velocities may reflect the uncertainties associated with each method. However, given the noted difference in particle sizes between the initial sediment plume (likely very fine material) and DST -floc (matched to the larger, pre-flow sizes), these findings may indicate different velocities among sediment types (e.g., size and chemistry). Sediment velocities tended to be similar to those estimated by the landscape-level water tracer SF6. To some extent SF6 velocities were estimated at locations farther from the S152 than ADVs or dye studies, so the similarity of DST and SF6-based velocities may be similar, but for different reasons (size-related effects versus distance-related effects on velocity).

Under high flows, vegetation pattern clearly impacts the direction and velocity of water flow, explaining some of the exceptionally high velocities measured by ADVs. As shown in Table 4-6, high velocities (8.3 cm s-1) were measured during the November 2013 S152 openning, at a site south of the RS1d boardwalk. At this location the slough narrows to roughly 5-m across.. Similarly high velocities (>10 cm s-1) are observed in the actively created slough, approximately 2-m across and 100-m long (**Figure PF27**).

Benefits of Sustained Flow: Biological Feedbacks on Flow

Findings from the three flow events together suggest that sediment dynamics in the ridge and slough are complex, involving the interplay of biological responses to flow as well as physical impacts. Using findings presented here and previous reports, we present a conceptual model (**Figure SYN2**) to synthesize the sequence by which these feedbacks occur, their ramifications for restoration, and to provide insights about landscape-scale and longer-term responses to flow. The model also highlights new information needed to explain processes which help predict the pace and scale of benefits from sheetflow restoration.

In areas within 500 m of S152 inflows (**top, Figure SYN2**), the most immediate responses to high flow included increased slough velocities of ~3 cm s^{-1}, within hours. In addition, most slough metaphyton community in those areas also broke up and/or sank to the sediment floor, a process which typically occured within days of flow and best exemplified at RS1 (see **section 4.4**). Though the exact mechanism is unknown, we hypothesize periphyton loss reflects increased loading of P with flow, even though water column TP was maintained below 10 ppb. Experimental results have previously shown that increased P loading leads to mat disintegration (Gaiser et al., 2006), though in non-flowing and higher water TP conditions. We have observed metaphyton collapse leading to initial, rapid floc accumulation, but metaphyton does not recover. We hypothesize that floc production is reduced with the loss of metaphyton. Possibly as a result to reduced metaphyton, green algae production increases with sustained flow, confirmed by biomarker and taxonomic analyses of periphyton, advected sediments and benthic floc samples. While our pilot algal study suggested flow may stimulate biomass and productivity, floc measurements suggest this stimulation is insufficient to maintain original pre-flow floc levels. Benthic flume measurements show floc becomes more erodible after sustained flows, likely reflecting a change in OM source influenced to some degree by green algal sources. As green algal-dominated sloughs have been shown to have higher aquatic respiration than ones dominated by cyanobacterial metaphyton (Hagerthey et al., 2010), we hypothesize increased green algal floc sources may increase sediment decomposition (and ultimately accumulation) rates. The combination of reduced floc production, increased floc erodibility, and potentially more labile floc likely contribute, to varying degrees, to reduced floc stocks observed after 8-10 weeks of sustained flow. Finally, since biomass (live + dead) frontal area has been shown to reduce slough velocities, the combined loss of metaphyton, along with floc, after sustained flows provides a positive feedback increasing slough velocities, which typically peaked after 2 months of flow. This positive feedback would then amplify the physical and biological responses described above.

These processes likely have downstream impacts (**Figure SYN2, bottom**), at sites 500–1000 m from S152. In these areas, slough velocities increased, but slightly. Increased sediment transport (presumably with associated P) was not readily detectable, suggesting the increased sediment transported observed closer to the S152 mostly settles within the 500-m boundary. We hypothesize that P loading beyond 500-m was insufficient to disrupt slough metaphyton. At sites

700-m (Z5-3) to 1000-m (C1) from S152, green algal abundance did increase in floc, particularly after the second flow. This lagged response indicates there is some transport of green algae-derived OM and/or algal community changes beyond the 500-m boundary. Should these biogeochemical changes of algae and floc continue in future flow events, then we hypothesize the striking changes observed within 500-m of S152 (i.e., higher velocities and sediment transport, metaphyton collapse, increased green algae, and reduced floc) will eventually happen farther away. Ultimately, the pace by which these sheetflow impacts "spread" across the greater landscape remains a key unknown. Repeated flow events over multiple years will ultimately determine whether such sheetflow benefits are spreading at a snail's pace (e.g., a few meters per decade) or something more substantial for restoration (100-1000's of meters per year). The former would indicate the need for active management approaches.

5. Lessons Learned and Relevance for Water Management

DPM objectives were aimed at providing information regarding critical uncertainties for the decompartmentalization of WCA3:

1. How much water flow is needed to redistribute sediment from sloughs onto ridges? How far downstream from the culverts and levee gaps will the high-flow be maintained? What is the role of vegetation in shaping and attenuating water flow at the landscape scale?
2. How will increased loading of sediment and nutrients affect local biogeochemical processes such as periphyton metabolism and organic matter decomposition? What ecosystem structural and functional measurements are likely to be the key indicators of altered nutrient cycling rates, even if the water entering the system is low in TP?
3. To what extent will canals sequester and reduce the transport of sediment? To what extent will they be a source of high nutrient sediments downstream? Will backfilling or partial backfilling of canals sufficiently reduce negative impacts to water quality and promote greater connectivity of marsh sediment transport?
4. How will flow affect habitat use and seasonal movements of fish? To what extent will canal fish populations be affected by canal backfill treatments?

The baseline (pre-flow) information of the hydrology, water chemistry and sediment budgets in the DPM footprint indicated that in the current state, restoration of the ridge and slough landscape patterning and microtopography is unlikely without increasing sheetflow. Water velocities were not high enough, based on measured critical entrainment velocities (CET), to entrain sediments and thereby redistribute sediments from sloughs onto ridges. In addition, marsh sediment traps indicated rates of transport were equivalent in sloughs and ridges.

DRAFT

Operational strategies to maximize sediment redistribution – the importance of pulse flows, steady state flows and sediment types

While the three flow events were conducted during hydrologically contrasting years (2013 being the wettest), certain findings from these events appear robust. In the first two events, dye and SF6 tracers injected at or near the S-152 spread radially across the pocket, but moved preferentially eastward. High flow velocities (>3 cm s^{-1}) were achieved primarily in sloughs, but limited to areas within 500-m of the S-152. Velocities and shear stress measured at the sediment-water interface in sloughs were at or above the critical thresholds required to resuspend sediments. Greater ridge-slough differences, however, were observed in the wetter flow year. Several independent field measurements (e.g., traps, synthetic tracers, water samples) demonstrated sediment transport increased several-fold above baseline conditions, more so in sloughs than ridges and of greater magnitude (though short in duration) shortly after the culverts were opened. Analysis of floc biomarkers and synthetic floc tracer experiments provided evidence of slough-sediments moving and settling in ridges under high flow, a critical mechanism in rebuilding topography.

The third DPM flow event continued to support previous findings that sustained flow operations of 8-10 weeks, rather than multiple pulses, are needed to maximize slough velocities, sediment transport and sediment redistribution, critical steps for landscape restoration. The pulse study indicated that successive pulse events do not have large-scale or lasting effects. As described in the conceptual model above (**section 4.8**), the advantage of maintaining continuous sheetflow (as opposed to pulses) is that structural changes to sloughs (loss of periphyton) may then lead to changes in the biological and physical properties of floc (i.e., more erodible, possibly more labile sources), which further accelerate flow and sediment redistribution.

The effectiveness of the S152 in restoring large areas still remains a key unknown. At this time, our results suggest three potential trajectories for restoration within the DPM study area: (1) sheetflow generated by the S152 will only restore small areas (500-m radius), therefore active management is needed; (2) sheetflow impacts may eventually "spread" across the landscape, likely involving feedbacks between sheetflow and biogeochemical responses; or (3) some combination of 1 and 2. Whether high velocities can be extended beyond 500-m appears to be linked to biogeochemical responses of slough SAV and periphyton to both water column TP and velocity (P loading).

Understanding the responses of algal communities to low-level P loading may help guide S152 operations by elucidating discharge and inflow TP conditions that maximize ecological benefits. The pilot study initiated in flow event 3 was a first attempt at evaluating the ecological responses to flow and P load under low TP conditions. Going forward, we will prioritize evaluating algal responses to P load, particularly at distances where high velocities and sediment transport currently taper off (~500-m from S152). Across the DPM study area, water TP has remained low, including

at sites close to the inflow (≤10 ppb); however, it is unclear at this time whether subtle changes in TP (by ±2-4 ppb) versus velocity changes drive the fundamental changes in slough algae, as at RS1. Flow impacts on long-term sediment TP dynamics will also be presented in future reporting as increased green algae dominance and P loading to soils could potentially promote cattail growth (Hagerthey et al., 2008), although such changes have not been observed in this study. Taken together, this information may be useful for evaluating sediment and nutrient spiraling in other water management efforts, including monitoring for the Everglades Stormwater Treatment Areas and the Central Everglades Planning Project.

Active Management

Initial findings of a pilot study, started in the second flow event, showed that flow and sediment transport can be increased using an active management approach. In this case, a 100-m long by 2-m wide slough was created by manually removing live and dead aboveground sawgrass biomass (including basal culms). The slough was aligned to the predominant flow direction during high flows. The latter study was motivated by the limited spatial extent of high velocities observed in the first flow event (and confirmed in the second flow event). Velocities in the created slough were raised 5-fold (approximately 15 cm s^{-1}) above those of the surrounding sawgrass-dominated landscape (2-3 cm s^{-1}). The shape, width in particular, of the slough may be an important factor in achieving target velocities for sloughs. On a larger scale, active management may be a useful tool to re-orient flow towards the natural landscape pattern (north-south). Given evidence showing the importance of vegetation in shaping the direction and speed of flows, we anticipate larger-scale active management of sloughs could be used to redirect more flow toward the natural (south) orientation of the landscape, and to increase the areal extent of sheetflow and sediment redistribution (i.e., to kilometers rather than a few hundred meters).

Ecological Responses to Canal Backfilling Treatments and Levee Removal

High flows were associated with large increases in sediment accumulation in the northern-most (open) canal backfill treatmentAdditional sampling of canal sediments (benthic and along canal-marsh edge) is underway, and chemistry and biomarker analyses of these sediments should highlight the source of this material and associated P. This remains a key priority for ongoing sampling leading up to and during the fourth flow event.

Ecological responses in the canal backfill treatments and levee gap

Additional years will be required to evaluate how backfill treatment and construction impact sediments dynamics and sediment chemistry in and downstream of the canal treatments.

While flows around the L-67C gap are quite variable spatially, there is evidence of greater flows on the north end of the L-67C canal area which receives water that flows east and southeast from the S152. In the first flow event, these increased flows correspond with greater sediment accumulation in the northernmost (open) canal treatment. This likely results from sediment entering (or being entrained in) the portion of the L67C canal north of the backfill, followed by the transport of sediment southwest to the open canal treatment. Velocimeters in the canal backfill treatments indicated canal velocities roughly doubled under high flow, reaching 7-8 cm s^{-1}. Therefore, sediment dynamics may be strongly influenced by velocity changes within the canal. In order to determine the extent to which changes in canal sediment accumulation reflect sediments mobilized within the canal, along the canal-marsh edge or from more interior marsh sites, sampling in the third and fourth flow years has been expanded to include canal benthic sediments and edge sediments for biomarker and nutrient analysis and additional velocity and water quality monitoring in and around the backfill treatments. Given the high TP of canal sediments, this process could potentially alter P cycling in the canal. Biomarker analysis of sediments accumulating in canals showed widespread sediment source changes with flow, even at control sites.

Results from fish sampling suggest there has been no loss of fishing habitat with the partial or complete fills. The partial fill and complete fill areas have created a new deeper water habitat that supports a similar community to the one currently only found on the canal edge. This finding may be important as canal-edge habitats support much higher fish densities than marsh habitats.

DRAFT

6. Literature Cited

Belicka, L. L., E. R. Sokol, J. M. Hoch, R. Jaffé, and J. C. Trexler. 2012. A molecular and stable isotopic approach to investigate the importance of algal and detrital energy pathways in a freshwater marsh. Wetlands 32:531-542.

Bernhardt, C.E., D. A. Willard. 2009. Response of the Everglades ridge and slough landscape to climate variability and 20th-century water management. *Ecological Applications* 19:1723-1738.

Black, K. S. and D. M. Paterson. 1997. Measurement of the erosion potential of cohesive marine sediments: A review of current *in situ* technology. *J. Marine Environmental Engineering* 4:43-83.

Budge, S. M., S. J. Iverson, and H. N. Koopman. 2006. Studying trophic ecology in marine ecosystems using fatty acids: a primer on analysis and interpretation. Marine Mammal Science 22:759–801.

Chick, J. H., S. Coyne, and J. C. Trexler. 1999. Effectiveness of airboat electrofishing for sampling fishes in shallow vegetated habitats. North American Journal of Fisheries Management 19:957-967.

Chick, J. H., C. R. Ruetz III, and J. C. Trexler. 2004. Spatial scale and abundance patterns of large fish communities in freshwater marshes of the Florida Everglades. *Wetlands* 24:652-664

Chick, J. H., P. Geddes, and J. C. Trexler. 2008. Periphyton mat structure mediates trophic interactions in a subtropical wetland. Wetlands 28:378–389.

Choi, J., C. Coronado-Molina, J. Harvey, D. T. Ho, L. Larsen, S. Newman, C.J. Saunders, K. Skalak, F. H. Sklar, E. Tate-Boldt, J. Trexler. 2013. The Decomp Physical Model (DPM), Year 3 Annual Report: Pre-Flow Baseline Monitoring of the Water Conservation Area (WCA) 3 Decompartmentalization and Sheet Flow Enhancement Project, US Geological Survey.

Collins, D.L., 1977, Computation of records at control structures: U.S. Geological Survey Water-Resouces Investigations Report 77-8, 57 p.

Dorn, N. J., J. C. Trexler, and E. E. Gaiser. 2006. Exploring the role of large predators in marsh food webs: evidence for a behaviorally-mediated trophic cascade. Hydrobiologia 569:375-386

Eaton A.D., Clesceri L.S., A.E. Greenberg eds (1995). Standard methods for the examination of water and waste water; American Public Health Association (APHA), Washington, USA

Elçi, S., R. Aydin and P. A. Work. 2009. Estimation of suspended sediment concentration in rivers using acoustic methods. *Environmental Monitoring and Assessment*. 159:255–265.

DRAFT

Field, M. S., R. G. Wilhelm, J. F. Quinlan, and T .J. Aley. 1995. An assessment of the potential adverse properties of fluorescent tracer dyes used for groundwater tracing. *Environmental Monitoring and Assessment* 38:75-96.

Gaiser, E. E., P. Sullivan, F. A. C. Tobias, A. J. Bramburger, and J. C. Trexler. 2013. Boundary effects on benthic microbial phosphorus concentrations and diatom beta diversity in a hydrologically-modified, nutrient-limited wetland. *Wetlands* doi: 10.1007/s13157-013-0375-3

Gao, M. 2007. Chemical Characterization of Soil Organic Matter in an Oligotrophic, Subtropical, Freshwater Wetland System: Sources, Diagenesis, and Preservation, Ph.D. Thesis, Florida International University, Miami, FL, p. 255 pp.

Gao, M., B. R. T. Simoneit, M. Gantar, and R. Jaffe. 2007. Occurrence and distribution of novel botryococcene hydrocarbons in freshwater wetlands of the Florida Everglades. *Chemosphere* 70:224-236.

Geddes, P., and J. C. Trexler. 2003. Uncoupling of omnivore-mediated positive and negative effects on periphyton mats. Oecologia 136:585-595.

Goring, D. G., and V. I. Nikora. 2002. Despiking acoustic Doppler velocimeter data. *J. Hydraul.Eng.*, 128(1):117–126.

Green, D. P. J., J. C. Trexler, J. J. Lorenz, C. C. McIvor, and T. Philippi. 2006. Spatial Patterns of Fish Communities Along Two Estuarine Gradients in Southern Florida. *Hydrobiologia* 569:387-399.

Hagerthey, S. E., J. J. Cole, and D. Kilbane. 2010. Aquatic metabolism in the Everglades: The dominance of net heterotrophy. *Limnol. Oceanogr.* 55:653–666.

Harvey, J. W., G. B. Noe, L. G. Larsen, D. J. Nowacki, and L. M. McPhillips. 2011. Field flume reveals aquatic vegetation's role in sediment and particulate phosphorus transport in a shallow aquatic ecosystem. *Geomorphology.* 126:297–313,doi:10.1016/j.geomorph.2010.03.028.

Harvey, J. W., R. W. Schaffranek, G. B. Noe, L. G. Larsen, D. J. Nowacki, and B. L. O'Connor. 2009. Hydroecological factors governing surface-water flow on a low gradient floodplain. *Water Resources Research*, Vol. 45, W03421, doi:10.1029/2008WR007129.

Hedley, M. J. and J. W. B. Stewart. 1982. Method to measure microbial phosphate in soils. *Soil Biol. Biochem.* 14:377-385.

Hijuelos, A. C. 2012. Spatial and temporal patterns in the distribution, behavior, and activity of fishes in canals of the Everglades. M. S. Thesis, Florida International University, Miami. 47pp.

DRAFT

Hill, M. O., P. M. Latter, and G. Bancroft. 1985. A standard curve for inter-site comparison of cellulose degradation using the cotton strip method. *Canadian Journal of Soil Science*, 65(4):609-619, doi:10.4141/cjss85-067

Ho, D.T., P. Schlosser, and T. Caplow. 2002. Determination of longitudinal dispersion coefficient and net advection in the tidal Hudson River with a large-scale, high resolution SF_6 tracer release experiment, *Environ. Sci. Technol.*, *36*(15):3234 - 3241, doi:10.1021/es015814+.

Ho, D.T., V. C. Engel, E. A. Variano, P. J. Schmieder, and M. E. Condon. 2009. Tracer studies of sheet flow in the Florida Everglades, *Geophys. Res. Lett.*, *36*(9), L09401, 10.1029/2009GL037355.

Hoffman, W., G. T. Bancroft, and R. J. Sawicki. 1994. Foraging habitat of wading birds in the Water Conservation Areas of the Everglades. Pages 585-614 *in* S. M. Davis and J. C. Ogden, editors. *Everglades: The Ecosystem and its Restoration*. St. Lucie Press, Delray Beach

Hubbard, E. F., F. A. Kilpatrick, L. A. Martens, and J. F. Wilson, Jr. 1982. Measurement of time of travel and dispersion in streams by dye tracing, Techniques of Water-Resource Investigations, Book 3, Applications of Hydraulics, Chapter A9, USGS.

Jordan, C. F., S. Coyne, and J. C. Trexler. 1997. Sampling fishes in heavily vegetated habitats: the effects of habitat structure on sampling characteristics of the 1-m2 throw trap. Transactions of the American Fisheries Society 126:1012-1020.

Kerfoot, W,C., J. W. Budd, B. J. Eadie, H. A. Vanderploeg, and M. Agy. 2004. Winter storms: Sequential sediment traps record *Daphnia* ephippial product, resuspension, and sediment interactions. *Limnol. Oceanogr.* 49:1365-1381.

Kenney, T. A., 2010. Levels at gaging stations: U.S. Geological Survey Techniques and Methods 3-A19, 60 p.

Larsen, L. G., J. W. Harvey, et al. 2009a. Morphologic and transport properties of natural organic floc. *Water Resources Research* 45. W01410. doi:10.1029/2008WR006990.

Larsen, L. G., J. W. Harvey, and J. P. Crimaldi. 2009b. Predicting bed shear stress and its role in sediment dynamics and restoration potential of the Everglades and other vegetated flow systems. *Ecological Engineering* 35:1773-1785.

Larsen, L. G. and J. W. Harvey, 2010. How vegetation and sediment transport feedbacks drive landscape change in the Everglades and wetlands worldwide. *The American Naturalist* 176 (3), p. E66-E79. doi: 10.1086/655215..

Larsen, L., N. Aumen, C. Bernhardt, V. Engel, T. Givnish, S. Hagerthey, J. Harvey, L. Leonard, P. McCormick, C. McVoy, G. Noe, M. Nungesser, K. Rutchey, F. Sklar, T. Troxler, J. Volin, and D. Willard. 2011. Recent and Historic Drivers of Landscape Change in the Everglades

DRAFT

Ridge, Slough, and Tree Island Mosaic. *Critical Reviews in Environmental Science and Technology* 41:344-381.

Leonard, L., A. Croft, D. Childers, S. Mitchell-Bruker, H. Solo-Gabriele, M. Ross. 2006. Characteristics of Surface-Water Flows in the Ridge and Slough Landscape of Everglades National Park: Implications for Particulate Transport. *Hydrobiologia* 569:5-22.

Levesque, V.A., K. A. and Oberg. 2012. Computing discharge using the index velocity method: U.S. Geological Survey Techniques and Methods 3–A23, 148 p. http://pubs.usgs.gov/tm/3a23//

Lightbody, A. F., and H. M. Nepf. 2006. Prediction of velocity profiles and longitudinal dispersion in emergent salt marsh vegetation. *Limnol. Oceanogr.* 51(1): 218-228.

McVoy, C. W., W. Park Said, J. Obeysekera, J. A. VanArman and T. W. Dreschel. 2011. *Landscapes and Hydrology of the Predrainage Everglades*. University Press of Florida, Gainesville, FL. 342 pp. + 297 pp. on DVD

Mead, R., Y. P. Xu, J. Chong, R. Jaffe. 2005. Sediment and Soil Organic Matter Source Assessment as Revealed by the Molecular Distribution and Carbon Isotopic Composition of N-Alkanes. *Organic Geochemistry* 36:363-370.

Merkel, Robert S. and R. Hickey-Vargas. 2000. Element and sediment accumulation rates in the Florida Everglades. *Water, Air, and Soil Pollution*. 122:327-349.

Mulcahy, D.M. 2003. Surgical implantation of transmitters into fish. ILAR Journal 44:295 306.

Neto, R. R., R. N. Mead, J. W. Louda, R. Jaffe. 2006. Organic Biogeochemistry of Detrital Flocculent Material (Floc) in a Subtropical, Coastal Wetland. *Biogeochemistry* 77:283-304.

Newman, S., H. Kumpf, J. A. Laing, J.A., W. C. Kennedy. 2001. Decomposition Responses to Phosphorus Enrichment in an Everglades (USA) Slough. *Biogeochemistry* 54:229-250.

Newman, S., P. V. McCormick, and J. G. Backus. 2003. Phosphatase activity as an early warning indicator of wetland eutrophication: Problems and prospects. *J. of Applied Phycology*, 15:45–59.

Noe, G.B., D.L. Childers, A.L. Edwards, E. Gaiser, K. Jayachandran, D. Lee, J. Meeder, J. Richards, L.J. Scinto, J.C. Trexler and R.D. Jones, 2002. Short-term changes in phosphorus storage in an oligotrophic Everglades wetland ecosystem receiving experimental nutrient enrichment. Biogeochem., 59:239-267.

Noe, G. B., J. W. Harvey, and J. E. Saiers. 2007. Characterization of suspended particles in Everglades wetlands. *Limnol. Oceanogr.* 52:1166-1178.

DRAFT

Noe, G. B., J. W. Harvey, R. W. Schaffranek, L. G. Larsen. 2010. Controls of Suspended Sediment Concentration, Nutrient Content, and Transport in a Subtropical Wetland. *Wetlands* 30: 39-54.

Obaza, A., D. L. DeAngelis, J. C. Trexler. 2011. Using data from an encounter sampler to model fish dispersal. Journal of Fish Biology. 78(2):495-513.

Parkos, J. J., C. R. Ruetz III, and J. C. Trexler. 2011. Disturbance regime and limits on benefits of refuge use for fishes in a fluctuating hydroscape. *Oikos* 120:1519-1530.

Parkos, J. J., III, L. F. Wolski, W. F. Loftus, and J. C. Trexler. 2015. Dynamic movement patterns of Florida gar within a fluctuating hydroscape. Copeia 103:132–140.

Partrac. 2005. Measurement of floc transport in the Everglades, Florida. Report to SFWMD. 46p.

Partrac. 2006. Measurement of floc transport in the Everglades, Florida. Report to SFWMD. 55p.
21
Partrac. 2008. Quantifying floc transport in vegetated and non-vegetated habitats in the Florida Everglades. Report to SFWMD. 88p.

Phillips, J. M., M. A. Russell, and D. E. Walling. 2000. Time-integrated sampling of fluvial suspended sediment: a simple method for small catchments. *Hydrological Processes* 14:2589-2602.

Pisani, O., J. W. Louda, R. Jaffé. 2013. Biomarker assessment of spatial and temporal changes in the composition of flocculent material (floc) in the subtropical wetland of the Florida Coastal Everglades. *Environmental Chemistry* 10:424-436.

Riscassi, A. L., and R. W. Schaffranek. 2002. Flow velocity, water temperature, and conductivity in Shark River Slough, Everglades National Park, Florida, July 1999-August 2001: US Geological Survey Open-File Report 02-159, 32 p.

Ross, M. S., S. Mitchell-Bruker, J. P. Sah, S. Stothoff, P. L. Ruiz, D. L. Reed, K. Jayachandra, and C. L. Coultas. 2006. Interaction of hydrology nutrient limitation in the Ridge and Slough landscape of the southern Everglades. *Hydrobiologia* 569:37–59.

Saunders, C. J., M. Gao, J. A. Lynch, R. Jaffe, D. L. Childers. 2006. Using Soil Profiles of Seeds and Molecular Markers as Proxies for Sawgrass and Wet Prairie Slough Vegetation in Shark Slough, Everglades National Park. *Hydrobiologia* 569:475-492.

SFWMD. 2015c, SFWMD-EVER-SOP-DPM-Periphyton Primary Production-01Standard Operating Procedure for Measuring Periphyton Primary Production. SFWMD. West Palm Beach, FL.

SFWMD. West Palm Beach, FL. Sklar, F., S. Hagerthey, V. Engel, J. Harvey, L. Larson, K. Legault, S. Newman, G. Noe, J. Redwine, C. Saunders, J. Trexler. 2010. DECOMP Physical

DRAFT

Model Science Plan, http://www.evergladesplan.org/pm/projects/project_docs/pdp_12_decomp/060410_decomp_ea_final/april_2010_decomp_ea_app_e_bk.pdf.

Sklar, F. H. and T. Dreschel, 2015. Chapter 6 of the 2014 South Florida Environmental Report.

SonTek. 2001. SonTek ADV Acoustic Doppler Velocimeter Technical Documentation, 202 pp., San Diego, Calif.

Turner, A., and J. C. Trexler. 1997. Sampling invertebrates from the Florida Everglades: a comparison of alternative methods. *J. North American Benthological Society* 16:694-709

Variano, E.A., D. T. Ho, V. C. Engel, P. J. Schmieder, and M. C. Reid. 2009. Flow and mixing dynamics in a patterned wetland: Kilometer-scale tracer releases in the Everglades, *Water Resour. Res.*, *45*, doi: 10.1029/2008wr007216.

Venne, L. S. 2012. Wading Bird (Ciconiiformes) Response to Fire and the Effects of Fire in the Everglades. PhD. Dissertation, University of Florida, Gainesville. 154pp.

Wahl, T. L. 2003. Discussion of 'Despiking acoustic doppler velocimeter data'. *J. Hydraul. Eng.*, 129(6):484–488.

Watts, D. L., M. J. Cohen, J. B. Heffernan, and T. Z. Osborne. 2011. Hydrologic Modification and the Loss of Self-organized Patterning in the Ridge-Slough Mosaic of the Everglades. *Ecosystems* 13:813-827.

Winter, J. 1996. Advances in underwater telemetry, pp 555-590. *In* B. R. Murphy and D. W. Willis. *Fisheries Techniques*, 2nd Ed. American Fisheries Society, Bethesda, MD

Xu, Y. P., R. N. Mead, R. Jaffe. 2006. A Molecular Marker-Based Assessment of Sedimentary Organic Matter Sources and Distributions in Florida Bay. *Hydrobiologia* 569:179-192.

DRAFT

APPENDIX A – DPM Workshop, April 2015

DPM Workshop – Key Findings and Remaining Uncertainties

April 24, 2015

Attendees:
Allison Swartz, Barry Rosen, Brendan Buskirk, Carlos Coronado-Molina, Chris Hansen, Colin Saunders, Christa Zweig, David Ho, Erik Tate-Boldt, Fred Sklar, Jay Choi, Jesus Gomez-Velez, Jud Harvey, Joel Trexler, Laurel Larsen, Mark Dickman, Megan Jacoby, Peter Regier, Rudolf Jaffé, Sue Newman

Workshop objectives:

1. To discuss and summarize the most important findings from DPM flows 1 and 2
2. To list the remaining uncertainties or new uncertainties that would guide a next phase of DPM

PART 1. Important findings to date

We went around the room asking each person: What are the most important findings based on the baseline and first 2 flow events in DPM? Findings ranged substantially in type. Mostly they related to how well we are addressing the original DPM hypotheses. Other findings related to results that were unexpected, results that have important implications for how to restore sheetflow at the larger (CEPP) scale, or results that suggest additional data analyses or data-mining are needed. This list could potentially lead to sampling changes in the third flow event and/or indicate an uncertainty that would have to be addressed with additional field testing, after the third flow event.

Below are the bullet statements written on the flip charts, including who we think made each comment, but request corrections if we have transcribed it wrong.

Authors/Initials; AS = Allison Schwartz; CC = Carlos Coronado-Molina; CH = Chris Hansen; CS = Colin Saunders; CZ = Christa Zweig; DH = David Ho; ETB = Erik Tate-Boldt; FS = Fred Sklar; JC = Jay Choi; JG = Jesus Gomez; JH = Jud Harvey; JT = Joel Trexler; LL = Laurel Larsen; MD = Mark Dickman; SN = Sue Newman

1. (JC) increased flow increased suspended sediment and sediment movement, but S152 had a smaller spatial footprint than expected
2. (JT) For consumers, landscape (i.e., canal & levee gap & connectivity) effects were more important than flow. Those landscape effects had large impacts on fish populations and community structure.
3. (JT) Fish community structure converges with the levee gap (DB = CB = UB)

4. (JT) A biogeochemical effect, mainly from P loading, is expected to be important for fish, but findings still in-progress.
5. (JH) Flow generated a spike then relaxation of water column fine sediments
6. (MD) S152 flows were low, due to tailwater buildup. Local S152 scouring may have occurred (indicated by Lars' data). Remnant sloughs near the structure controlled flow.
7. (JG, JH) Discussion as to what extent shallow water aquifer connection may or may not have been changed by flow.
8. (SN) Water TP changes with S152 opening and closing events and initial pulses
9. (LL, CS, SN) Flow impacts changed over a weekly to monthly time-scale. These included increased velocity and sediment transport toward the middle and later stages of the high flow events. Potential ecosystem feedbacks may have caused this. Such feedbacks include the loss of slough metaphyton, development of preferential flowpaths within sloughs, and decreases in the CET of benthic floc.
10. (LL) Enrichment gradients existed pre-flow and were possibly altered or extended with flow
11. (RJ, CC) There is a preferential movement of slough-derived organic matter in canals, but this changes with flow, which indicates either more ridge-derived OM or an un-measured source near or within the canals themselves. Since canal velocities increased with flow, sediment source from edges or benthic areas in canal are plausible and require additional sampling.
12. (JT) Fill improves fish habitat. Extent to which it improves fishing habitat depends on vegetation regrowth and accessibility
13. (CC) Revegetation in canal fill areas is fast, extensive in some areas, but varies spatially.
14. (JT, CC) Backfill topography varies substantially, generating sediment accumulation "hotspots" and altering local velocities
15. (LL, CS) Landscape pattern analysis is needed to understand how underlying spatial variability in ridge and slough patterns controls local-scale water flows, sediment movement and biogeochemical processes.
16. (DH) Low lateral dispersion during high flows and over long distances – this was unexpected. Having data on the landscape flow fields is critical information gap for understanding dispersions results from SF6.
17. (LL) Differences were observed between 2013 and 2014 in flow and shear stress. In 2013, bed shear stress was high, and ridge-slough differences were greater. In 2014, these effects were muted at the RS1 boardwalk sites.
18. (ETB) In 2013, on the west side of RS1 slough, the bed developed "floc mounds" and "periphyton snow drifts". In 2014, the bed appeared more scoured, fewer "snow drifts". These may be interrannual or cumulative effects of flow that require several years of study to fully understand.
19. (AS) At RS1u, the floc height increased at first (within the first day or so), then varied a lot.

DRAFT

20. (CZ) At the actively managed "Zweig" slough, the ridge velocity varied not as a function of ridge density and not as a function of distance to the slough.
21. (CH) Macro-invertebrates increased with flow at RS1, based on occurrences in the horizontal sediment traps.
22. (JT) Canal sonar data could be utilized to evaluate temporal changes in sediment concentration, sediment flow and SAV abundance.

PART 2. What's the next step? Brainstorming field tests beyond flow event #3

We went around the room asking each person: Do your results suggest changes to our original design and/or hypotheses? Given results so far, what additional field tests and monitoring would be needed to resolve the major uncertainties?

Below are the bullet statement that were written on the flip charts, including who we think made each comment. Bullet statements and hypotheses have not been edited and should be considered in draft form at this time.

1. Possible impacts of high velocity on small fish recruitment (Joel Trexler).
2. Community Linkages: Hg and Sulfur linkage to flow -> to algae -> to fish (Joel Trexler).
3. Pulsing may be needed by CEPP, but what are the biogeochemical implications and how is it related to sediment sources and sinks? (Saunders, Newman, Larsen, Harvey)
4. Modifications to the S-152: a) Impacts of "mounding" of sediments downstream of S-152? (Mark Dickman) and b) create a mixing model for L-67A to expand operational window (Saunders).
5. Ecological role/function of preferential flow paths (David Ho).
6. Impacts of flow on groundwater – surface water interactions and the effects of this interaction on water quality (porewater and SW), floc and hydrology (Sue Newman and ?).
7. Long-terms impacts of flow on TP loadings, changes in entrainment and vegetation structure and function (Sue Newman, Christa Zweig and Laurel Larsen).
8. Temporal cascade of biological impacts due to operating the S-152 just during the winter (Joel Trexler?).
9. Expand the S-152 operational window: Test implications of the Q-bell (Fred Sklar)
10. Expand canal studies and evaluate sediment sources and sinks, TP and fish communities by: a) changing canal backfill and levee options and b) developing more canals measures of ecological function, sediment characteristics and WQ (Jaffe, Trexler, Saunders and Newman).
11. Pattern Analysis and Resilience: Evaluating the short and long-term impacts of historical flow velocities, but non-historical flow direction (?).
12. Drop S-1 and add new stations along the levee and canal (Sue Newman).
13. More Active Management: a) reconnect sloughs, b) create more open habitats (AMI example), and c) modification/expansion of RS-1 slough (Christa Zweig, Sue Newman).

DRAFT

14. Impacts of flow on accretion rates: Add marker horizons (Saunders and Coronado).
15. High resolution imaging: a) side scanning of canal-marsh interface (Trexler) and b) aerial scanning of slough-marsh interface (Zweig).
16. Biomass – Velocity Relationship (?).
17. Incremental adaptive management for WCA-3B: a) tree island restoration (Coronado); b) food-web restoration (Trexler), c) Active Marsh Improvement (AMI) in WCA-3B (Newman), d) climate change (add a met station – David Ho?), e) develop a water budget (Jay Choi and Jud Harvey).

Parameters to monitor during "baseline period"

1. Water level and structure flow
2. Algae composition & TP
3. Hydrolabs (DO, conductivity, pH, temperature, turbidity)
4. MET station
5. Porewater and surface water nutrients
6. Feldspar deployment (accretion)
7. Flow/depths
8. Floc & sediment
9. Canal sediment traps
10. Canal sediment stocks
11. Fish community structure

DRAFT

Figures - Study area and sampling design (iA-E)

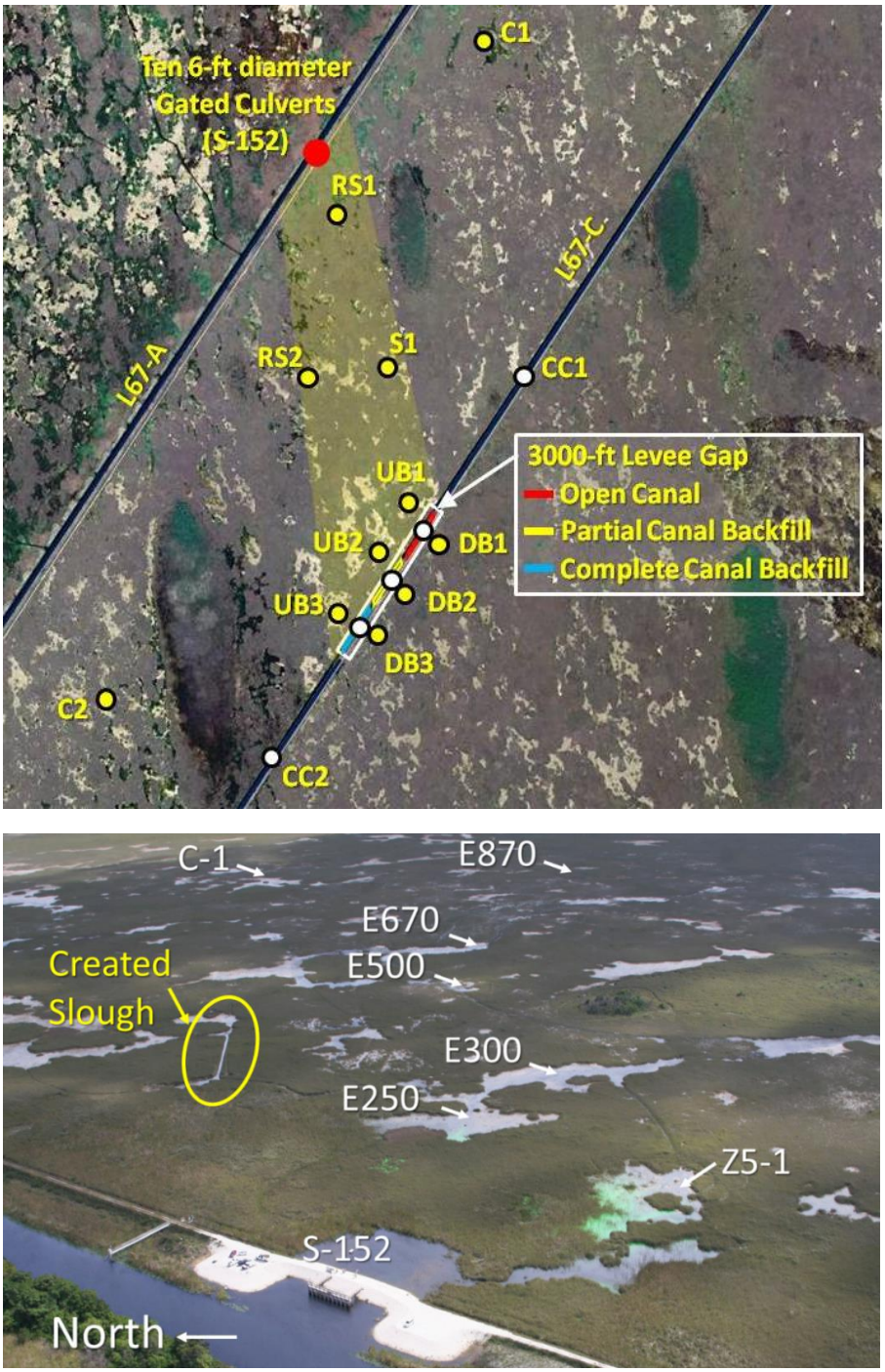

Figure i-A. (Top) Map of the DECOMP Physical Model (DPM) experimental site, located in "the pocket" between the L67A and L67C canal/levee structures. Hydrologic and biological response variables are measured at 11 marsh sites and 5 canal sites using a Before-After-Control-Impact (BACI) experimental design. (Bottom) Location of east transect sites (E250, 300, 500, 670 and 870) added in 2014 to examine hydrological and ecological parameters along the preferential, eastward flowpath and location of a 3-m x 100-m created slough (circled, yellow) used to assess the benefits of active management in restoring flow and sediment redistribution.

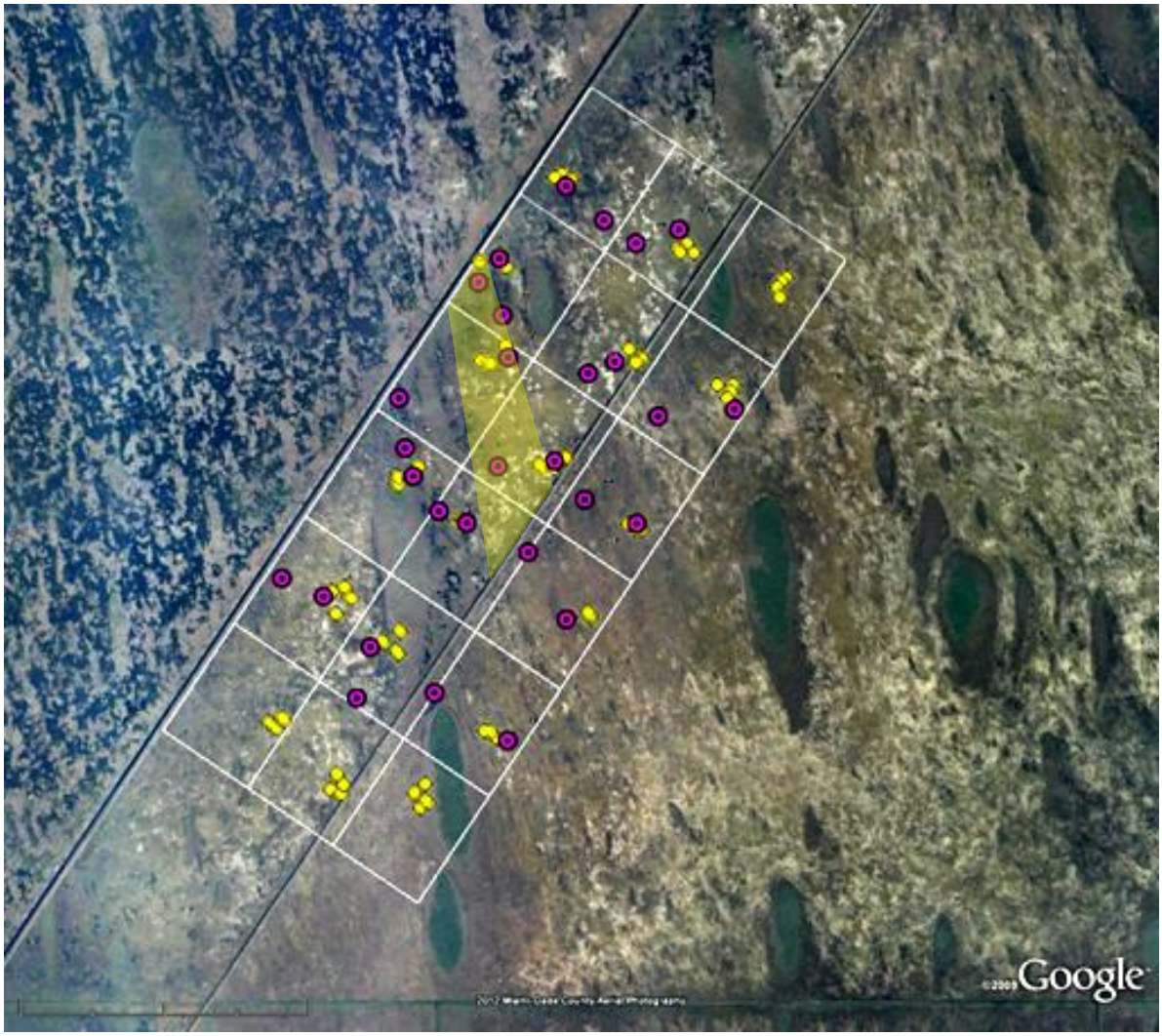

Figure i-B. A spatial sampling design was generated by Dr. Michael Ross and colleagues as part of the RECOVER-MAP in order to quantify and understand landscape gradients in floc and soil chemistry. Yellow symbols represent the 216 subplots used to survey standing vegetation in each of 18 zones. The pink symbols represent the subplots used to sample floc and soil (in 14 of the 18 zones). Shaded polygon indicates flowpath highlighted in Figure i-A.

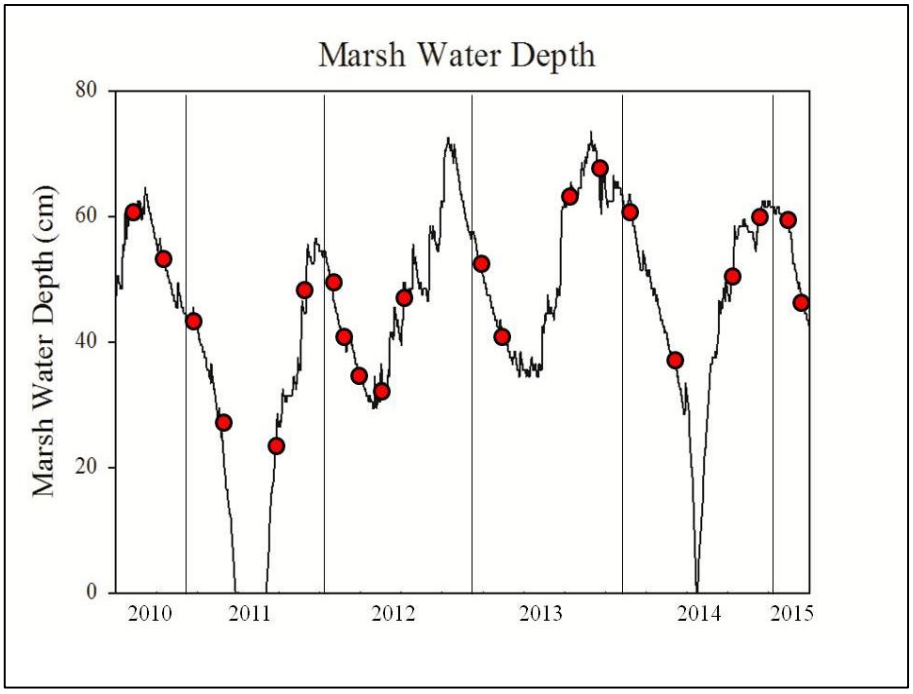

Figure i-C. Marsh water depth versus time for this study. Red dots indicate approximate dates when small and large fish were sampled.

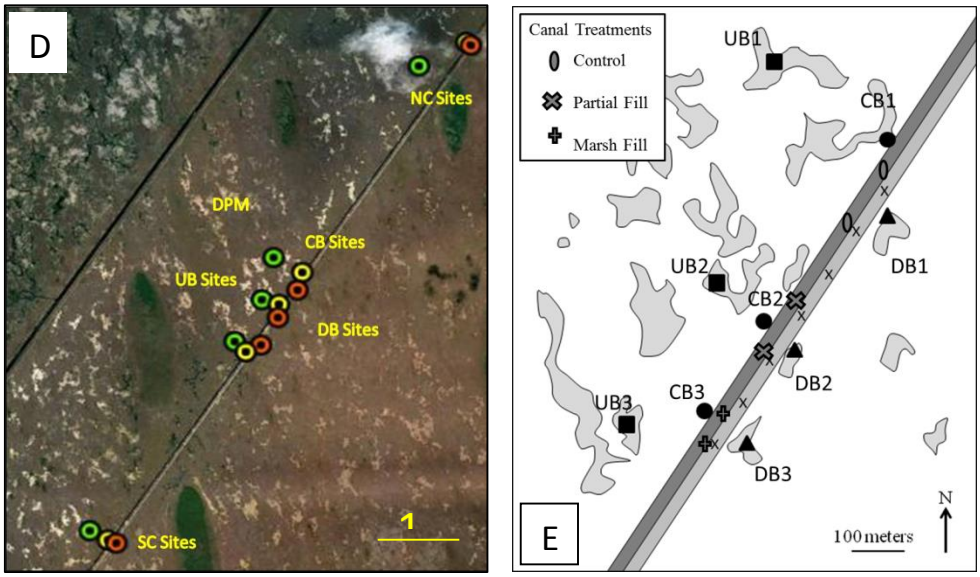

Figure i-D & E. Locations of the throw trap and drift fence sampling locations. Electroshocking transects take place in approximately the same areas. Map on the left shows DPM and control sites; map on the right illustrates the position of DPM sites with respect to canal fill treatments.

This page deliberately left blank.

Figures – Hydrology (H1-20)

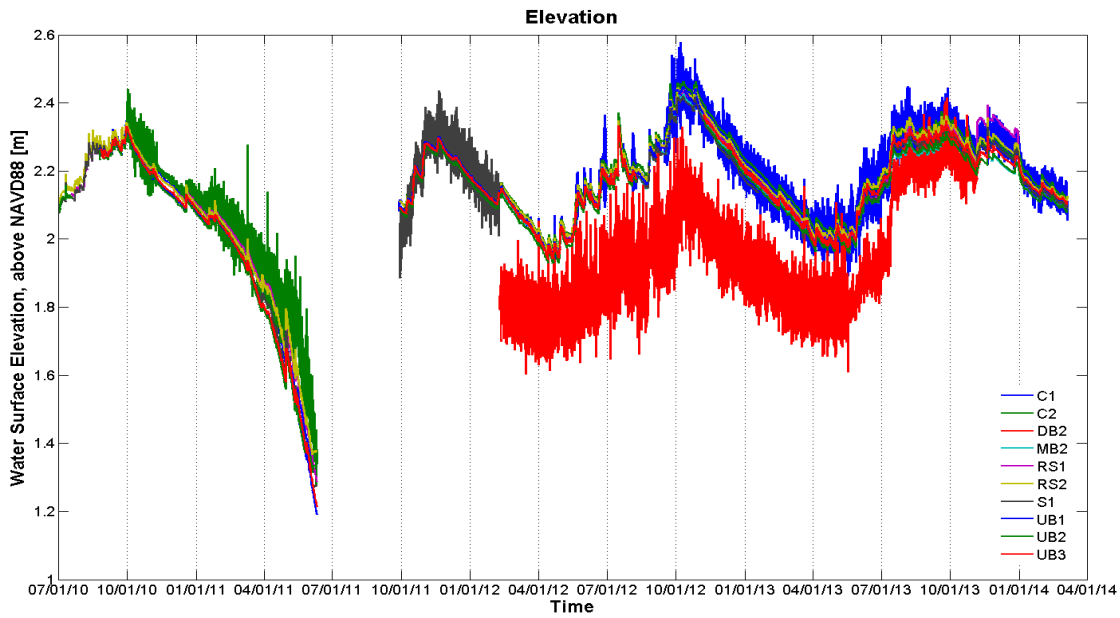

Figure H1. Water level elevations for all sites in DPM.

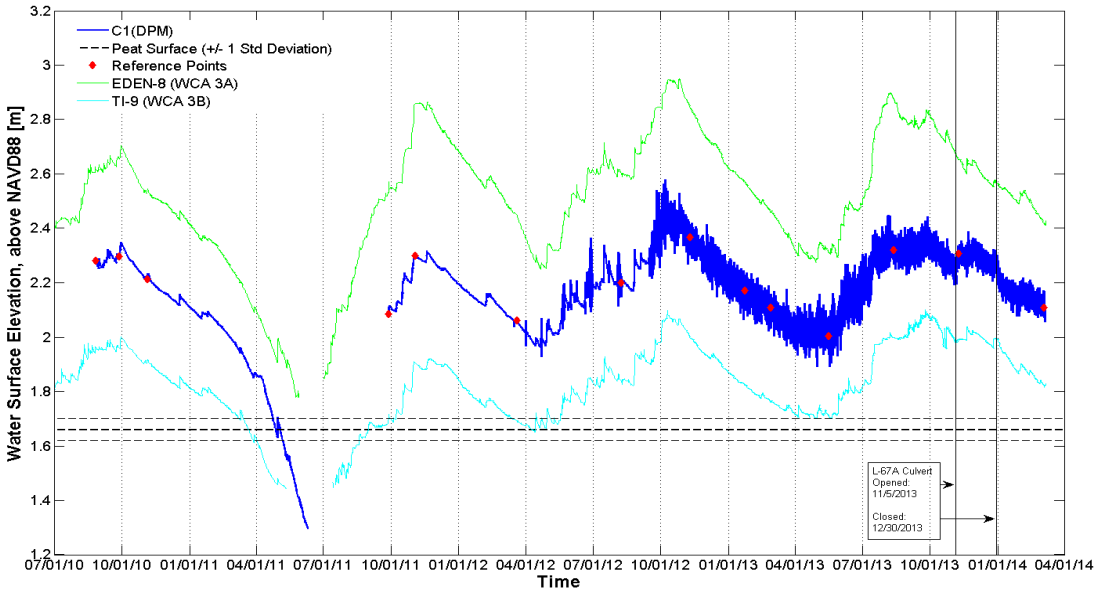

Figure H2. Water level and ground surface elevation at C1 in DPM. The mean ground surface elevation ± 1 standard deviation is shown for nearby areas of ridge and slough vegetation is shown. Reference points are hand collected calibration measurements.

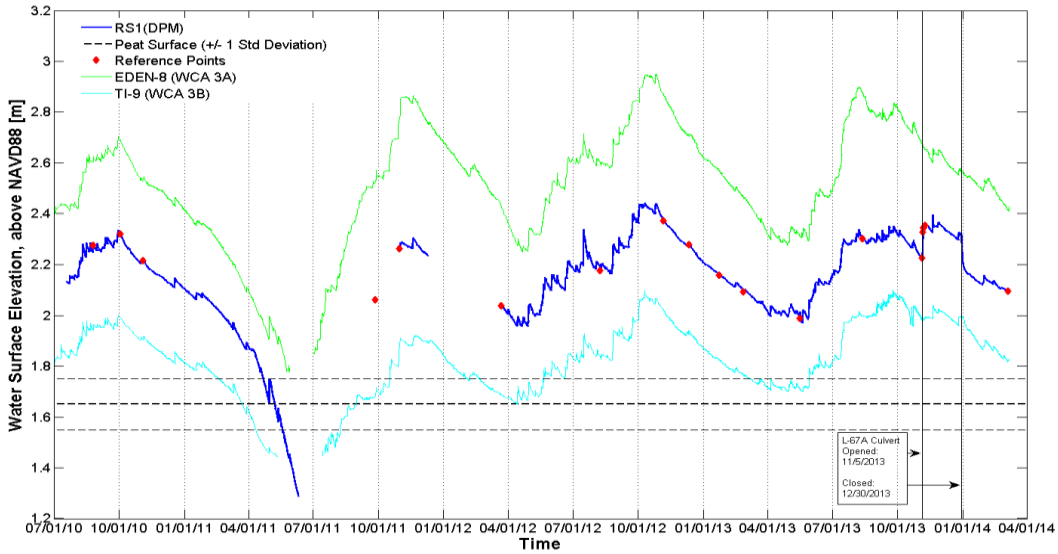

Figure H3. Water level and ground surface elevation at RS1 in DPM. Mean ground surface elevation ± 1 standard deviation in areas of ridge and slough vegetation is shown. Reference points are hand collected calibration measurements.

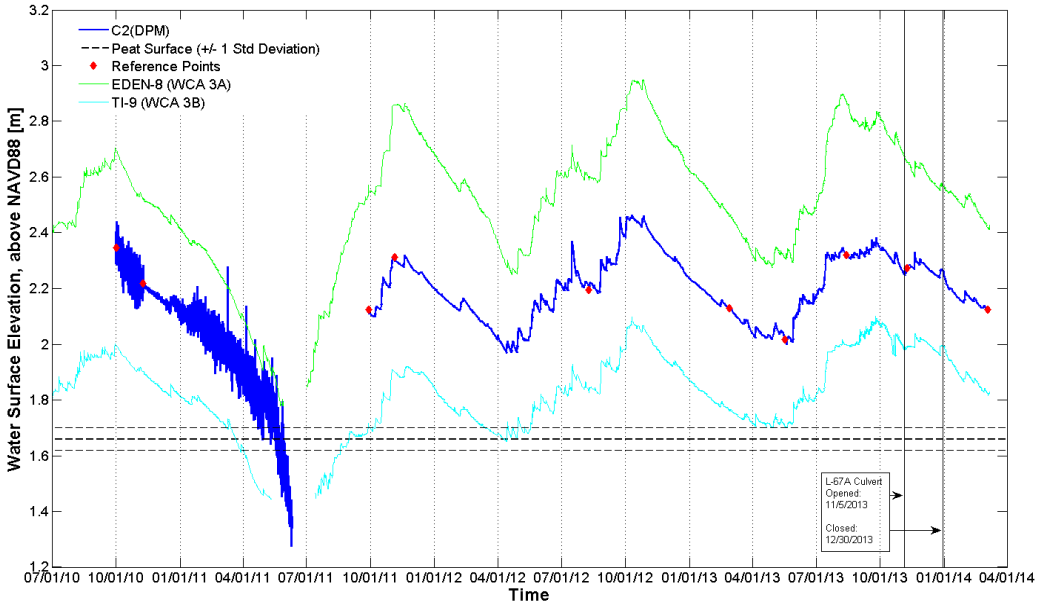

Figure H4. Water level and ground surface elevation at C2 in DPM. The mean ground surface elevation ± 1 standard deviation is shown for nearby areas of ridge and slough vegetation is shown. Reference points are hand collected calibration measurements.

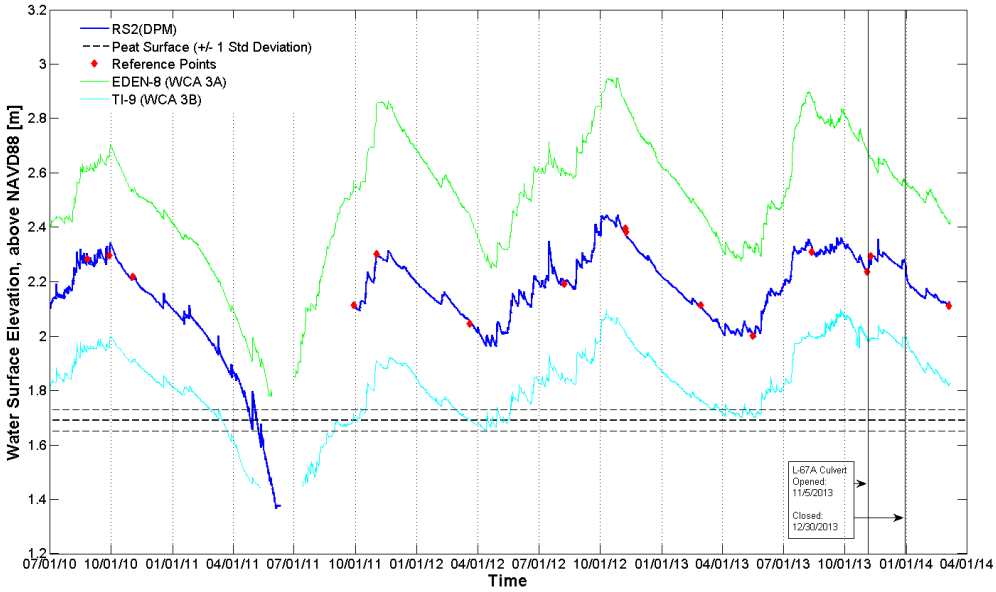

Figure H5. Water level and ground surface elevation at RS2 in DPM. The mean ground surface elevation ± 1 standard deviation is shown for nearby areas of ridge and slough vegetation is shown. Reference points are hand collected calibration measurements.

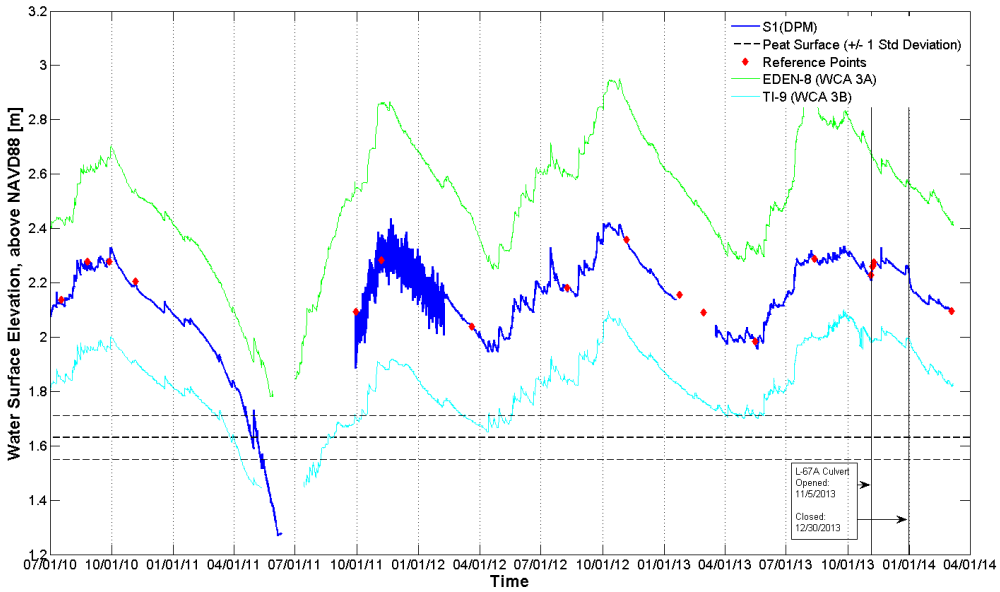

Figure H6. Water level and ground surface elevation at S1 in DPM. The mean ground surface elevation ± 1 standard deviation is shown for nearby areas of ridge and slough vegetation is shown. Reference points are hand collected calibration measurements.

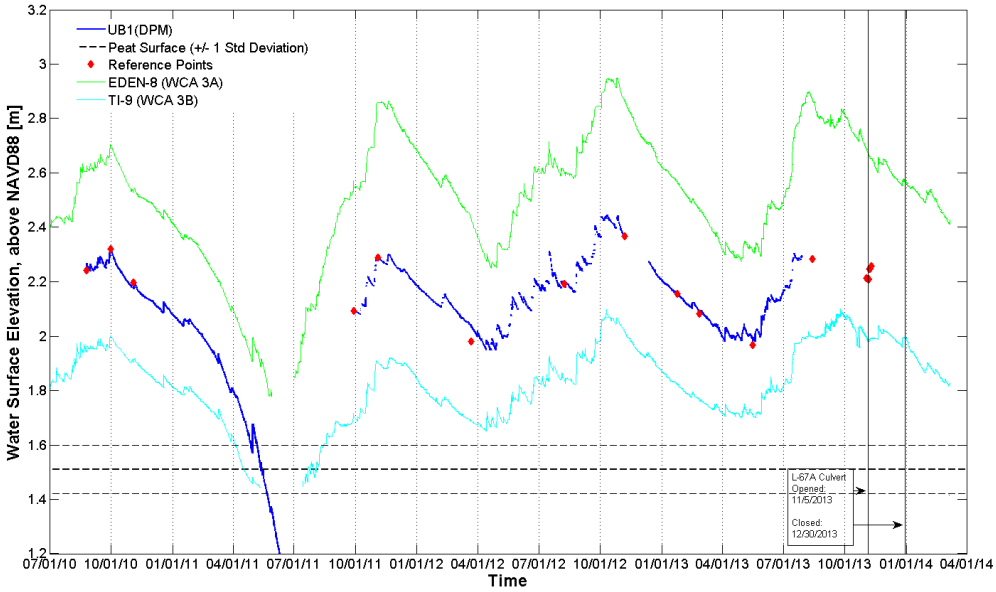

Figure H7. Water level and ground surface elevation at UB1 in DPM. The mean ground surface elevation ± 1 standard deviation is shown for nearby areas of ridge and slough vegetation is shown. Reference points are hand collected calibration measurements.

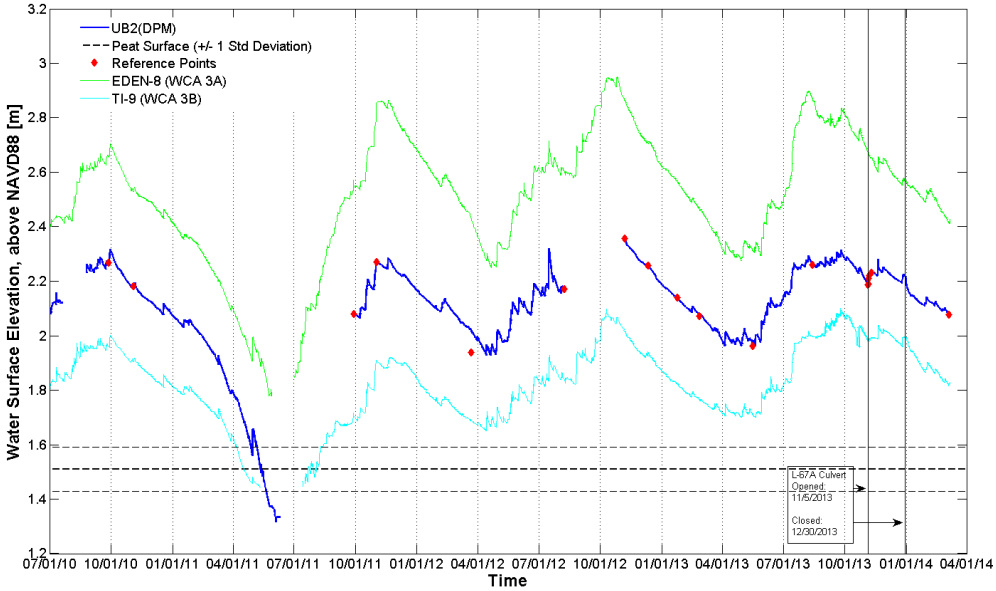

Figure H8. Water level and ground surface elevation at UB2 in DPM. The mean ground surface elevation ± 1 standard deviation is shown for nearby areas of ridge and slough vegetation is shown. Reference points are hand collected calibration measurements.

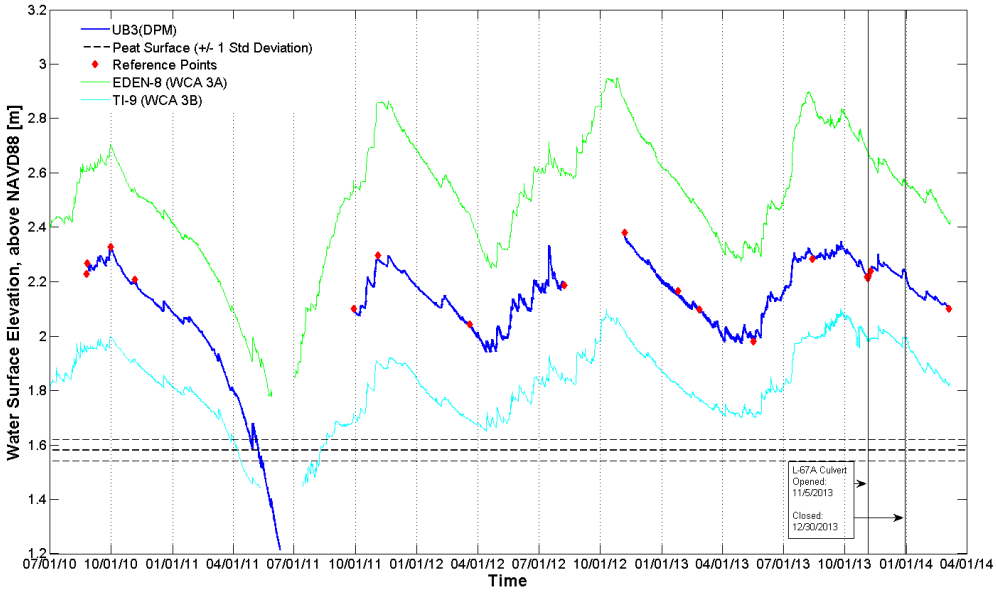

Figure H9. Water level and ground surface elevation at UB3 in DPM. The mean ground surface elevation ± 1 standard deviation is shown for nearby areas of ridge and slough vegetation is shown. Reference points are hand collected calibration measurements.

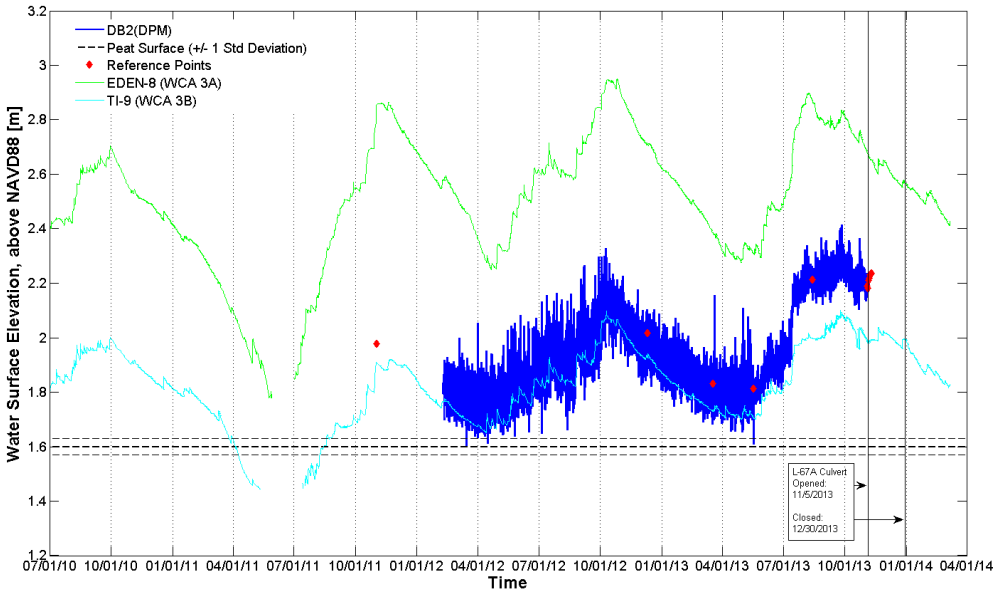

Figure H10. Water level and ground surface elevation at DB2 in DPM. The mean ground surface elevation ± 1 standard deviation is shown for nearby areas of ridge and slough vegetation is shown. Reference points are hand collected calibration measurements.

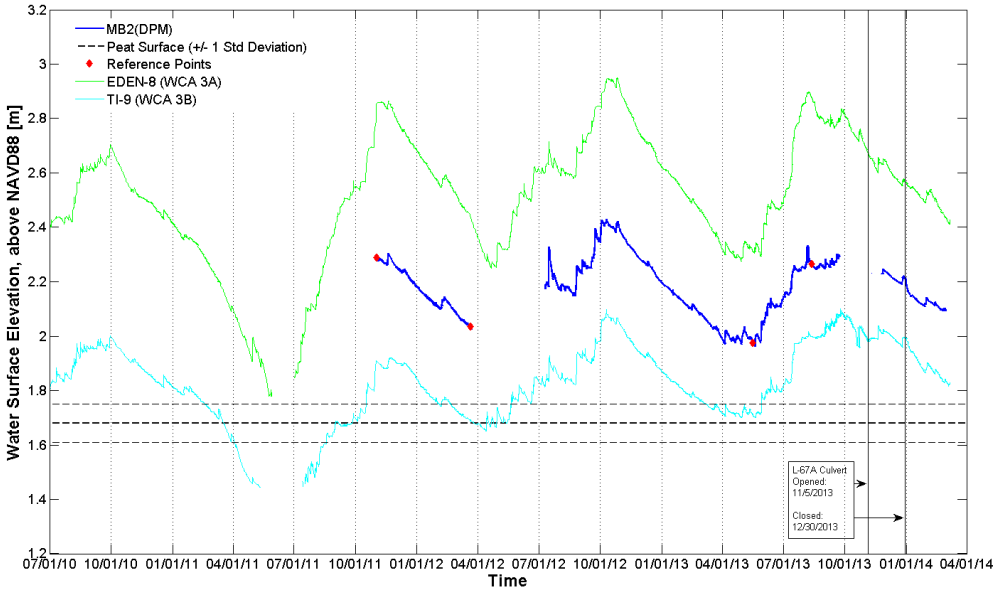

Figure H11. Water level and ground surface elevation at MB2 in DPM. The mean ground surface elevation ± 1 standard deviation is shown for nearby areas of ridge and slough vegetation is shown. Reference points are hand collected calibration measurements.

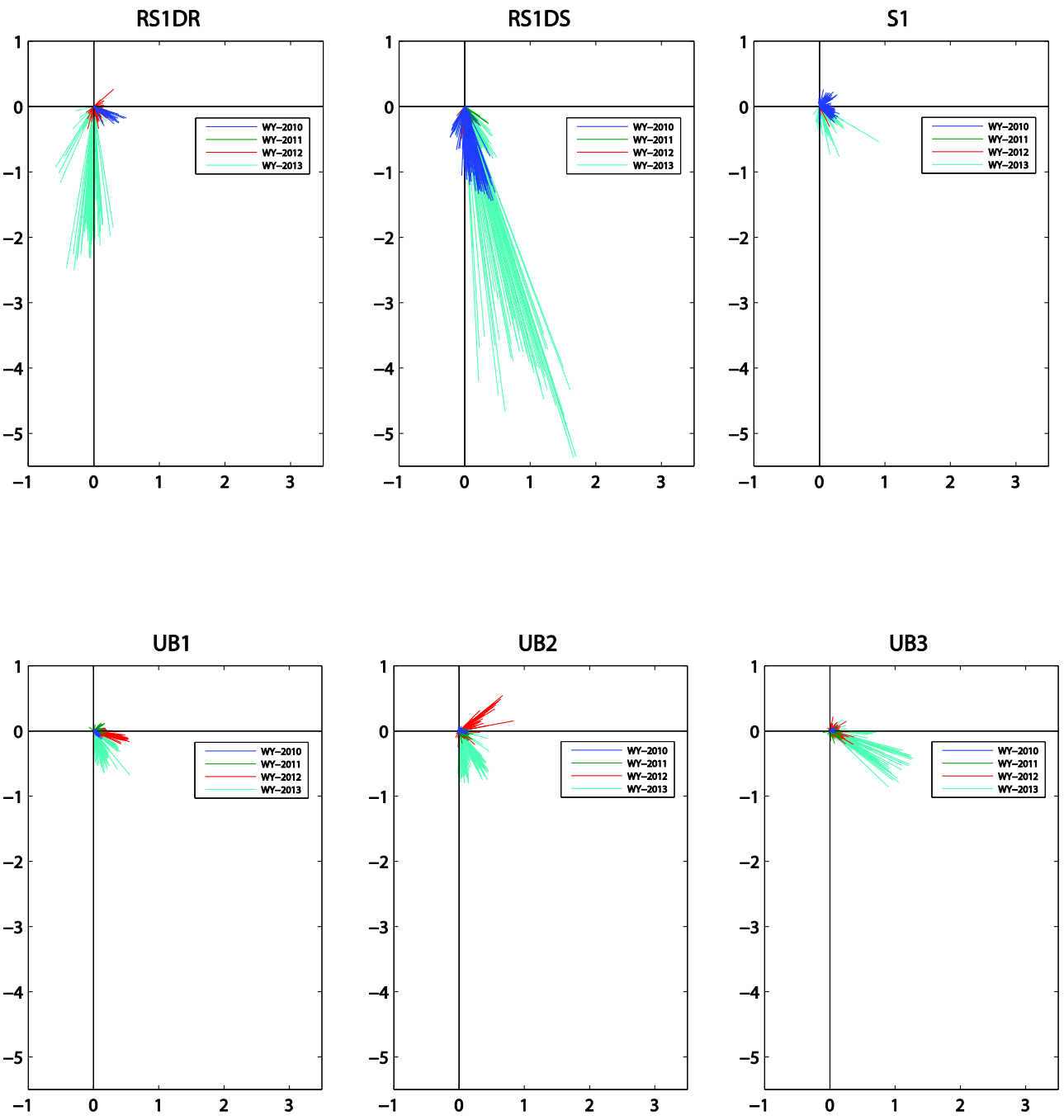

Figure H12. Daily average ADV flow vectors (cm/s) recorded at continuously sampled DPM sites. The axes represent cardinal directions with true north at the top of each plot.

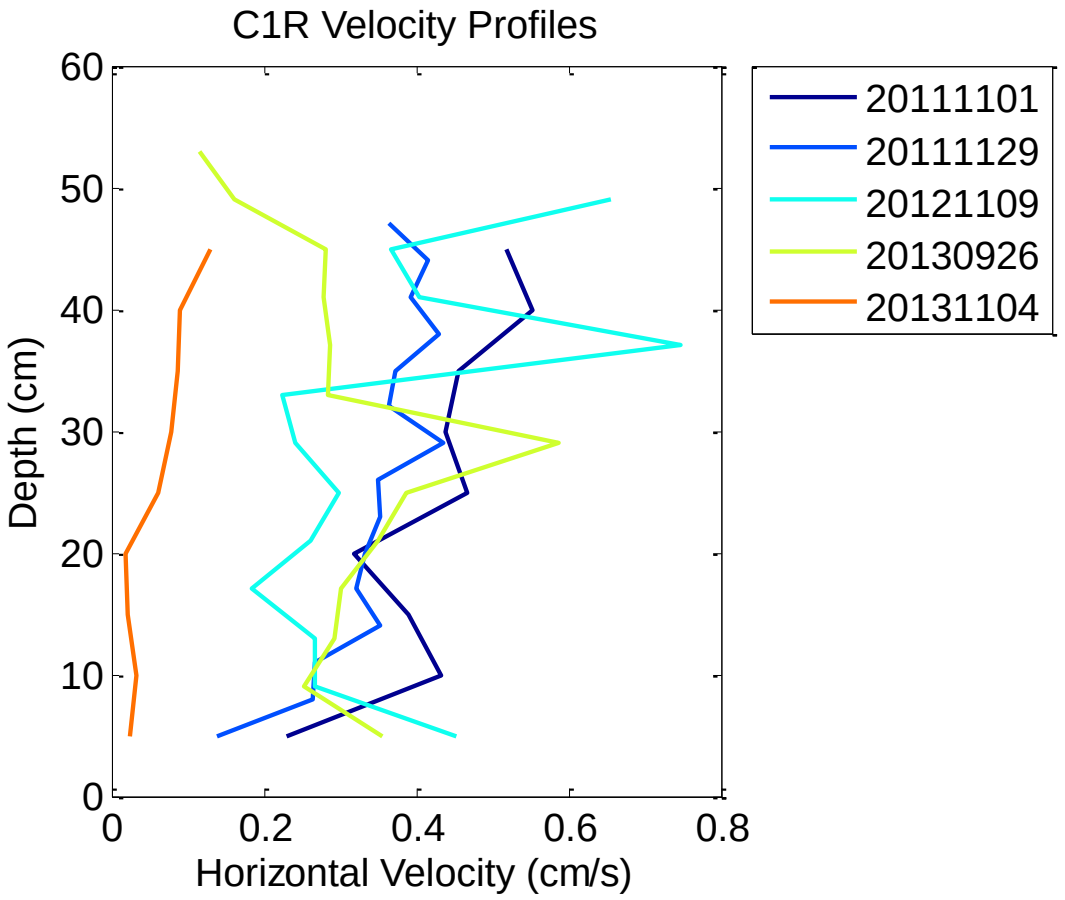

Figure H13. All ADV velocity profiles recorded at DPM site C1R prior to the flow release. Horizontal velocities in cm/s are shown. Dates are given in the format yyyymmdd.

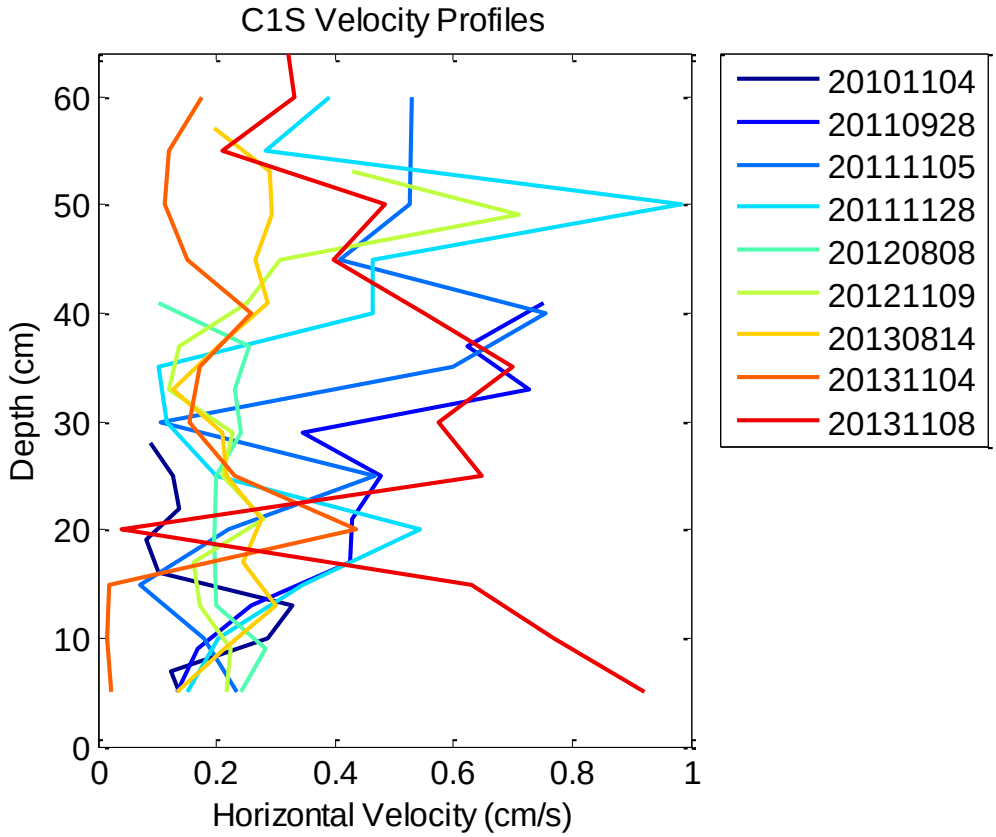

Figure H14. All ADV velocity profiles recorded at DPM site C1S. Horizontal velocities in cm/s are shown. Dates are given in the format yyyymmdd.

.

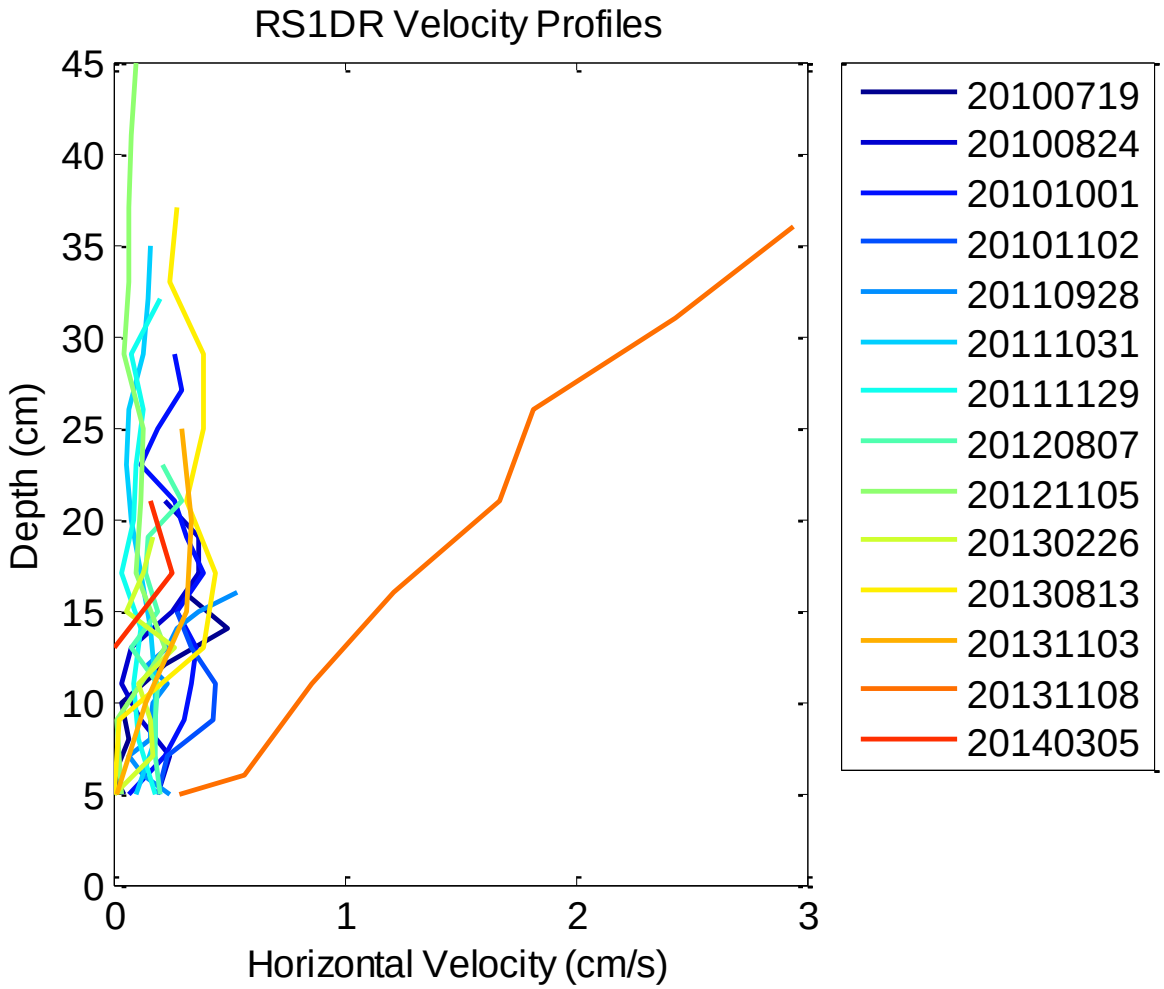

Figure H15. All ADV velocity profiles recorded at DPM site RS1DR. Horizontal velocities in cm/s are shown. Dates are given in the format yyyymmdd.

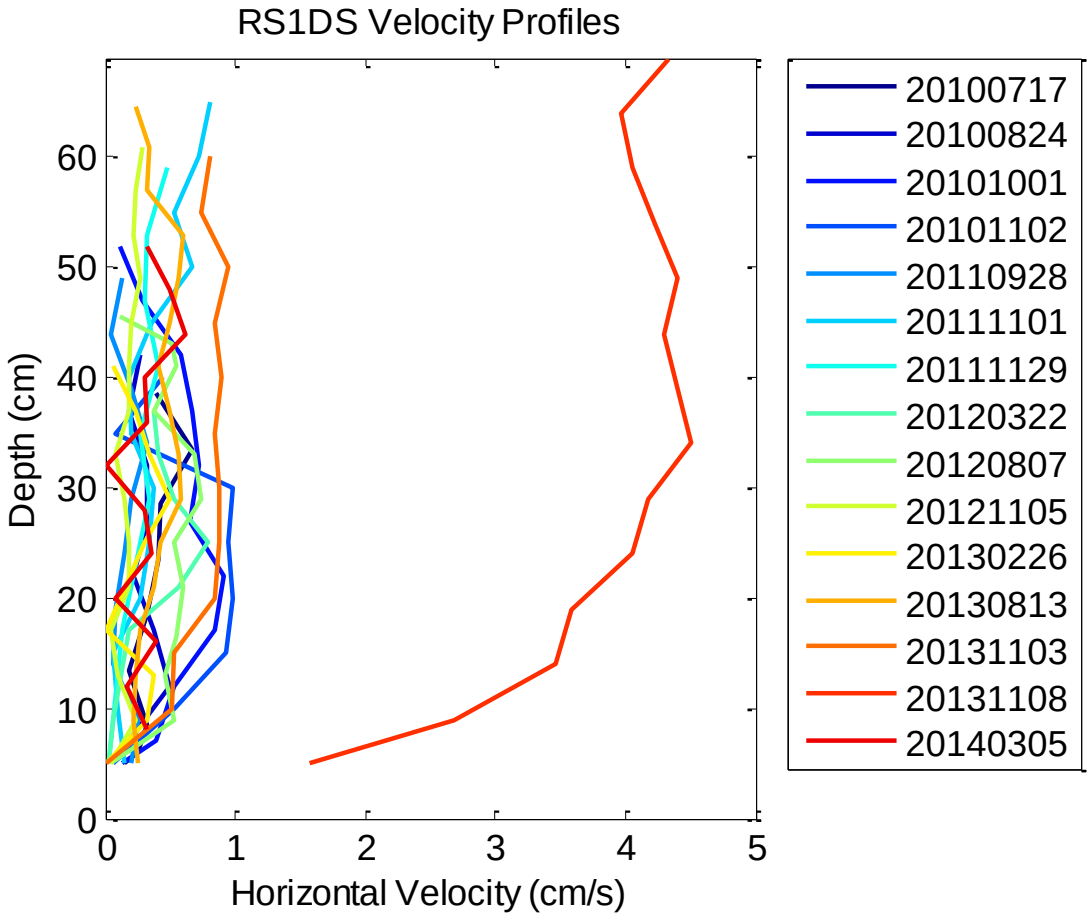

Figure H16. All ADV velocity profiles recorded at DPM site RS1DS. Horizontal velocities in cm/s are shown. Dates are given in the format yyyymmdd.

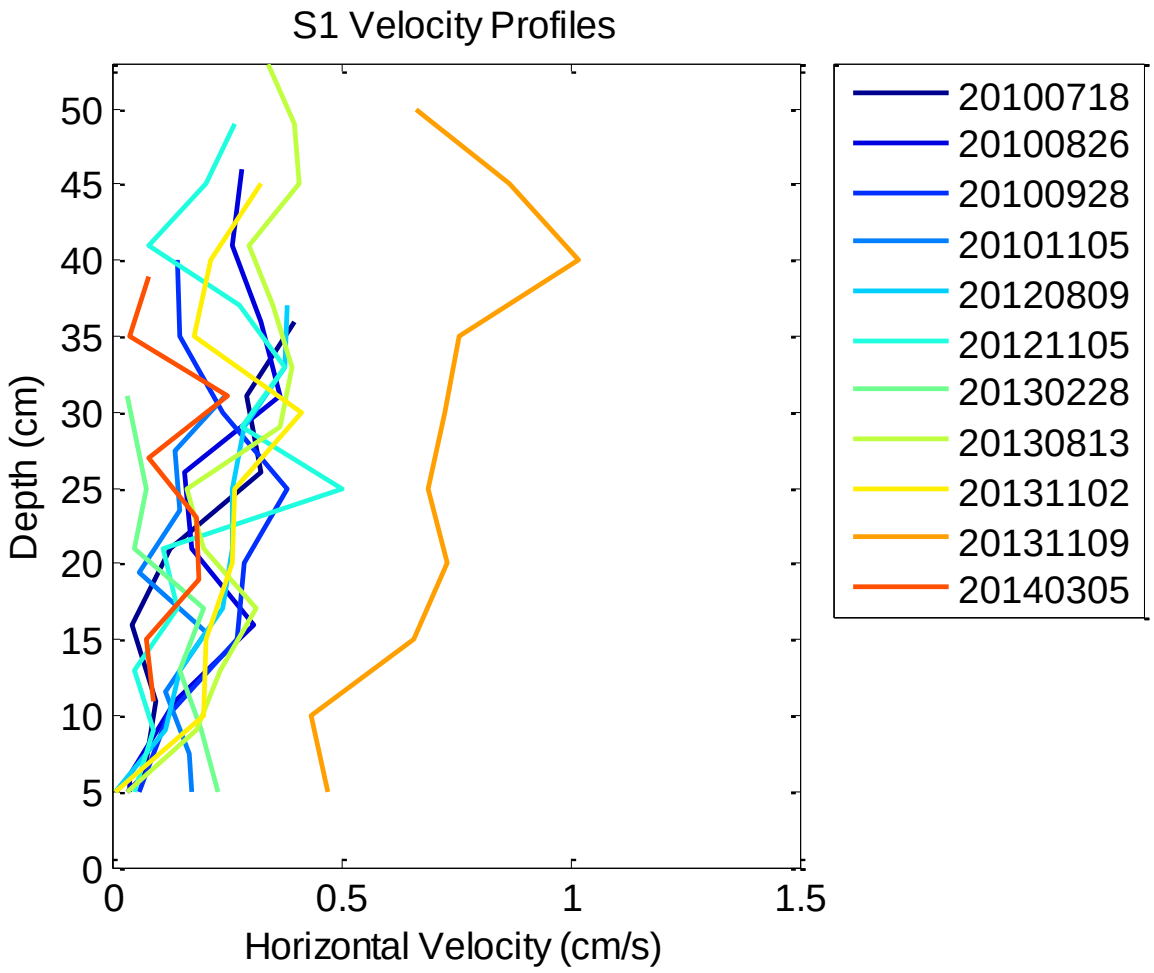

Figure H17. All ADV velocity profiles recorded at DPM site S1. Horizontal velocities in cm/s are shown. Dates are given in the format yyyymmdd.

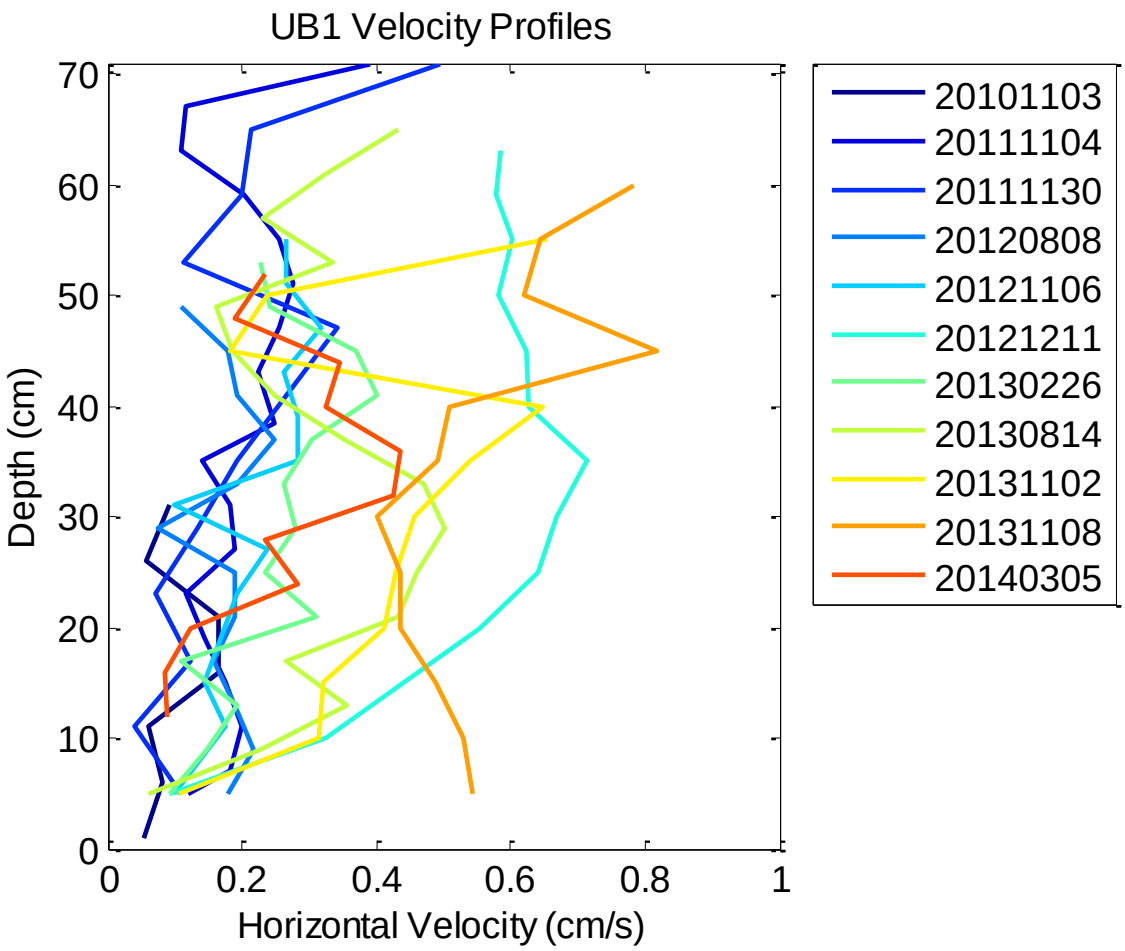

Figure H18. All ADV velocity profiles recorded at DPM site UB1. Horizontal velocities in cm/s are shown. Dates are given in the format yyyymmdd.

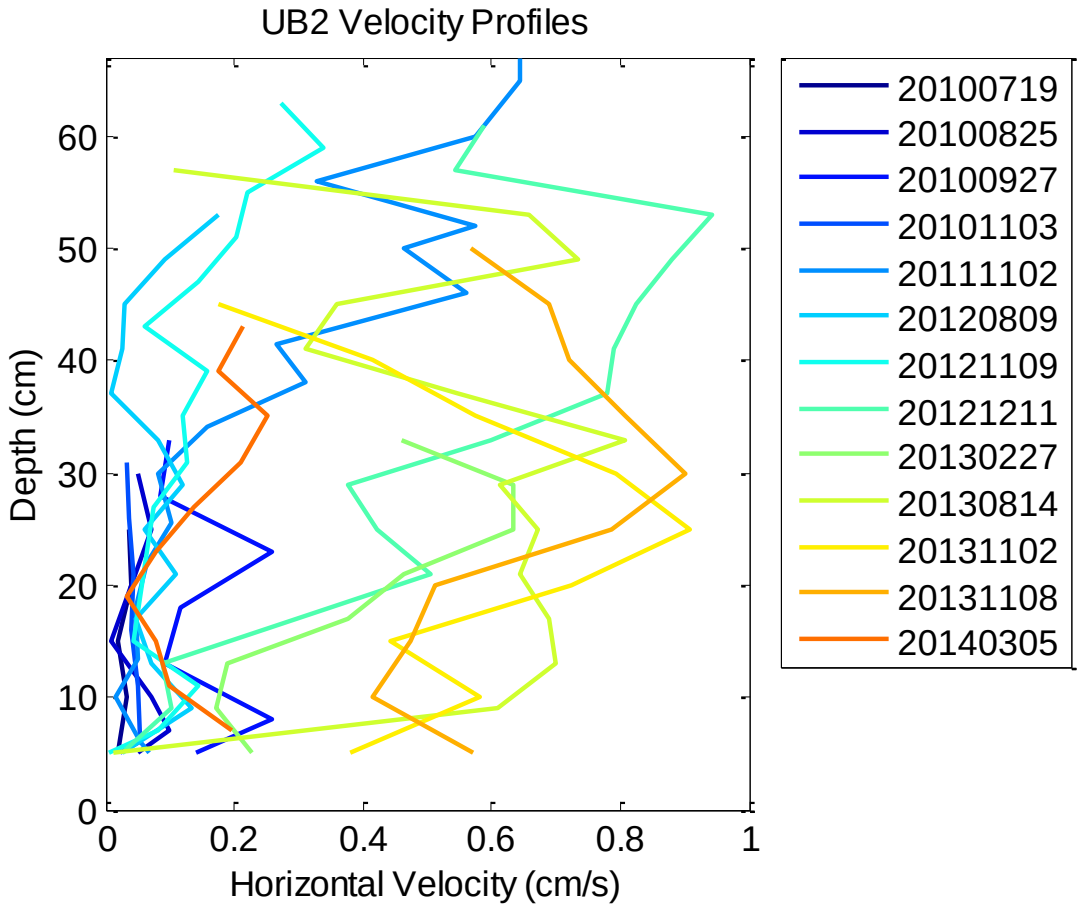

Figure H19. All ADV velocity profiles recorded at DPM site UB2. Horizontal velocities in cm/s are shown. Dates are given in the format yyyymmdd.

.

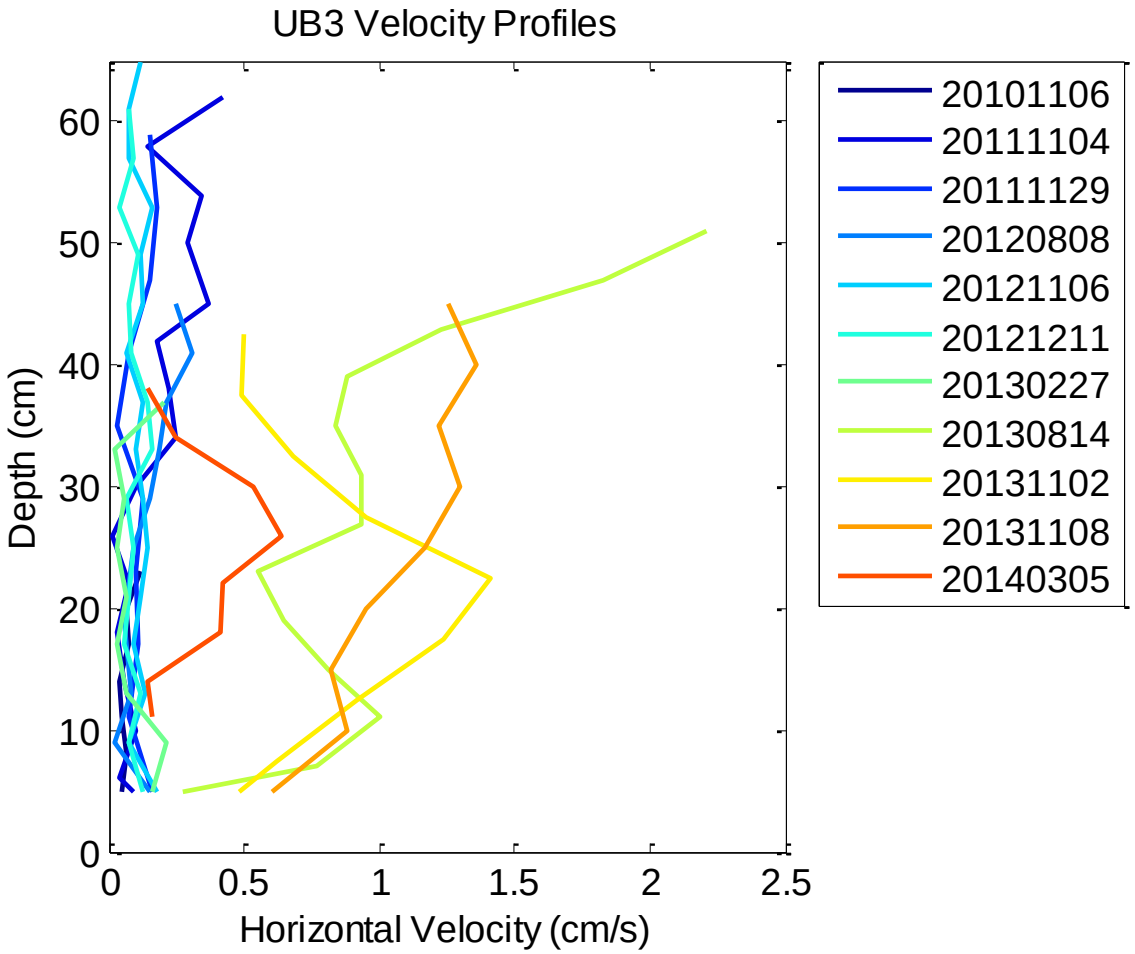

Figure H20. All ADV velocity profiles recorded at DPM site UB3. Horizontal velocities in cm/s are shown. Dates are given in the format yyyymmdd.

Figures – Hydrology (H21-30)

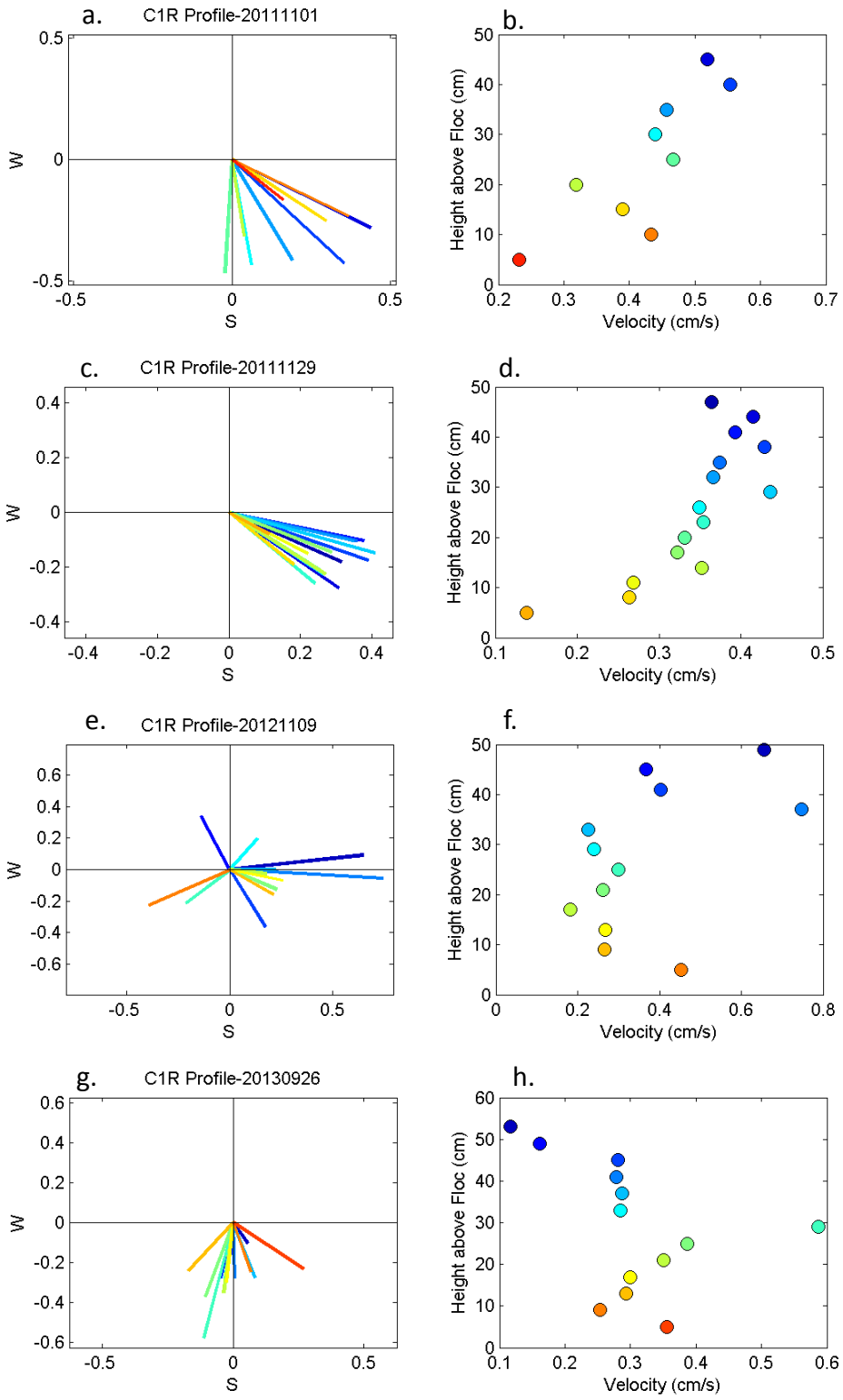
a.
C1R Profile-20111101
W
S
b.
Height above Floc (cm)
Velocity (cm/s)
c.
C1R Profile-20111129
W
S
d.
Height above Floc (cm)
Velocity (cm/s)
e.
C1R Profile-20121109
W
S
f.
Height above Floc (cm)
Velocity (cm/s)
g.
C1R Profile-20130926
W
S
h.
Height above Floc (cm)
Velocity (cm/s)

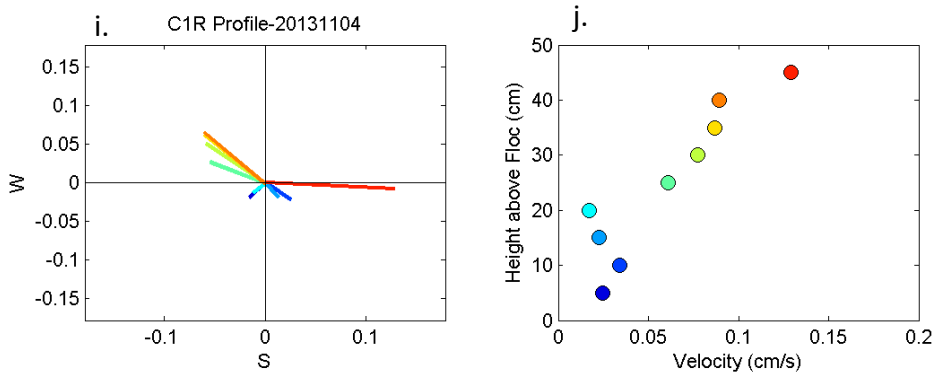

Figure H21. ADV velocity profiles recorded prior to the DPM flow release at site C1R. Profiles recorded on (a-b) Nov. 01, 2011, (c-d) Nov. 29, 2011, (e-f) Nov. 09, 2012, (g-h) Sept. 26, 2013, (i-j) Nov. 04, 2013. Panels (a), (c), (e), (g) and (i) show velocity vectors (cm/s) with the axes representing cardinal directions, such that the top of the plot is true north. Panels (b), (d), (f), (h) and (j) show horizontal velocities (cm/s). Dates are given in the format yyyymmdd.

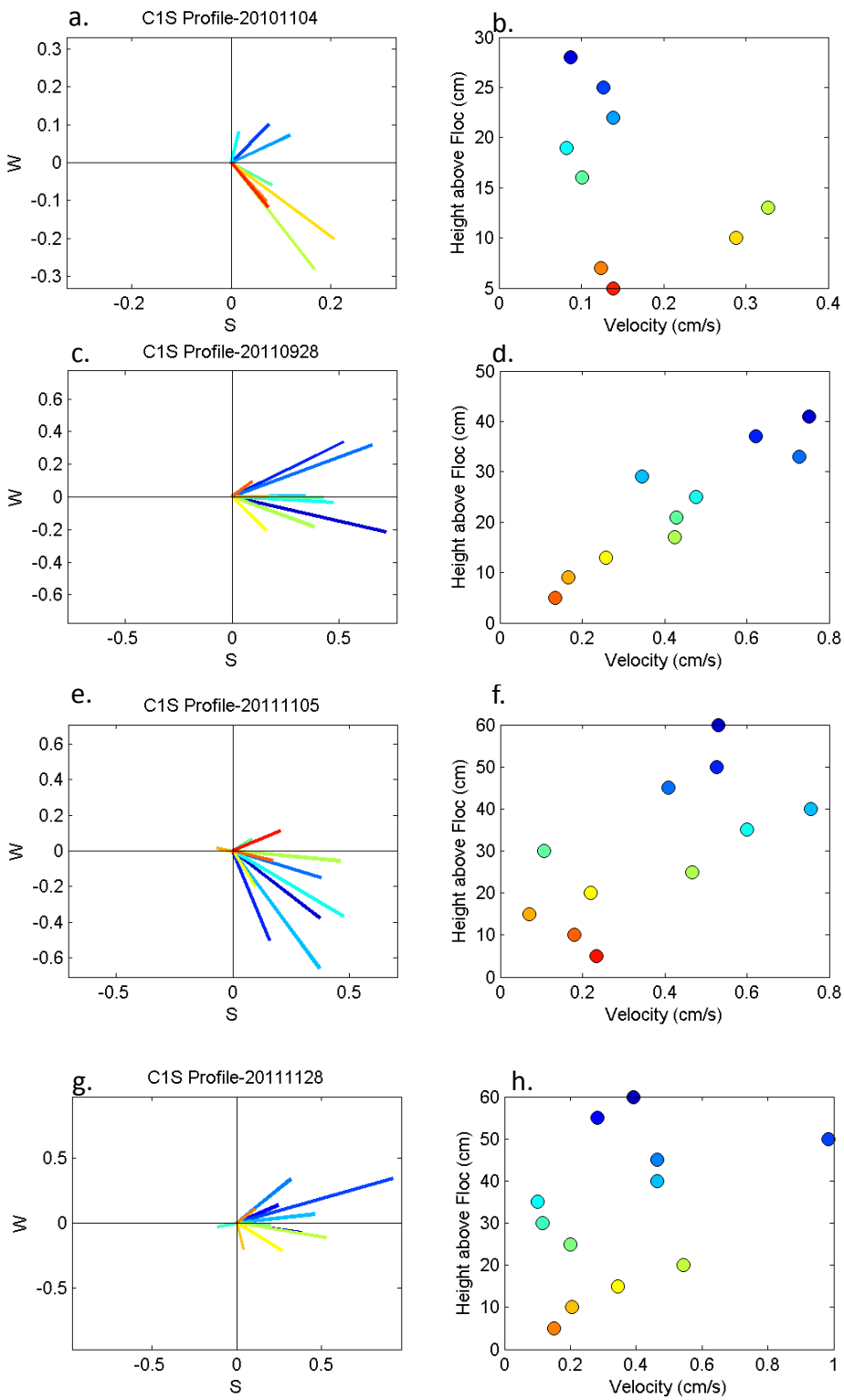
a.
C1S Profile-20101104
W
S
b.
Height above Floc (cm)
Velocity (cm/s)
c.
C1S Profile-20110928
W
S
d.
Height above Floc (cm)
Velocity (cm/s)
e.
C1S Profile-20111105
W
S
f.
Height above Floc (cm)
Velocity (cm/s)
g.
C1S Profile-20111128
W
S
h.
Height above Floc (cm)
Velocity (cm/s)

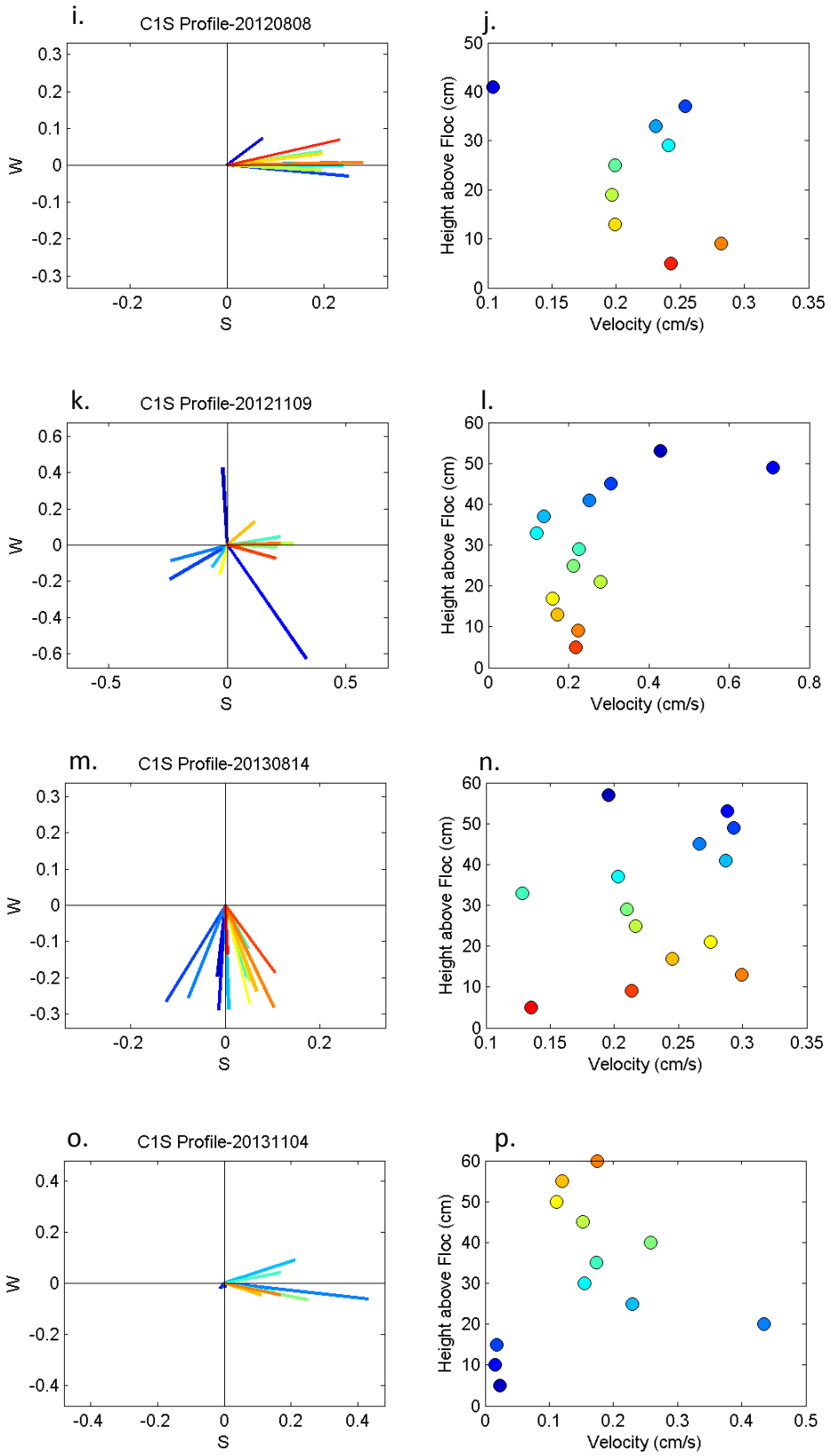
i.
C1S Profile-20120808
W
S
j.
Height above Floc (cm)
Velocity (cm/s)
k.
C1S Profile-20121109
W
S
l.
Height above Floc (cm)
Velocity (cm/s)
m.
C1S Profile-20130814
W
S
n.
Height above Floc (cm)
Velocity (cm/s)
o.
C1S Profile-20131104
W
S
p.
Height above Floc (cm)
Velocity (cm/s)

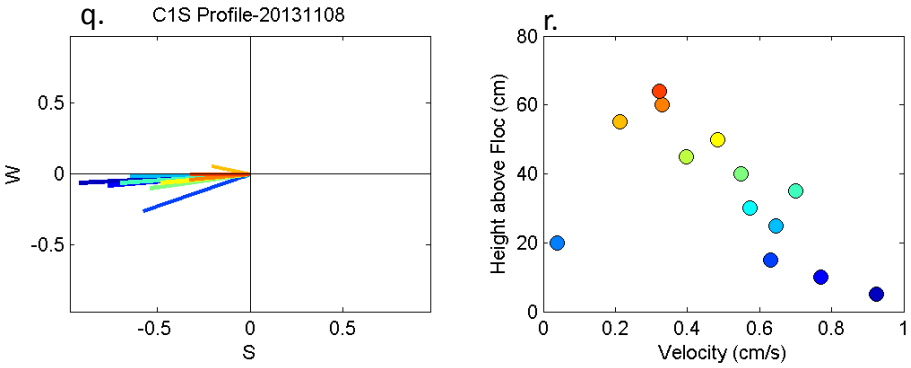

Figure H22. ADV velocity profiles recorded prior to the DPM flow release at site C1S. Profiles recorded on (a-b) Nov. 04, 2010, (c-d) Sep. 28, 2011, (e-f) Nov. 5, 2011, (g-h) Nov. 28, 2011, (i-j) Aug. 8, 2012, (k-l) Nov. 9, 2012, (m-n) Aug. 14, 2013, (o-p) Nov. 04, 2013, (q-r) Nov. 8, 2013. Panels (a), (c), (e), (g), (i), (k), (m), (o) and (q) show velocity vectors (cm/s) with the axes representing cardinal directions, such that the top of the plot is true north. Panels (b), (d), (f), (h), (j), (l), (n), (p) and (r) show horizontal velocities (cm/s). Dates are given in the format yyyymmdd.

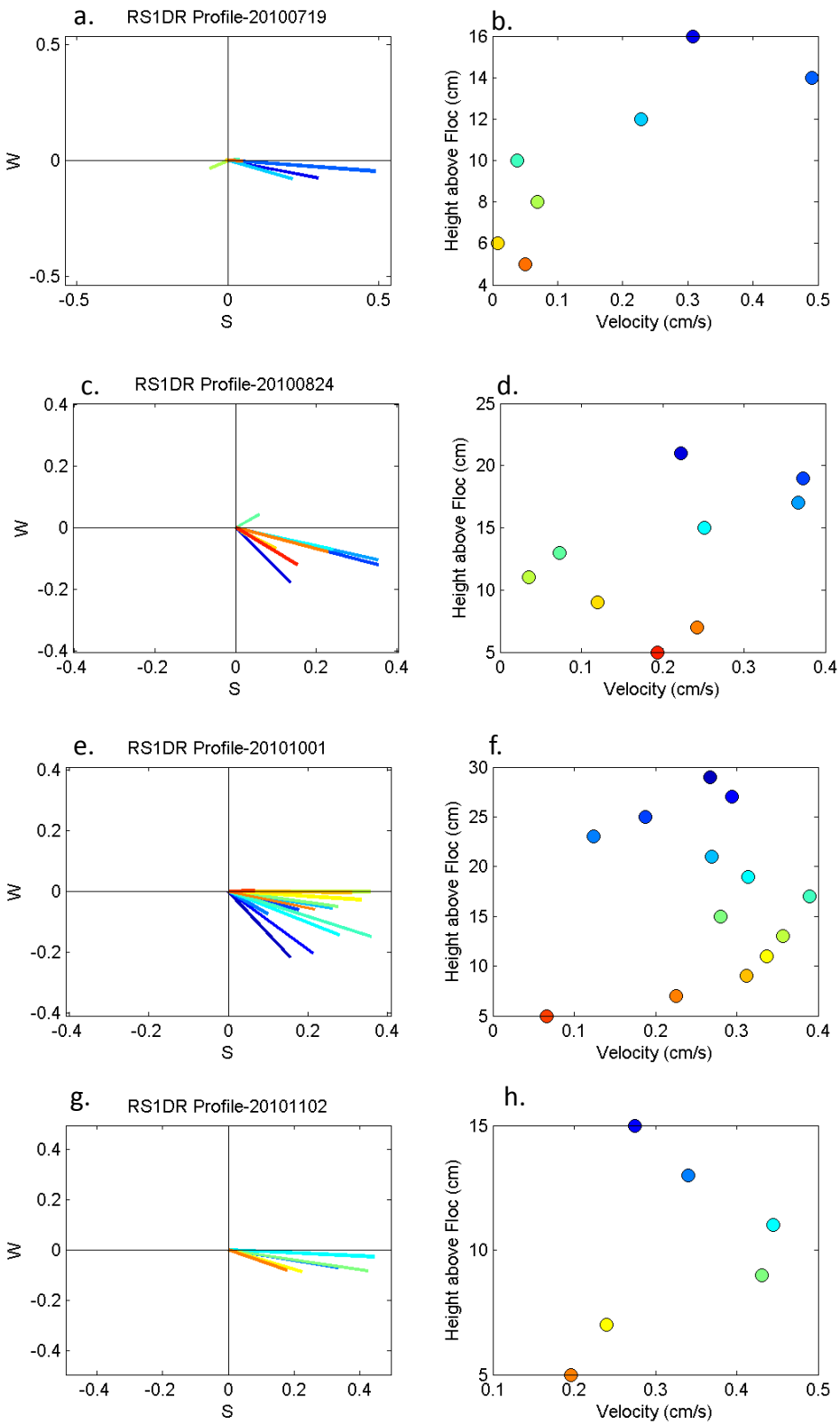
a.
RS1DR Profile-20100719
W
S
b.
Height above Floc (cm)
Velocity (cm/s)
c.
RS1DR Profile-20100824
W
S
d.
Height above Floc (cm)
Velocity (cm/s)
e.
RS1DR Profile-20101001
W
S
f.
Height above Floc (cm)
Velocity (cm/s)
g.
RS1DR Profile-20101102
W
S
h.
Height above Floc (cm)
Velocity (cm/s)

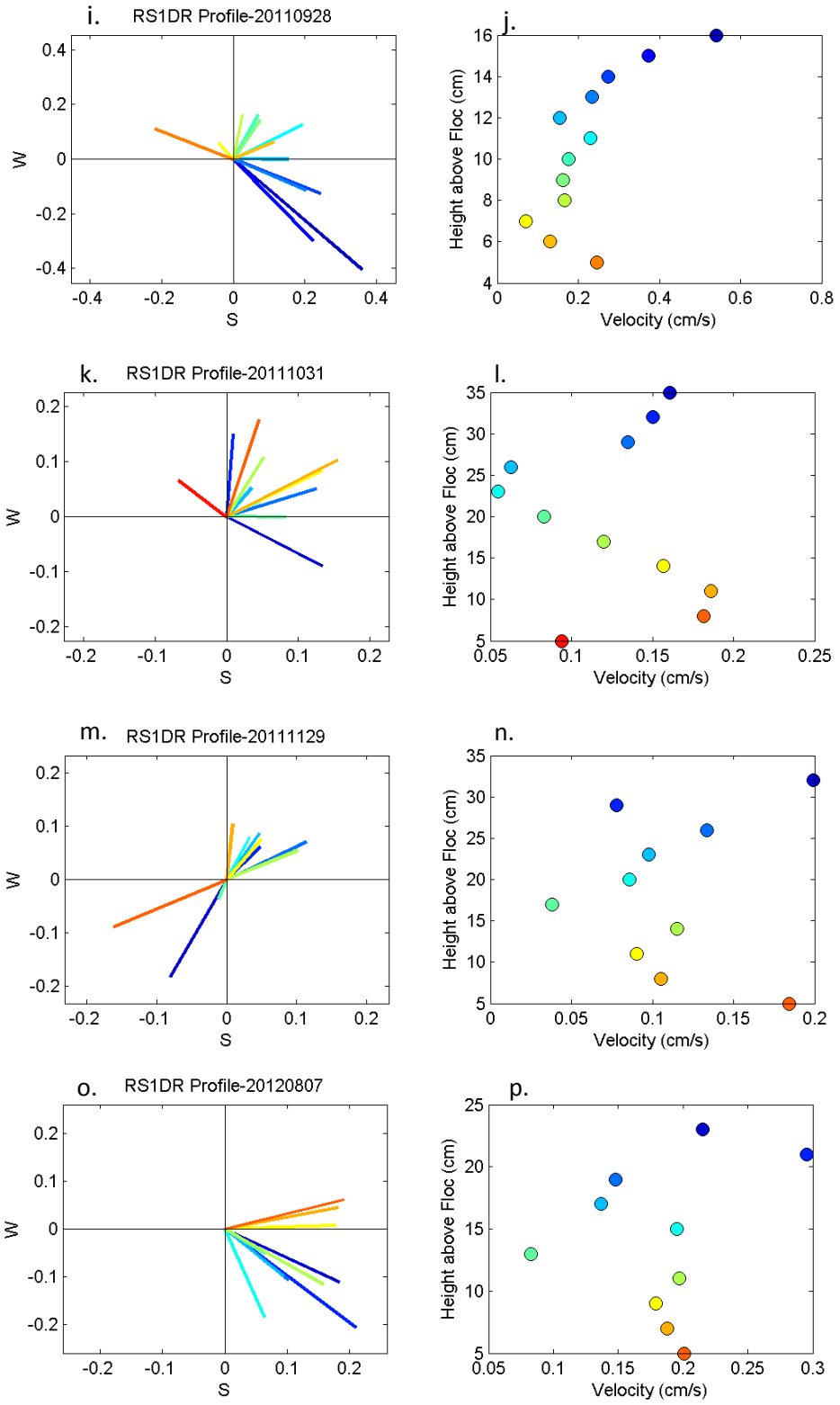
i.
RS1DR Profile-20110928
W
S
j.
Height above Floc (cm)
Velocity (cm/s)
k.
RS1DR Profile-20111031
W
S
l.
Height above Floc (cm)
Velocity (cm/s)
m.
RS1DR Profile-20111129
W
S
n.
Height above Floc (cm)
Velocity (cm/s)
o.
RS1DR Profile-20120807
W
S
p.
Height above Floc (cm)
Velocity (cm/s)

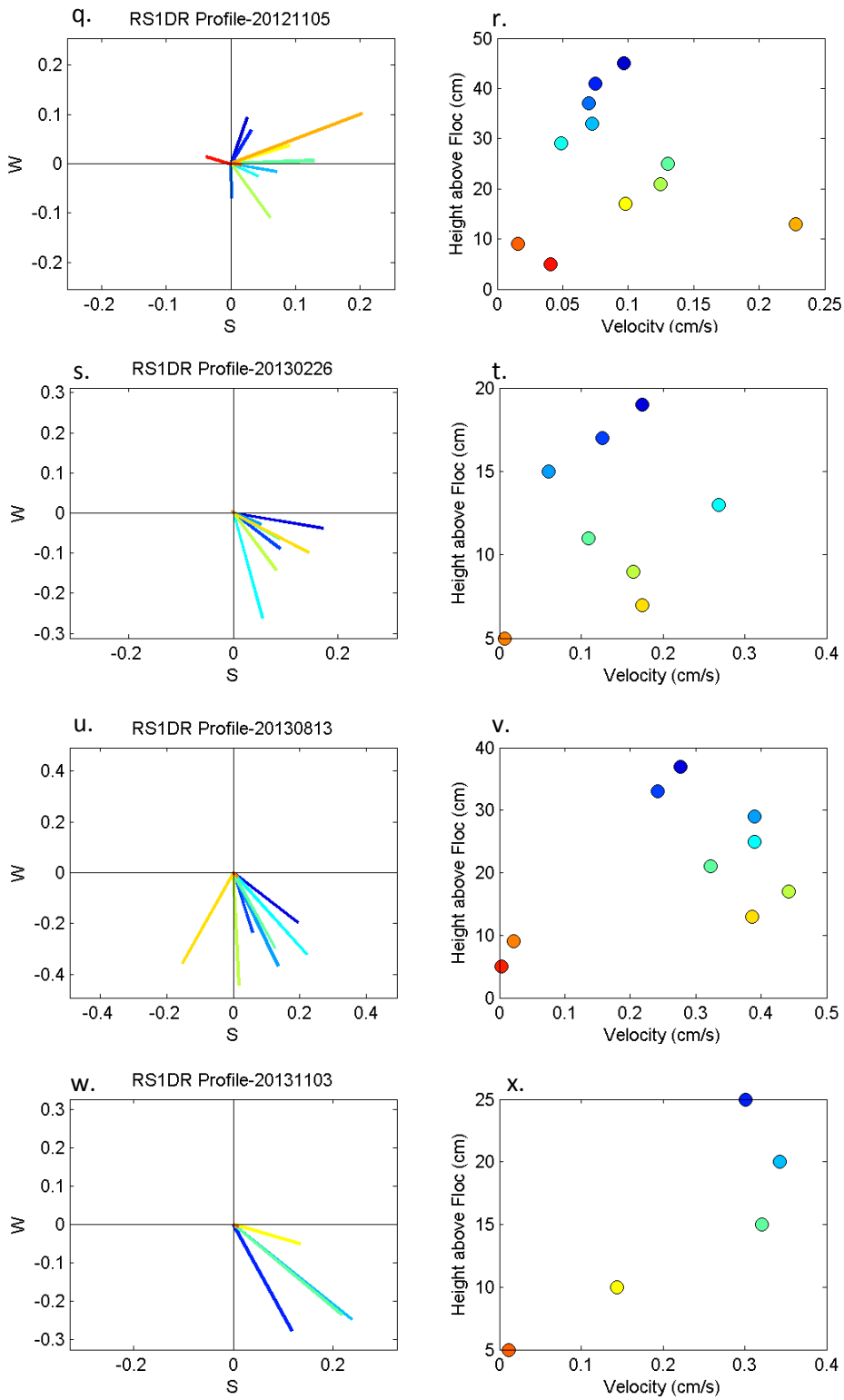
q.
RS1DR Profile-20121105
W
S
r.
Height above Floc (cm)
Velocity (cm/s)
s.
RS1DR Profile-20130226
W
S
t.
Height above Floc (cm)
Velocity (cm/s)
u.
RS1DR Profile-20130813
W
S
v.
Height above Floc (cm)
Velocity (cm/s)
w.
RS1DR Profile-20131103
W
S
x.
Height above Floc (cm)
Velocity (cm/s)

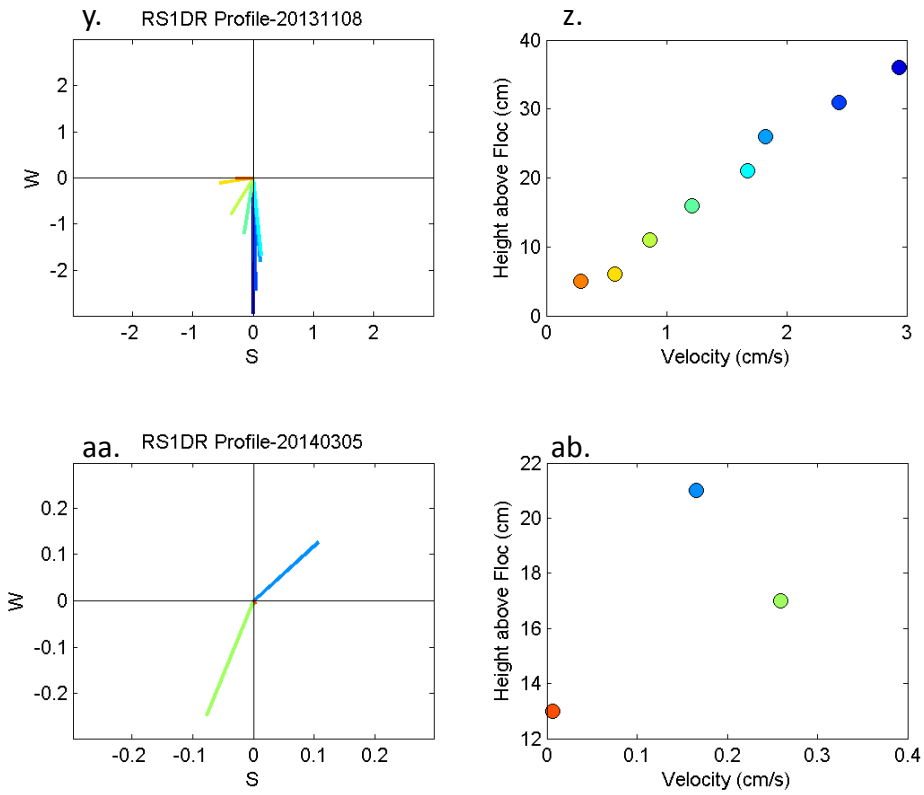

Figure H23. ADV velocity profiles recorded prior to the DPM flow release at site RS1DR. Profiles recorded on (a-b) Jul. 19, 2010, (c-d) Aug. 24, 2010, (e-f) Oct. 1, 2010, (g-h) Nov. 2, 2010, (i-j) Sep. 28, 2011, (k-l) Oct. 31, 2011, (m-n) Nov. 29, 2011, (o-p) Aug. 7, 2012, (q-r) Nov. 5, 2012, and (s-t) Feb. 26, 2013, (u-v), Aug. 13, 2013, (w-x) Nov. 03, 2013, (y-z) Nov. 8, 2013, and (aa-ab) Mar. 5, 2014. Panels (a), (c), (e), (g), (i), (k), (m), (o), (q), (u), (w), (y), and (aa) show velocity vectors (cm/s) with the axes representing cardinal directions, such that the top of the plot is true north. Panels (b), (d), (f), (h), (j), (l), (n), (p), (r), (t), (v), (x), (z) and (ab) show horizontal velocities (cm/s). Dates are given in the format yyyymmdd.

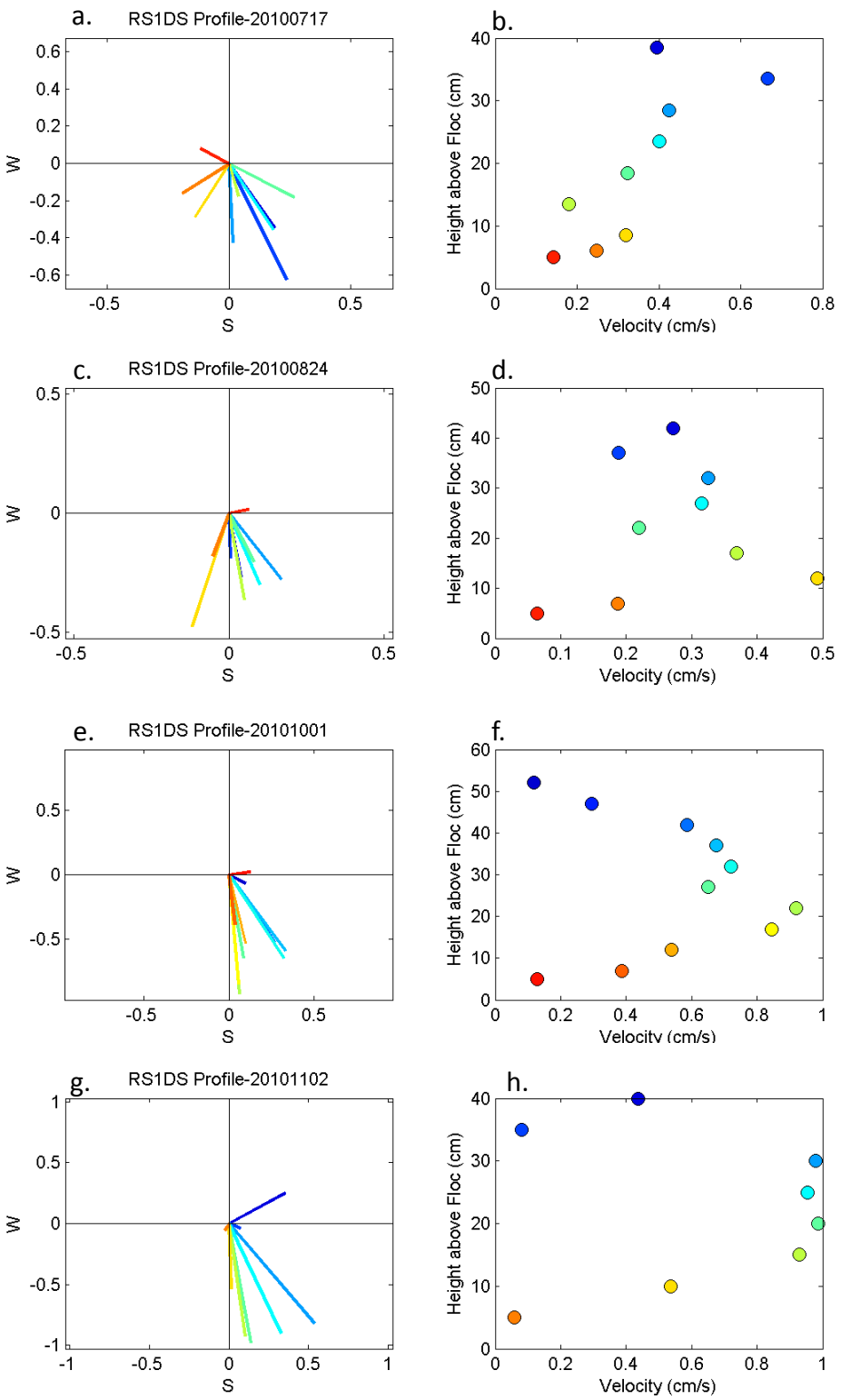
a.
RS1DS Profile-20100717
W
S
b.
Height above Floc (cm)
Velocity (cm/s)
c.
RS1DS Profile-20100824
W
S
d.
Height above Floc (cm)
Velocity (cm/s)
e.
RS1DS Profile-20101001
W
S
f.
Height above Floc (cm)
Velocity (cm/s)
g.
RS1DS Profile-20101102
W
S
h.
Height above Floc (cm)
Velocity (cm/s)

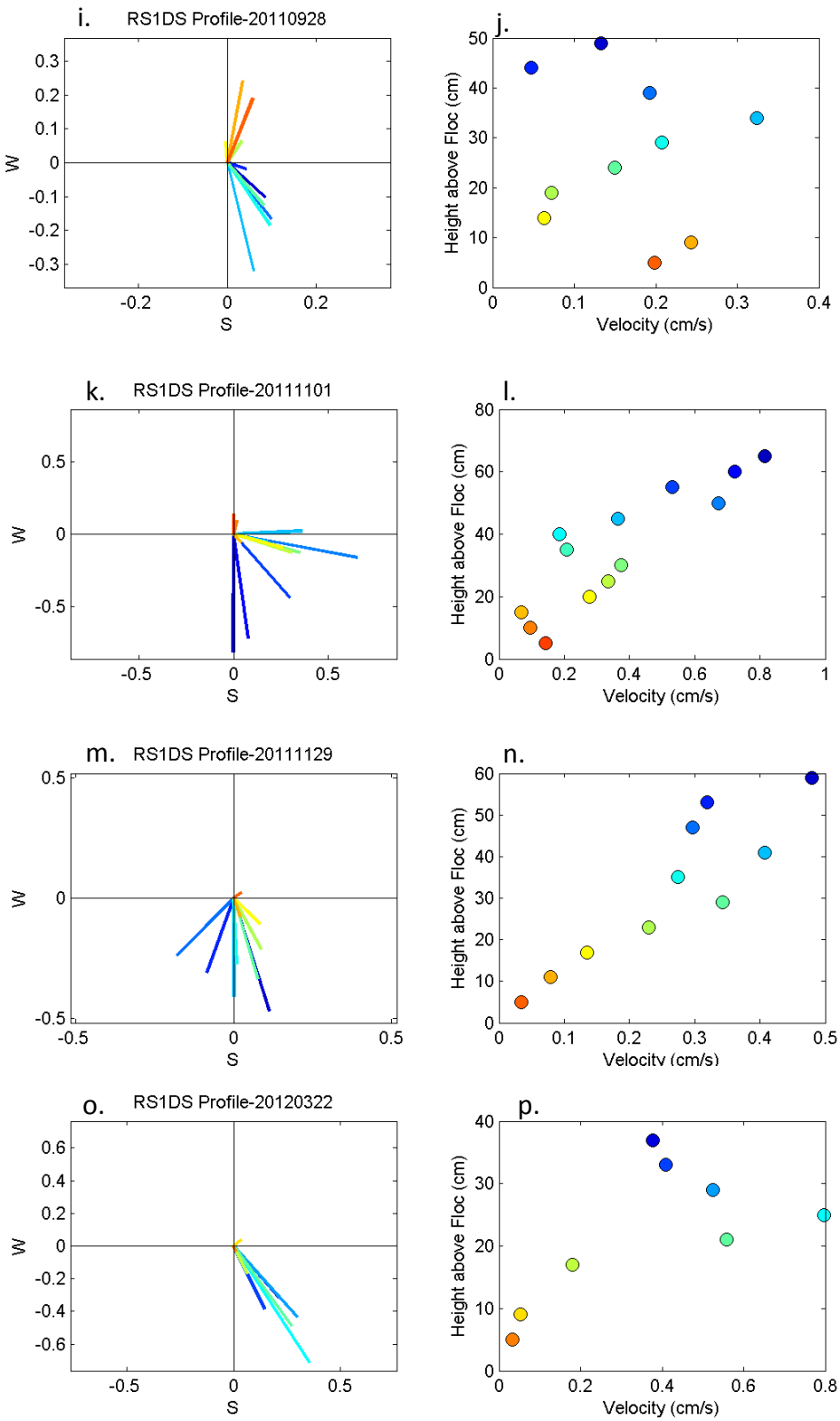
i.
RS1DS Profile-20110928
W
S
j.
Height above Floc (cm)
Velocity (cm/s)
k.
RS1DS Profile-20111101
W
S
l.
Height above Floc (cm)
Velocity (cm/s)
m.
RS1DS Profile-20111129
W
S
n.
Height above Floc (cm)
Velocity (cm/s)
o.
RS1DS Profile-20120322
W
S
p.
Height above Floc (cm)
Velocity (cm/s)

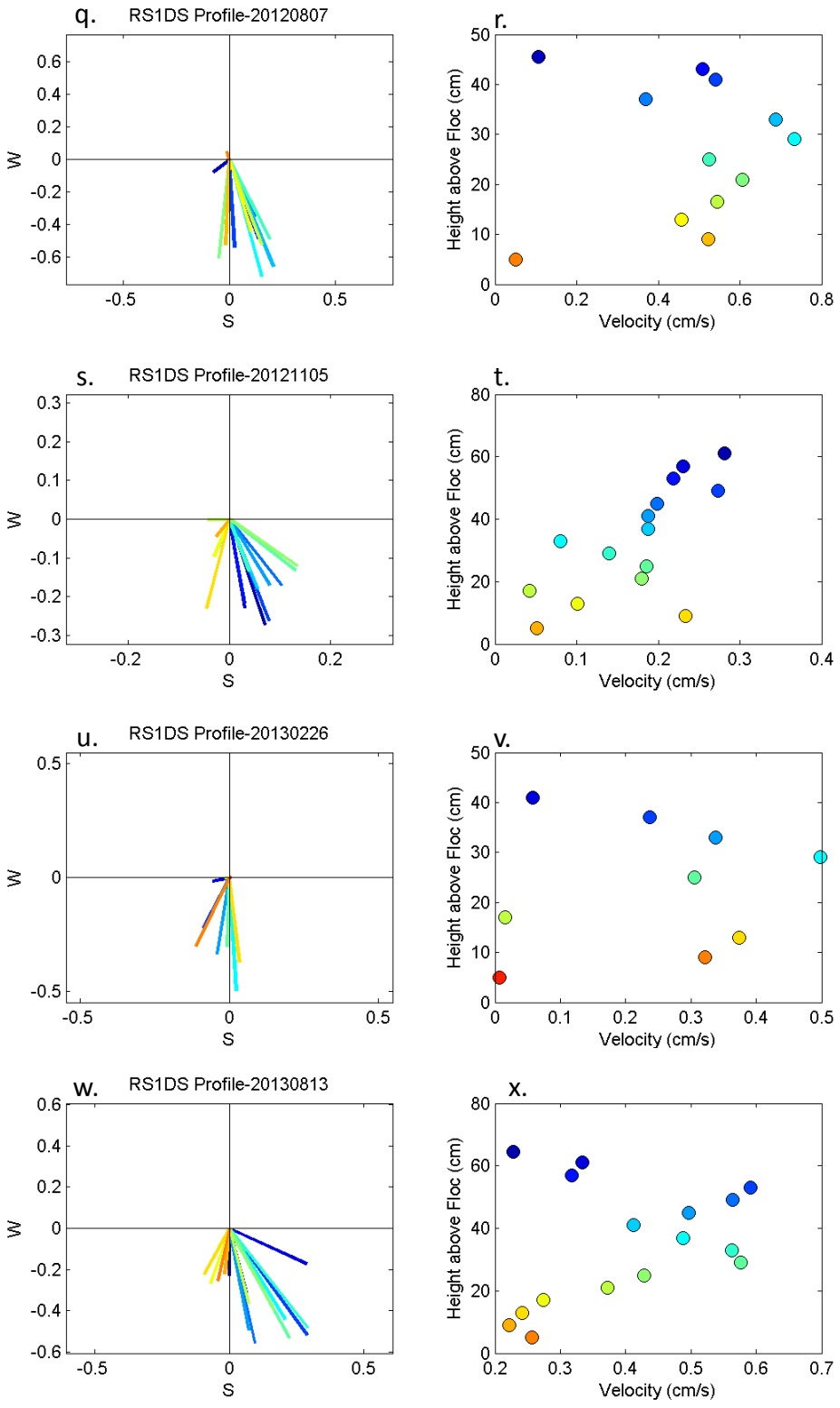
q.
RS1DS Profile-20120807
W
S
r.
Height above Floc (cm)
Velocity (cm/s)
s.
RS1DS Profile-20121105
W
S
t.
Height above Floc (cm)
Velocity (cm/s)
u.
RS1DS Profile-20130226
W
S
v.
Height above Floc (cm)
Velocity (cm/s)
w.
RS1DS Profile-20130813
W
S
x.
Height above Floc (cm)
Velocity (cm/s)

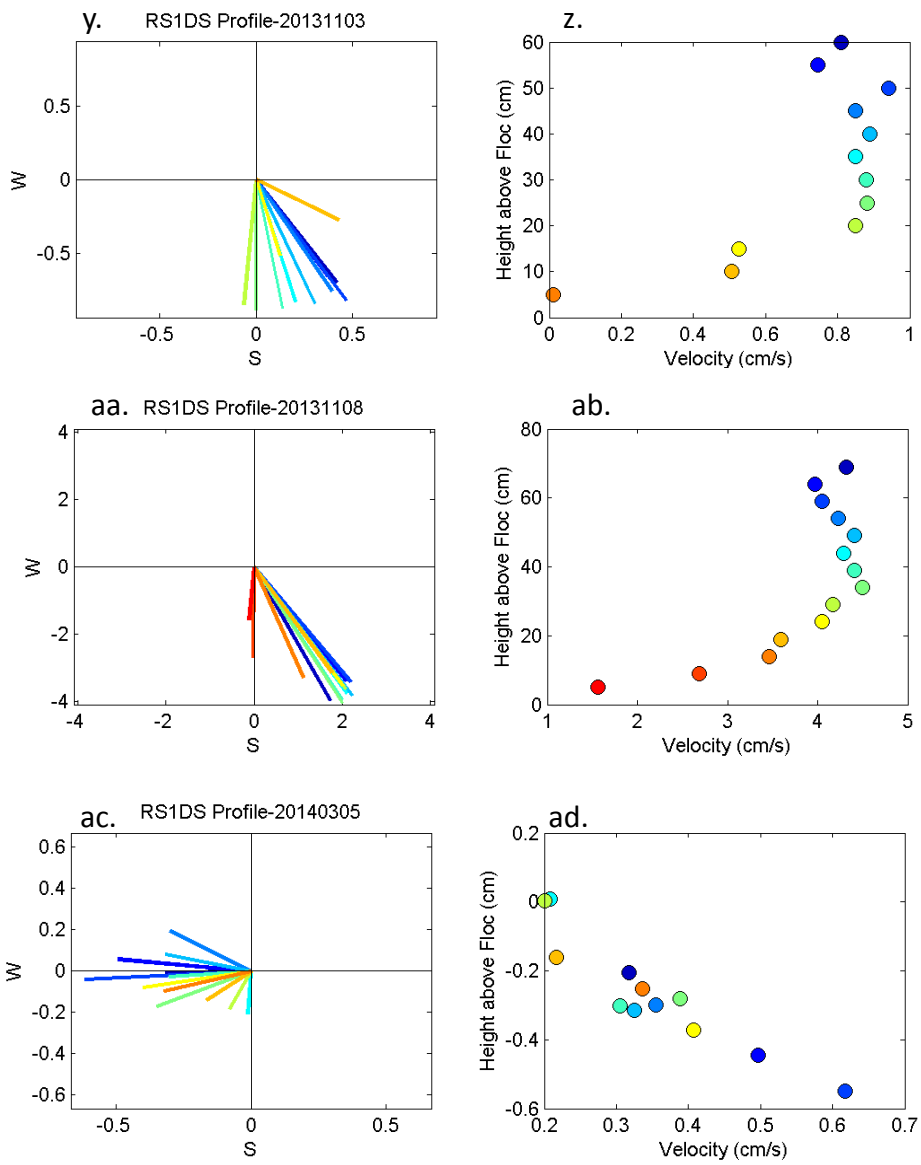

Figure H24. ADV velocity profiles recorded prior to the DPM flow release at site RS1DS. Profiles recorded on (a-b) Jul. 17, 2010, (c-d) Aug. 24, 2010, (e-f) Oct. 1, 2010, (g-h) Nov. 2, 2010, (i-j) Sep. 28, 2011, (k-l) Nov. 1, 2011, (m-n) Nov. 29, 2011, (o-p) Mar. 22, 2012, (q-r) Aug. 7, 2012, (s-t) Nov. 5, 2012, and (u-v) Feb. 26, 2013, (w-x) Aug. 13, 2013, (y-z) Nov. 03, 2013, (aa-ab) Nov. 08, 2013 and (ac-ad) Mar. 05, 2014. Panels (a), (c), (e), (g), (i), (k), (m), (o), (q), (s), (u), (w), (y), (aa) and (ac) show velocity vectors (cm/s) with the axes representing cardinal directions, such that the top of the plot is true north. Panels (b), (d), (f), (h), (j), (l), (n), (p), (r), (t), (v), (x), (z), (ab), and (ad) show horizontal velocities (cm/s). Dates are given in the format yyyymmdd.

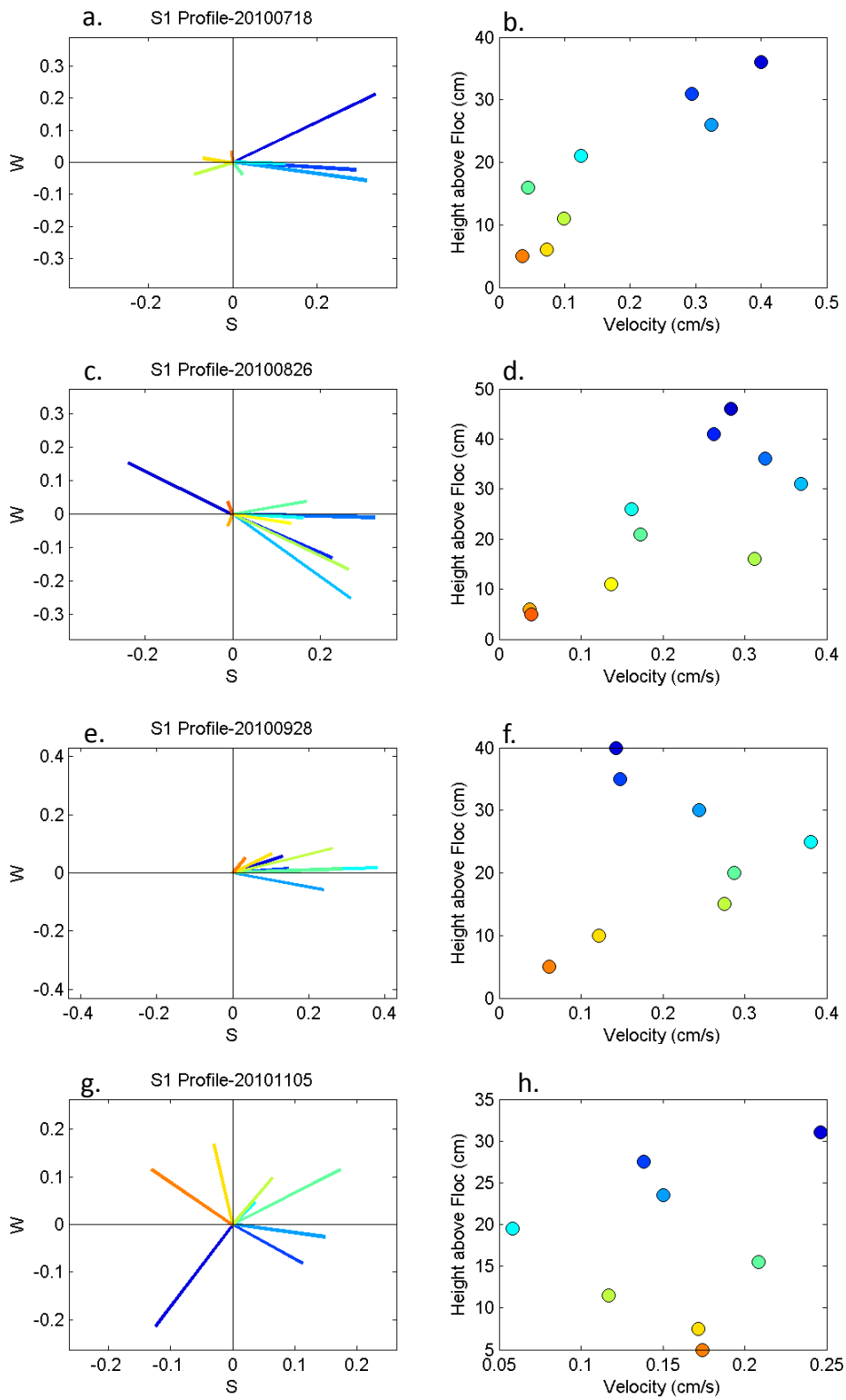
a.
S1 Profile-20100718
W
S
b.
Height above Floc (cm)
Velocity (cm/s)
c.
S1 Profile-20100826
W
S
d.
Height above Floc (cm)
Velocity (cm/s)
e.
S1 Profile-20100928
W
S
f.
Height above Floc (cm)
Velocity (cm/s)
g.
S1 Profile-20101105
W
S
h.
Height above Floc (cm)
Velocity (cm/s)

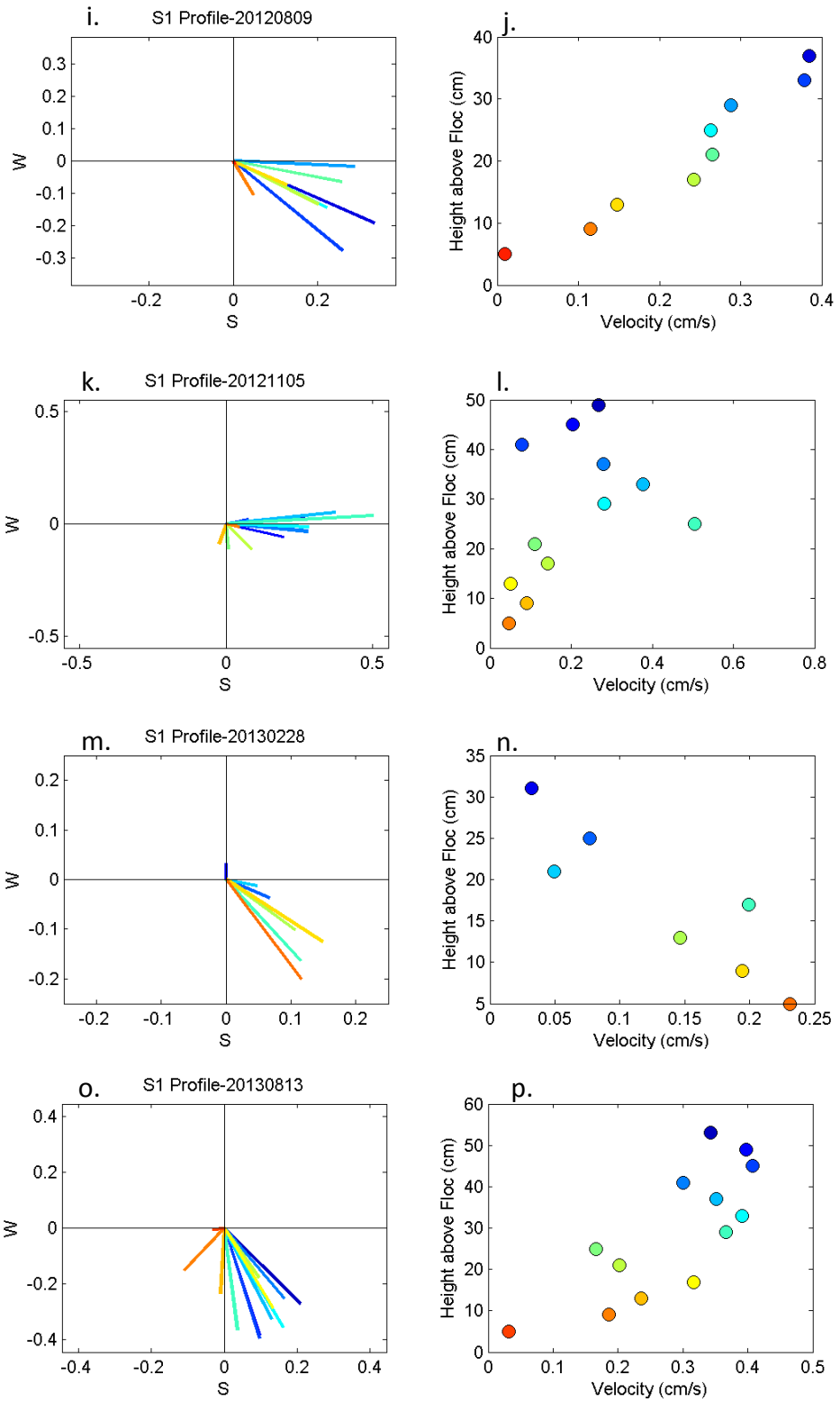
i.
S1 Profile-20120809
W
S
j.
Height above Floc (cm)
Velocity (cm/s)
k.
S1 Profile-20121105
W
S
l.
Height above Floc (cm)
Velocity (cm/s)
m.
S1 Profile-20130228
W
S
n.
Height above Floc (cm)
Velocity (cm/s)
o.
S1 Profile-20130813
W
S
p.
Height above Floc (cm)
Velocity (cm/s)

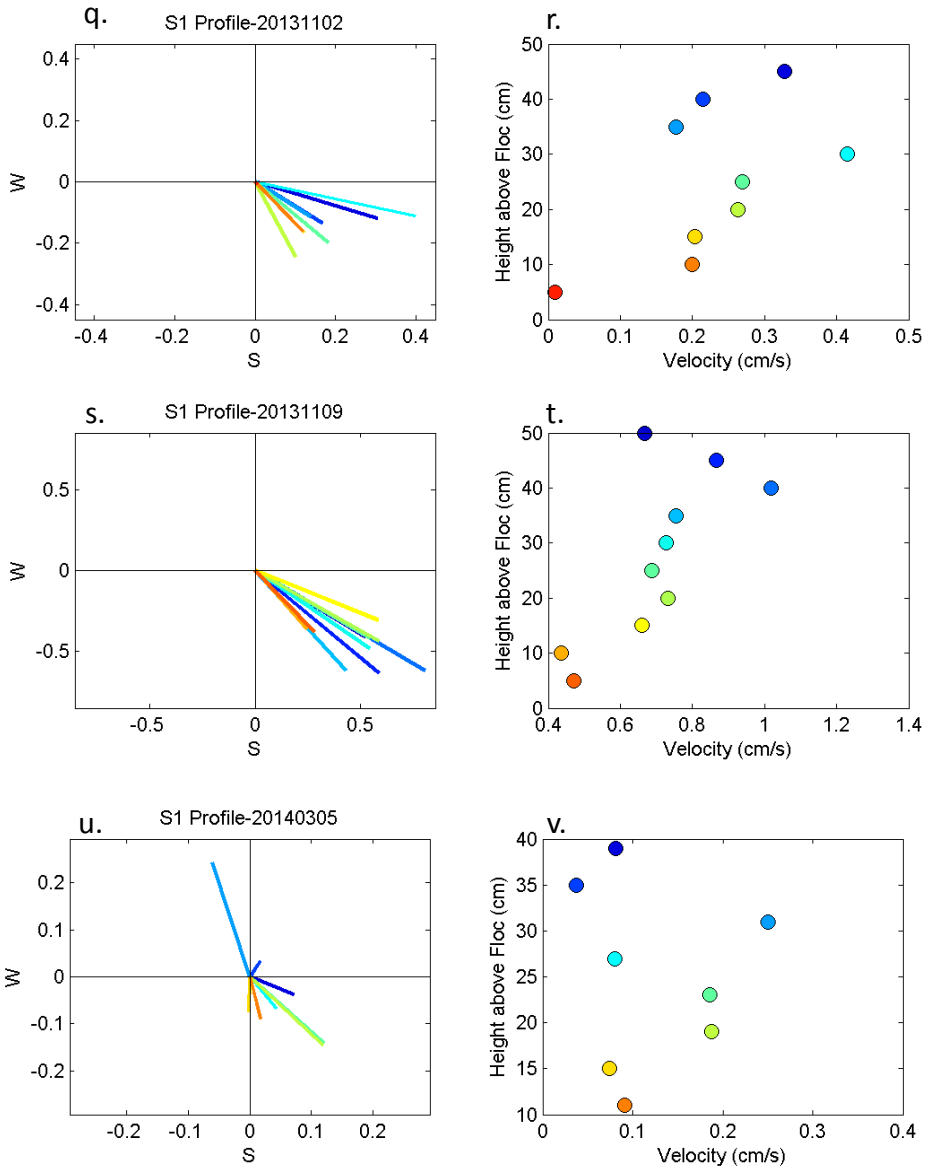

Figure H25. ADV velocity profiles recorded prior to the DPM flow release at site S1. Profiles recorded on (a-b) Jul. 18, 2010, (c-d) Aug. 26, 2010, (e-f) Sep. 28, 2010, (g-h) Nov. 5, 2010, (i-j) Aug. 9, 2012, (k-l) Nov. 5, 2012, and (m-n) Feb. 28, 2013, (o-p) Aug. 13, 2013, (q-r) Nov. 02, 2013, (s-t) Nov. 09, 2013, and (u-v) Mar. 05, 2014. Panels (a), (c), (e), (g), (i), (k), (m), (o), (q), (s) and (u) show velocity vectors (cm/s) with the axes representing cardinal directions, such that the top of the plot is true north. Panels (b), (d), (f), (h), (j), (l), (n), (p), (r), (t) and (v) show horizontal velocities (cm/s). Dates are given in the format yyyymmdd.

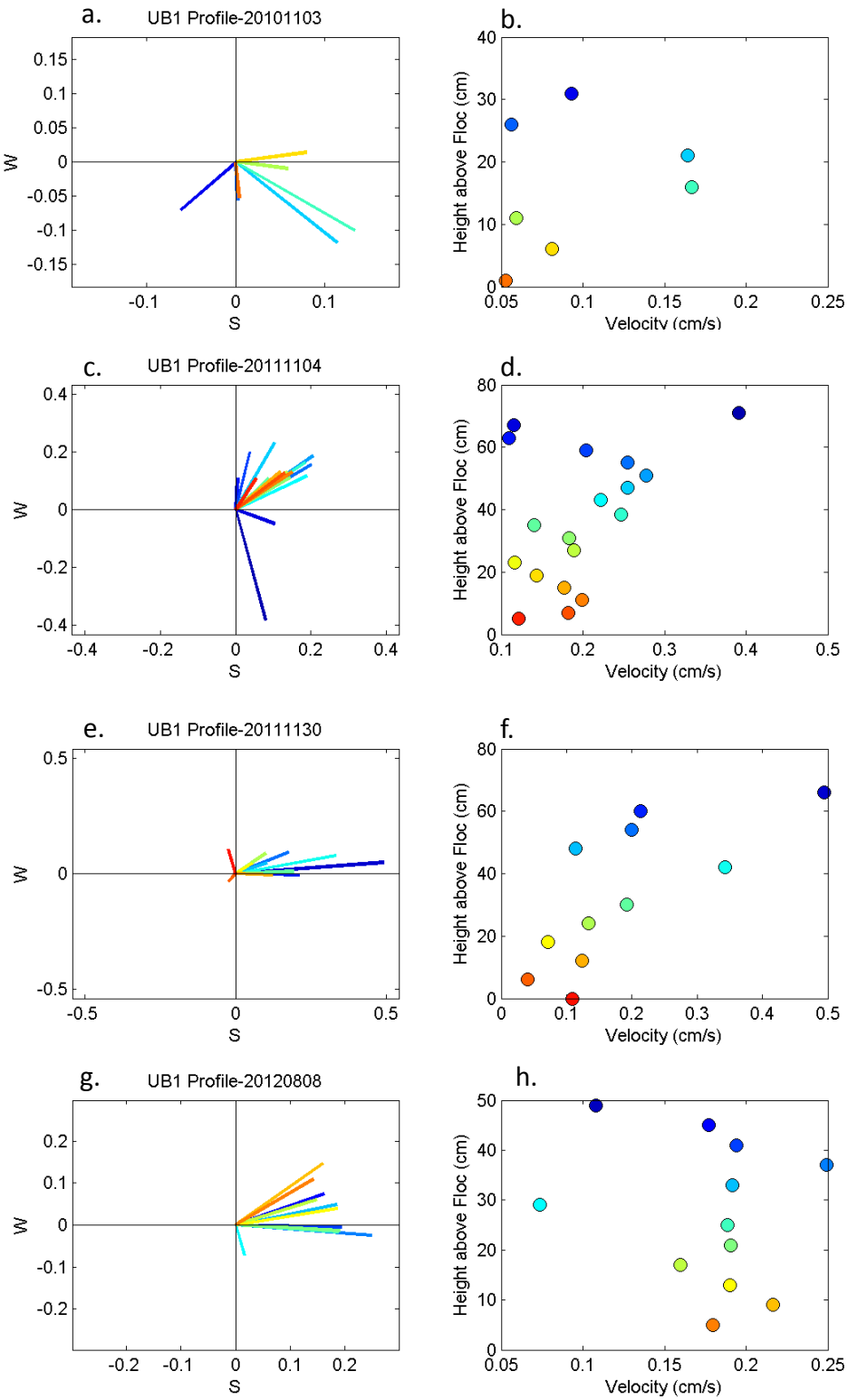
a.
UB1 Profile-20101103
W
S
b.
Height above Floc (cm)
Velocity (cm/s)
c.
UB1 Profile-20111104
W
S
d.
Height above Floc (cm)
Velocity (cm/s)
e.
UB1 Profile-20111130
W
S
f.
Height above Floc (cm)
Velocity (cm/s)
g.
UB1 Profile-20120808
W
S
h.
Height above Floc (cm)
Velocity (cm/s)

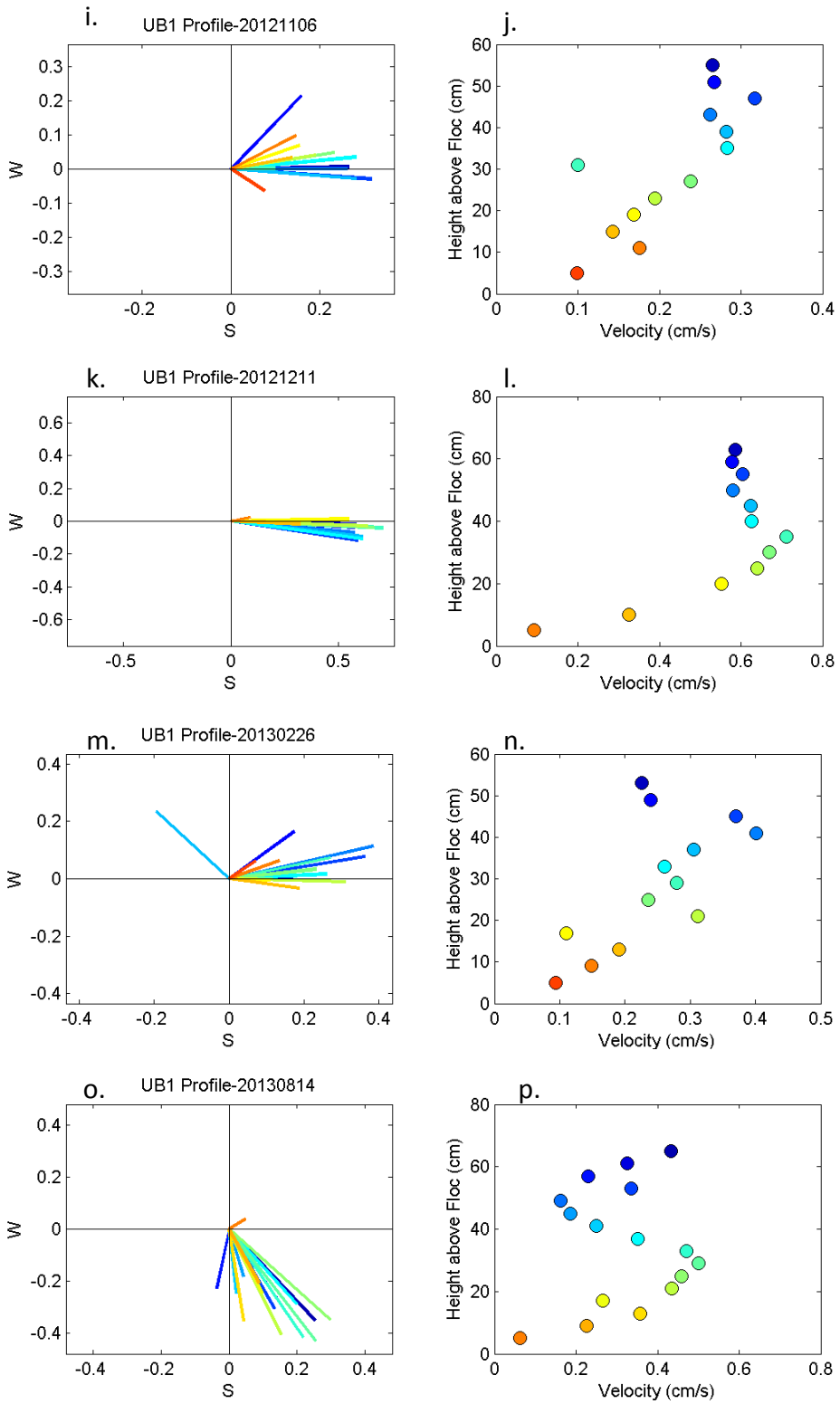
i.
UB1 Profile-20121106
W
S
j.
Height above Floc (cm)
Velocity (cm/s)
k.
UB1 Profile-20121211
W
S
l.
Height above Floc (cm)
Velocity (cm/s)
m.
UB1 Profile-20130226
W
S
n.
Height above Floc (cm)
Velocity (cm/s)
o.
UB1 Profile-20130814
W
S
p.
Height above Floc (cm)
Velocity (cm/s)

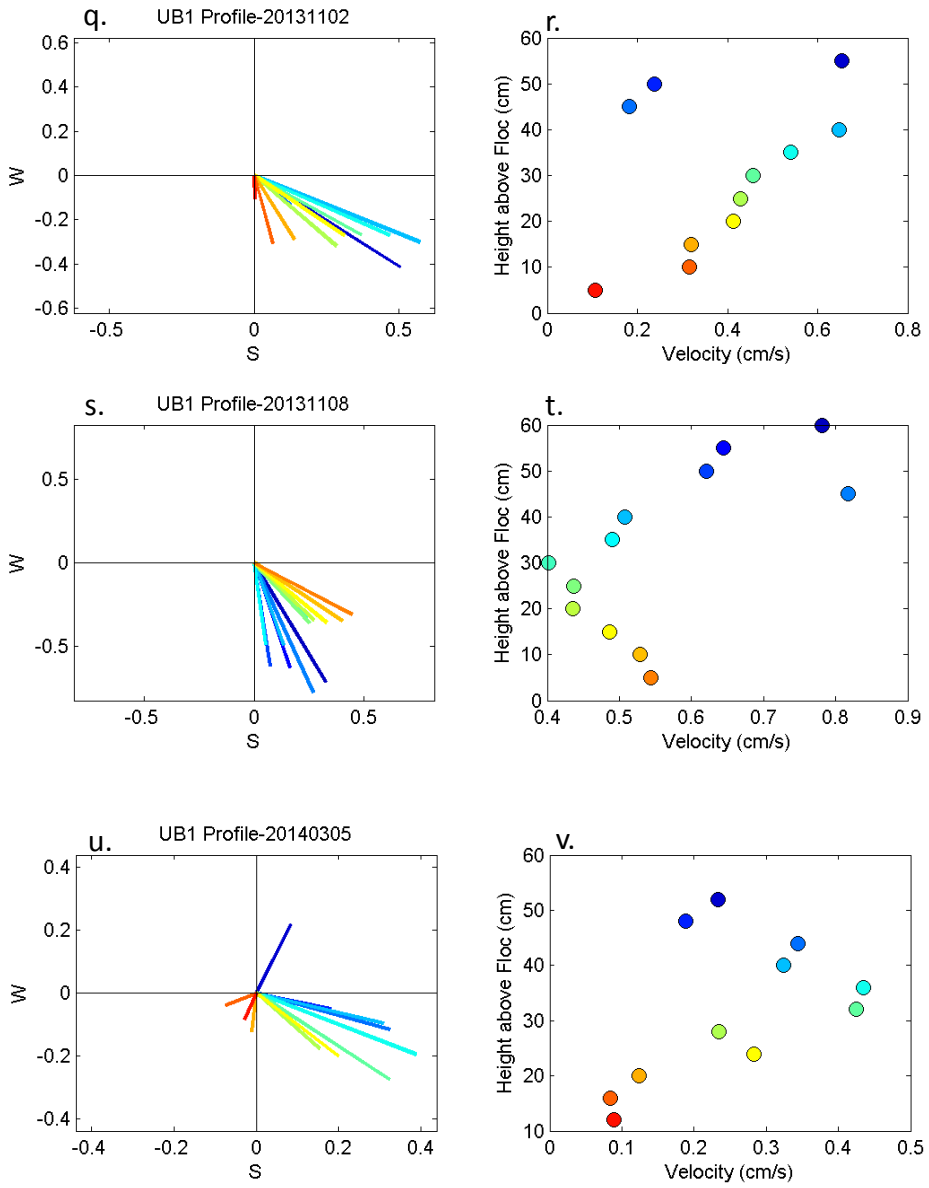

Figure H26. ADV velocity profiles recorded prior to the DPM flow release at site UB1. Profiles recorded on (a-b) Nov. 3, 2010, (c-d) Nov. 4, 2011, and (e-f) Nov. 30, 2011, (g-h) Aug. 8, 2012, (i-j) Nov. 6, 2012, (k-l) Dec. 11, 2012, (m-n) Feb. 26, 2013, (o-p) Aug. 14, 2013, (q-r) Nov. 02, 2013, (s-t) Nov. 08, 2013, and (u-v) Mar. 05, 2014. Panels (a), (c), (e), (g), (i), (k), (m), (o), (q), (s), and (u) show velocity vectors (cm/s) with the axes representing cardinal directions, such that the top of the plot is true north. Panels (b), (d), (f), (h), (j), (l), (n), (p), (r), (t), and (v) show horizontal velocities (cm/s). The profile shown in panels (a) and (b) was recorded on a SonTek Argonaut ADV. Dates are given in the format yyyymmdd.

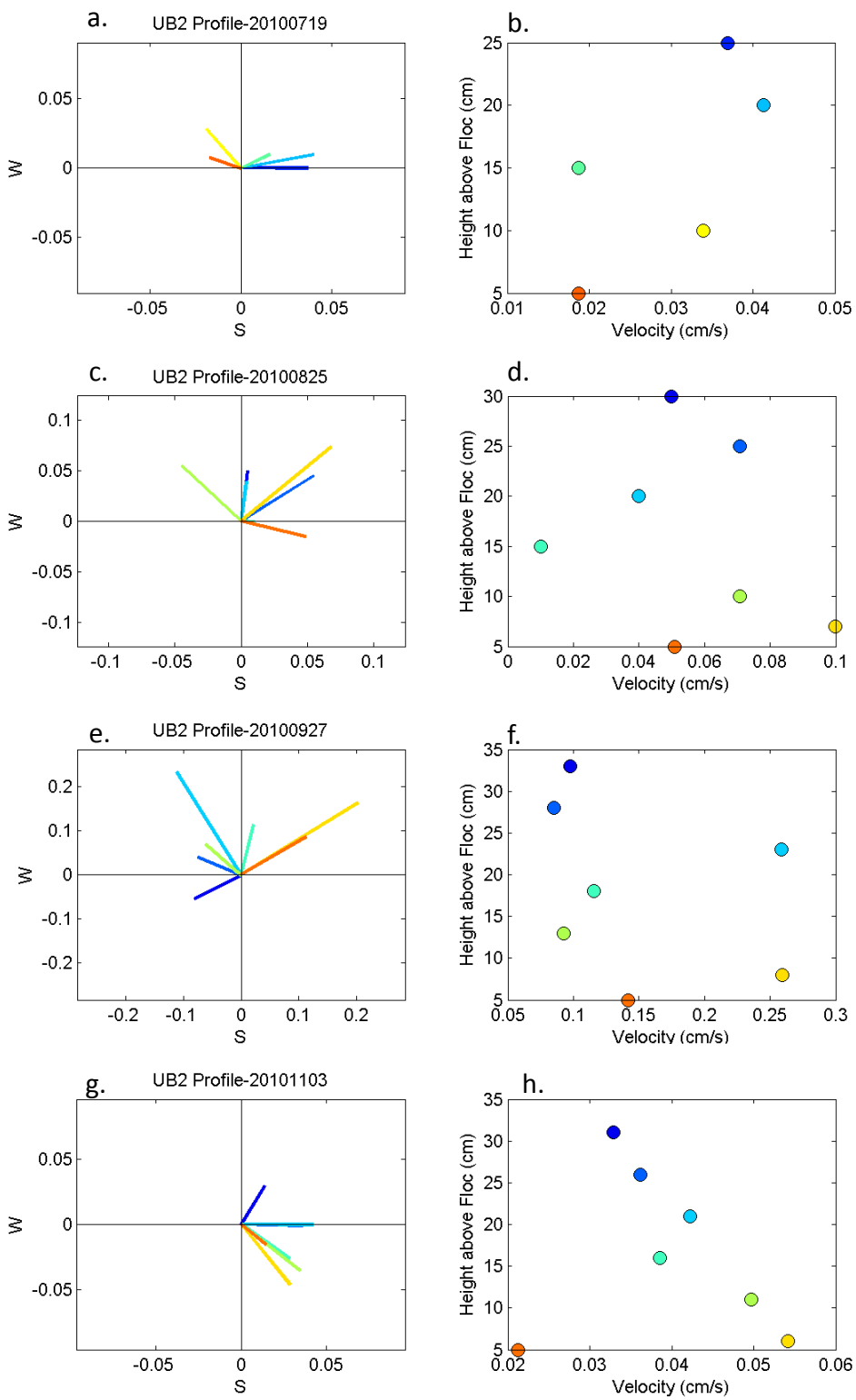
a.
UB2 Profile-20100719
W
S
b.
Height above Floc (cm)
Velocity (cm/s)
c.
UB2 Profile-20100825
W
S
d.
Height above Floc (cm)
Velocity (cm/s)
e.
UB2 Profile-20100927
W
S
f.
Height above Floc (cm)
Velocity (cm/s)
g.
UB2 Profile-20101103
W
S
h.
Height above Floc (cm)
Velocity (cm/s)

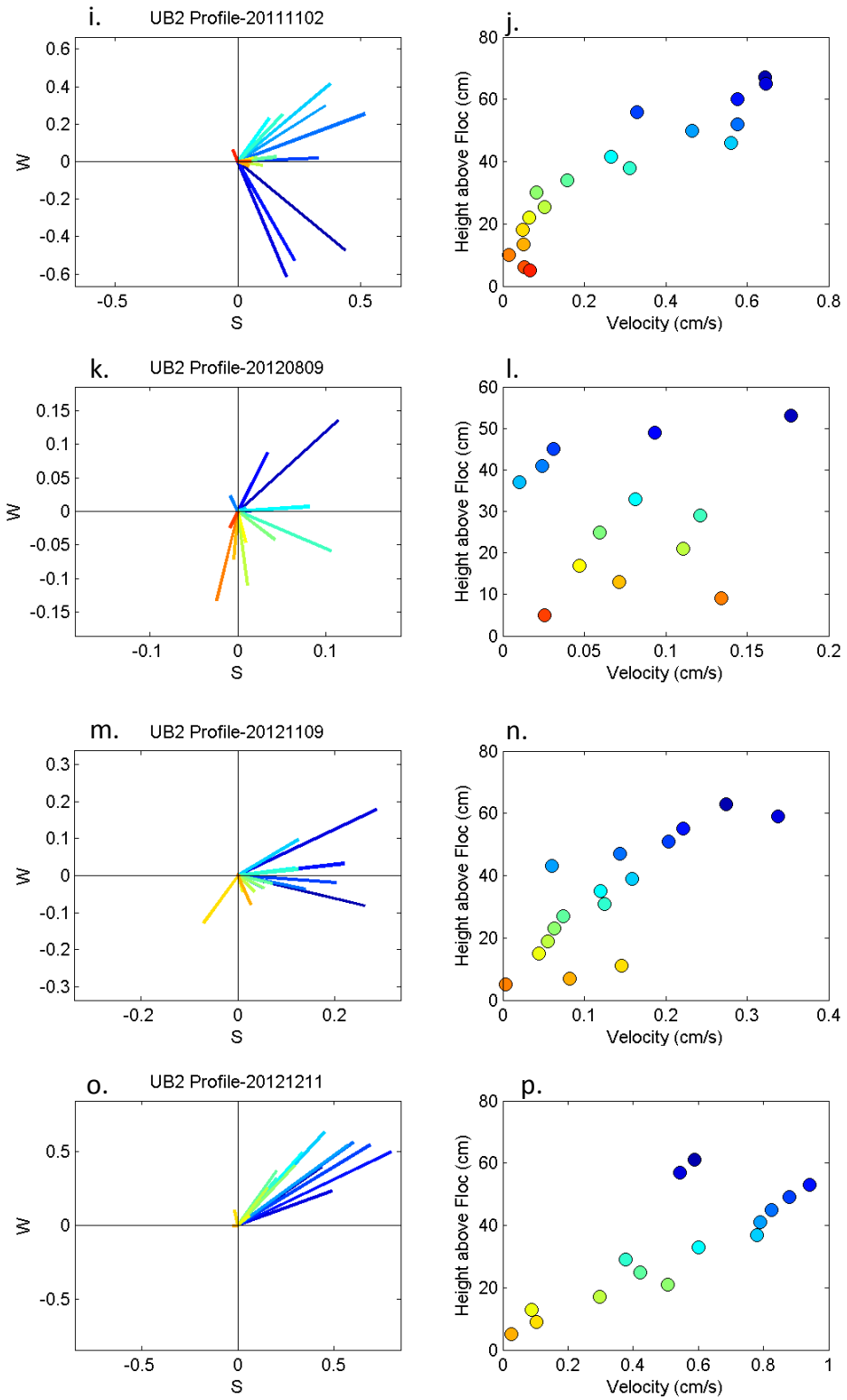
i.
UB2 Profile-20111102
W
S
j.
Height above Floc (cm)
Velocity (cm/s)
k.
UB2 Profile-20120809
W
S
l.
Height above Floc (cm)
Velocity (cm/s)
m.
UB2 Profile-20121109
W
S
n.
Height above Floc (cm)
Velocity (cm/s)
o.
UB2 Profile-20121211
W
S
p.
Height above Floc (cm)
Velocity (cm/s)

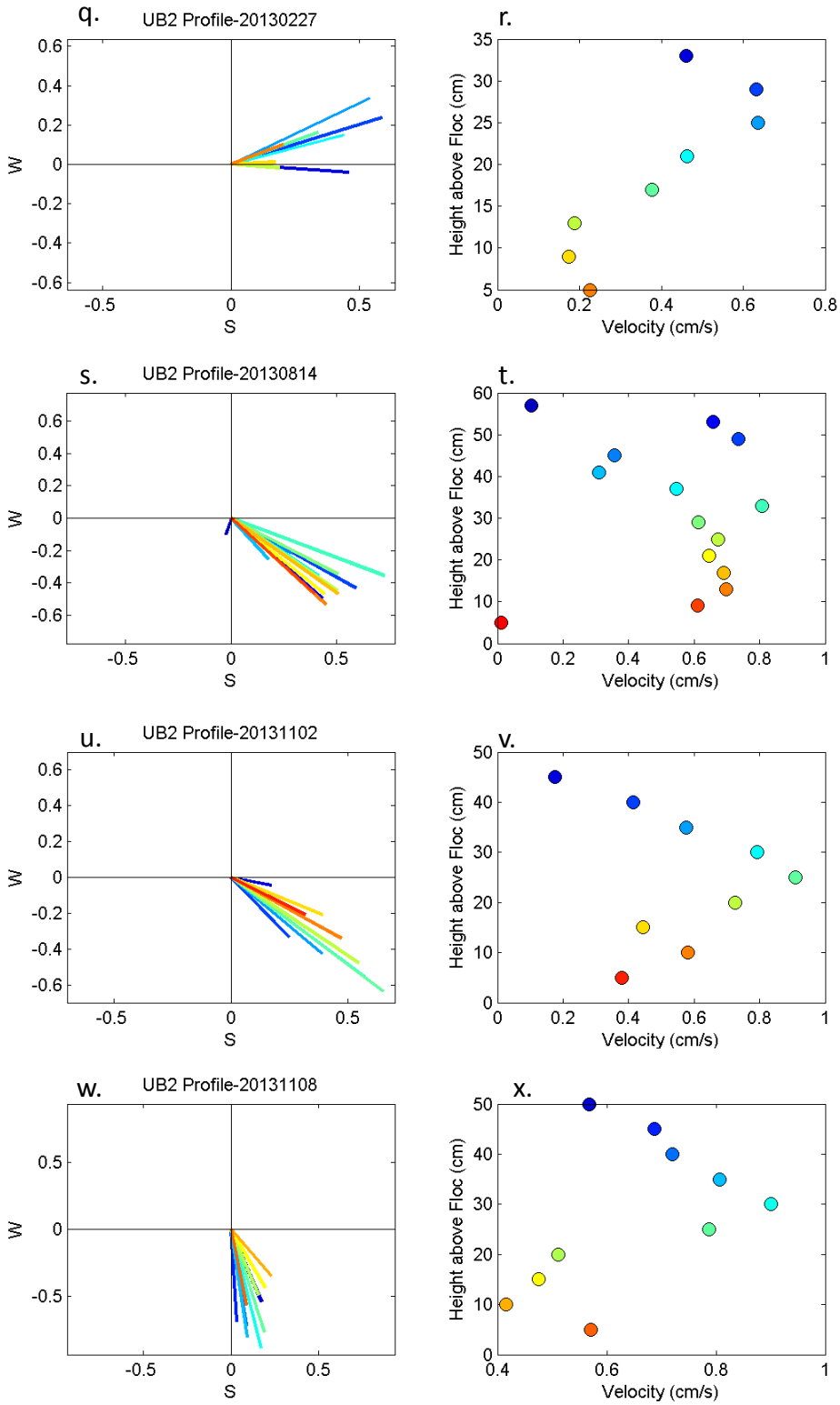
q.
UB2 Profile-20130227
W
S
r.
Height above Floc (cm)
Velocity (cm/s)
s.
UB2 Profile-20130814
W
S
t.
Height above Floc (cm)
Velocity (cm/s)
u.
UB2 Profile-20131102
W
S
v.
Height above Floc (cm)
Velocity (cm/s)
w.
UB2 Profile-20131108
W
S
x.
Height above Floc (cm)
Velocity (cm/s)

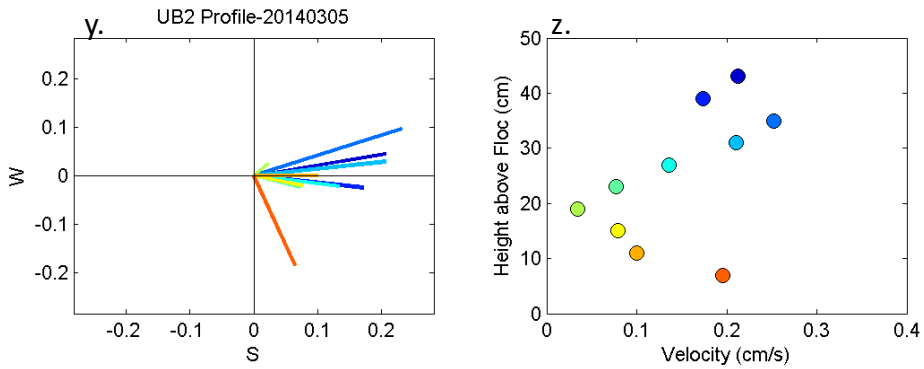

Figure H27. ADV velocity profiles recorded prior to the DPM flow release at UB2. Profiles recorded on (a-b) Jul. 19, 2010, (c-d) Aug. 25, 2010, (e-f) Sep. 27, 2010, (g-h) Nov. 3, 2010, (i-j) Nov. 2, 2011, (k-l) Aug. 9, 2012, (m-n) Nov. 9, 2012, (o-p) Dec. 11, 2012, (q-r) Feb. 27, 2013, (s-t) Aug. 14, 2013, (u-v) Nov. 02, 2013, (w-x) Nov. 08, 2013, and (y-z) Mar. 05, 2014. Panels (a), (c), (e), (g), (i), (k), (m), (o), (q), (s), (u), (w), and (y) show velocity vectors (cm/s) with the axes representing cardinal directions, such that the top of the plot is true north. Panels (b), (d), (f), (h), (j), (l), (n), (p), (r), (t), (v), (x), and (z) show horizontal velocities (cm/s). These profiles were recorded on a SonTek Argonaut ADV. Dates are given in the format yyyymmdd.

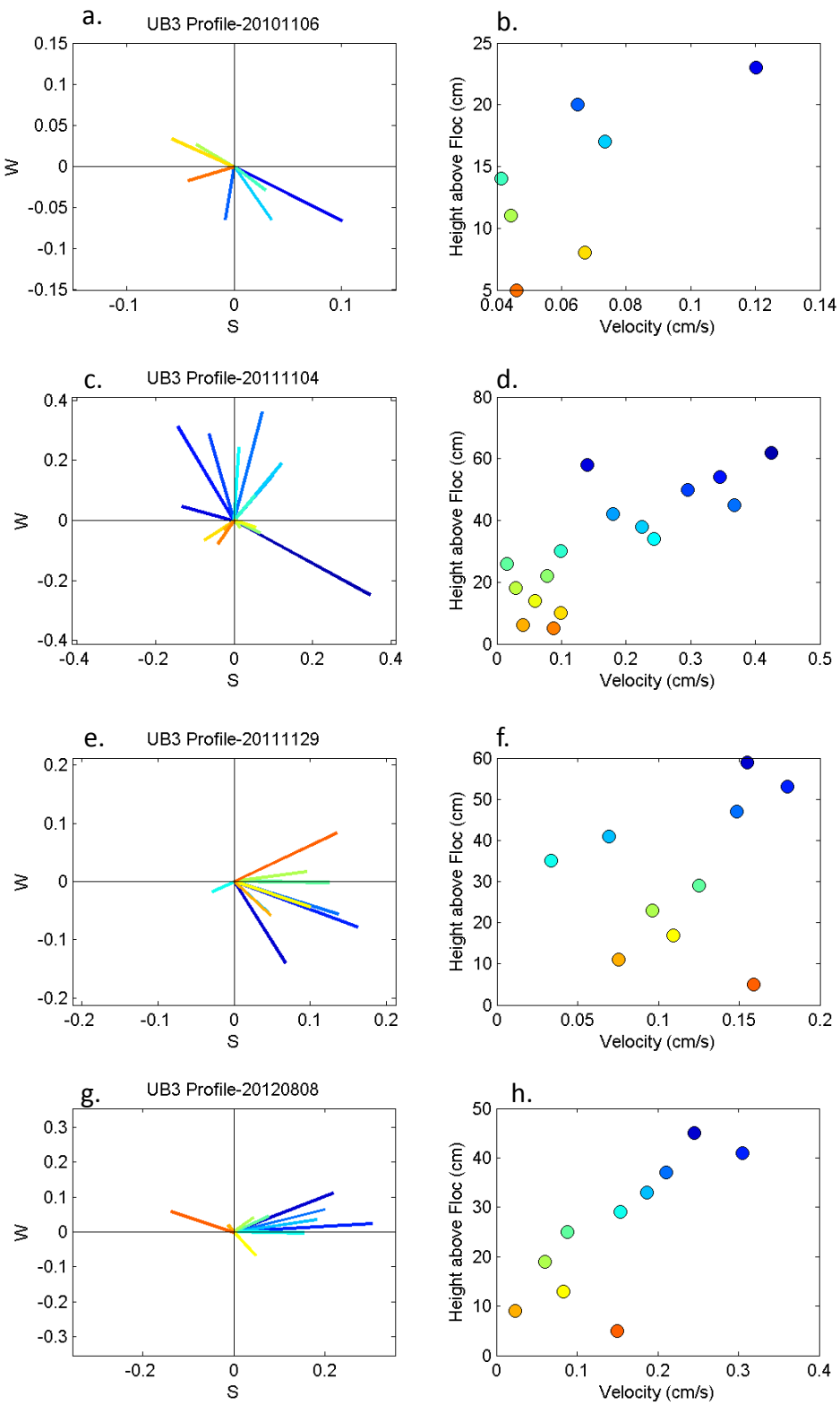
a.
UB3 Profile-20101106
W
S
b.
Height above Floc (cm)
Velocity (cm/s)
c.
UB3 Profile-20111104
W
S
d.
Height above Floc (cm)
Velocity (cm/s)
e.
UB3 Profile-20111129
W
S
f.
Height above Floc (cm)
Velocity (cm/s)
g.
UB3 Profile-20120808
W
S
h.
Height above Floc (cm)
Velocity (cm/s)

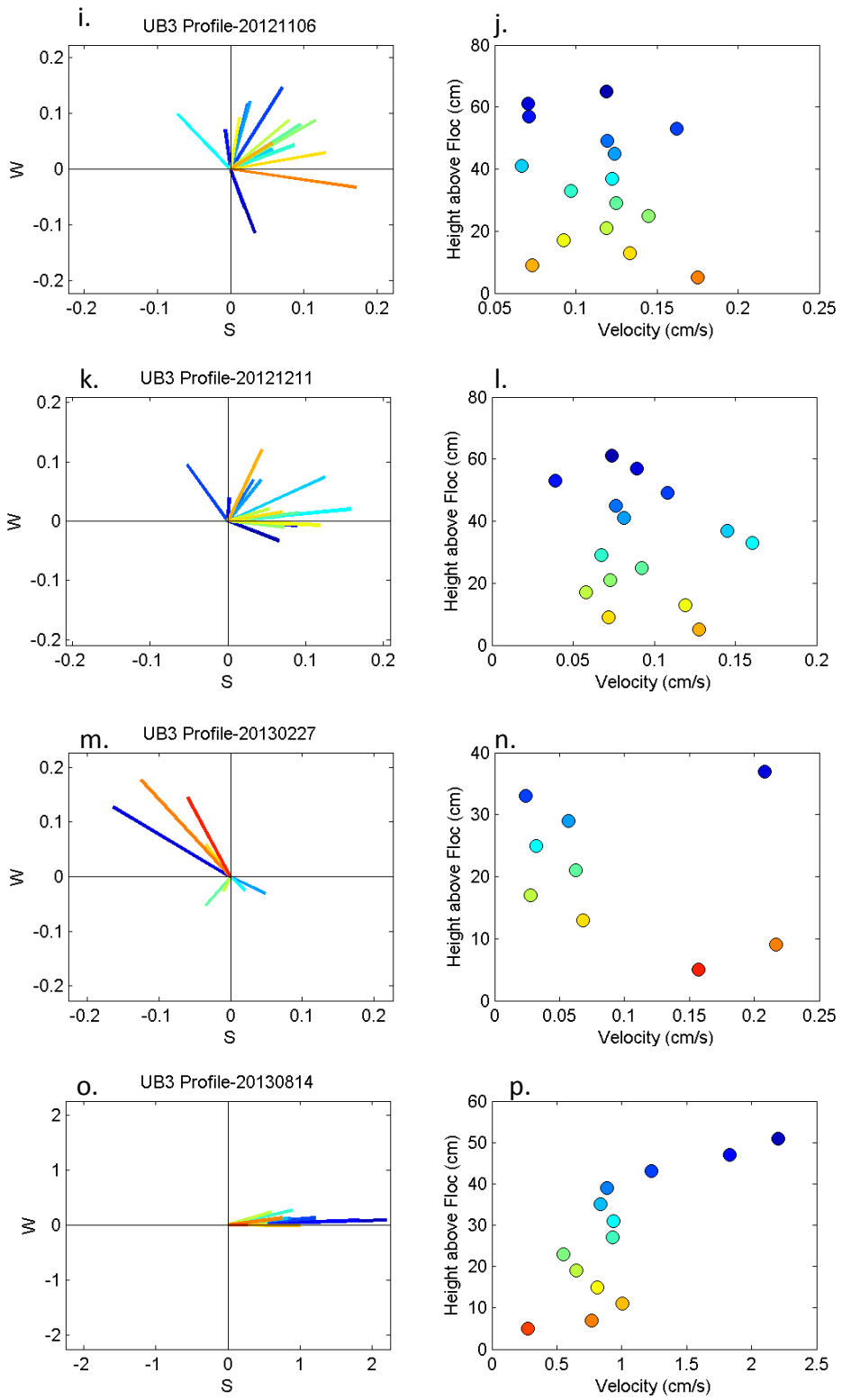
i.
UB3 Profile-20121106
W
S
j.
Height above Floc (cm)
Velocity (cm/s)
k.
UB3 Profile-20121211
W
S
l.
Height above Floc (cm)
Velocity (cm/s)
m.
UB3 Profile-20130227
W
S
n.
Height above Floc (cm)
Velocity (cm/s)
o.
UB3 Profile-20130814
W
S
p.
Height above Floc (cm)
Velocity (cm/s)

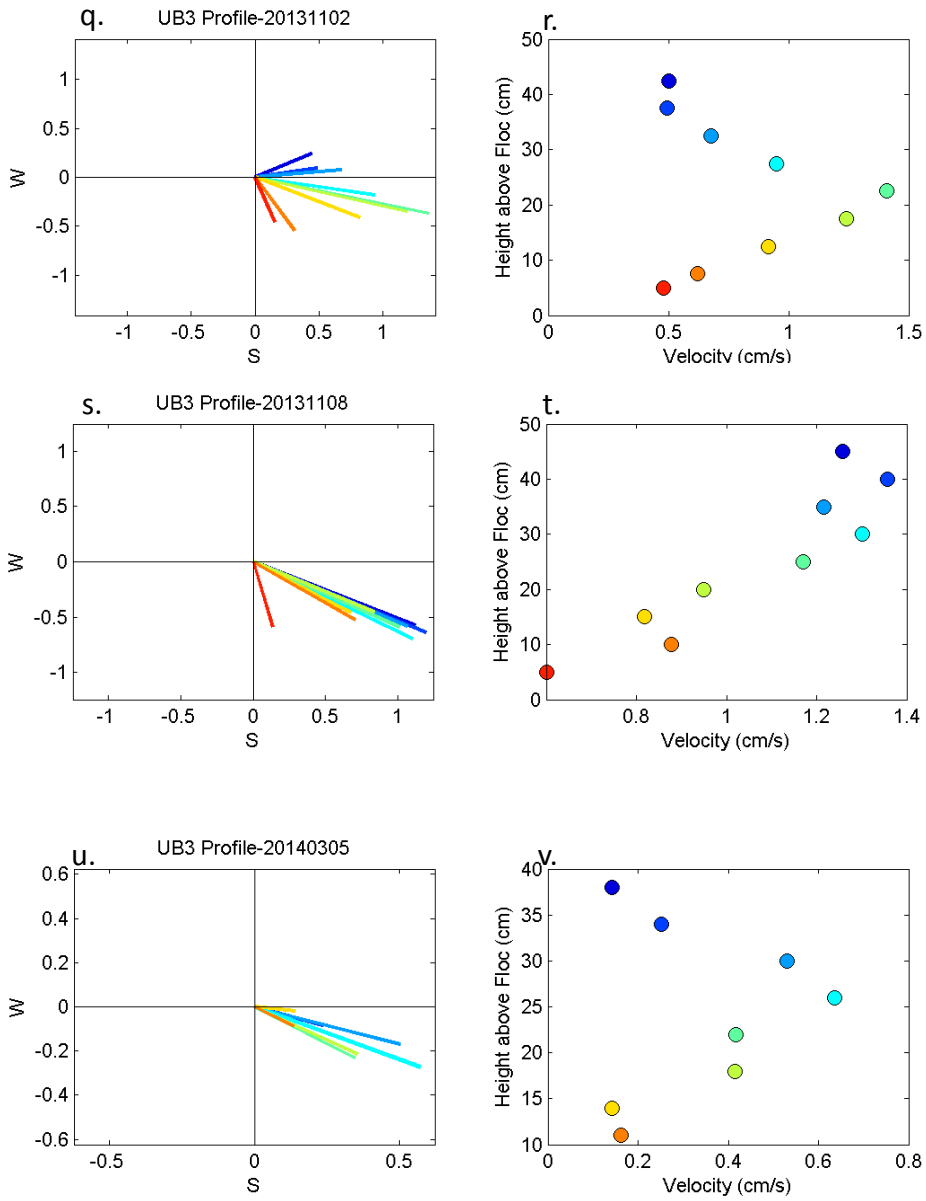

Figure H28. ADV velocity profiles recorded prior to the DPM flow release at site UB3. Profiles recorded on (a-b) Nov. 6, 2010, (c-d) Nov. 4, 2011, (e-f) Nov. 29, 2011, (g-h) Aug. 8, 2012, (i-j) Nov. 6, 2012, (k-l) Dec. 11, 2012, and (m-n) Feb. 27, 2013, (o-p) Aug. 13, 2013, (q-r) Nov. 02, 2013, (s-t) Nov. 08, 2013, (u-v) Mar. 05, 2014. Panels (a), (c), (e), (g), (i), (k), (m), (o), (q), (s), and (u) show velocity vectors (cm/s) with the axes representing cardinal directions, such that the top of the plot is true north. Panels (b), (d), (f), (h), (j), (l), (n), (p), (r), (t), and (v) show horizontal velocities (cm/s). The profile shown in panels (a) and (b) was recorded on a SonTek Argonaut ADV. Dates are given in the format yyyymmdd.

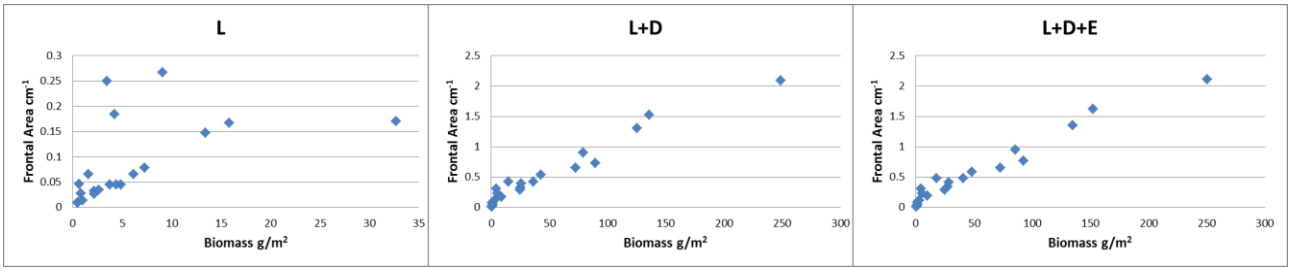

Figure H29. Plots of measured vegetation frontal area vs. biomass for (a) the live portion, (b) live and dead, and (c) live, dead, and epiphyton.

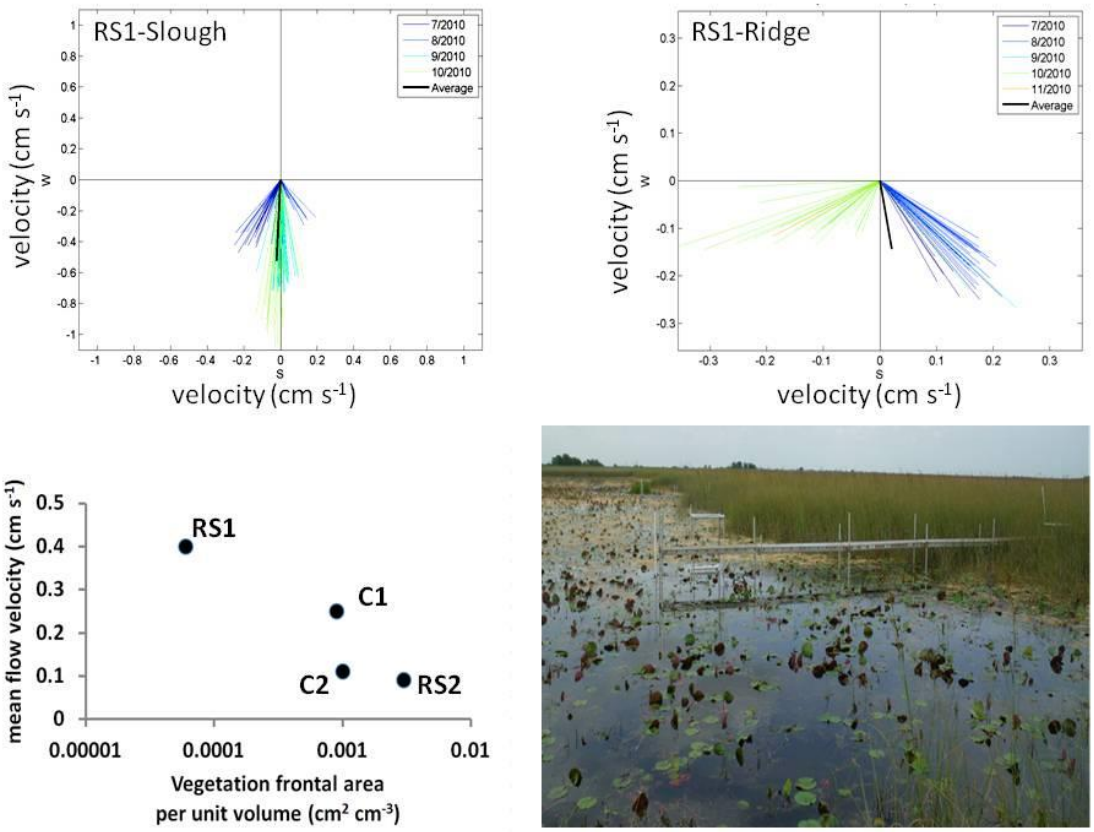

Figure H30. Water velocity and direction data in adjacent slough (top left) and ridge (top right) habitats at RS-1; and cross-site variation in mean flow velocity as a function of biomass frontal area (bottom left). The RS-1 boardwalk spanning the slough and ridge shown in the photo (facing North). ADV data are presented as daily means from July to November 2010.

Figures – Hydrology (H31-41)

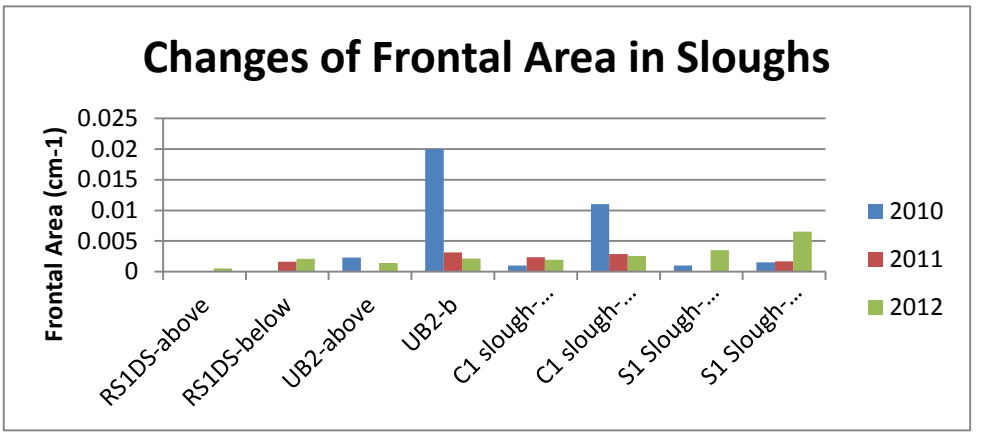

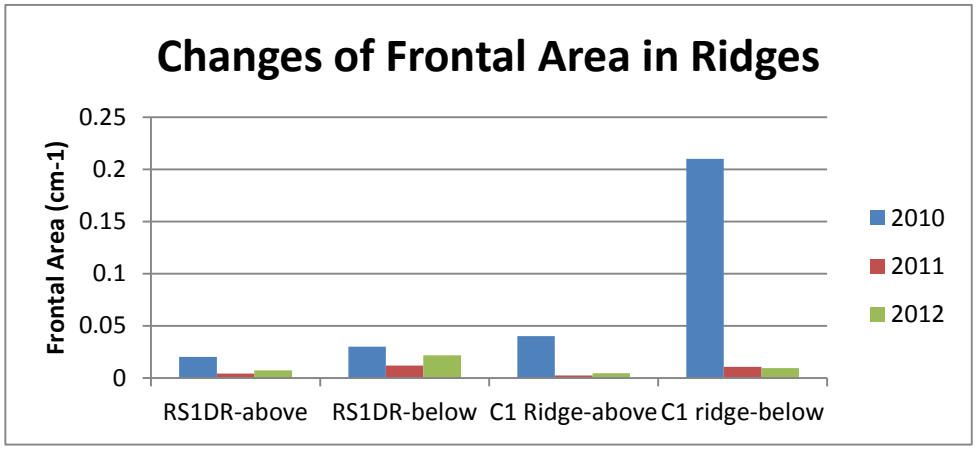

Figure H31. Changes in frontal area from 2010 to 2012 in a) slough environments and b) ridge environments. Both communities experienced signficant declines in frontal area after the fire.

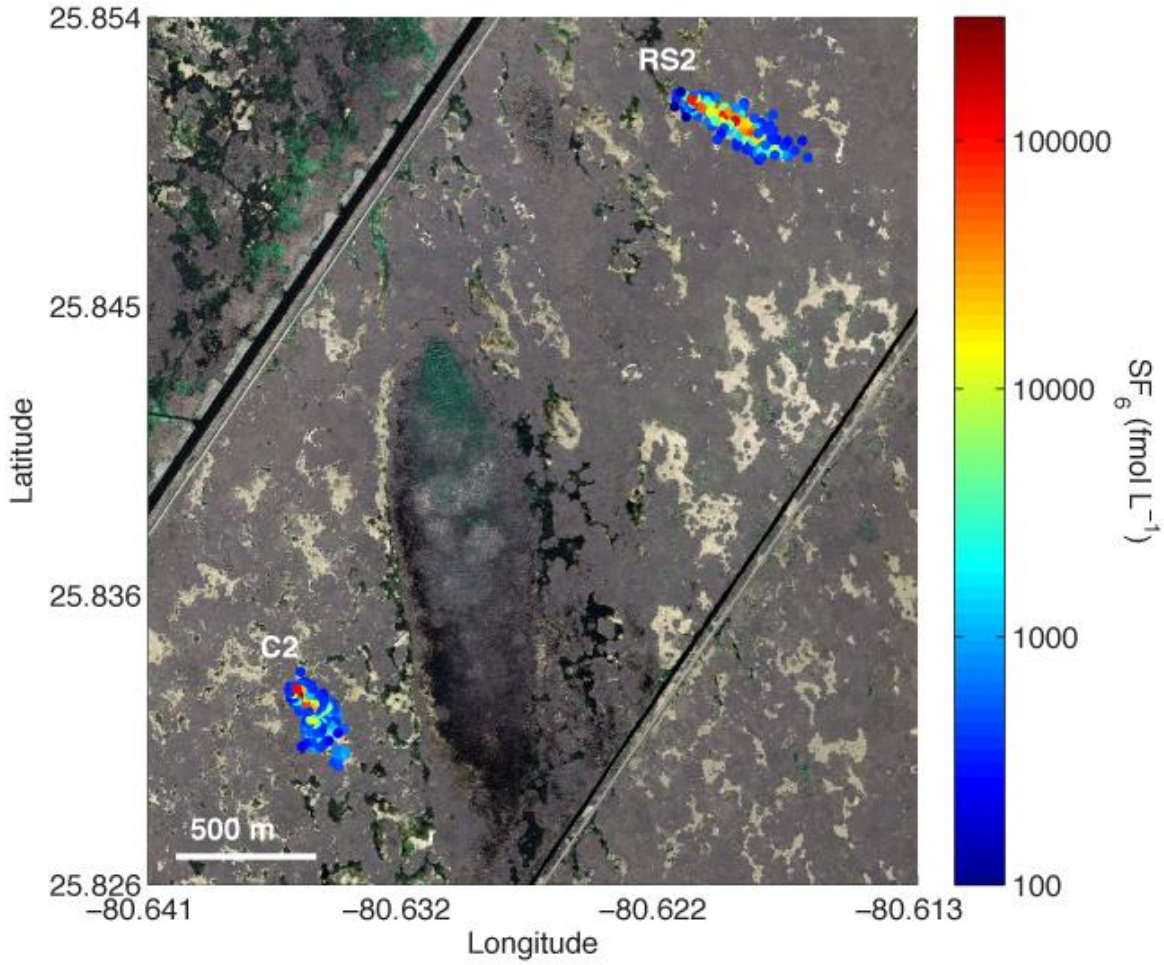

Figure H32. Composite of SF6 tracer measurements made in November 2010 at RS2 (EverTREx 7) and C2 (EverTREx 8).

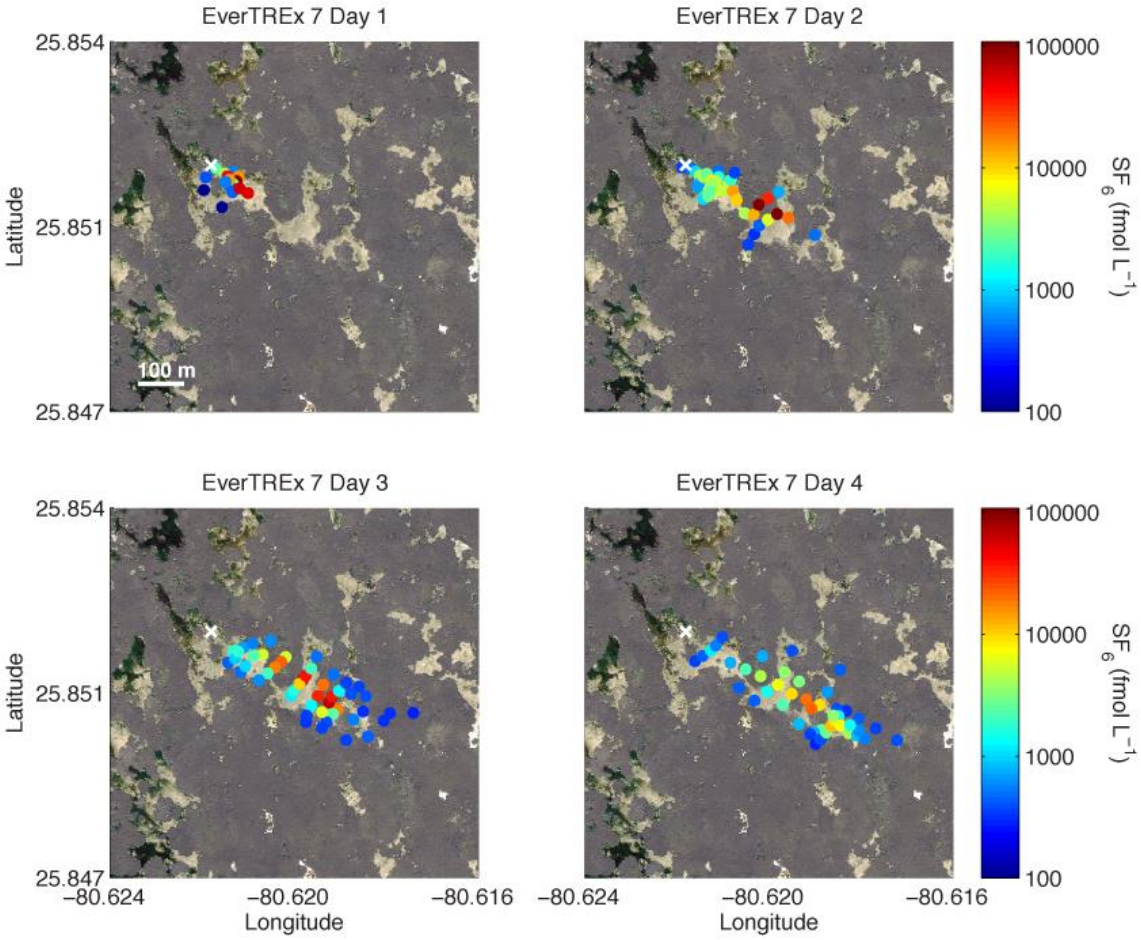

Figure H33. SF6 evolution at RS2 during EverTREx 7 (4-8 November 2010). SF6 was injected on Day 0 and measured for 4 consecutive days. White cross indicates the injection location.

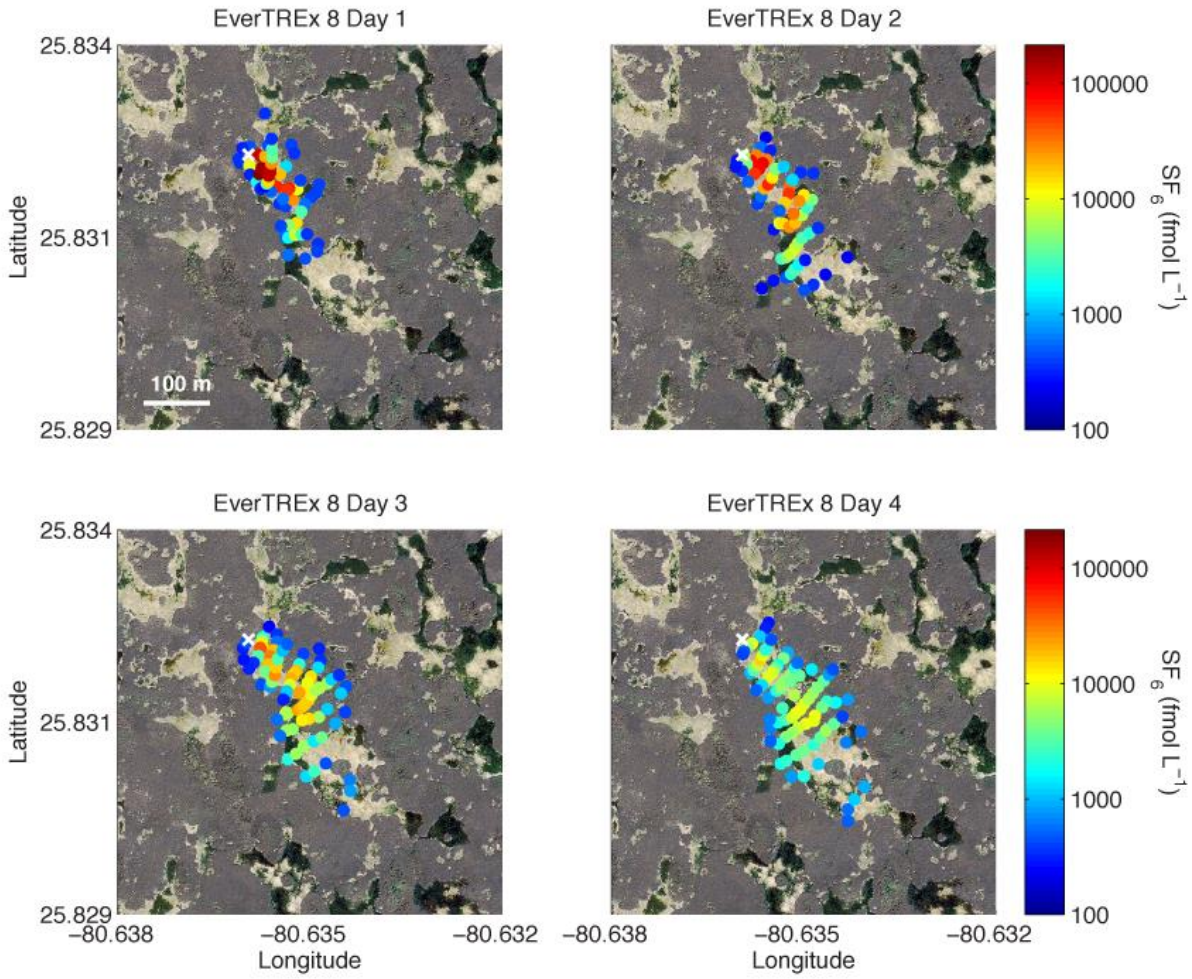

Figure H34. SF6 evolution at C2 during EverTREx 8 (8-12 November 2010). SF6 was injected on Day 0 and measured for 4 consecutive days. White cross indicates the injection location.

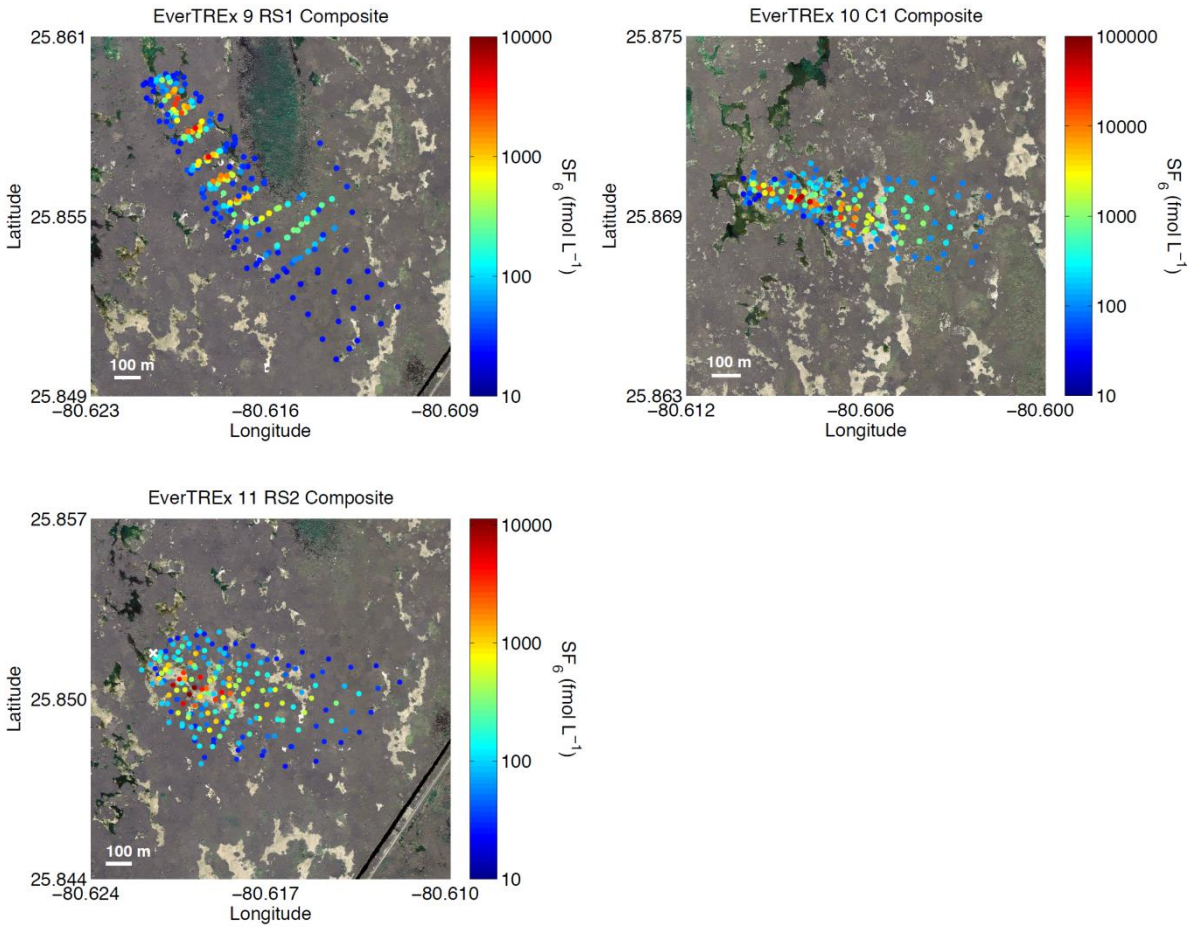

Figure H35. Composite of SF6 tracer measurements made in December 2011 at RS1, C1 and RS2.

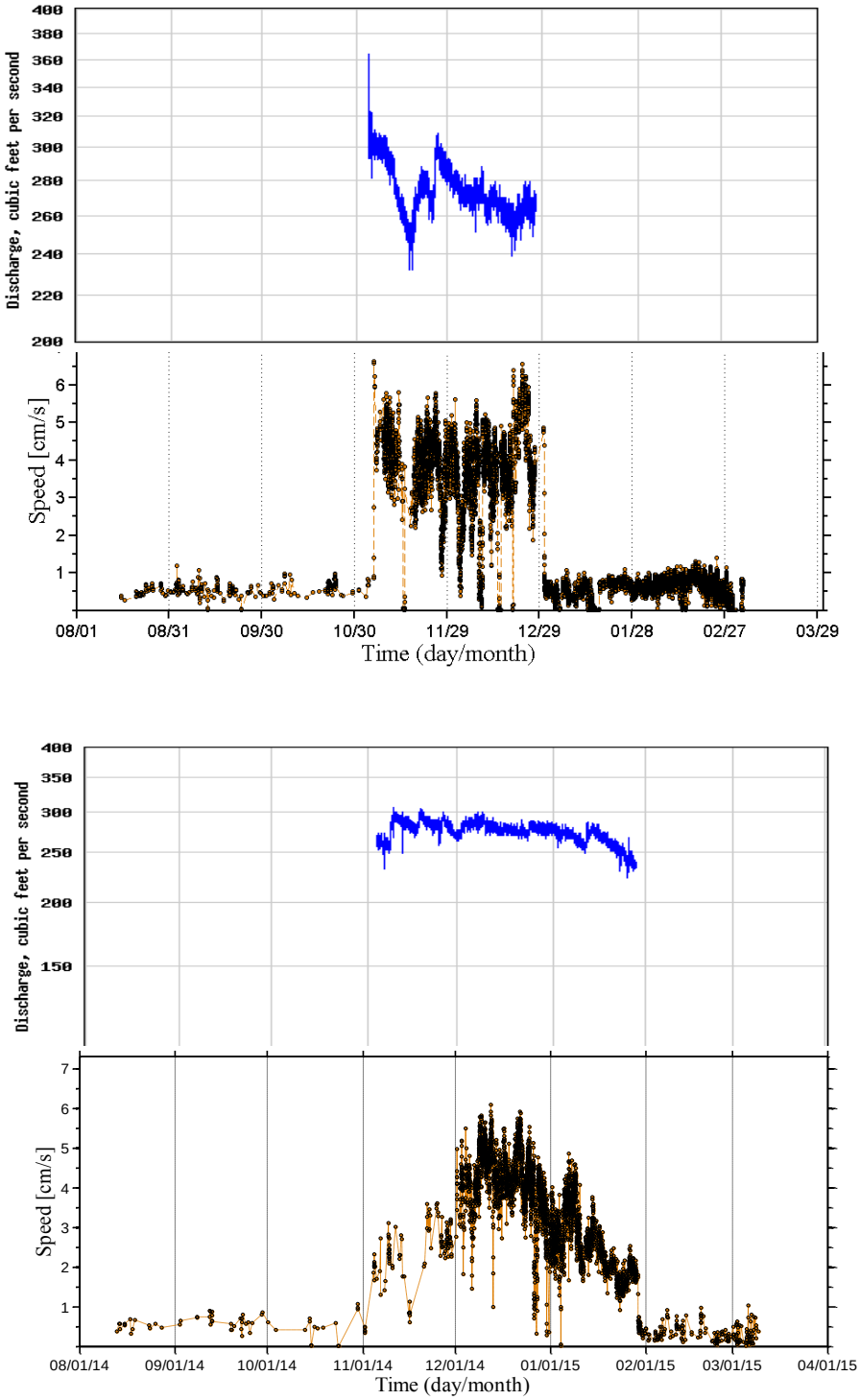

Figure H36. Discharge measurements at the outlet, or east end, of S152 and continuously sampled burst average ADV flow speed (cm s^{-1}) recorded at RS1DS from 8/1/2013 – 3/31/2014 (top 2 graphs) and from 8/1/2014 – 3/31/2015 (bottom 2 graphs).

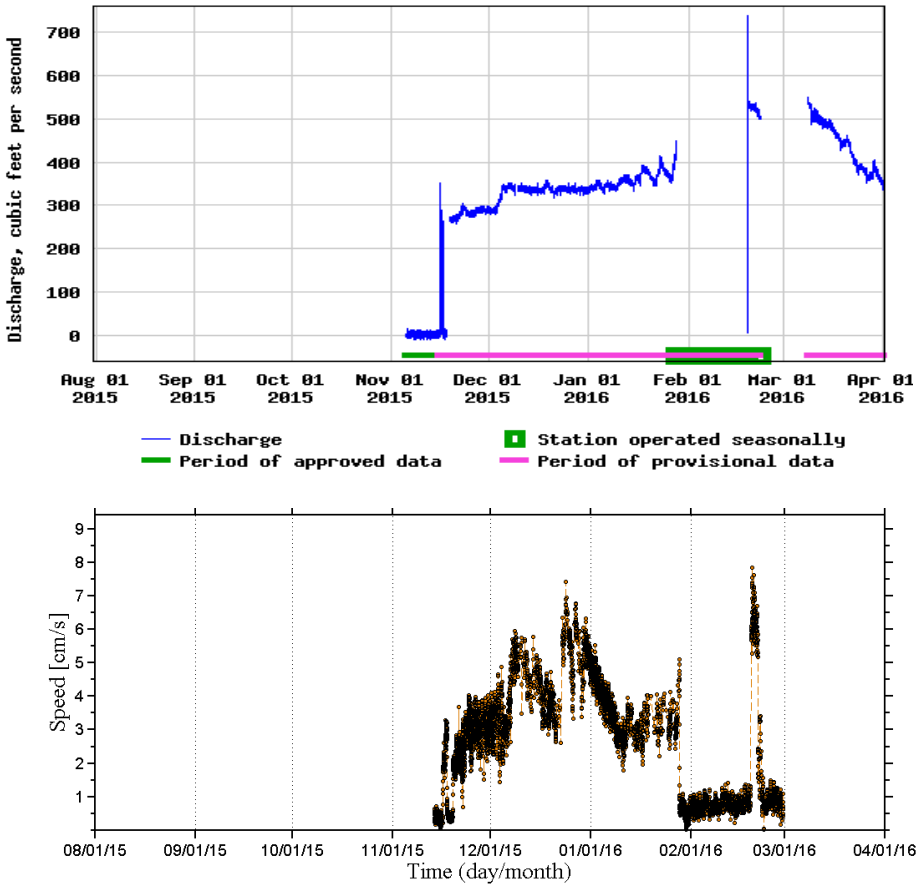

Figure H37. Discharge measurements at the outlet, or east end, of S152 during the 2015-2016 experiment (National Water Information System, 2015) and (bottom) continuously sampled burst average ADV flow speed (cm s^{-1}) recorded at RS1DS site during water year 2015 (8/1/2015 – 3/31/2016). Processing of ADV data after 3/31/16 from RS1DS is ongoing and therefore omitted. The large variation in S152 discharge in February indicates high, hourly variability associated with opening the structure; however, all S152 data shown should be considered provisional at this time.

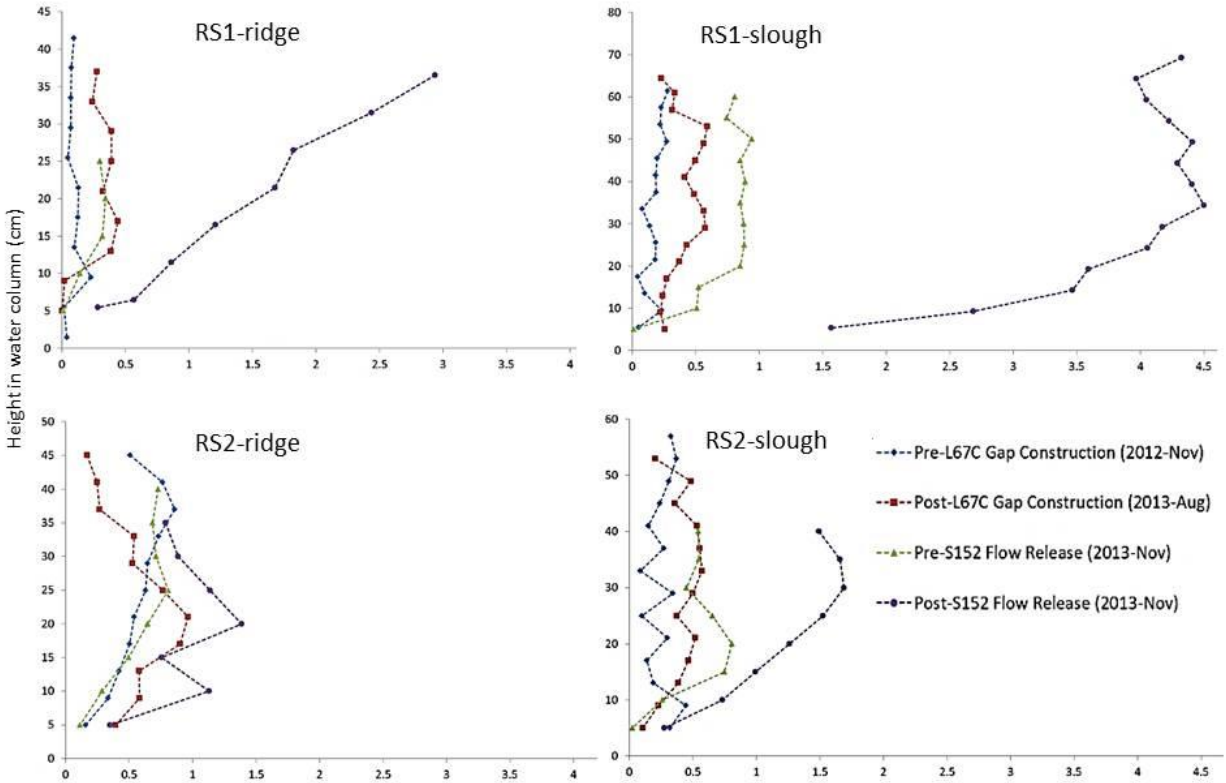

Figure H38. ADV-based velocities at RS1 (Left) and RS2 (Right) before and after flow was initiated through the S-152 structure in November 2013. Values, averaged per depth interval, are from sampling performed on one day in each of the periods indicated.

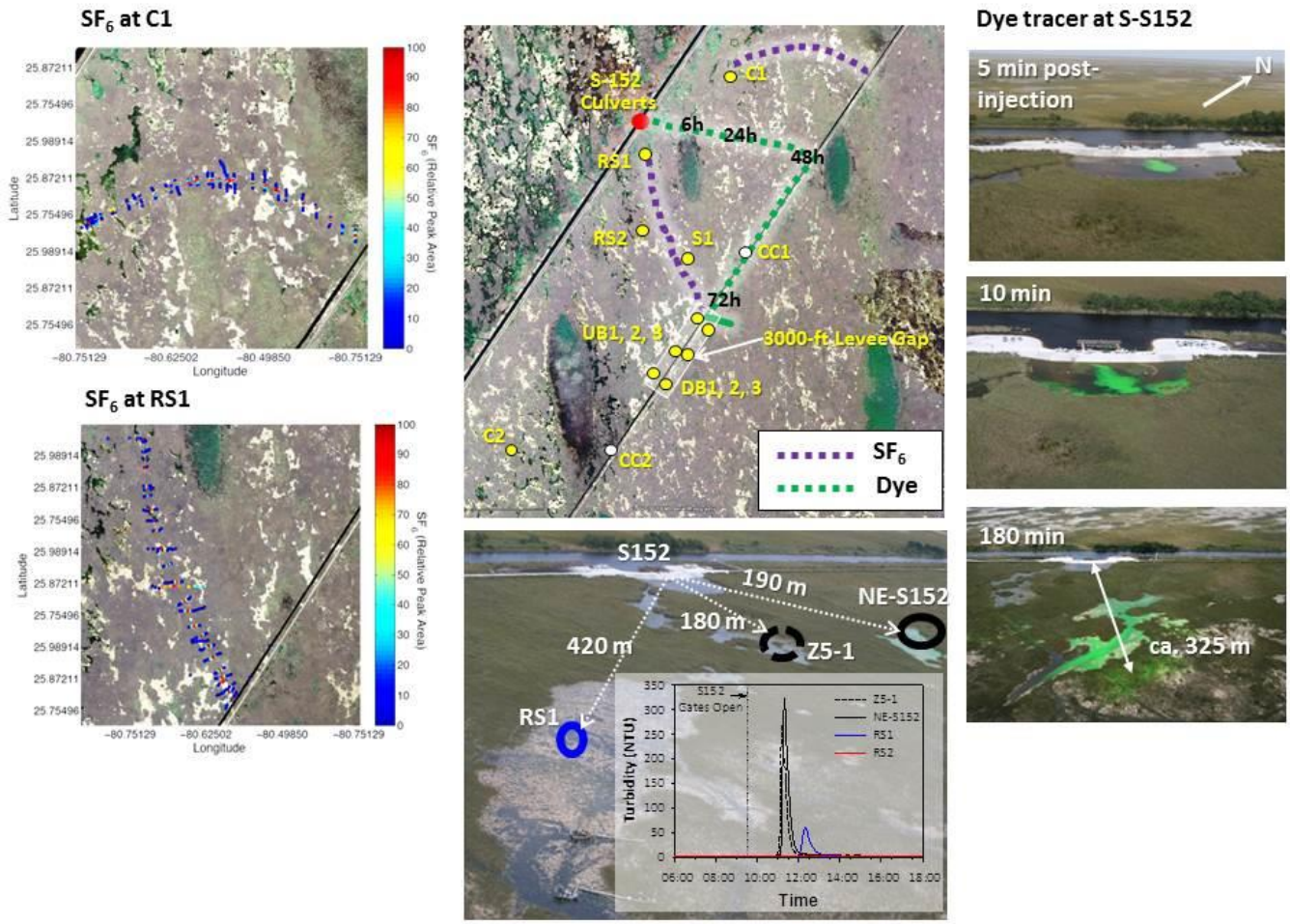

Figure H39. (Left column) Flowpaths of SF_6 at C1 and RS1. (Right column) Photographs of dye movement shortly after the opening of the S-152 culverts on November 5th, 2013. (Center - Top) Map of DPM study area showing sentinnel sites (circled) and flowpaths of SF_6 and dye from November 5 – 15th. Approximate locations of dye front after 6, 24, 48 and 72 hours post-injection are superimposed on flowpath. (Center – Bottom) Turbidity peaks measured at select sites on November 5th.

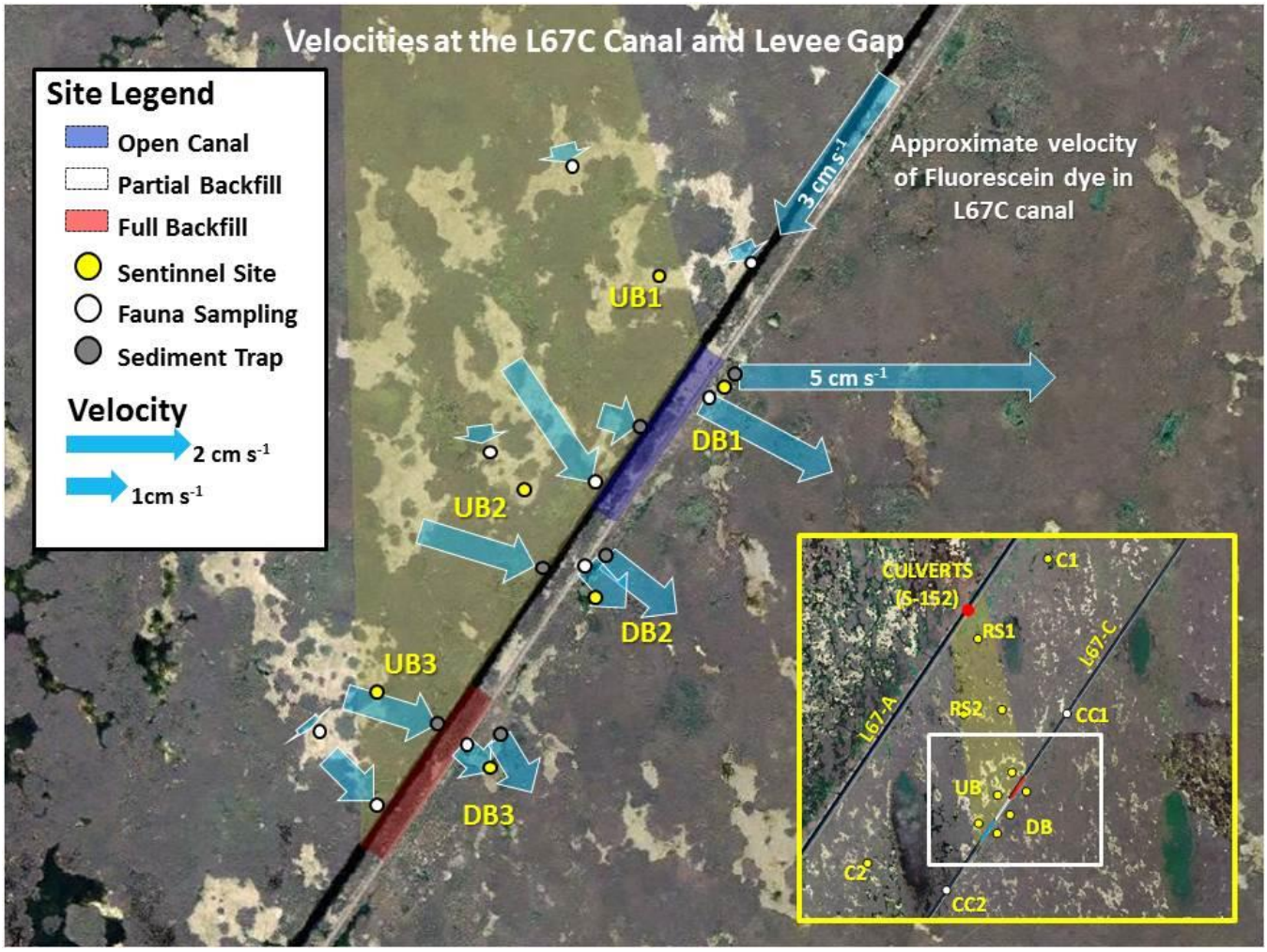

Figure H40. Flow vectors around the L67C canal & levee. Sampling points upstream of the canal are represented by arrow heads. Sampling points downstream of the canal are indicated by arrow tails. Inset map shows study area in relation to the entire DPM study. Flow vectors are ADV-based, with the exception of canal flow (based on dye movement, **Fig. H39**).

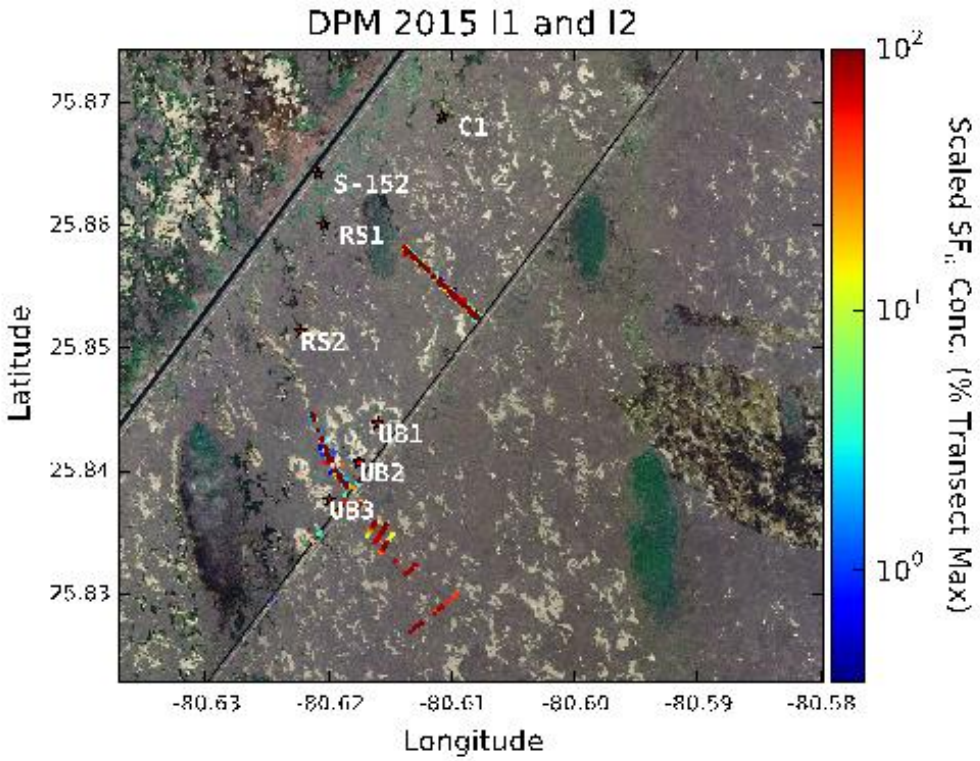

Figure H41. Composite of SF_6 tracer measurements made in December 2015, including a deployment site southwest of RS2 and another deployment southeast of RS1.

Figures – Water Quality (WQ1-13)

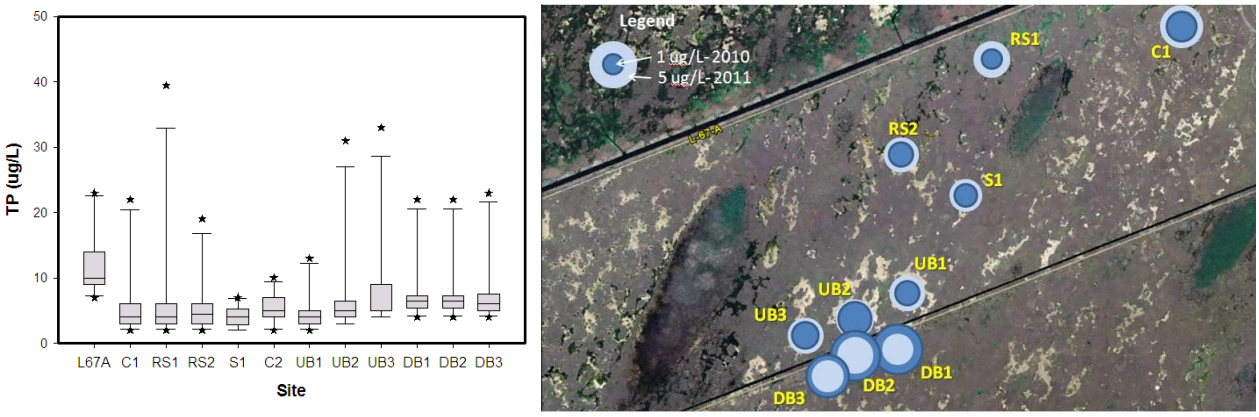

Figure WQ1. Summary of water quality parameters in the DPM. Left graph: Box plot of water column total phosphorus concentrations obtained at mid-water column from slough sites within the DPM footprint (includes data from October 2010 to January 2012). The top and bottom boundary of the box indicate the 75th and 25th percentiles, the line within the box marks the median, whiskers (error bars) above and below the box indicate the 90th and 10th percentiles and stars denote outliers from the 90th and 10th percentiles. Right: Spatial and temporal distribution of total particulate phosphorus. The size of the circle indicates the TPP concentration while the color denotes the year; dark blue= 2010, light blue=2011.

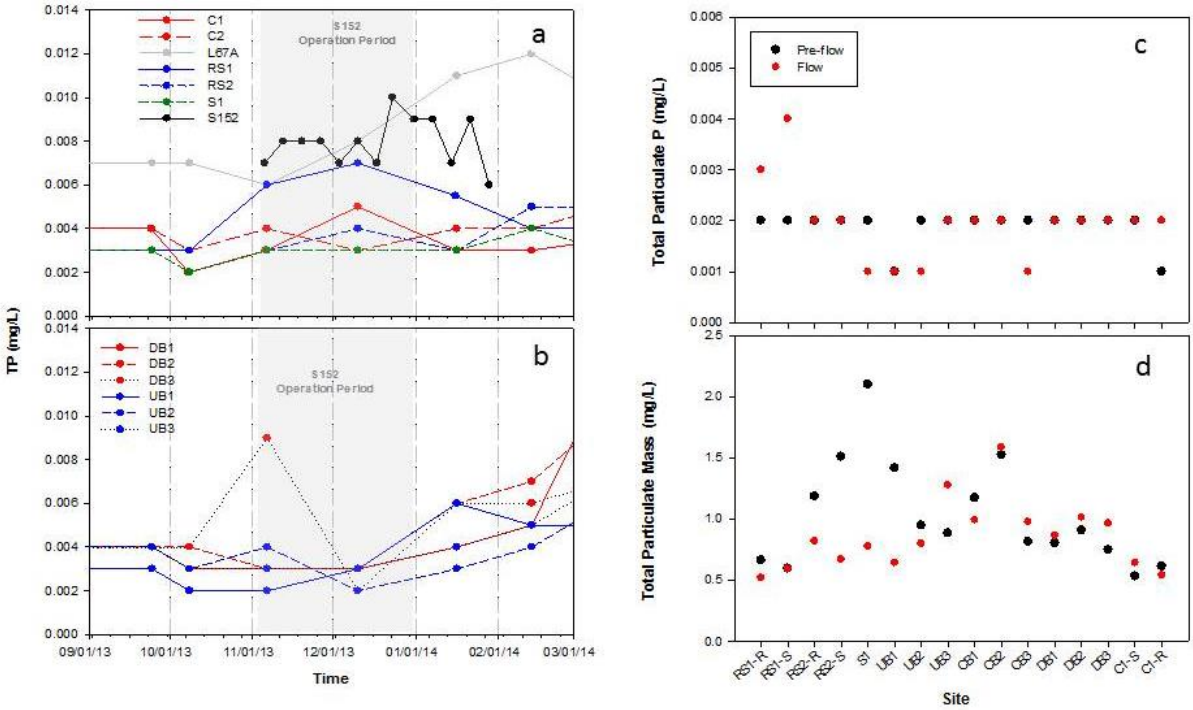

Figure WQ2. (a and b) Temporal TP concentrations in surface waters pre-, during and post-operation of the S-152. Total particulate P concentrations (c) and total mass (d) measured mid-water column depth at sites throughout the DPM project, pre and during flow. -R indicates ridge, -S slough, and CB sites are canal backfill sites.

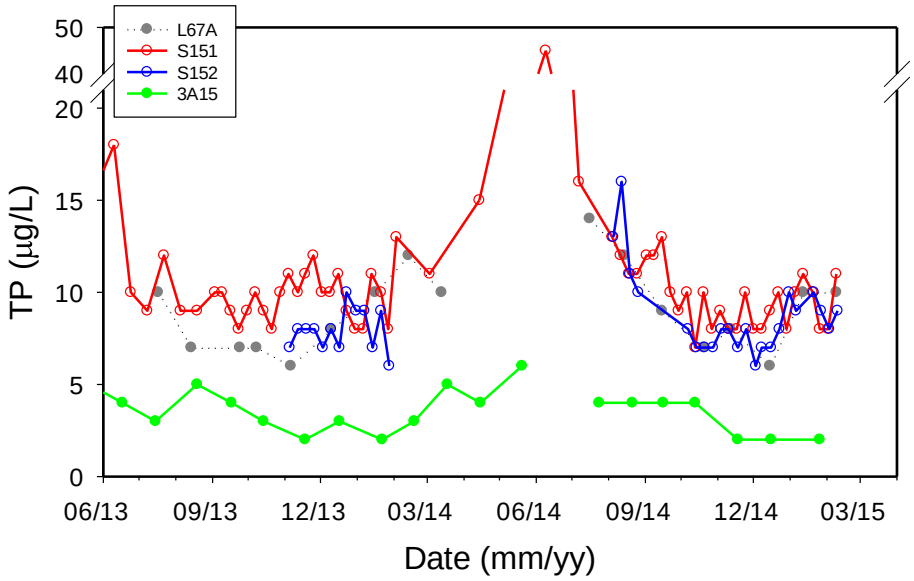

Figure WQ3. Total phosphorus concentrations measured at inflow (S152, L67A), upstream (S151), and reference wetland site (3A-15, in WCA-3A) during 2013 and 2014 sampling periods. Shaded areas depict durations the S152 structure was open.

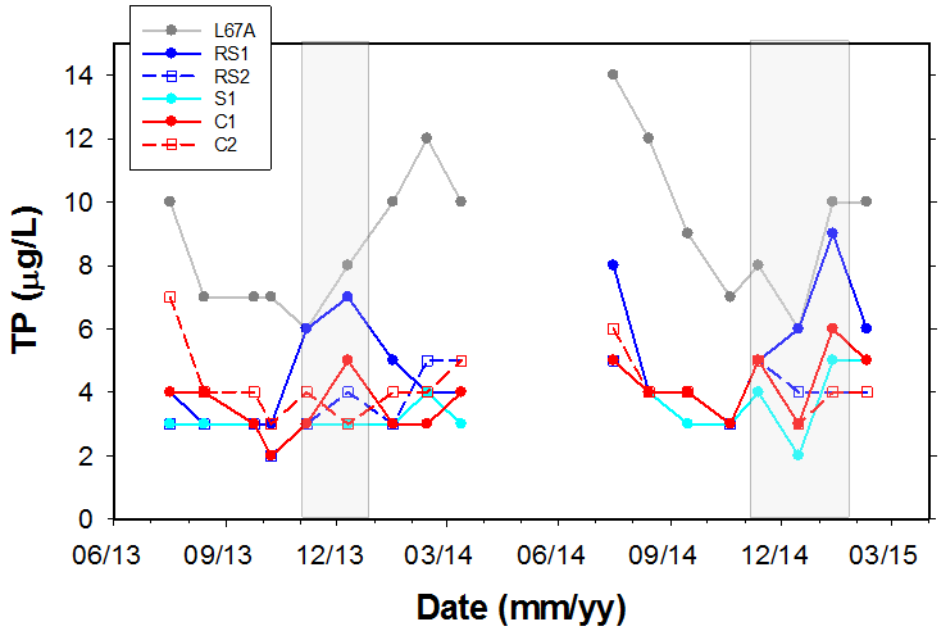

Figure WQ4. Changes in surface water TP concentrations observed pre, during and post flow at BACI sites throughout the DPM flow-way. Shaded areas depict durations the S152 structure was open.

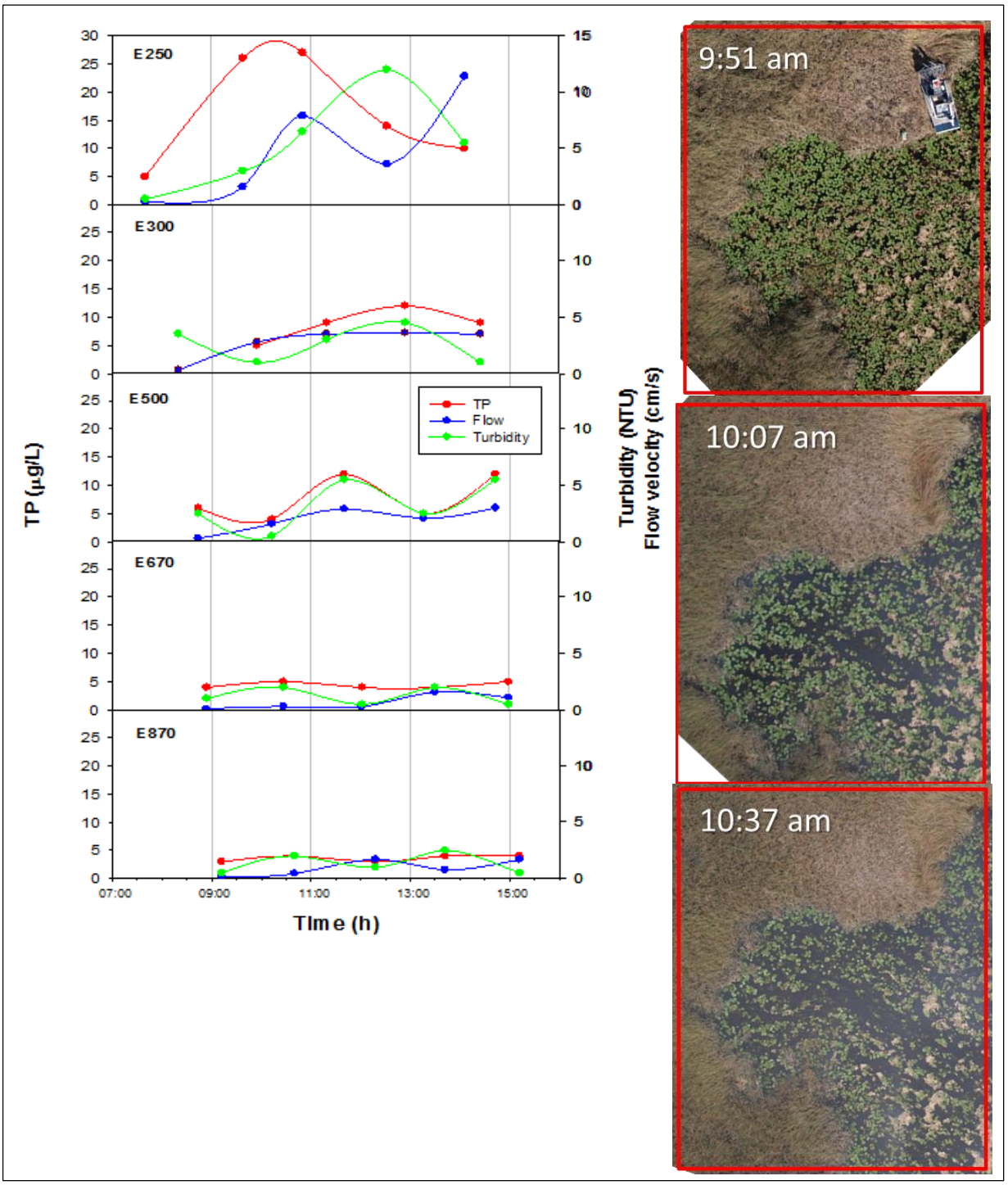

Figure WQ5. Changes in surface water TP concentrations, flow velocity and turbidity observed along the eastern flow path during flow day November 4, 2014 (left). Note structure opening began at approximately 9:30 am. Rapid changes in slough metaphyton at site E250 approximately one hour after flow was initiated [high-resolution images taken by Matt Burgess (UF) using the box-on-aircraft (BOA) system (right) (see 2015 SFER – Volume I, Chapter 6)].

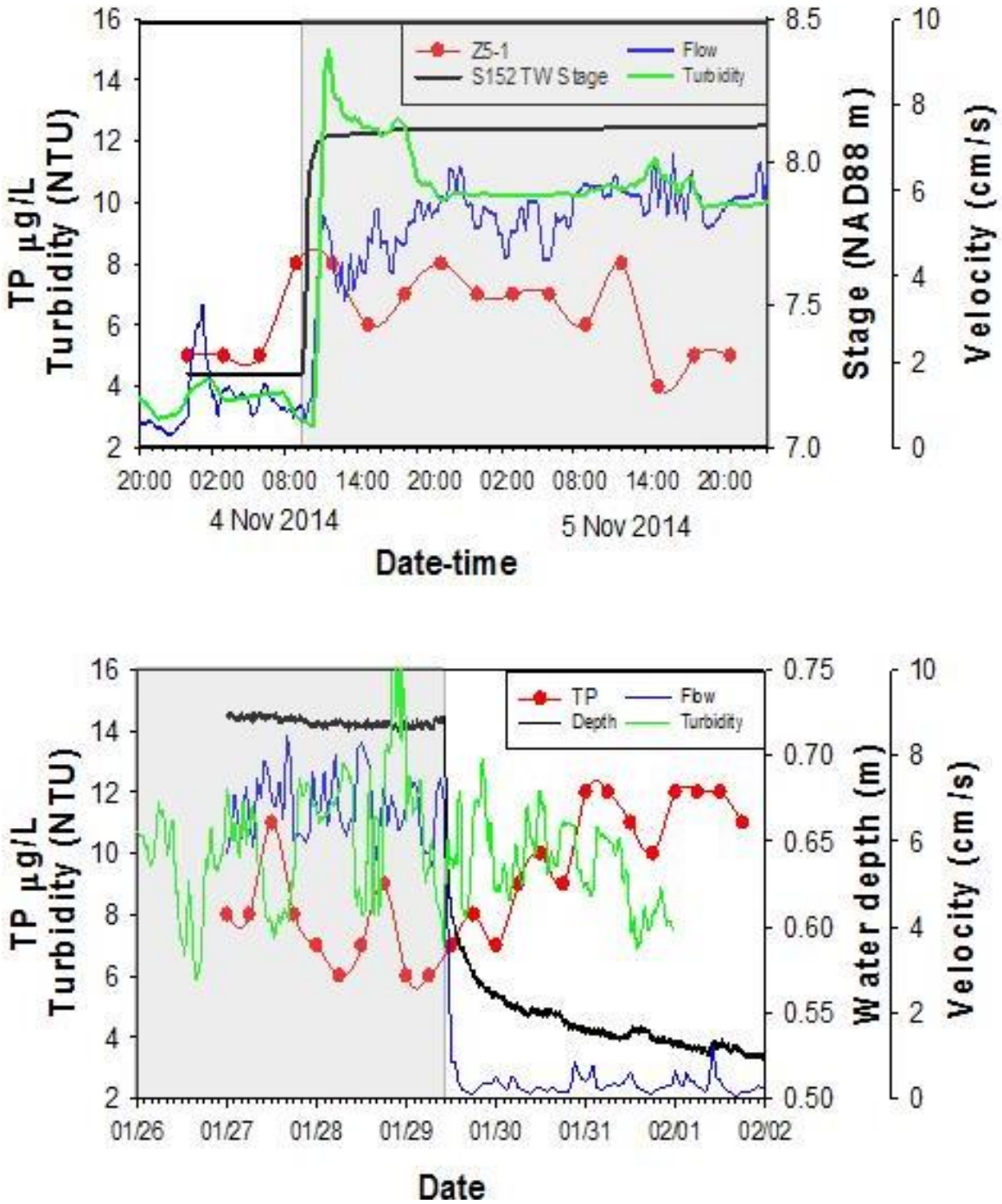

Figure WQ6. Intensive monitoring at site Z5-1 in response to opening (top image) and closing (bottom image) of the S152 structure. Shaded area depicts when structure was open.

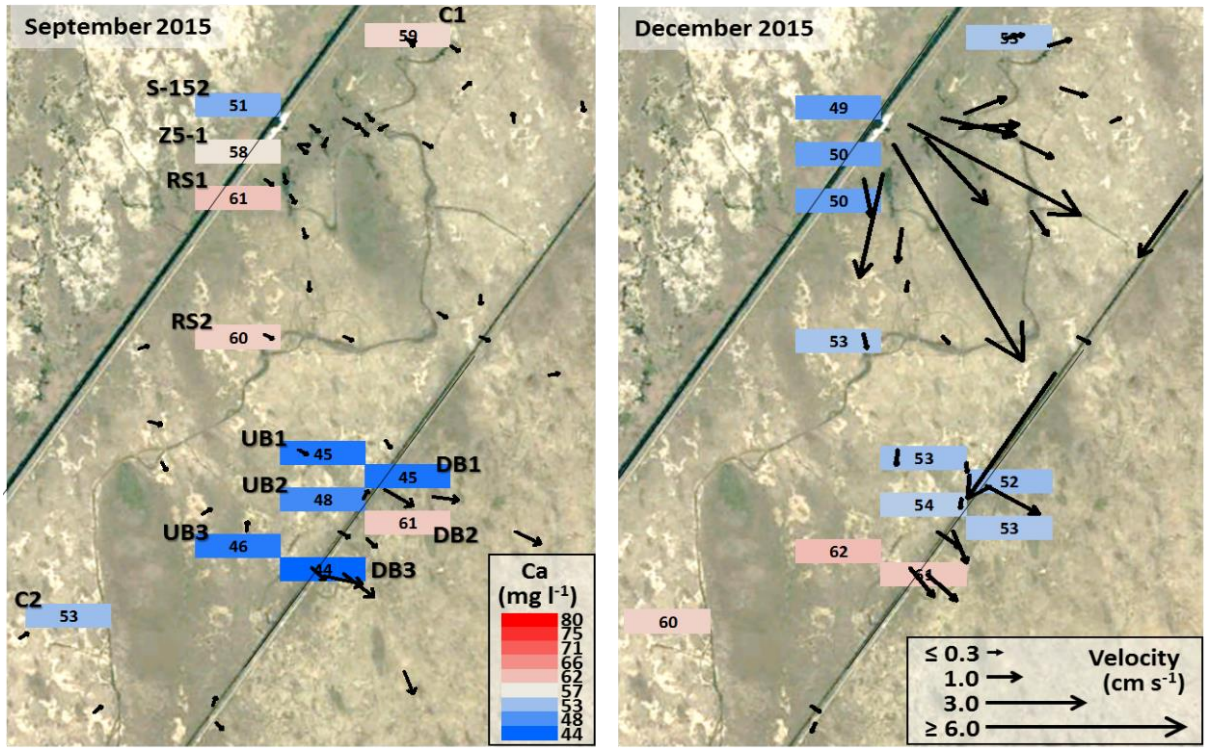

Figure WQ7. Spatial variation in velocities and Calcium (Ca) concentrations during pre-flow (left) and high-flow (right) periods. Dates indicate the sampling date for Ca. Pre-flow velocities represent average velocities from August to October (2012-2015) and high-flow velocities are averages of all three flow events. Velocities in the L67C canal are based on visual observations from dye studies but consistent with *in situ* measured velocities provided in the 2016 SFER (Saunders et al., 2016).

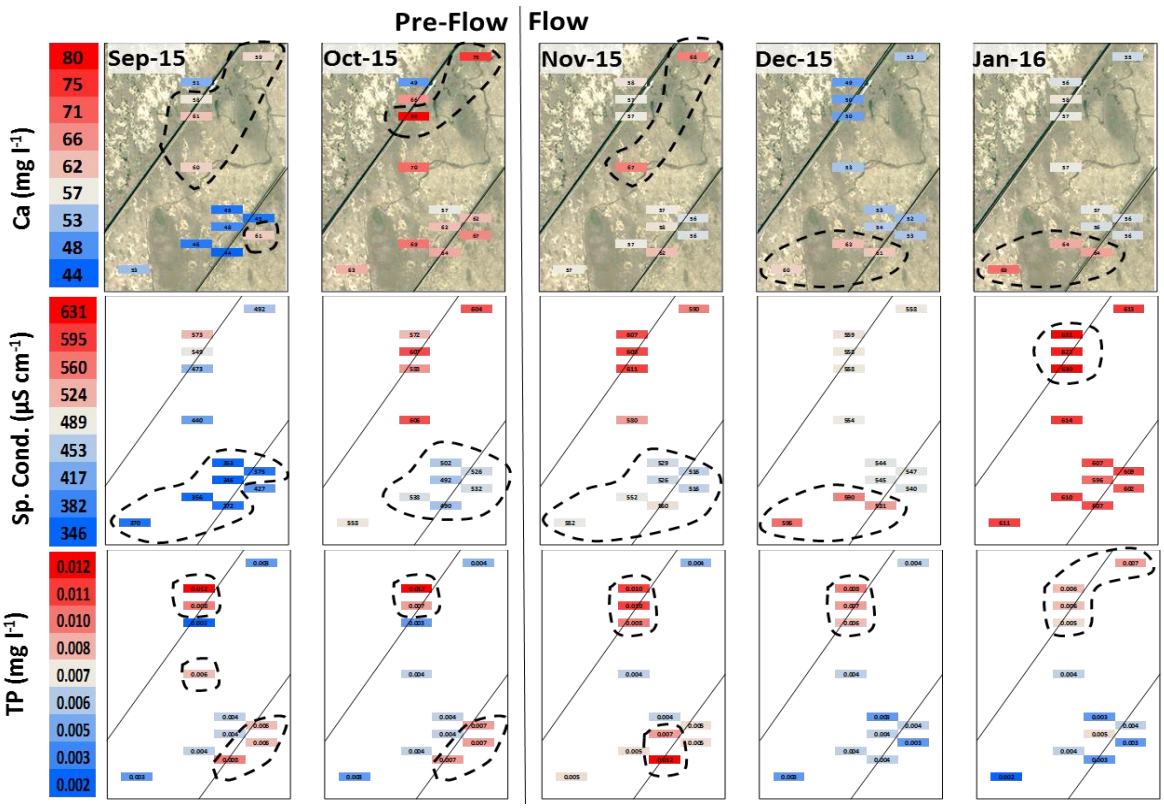

Figure WQ8. Monthly Calcium (top panel), Conductivity (middle) and Total Phosphorus (TP, bottom) from September 2015 through January 2016. For each month, dashed lines indicate sites that group together based on cluster analysis.

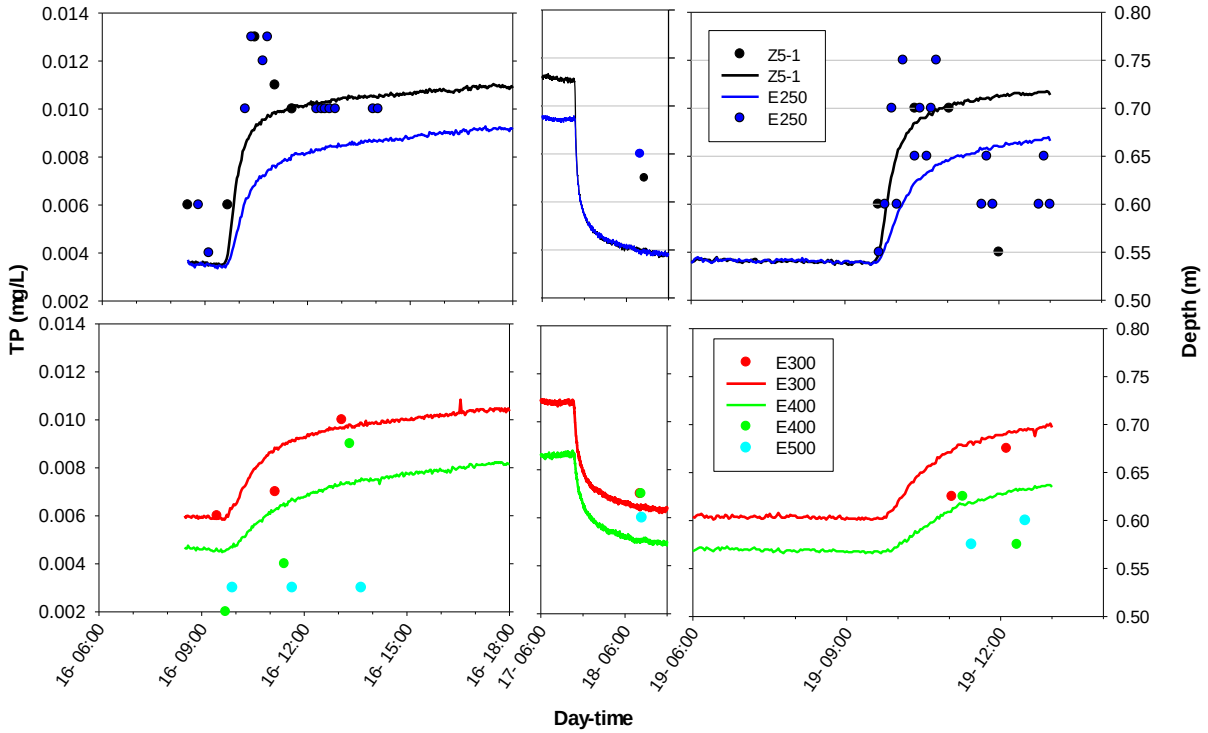

Figure WQ9. Water depths and surface water TP concentrations recorded at Z5-1 and at sites ranging 250-500 m along an eastern transect from S152, immediately before and during the 2015 pulse flow events. Vertical dashed lines indicate S152 opening, vertical solid line indicates S152 closure. There was no water level recorder at E500.

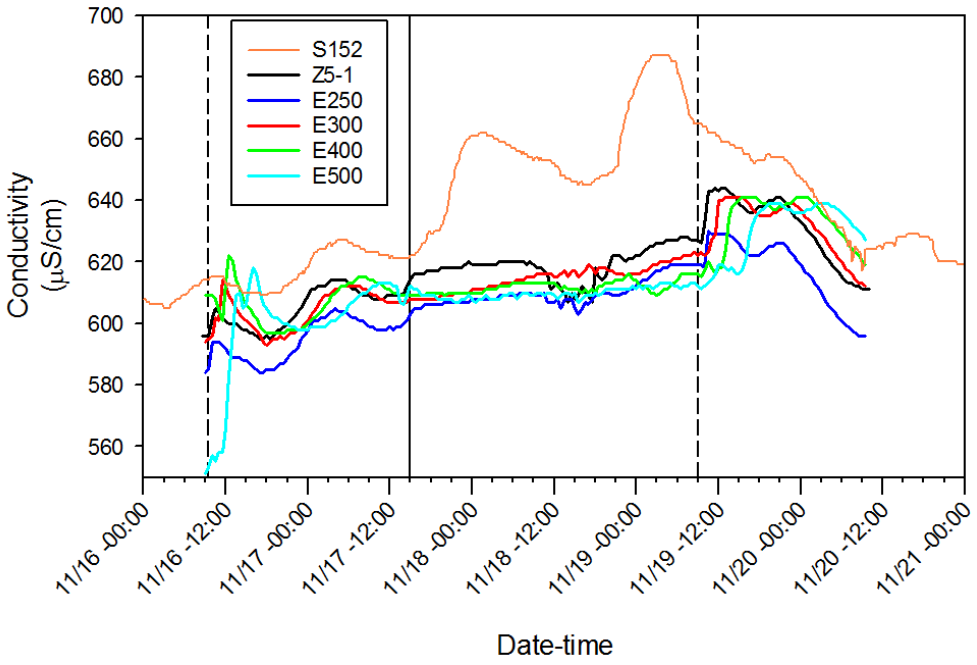

Figure WQ10. Specific conductivity recorded at S152, Z5-1 and at sites 250-500 m along an eastern transect from S152, immediately before and during the initial 2015 flow event. Vertical dashed lines indicate S152 opening, vertical solid line indicates S152 closure.

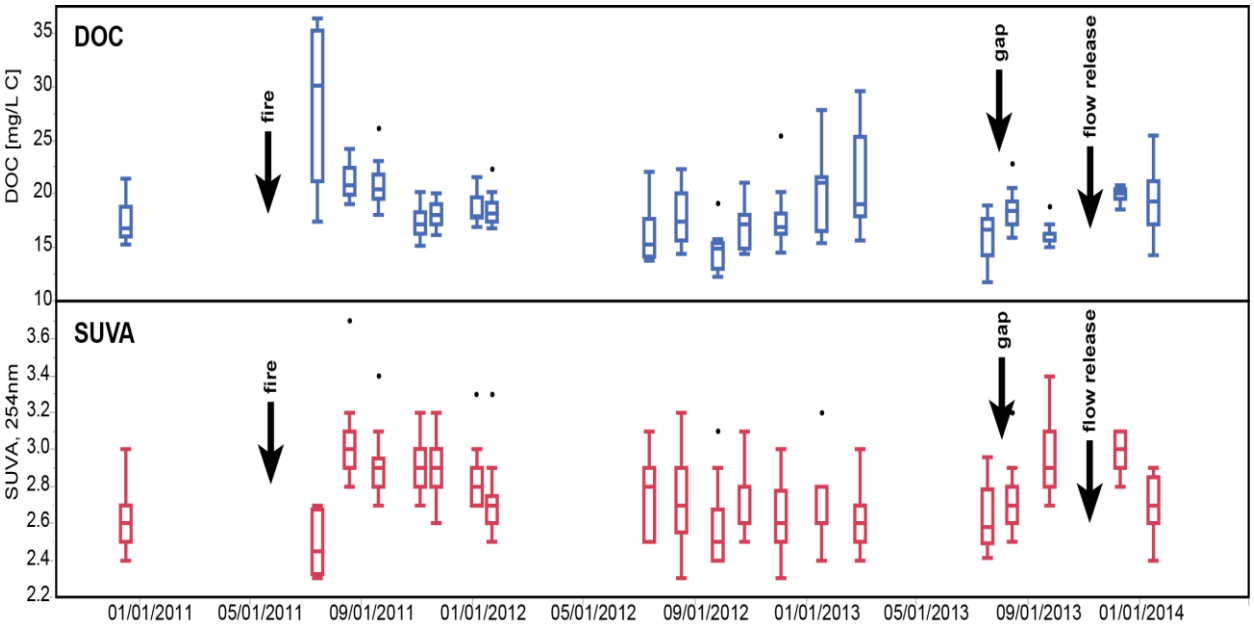

Figure WQ11. Distribution of DOC and SUVA over all study sites through the period of record. Box plots show the median (over all sites) and first and third quantiles. Whiskers represent 1.5 times the inter-quantile range

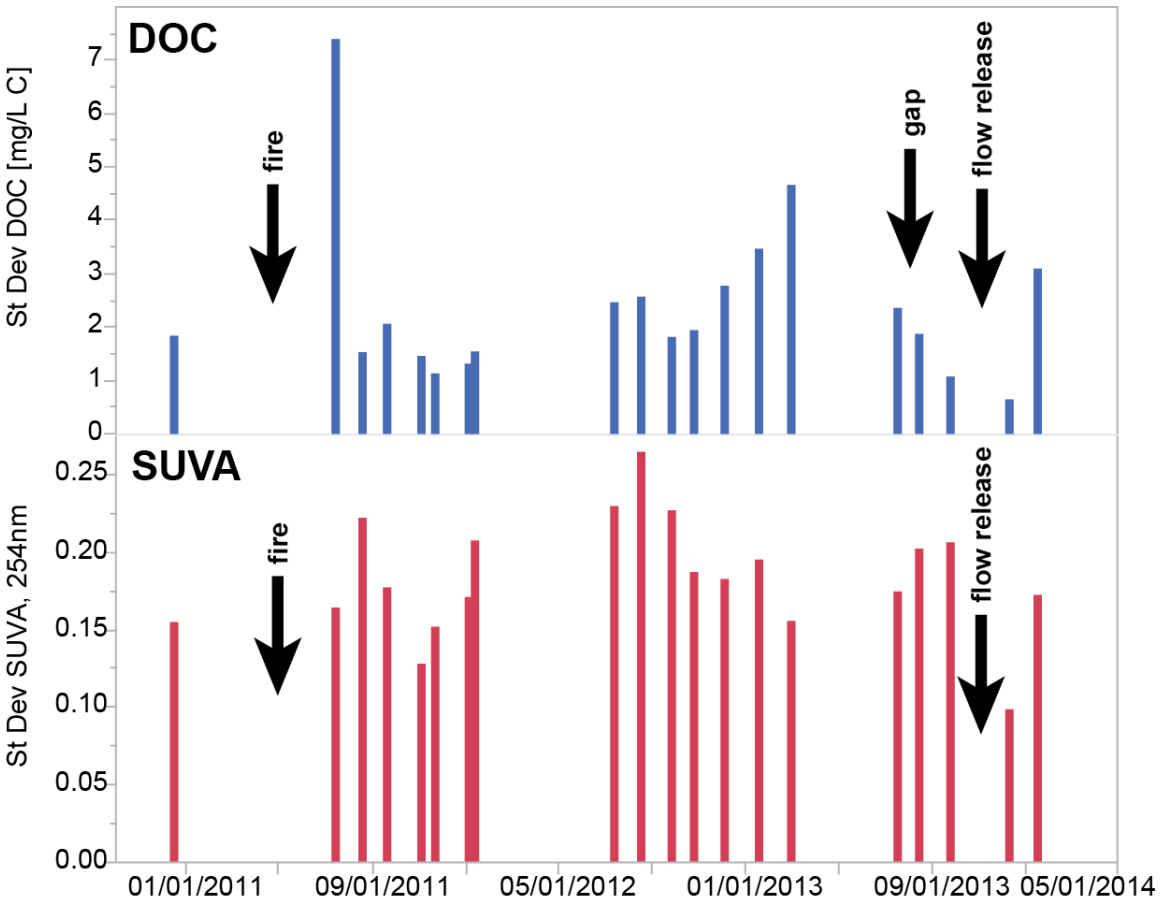

Figure WQ12. Standard deviation in DOC and SUVA over all sites for each sample collection period.

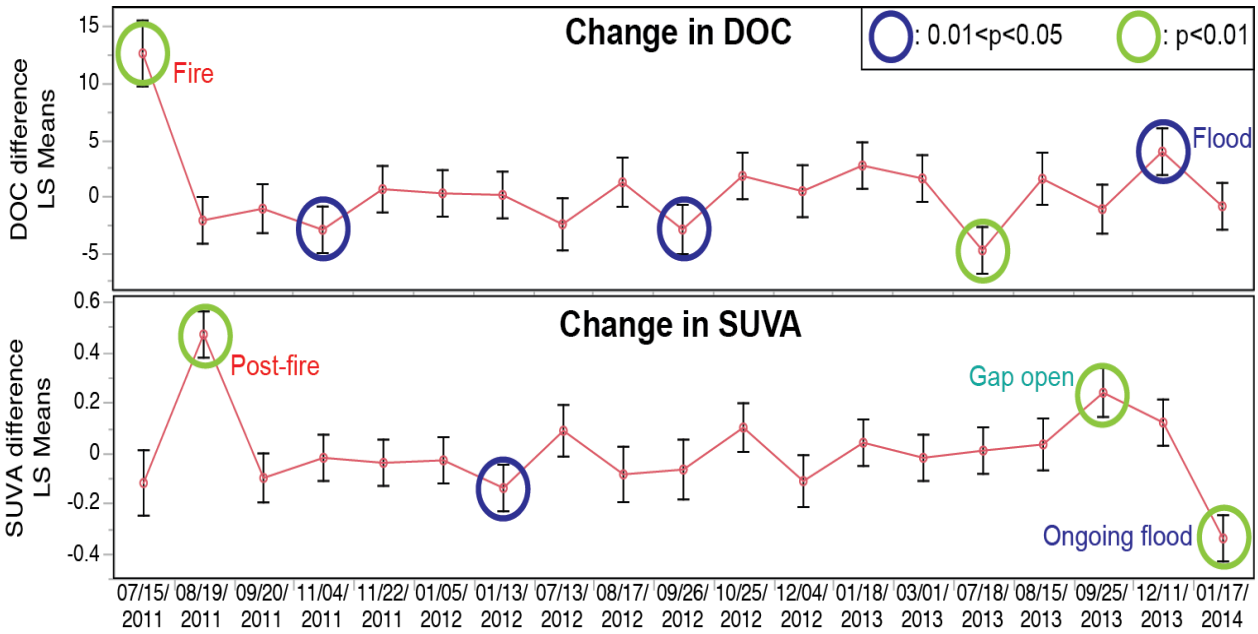

Figure WQ13. Least-squares means of the change in DOC and SUVA between sequential sampling events. Error bars represent standard errors. Circled points are those time periods for which the time effect in a general linear mixed model is significant.

Figures – Particle Characteristics (PC1-16)

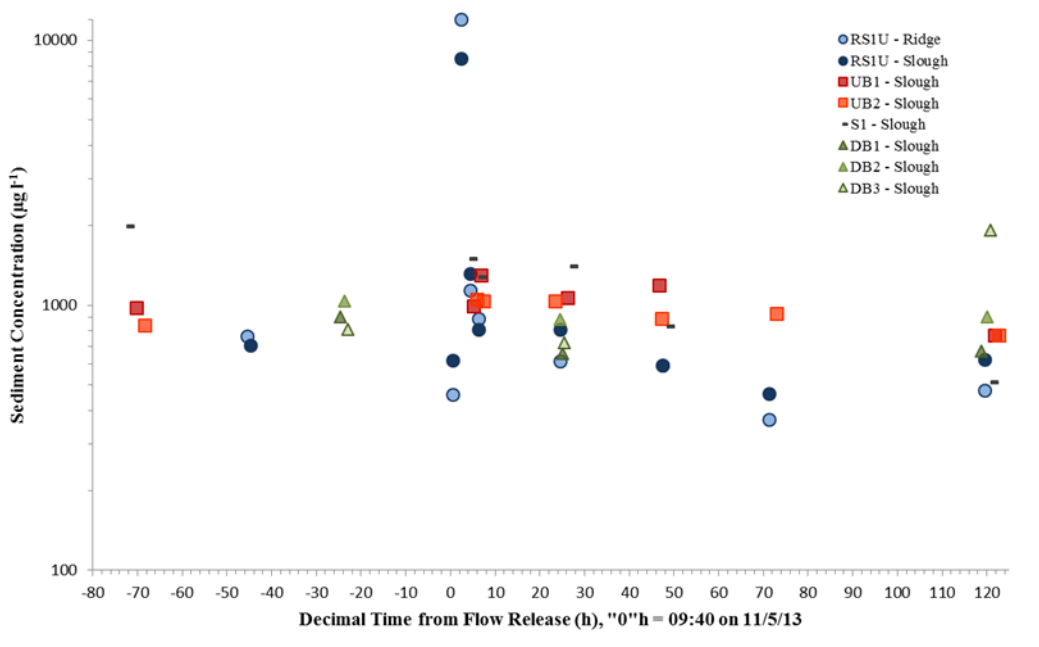

Figure PC1. Time series of depth-averaged suspended sediment concentration at all sites.

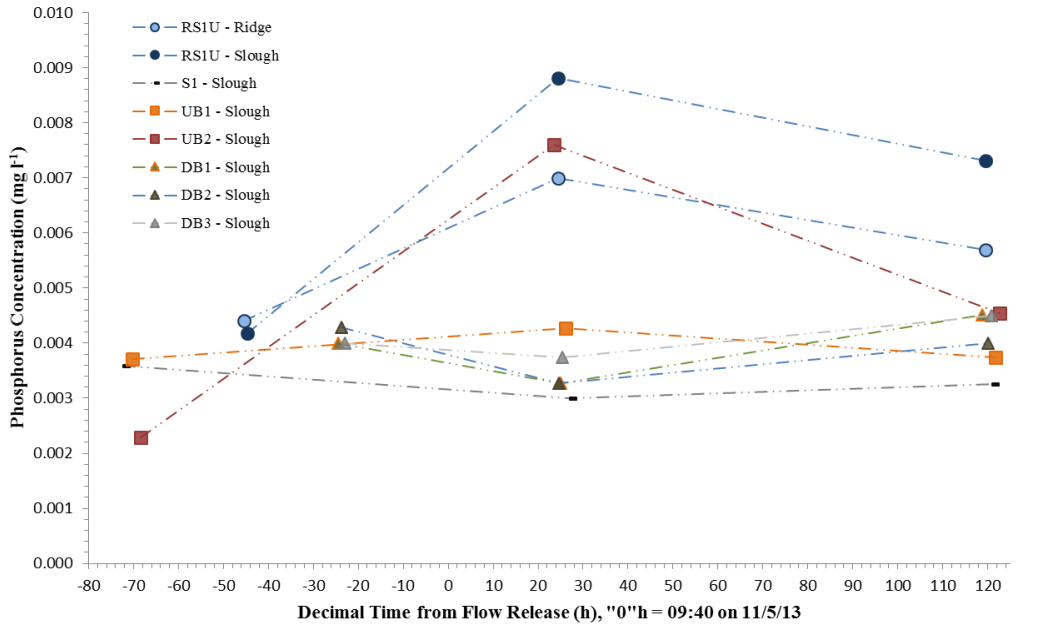

Figure PC2. Time series of depth-averaged phosphorus concentration at all sites.

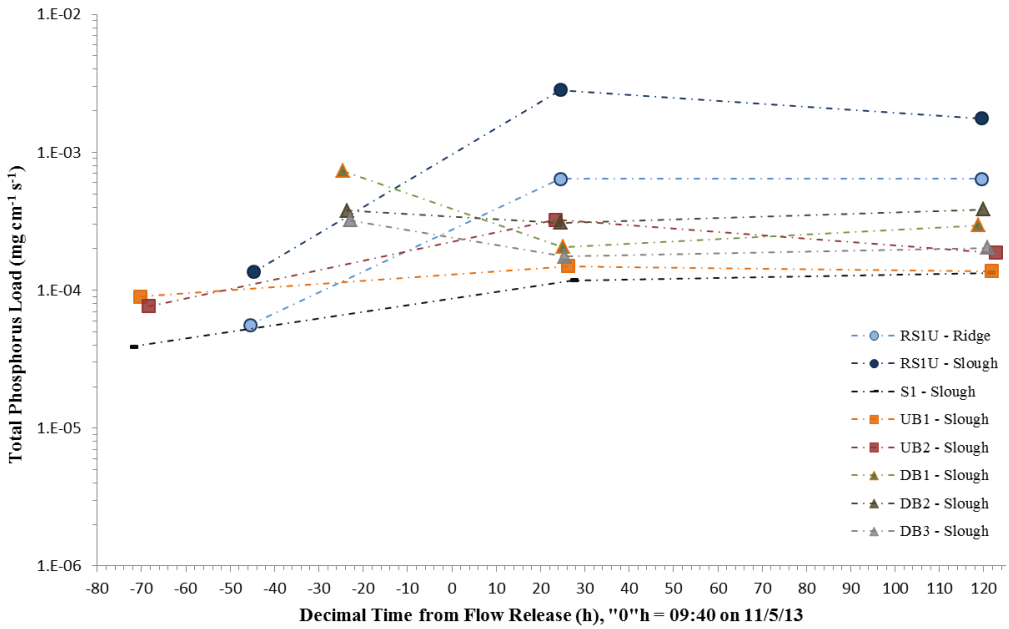

Figure PC3. Time series of depth-average phosphorus flux at all sites.

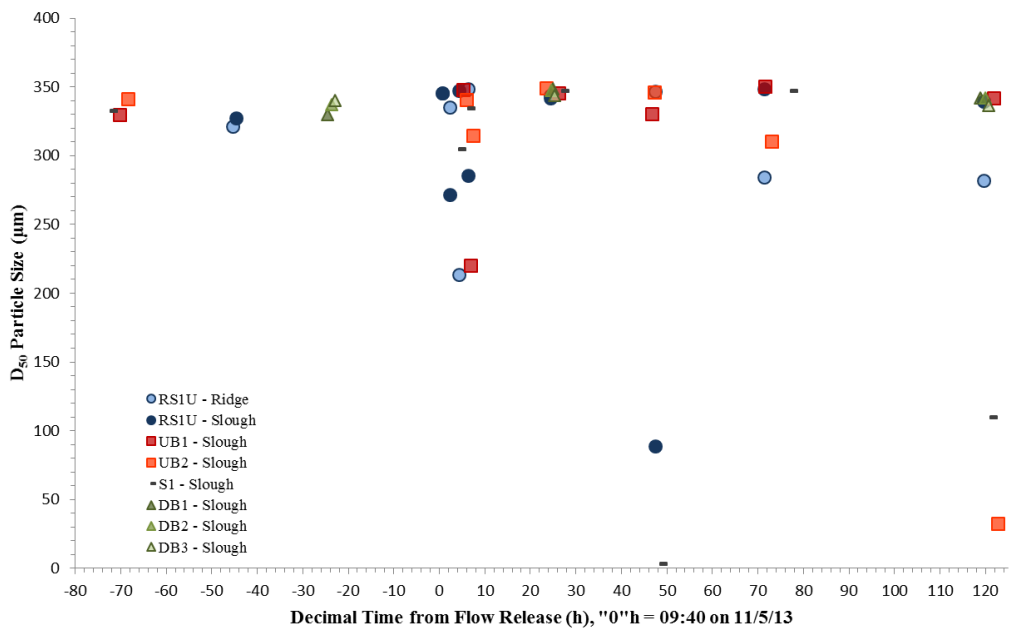

Figure PC4. Time series of depth-averaged D_{50} (median volume weighted size) of suspended particles at all sites.

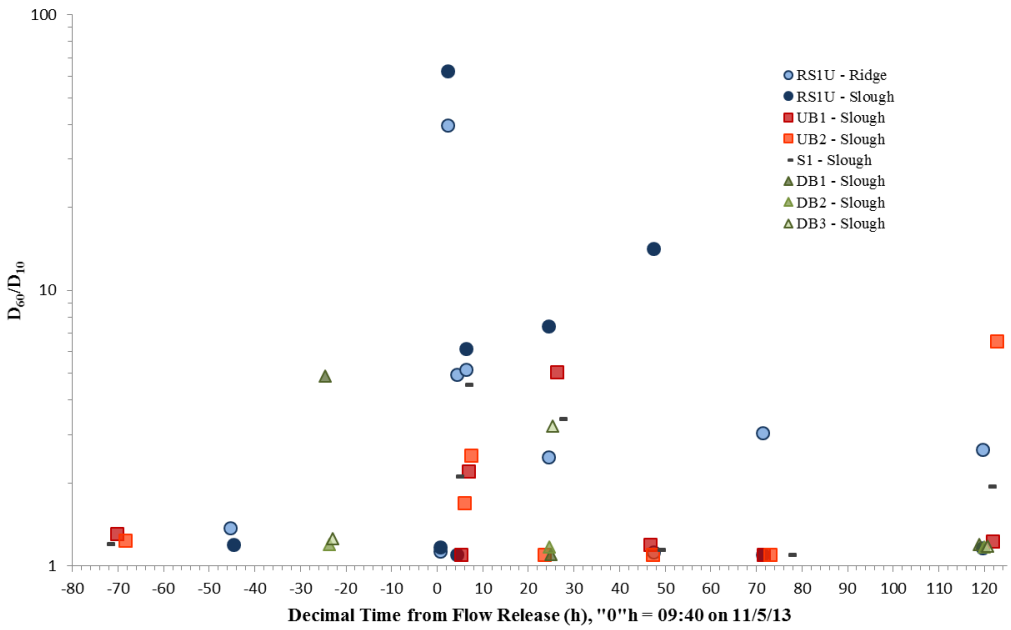

Figure PC5. Time series of depth-averaged D_{60}/D_{10} (particle size uniformity coefficient) of suspended sediment at all sites.

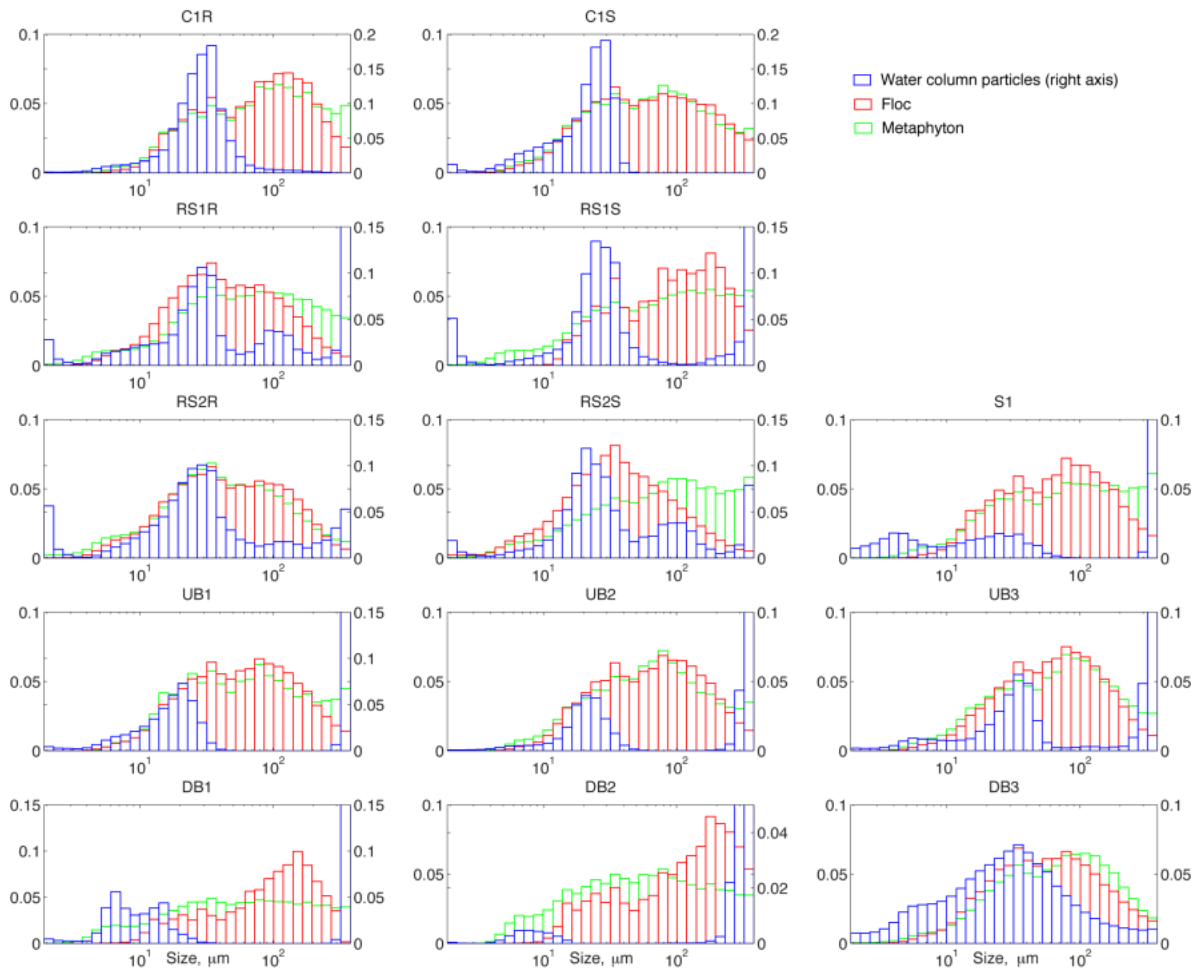

Figure PC6. Comparisons of distributions of Water Column, Floc and Epiphyton by size for samples collected 2010.

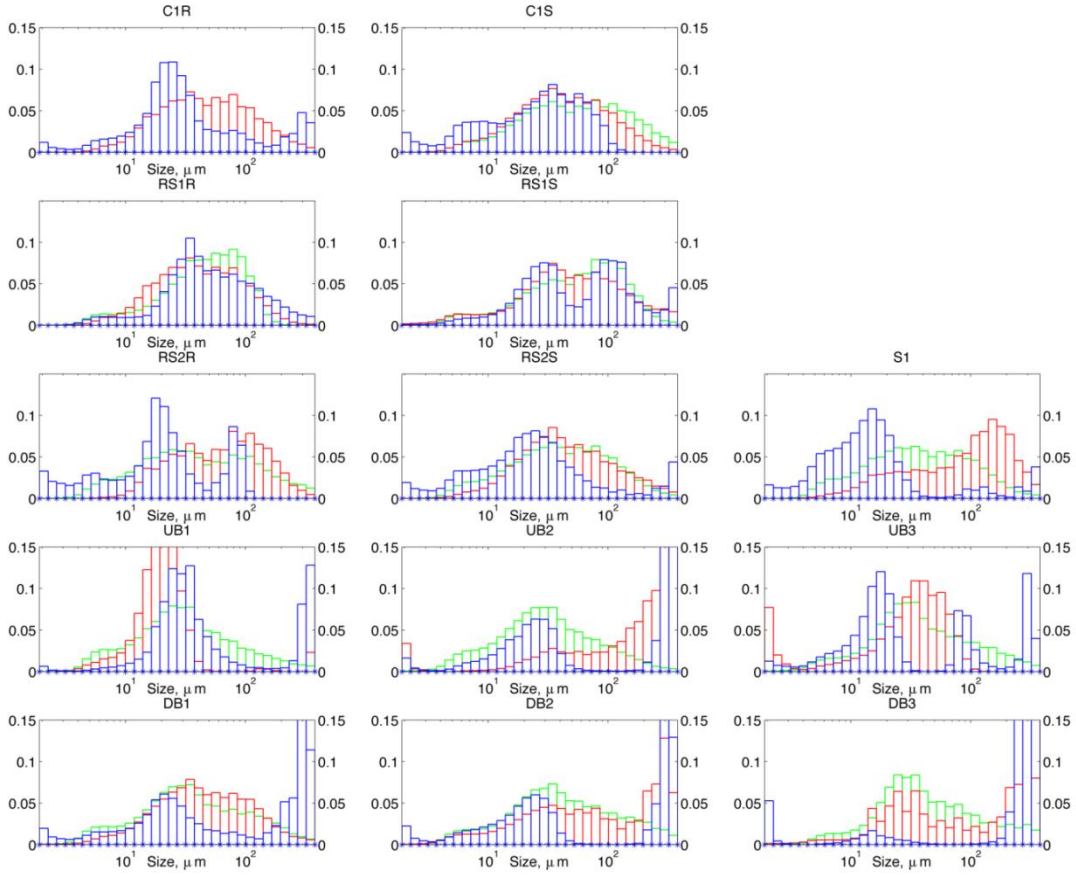

Figure PC7. Comparisons of distributions of Water Column, Floc and Epiphyton by size for samples collected 2011.

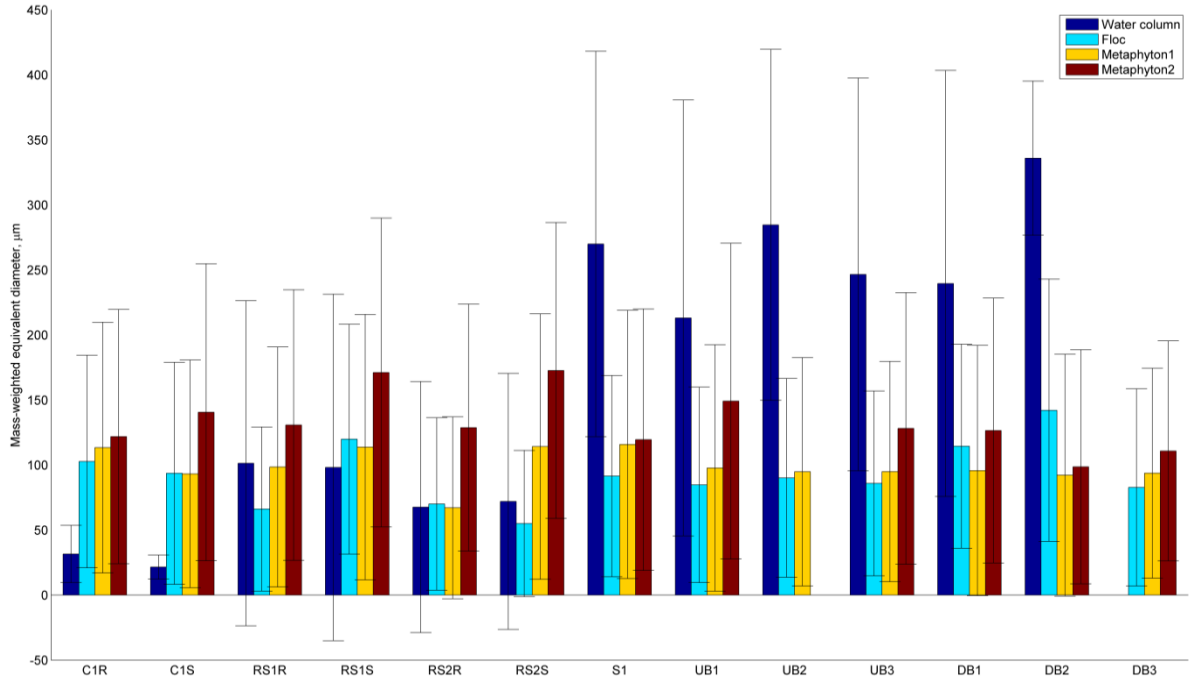

Figure PC8. Mass weighted equivalent diameter at all sites 2010.

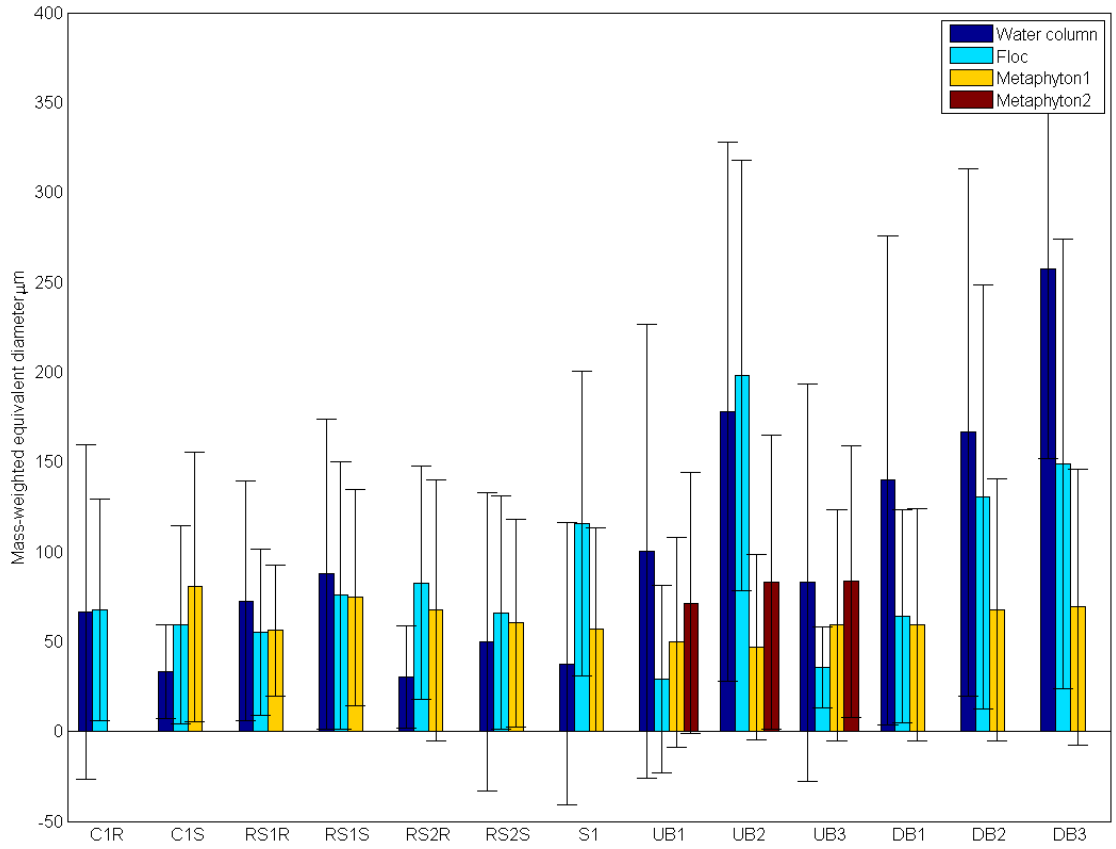

Figure PC9. Mass weighted equivalent diameter at all sites 2011.

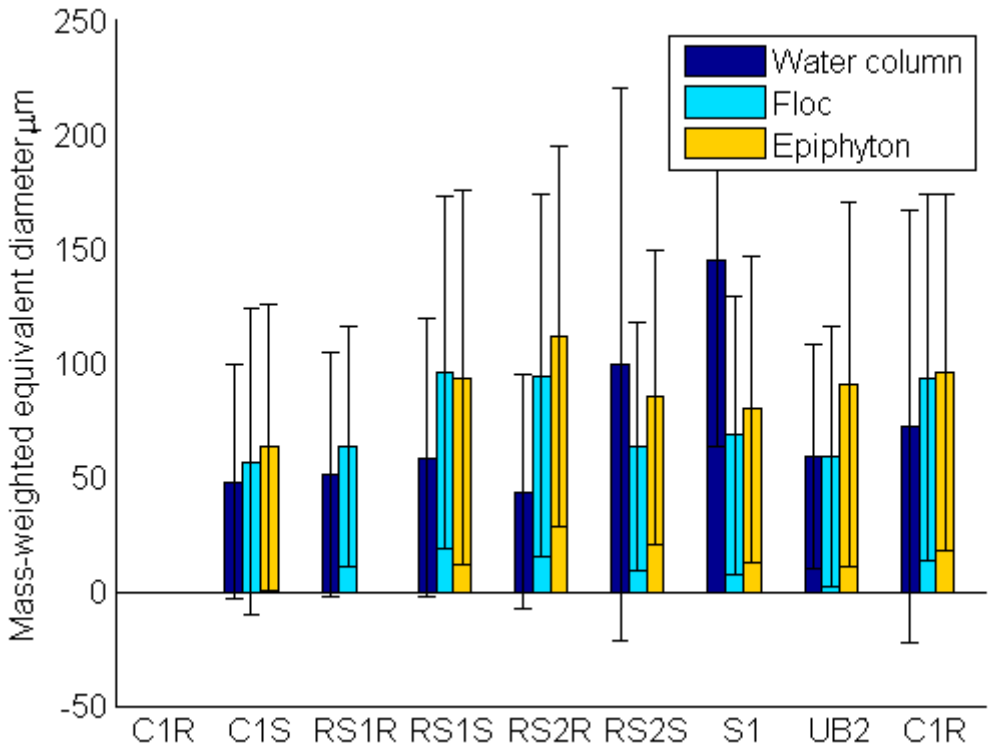

Figure PC10. Mass weighted equivalent diameter of particles

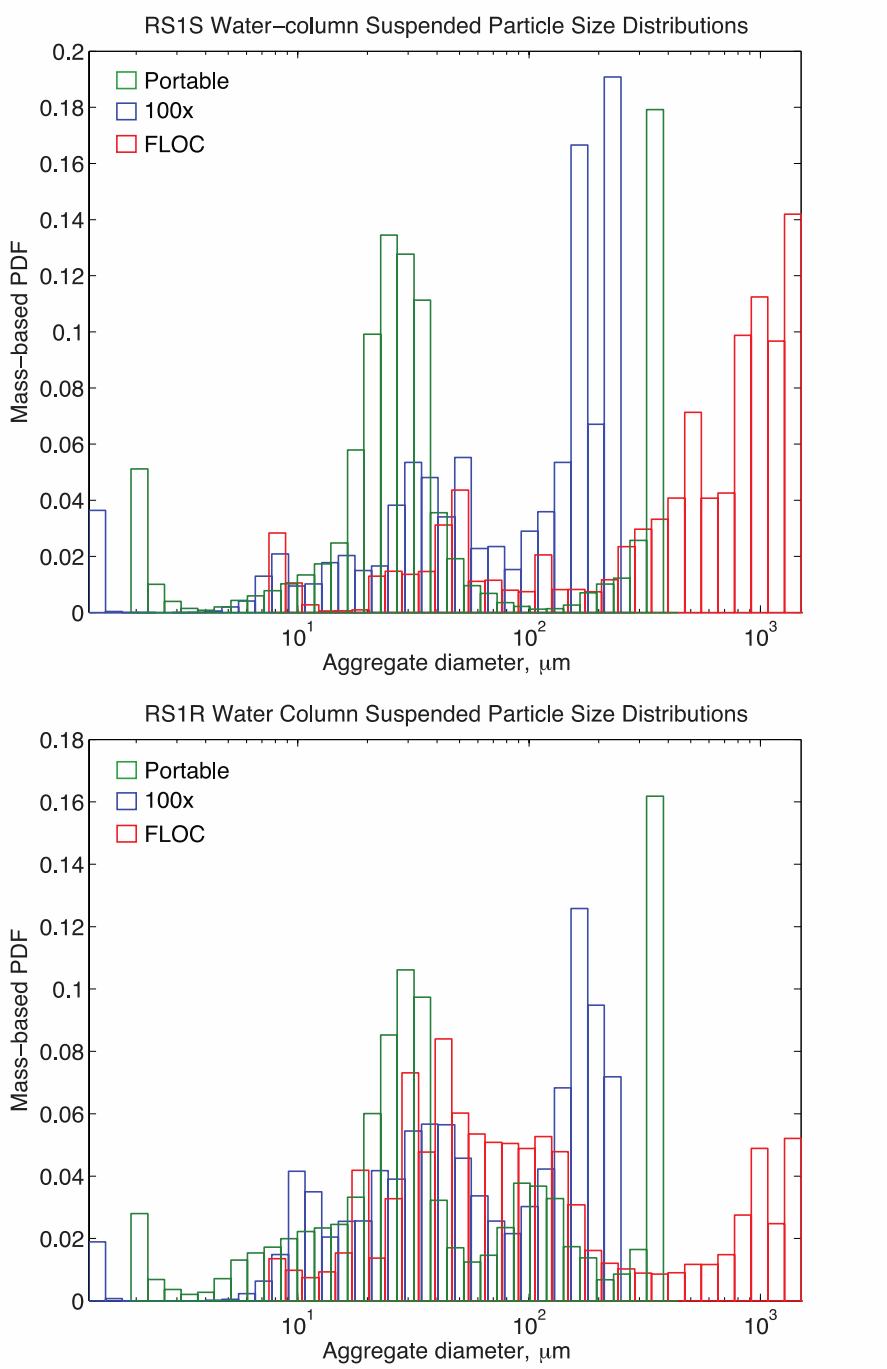

Figure PC11. Comparison of instruments measuring particle size and concentration. Limited comparability between different LISST instrumentation. Saturation in outer detector rings for all instrumentation. Some agreement in position of intermediate mode.

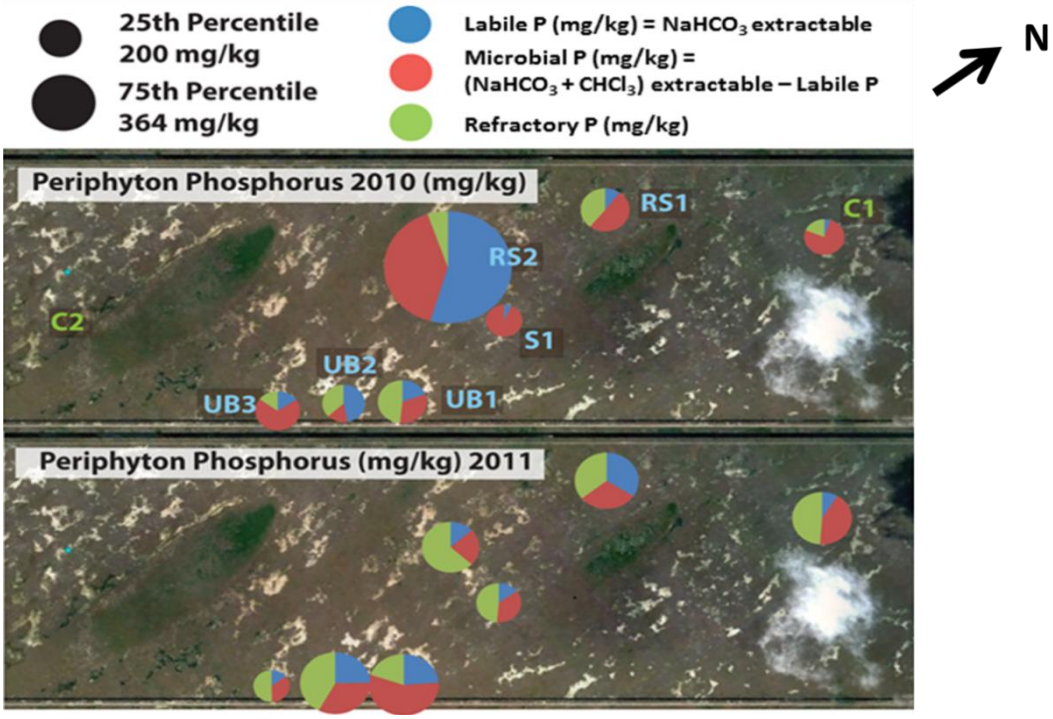

Figure PC12. Differences in TP concentrations were not detected between years though Periphyton phosphorus became more refractory in nature. This shift was accentuated in the interior sites RS2 and S1 away from the influence of the canal-levee system. The DB sites (not shown) on the south of the levee) were 2-fold higher in total P than canal sites in 2010 but similar to interior sites in 2011.

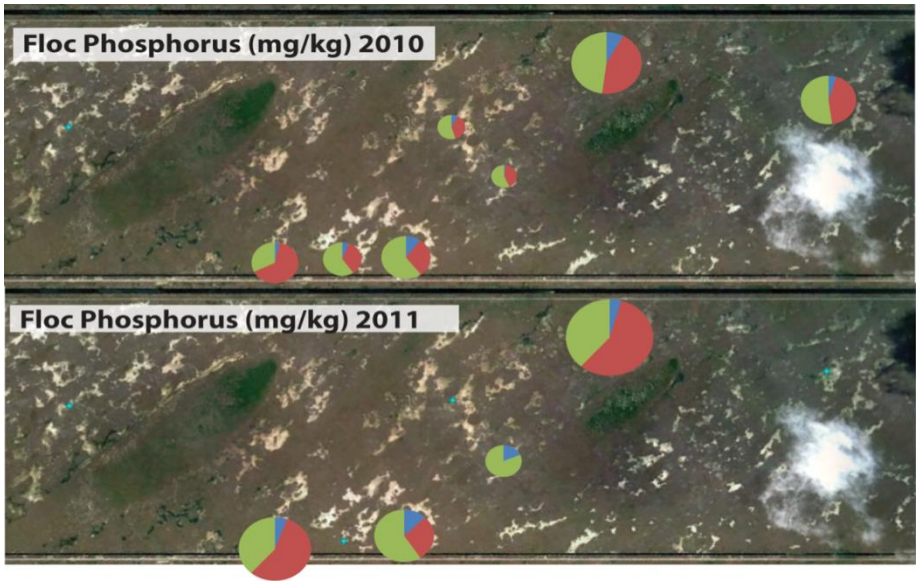

Figure PC13. Particulate phosphorus concentrations were also lower at the interior sites away from canals. Similar to periphyton derived phosphorus, distributions of particulate phosphorus in the different pools indicated that floc phosphorus became more refractory in nature.

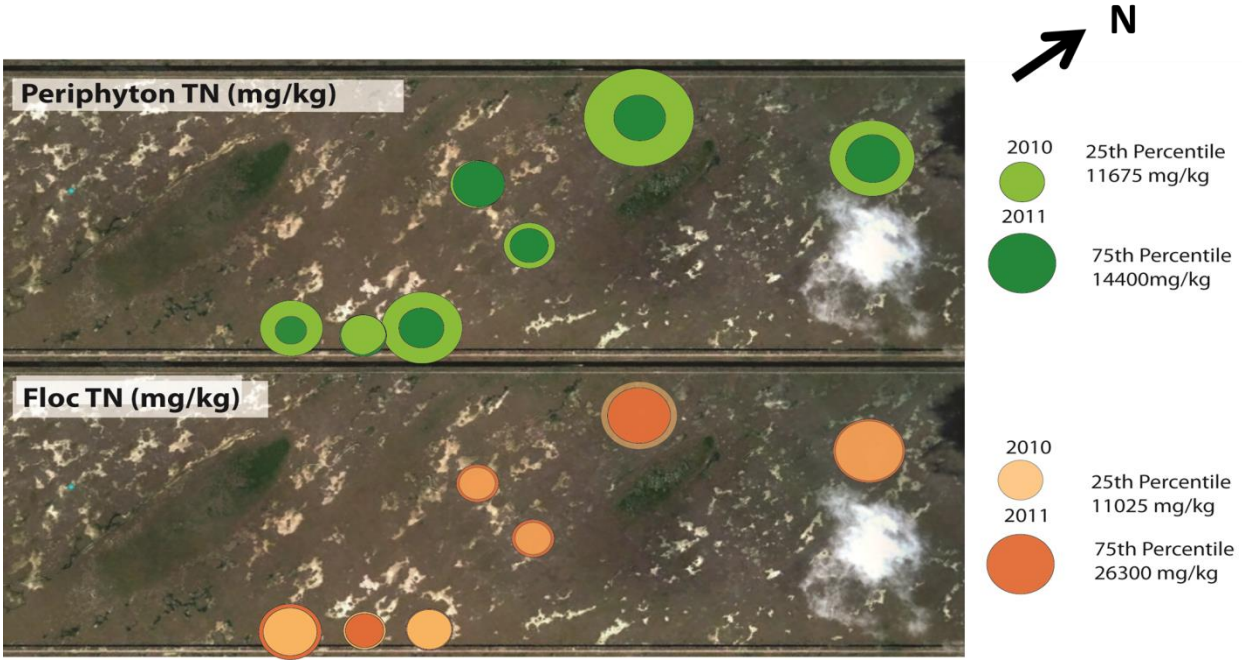

Figure PC14. Concentrations of particulate nitrogen were similar in both the periphyton and floc pools. Interannual changes were more accentuated in periphyton than in floc. Periphyton derived material contained more total nitrogen in 2010 than 2011 with greater differences observed in exterior sites than interior sites.

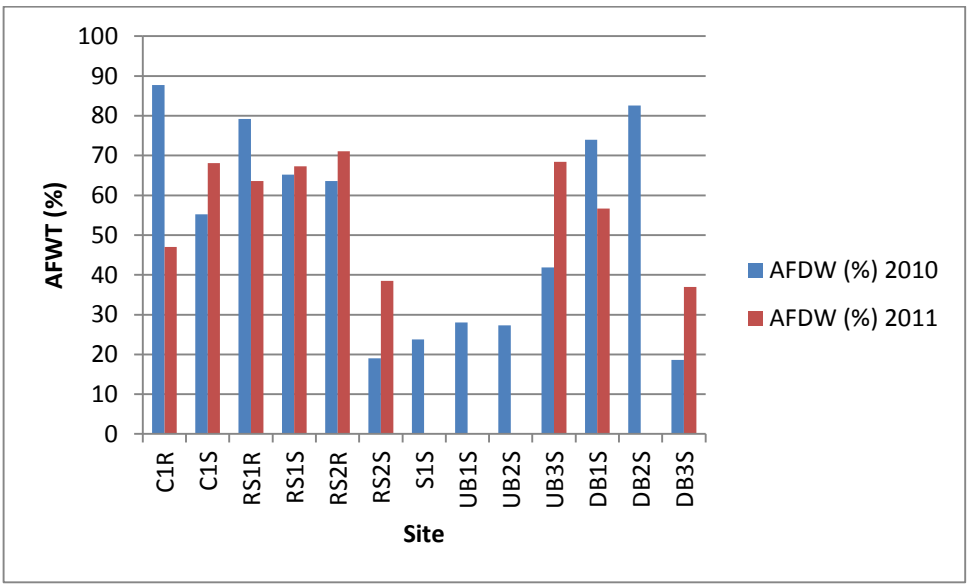

Figure PC15. Percent ash free dry weight (AFWT) at each site for 2010 and 2011.

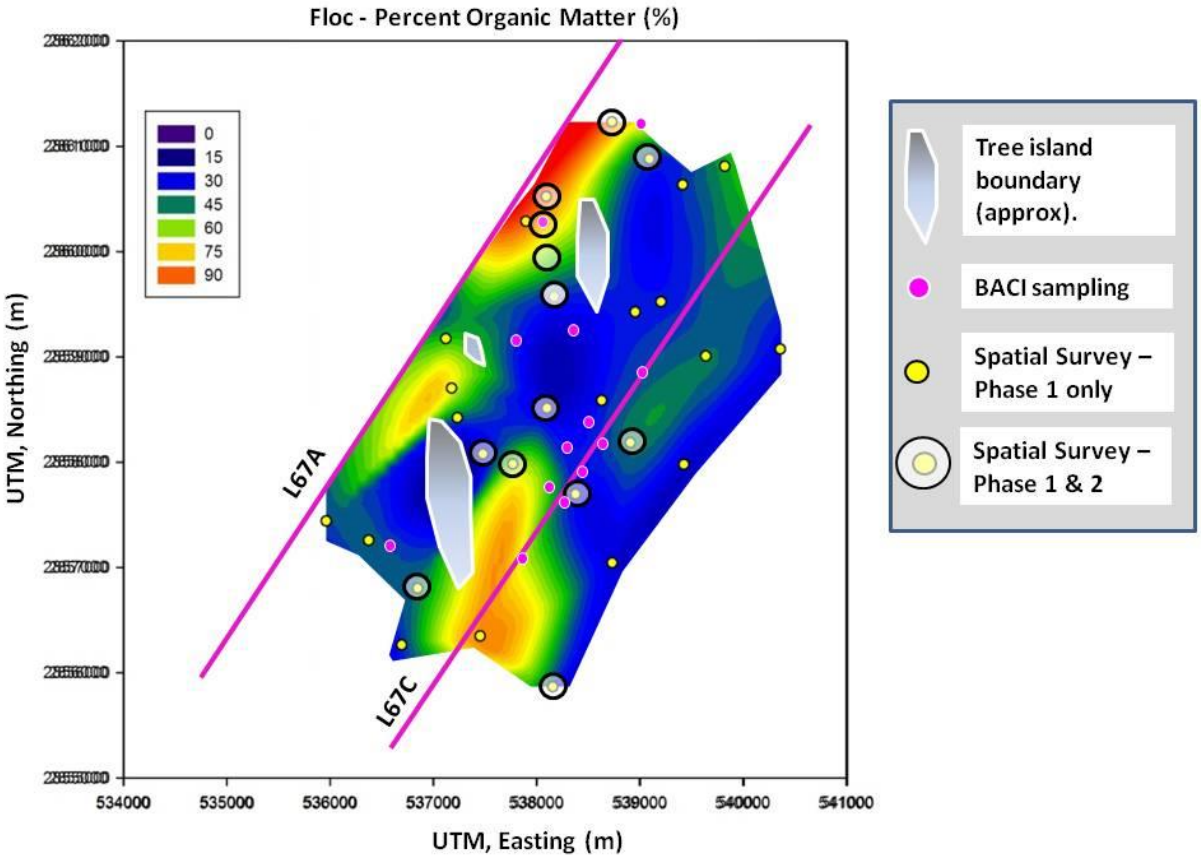

Figure PC16. Heat map of floc chemistry (% organic matter) over the DPM study area, based on the first spatial survey in July 2012 (Phase-1). These results provided the basis for Survey Phase-2 sampling, which is stratified based on gradients in substrate quality and distance from S-152 structure. Phase-2 includes sampling sediment chemistry and critical entrainment velocity, conducted once before and after each Nov-Dec window, and sediment transport measured over the Nov-Dec window.

Figures – Particle Fluxes (PF1-27)

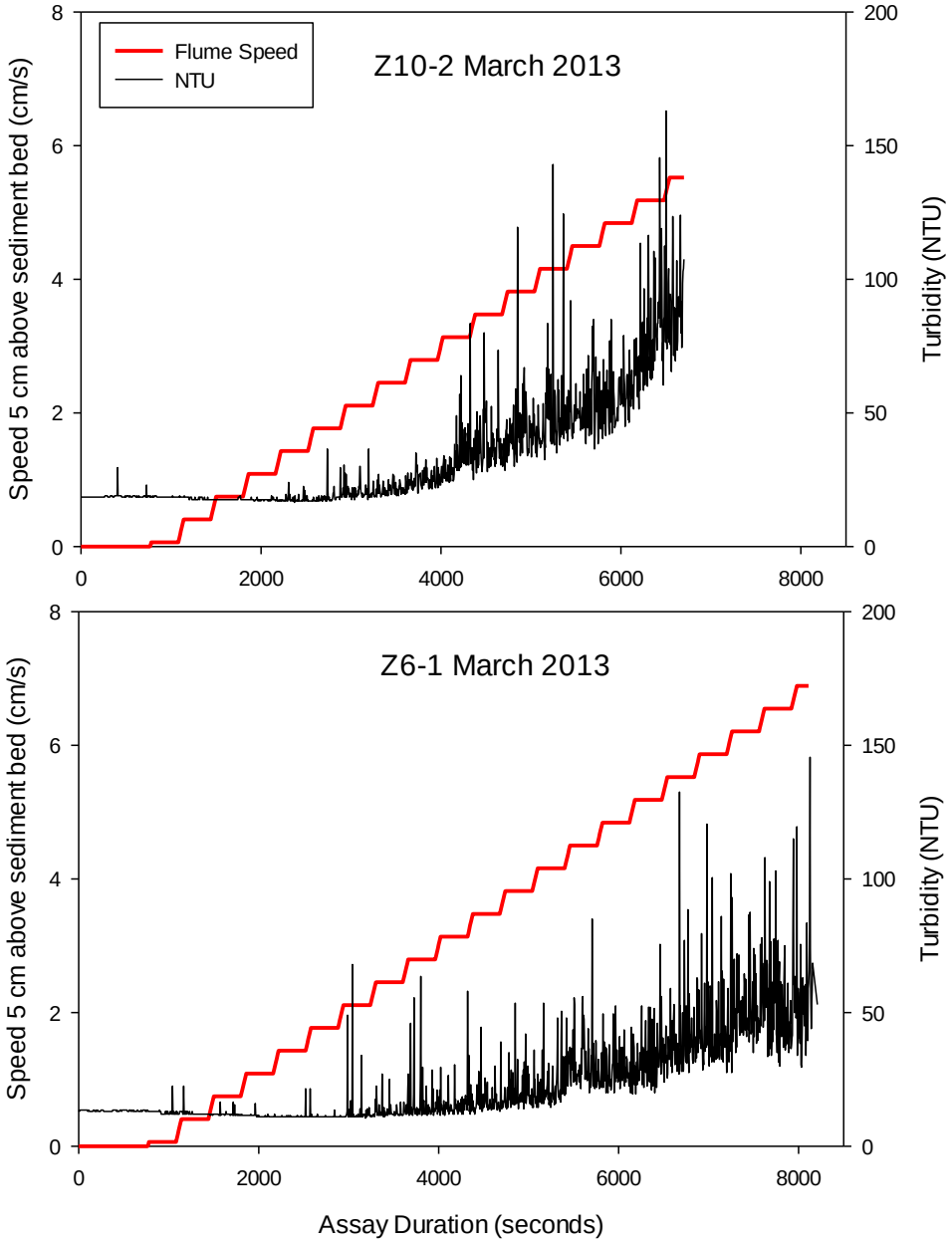

Figure PF1. Sediment erosion time series measured using the benthic annular flume at sites with mineral floc (site Z10-2) and organic floc (Z6-1).

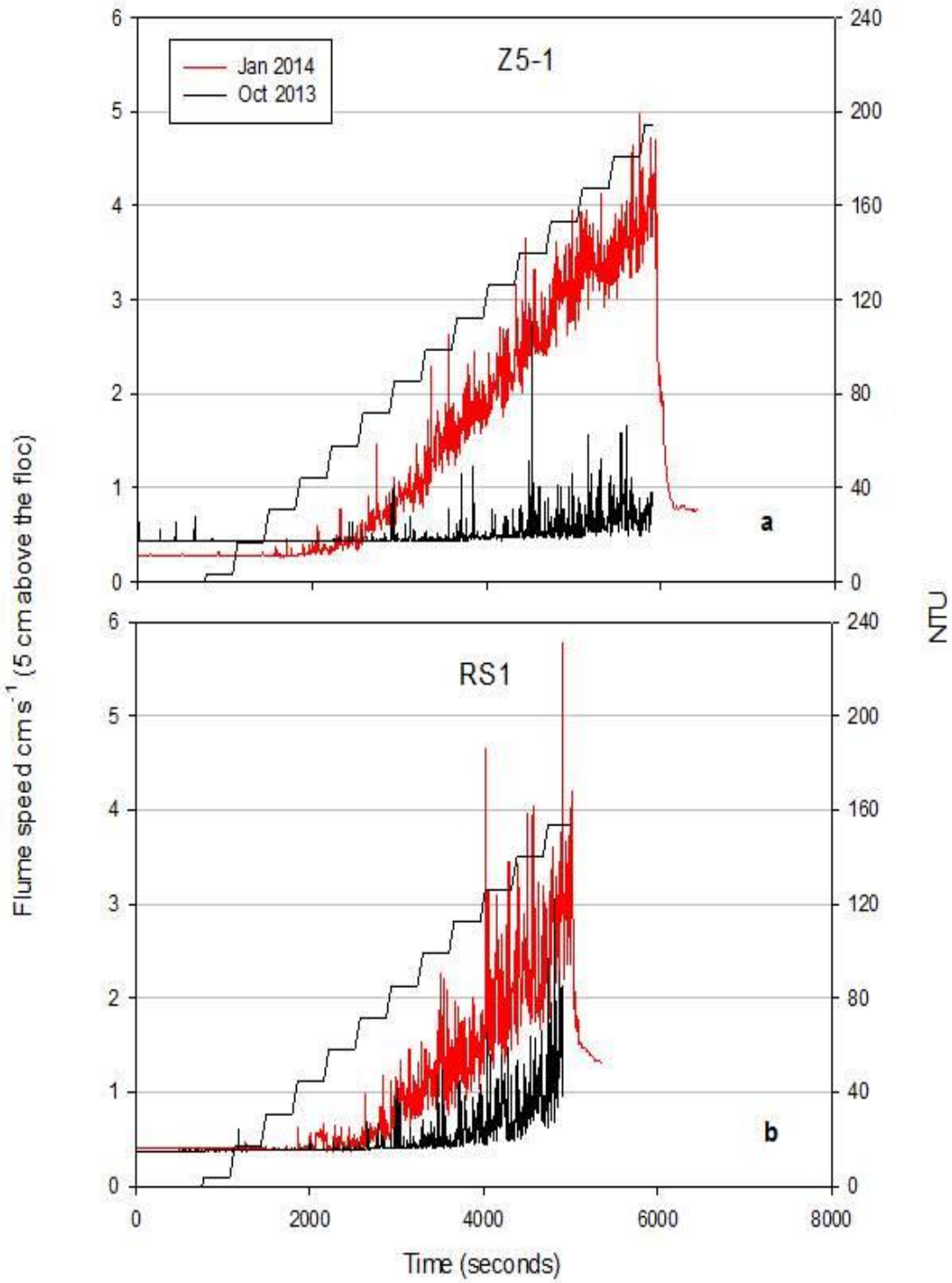

Figure PF2. (Left) Examples of pre- (Oct 2013) and post-flow (Jan 2014) critical entrainment velocities (CET) and Nephelometric Turbidity Units (NTU; an indication of sediment entrainment) at Z5-1 and RS1.

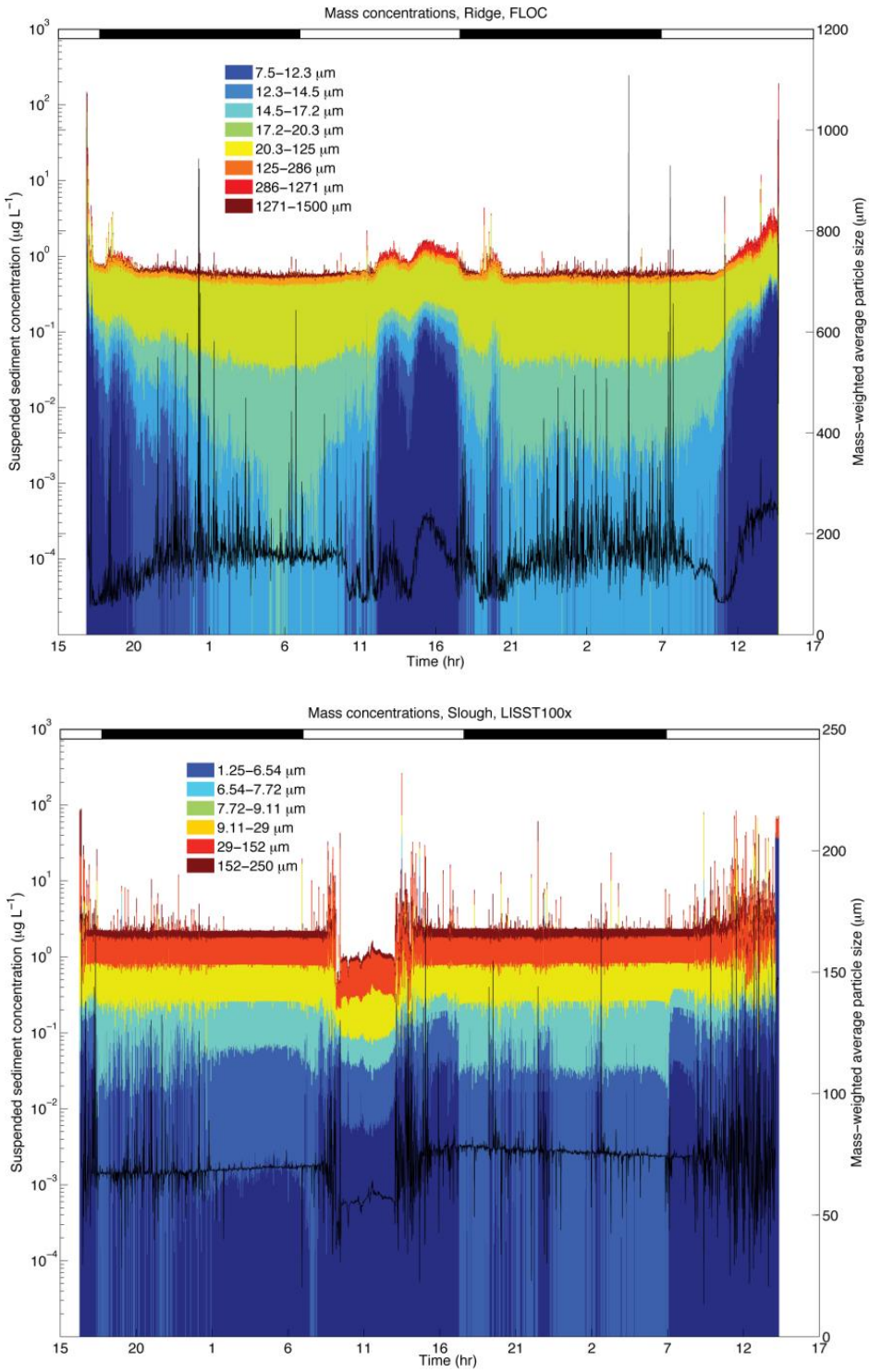

Figure PF3. Particle size distributions and mass-weighted equivalent diameters during a simultaneous deployment at RS1R (top) and RS1S (bottom) starting on November 7, 2010. Note that because different instruments were used for the two sites, the magnitudes of suspended sediment concentration or equivalent diameter are not directly comparable across sites; rather, we compare relative temporal trends in the diel dynamics. Black bars at the top of the figure represent nighttime periods; white bars represent daytime periods.

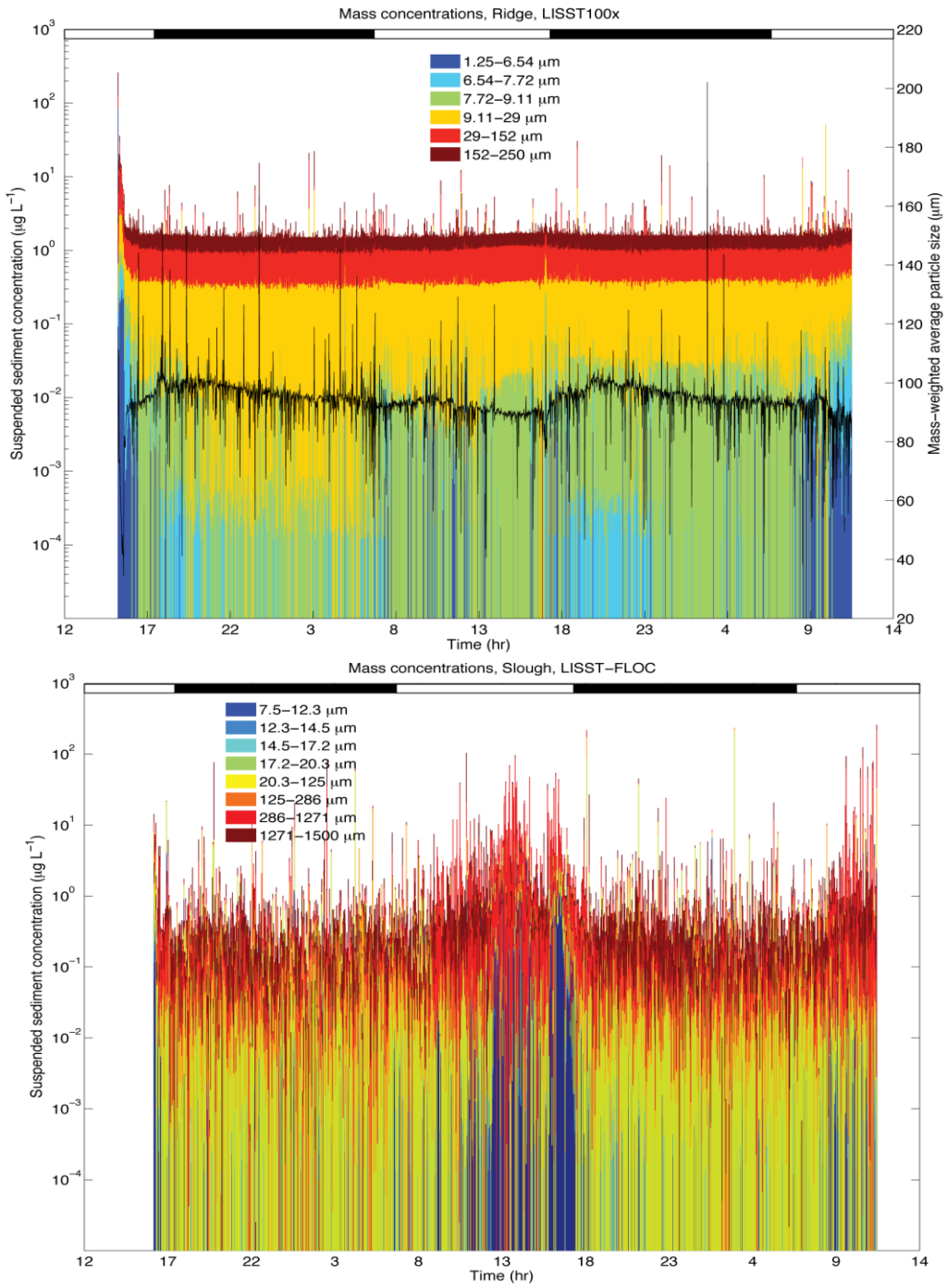

Figure PF4. Particle size distributions and mass-weighted equivalent diameters during the second simultaneous deployment at RS1S (top) and RS1R (bottom) starting on November 9, 2010. Note that because different instruments were used for the two sites, the magnitudes of suspended sediment concentration or equivalent diameter are not directly comparable across sites; rather, we compare relative temporal trends in the diel dynamics. Black bars at the top of the figure represent nighttime periods; white bars represent daytime periods.

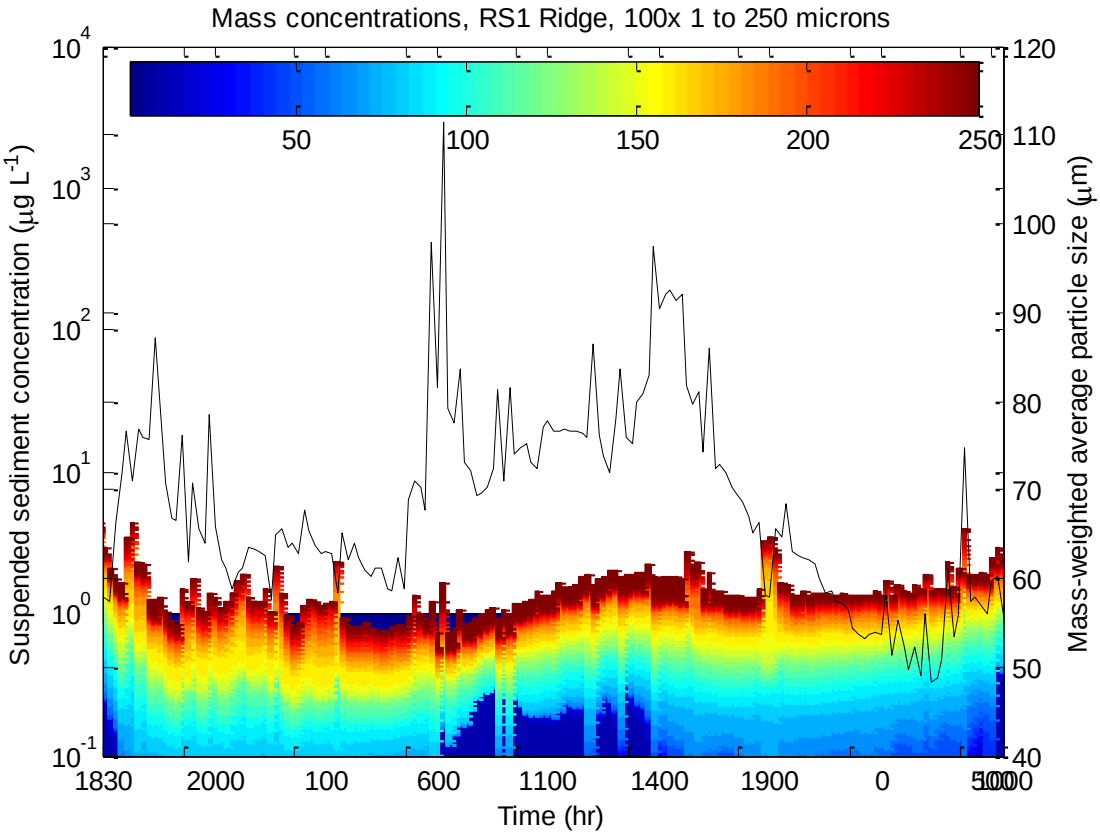

Figure PF5. Time series of mass weighted particle size distributions over forty hours at RS1 Ridge site. Data was binned into 32 size categories from 1.25 to 250 microns. Depth of water column was 42.5 cms. Distance of probe to peat was 19 cm and distance of probe to surface was 23 cm. Deployed August 7, 2012. Retrieved August 9, 2012.

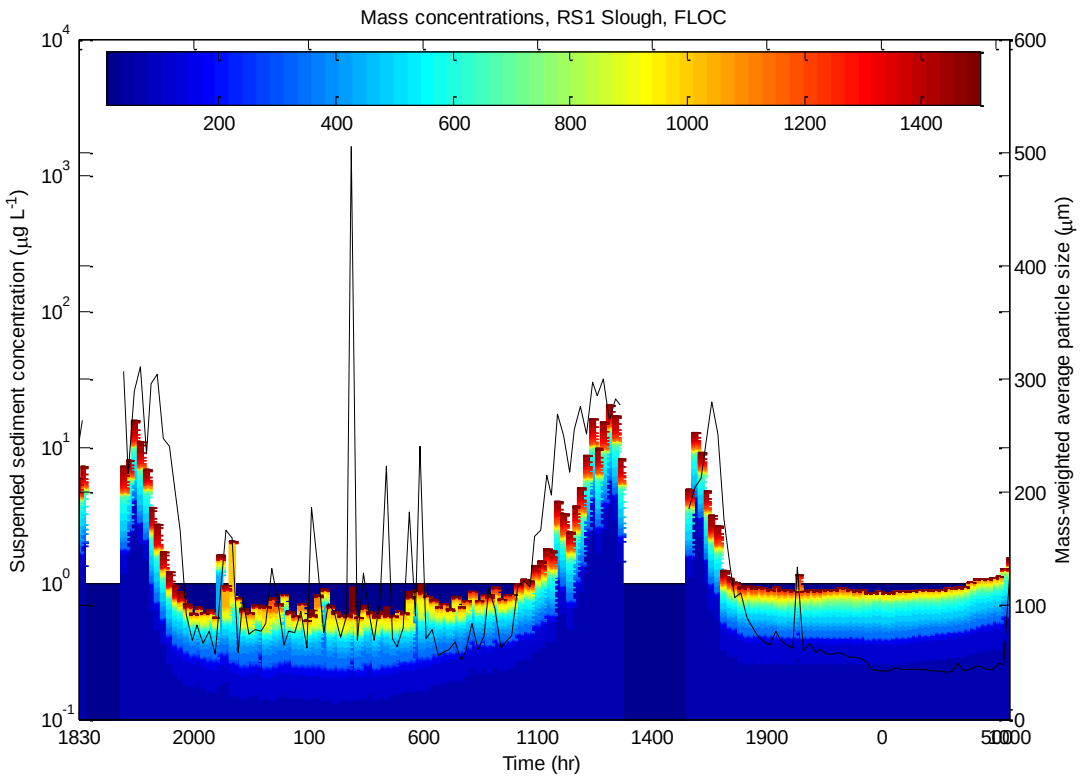

Figure PF6. Mass weighted suspended sediment concentrations and particle size over forty hours at RS1 Slough site. Data was binned in the 32 size classes from 7.5 microns to 1500 microns. Depth of water column was 55.8 cms. Distance of probe to peat was 32 cm and distance of probe to surface was 23 cm. Deployed August 7, 2012. Retrieved August 9, 2012.

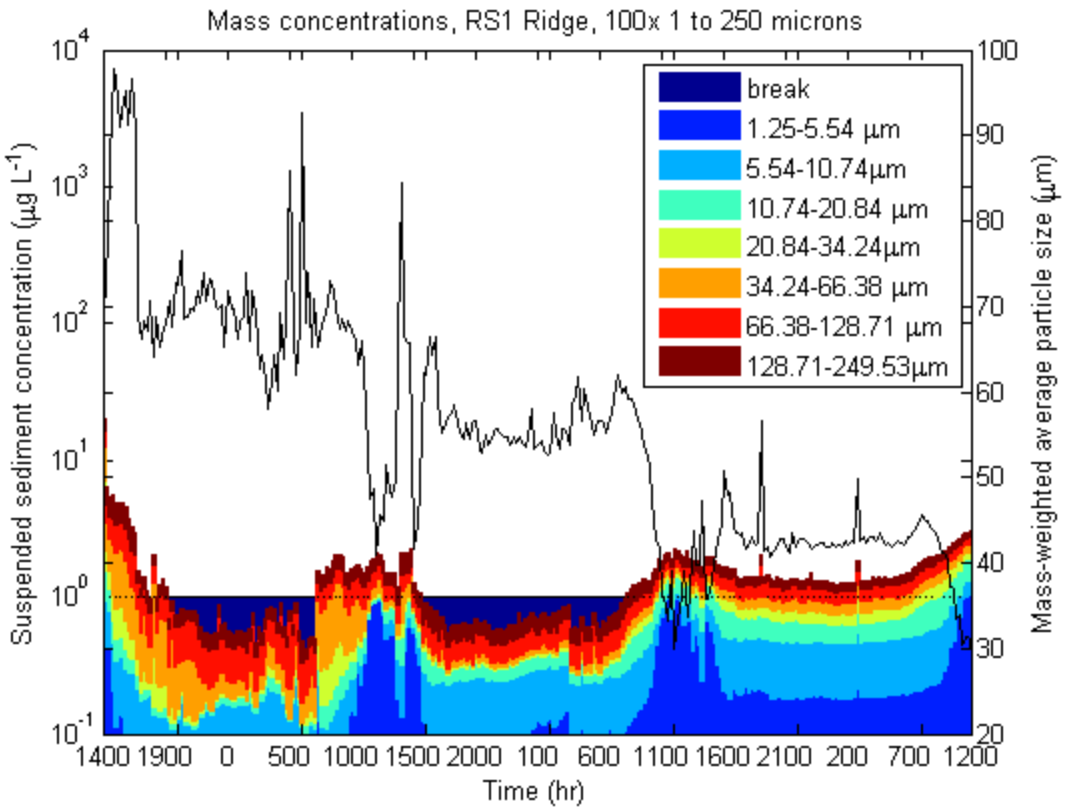

Figure PF7. Mass weighted suspended sediment concentrations and particle size of small component of sediment over forty hours at RS1 Slough site. Data was binned in the 7 size classes from 1.25 microns to 250 microns. Depth of water column was 55.8 cms. Distance of probe to peat was 32 cm and distance of probe to surface was 23 cm. Deployed August 7, 2012. Retrieved August 9, 2012.

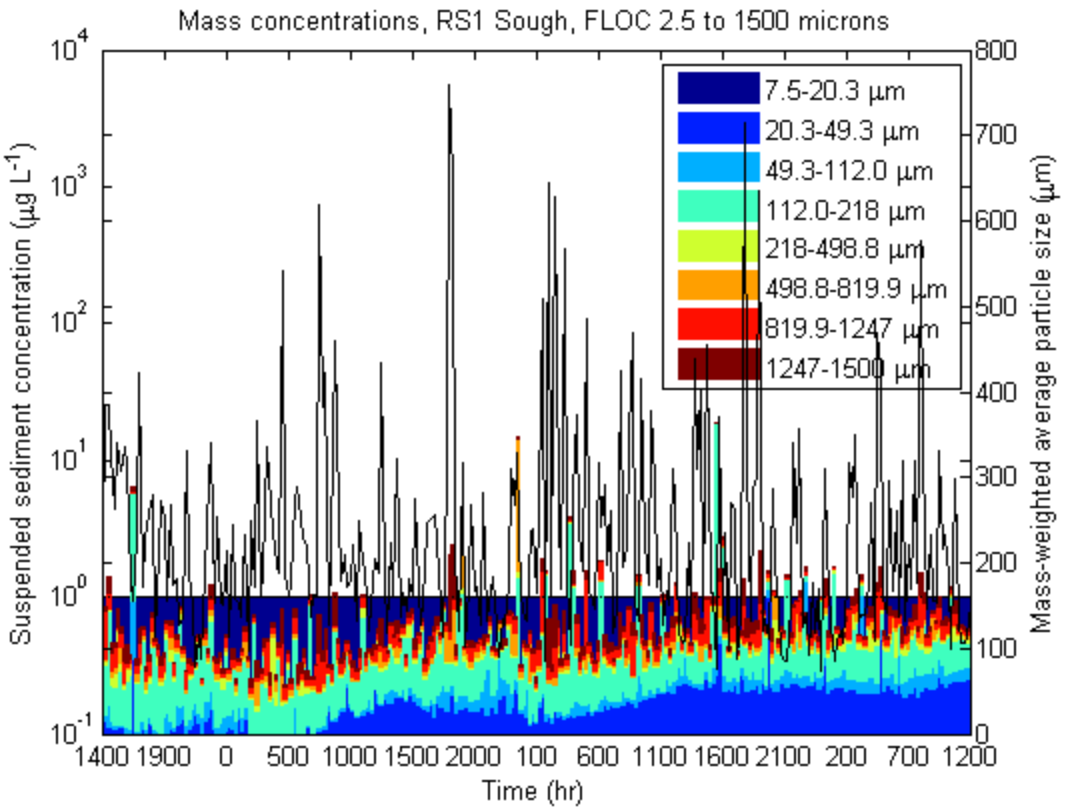

Figure PF8. Mass weighted suspended sediment concentrations and particle size of small component of sediment over forty hours at RS1 Slough site. Data was binned in the 7 size classes from 1.25 microns to 250 microns. Depth of water column was 55.8 cms. Distance of probe to peat was 32 cm and distance of probe to surface was 23 cm. Deployed August 7, 2012. Retrieved August 9, 2012.

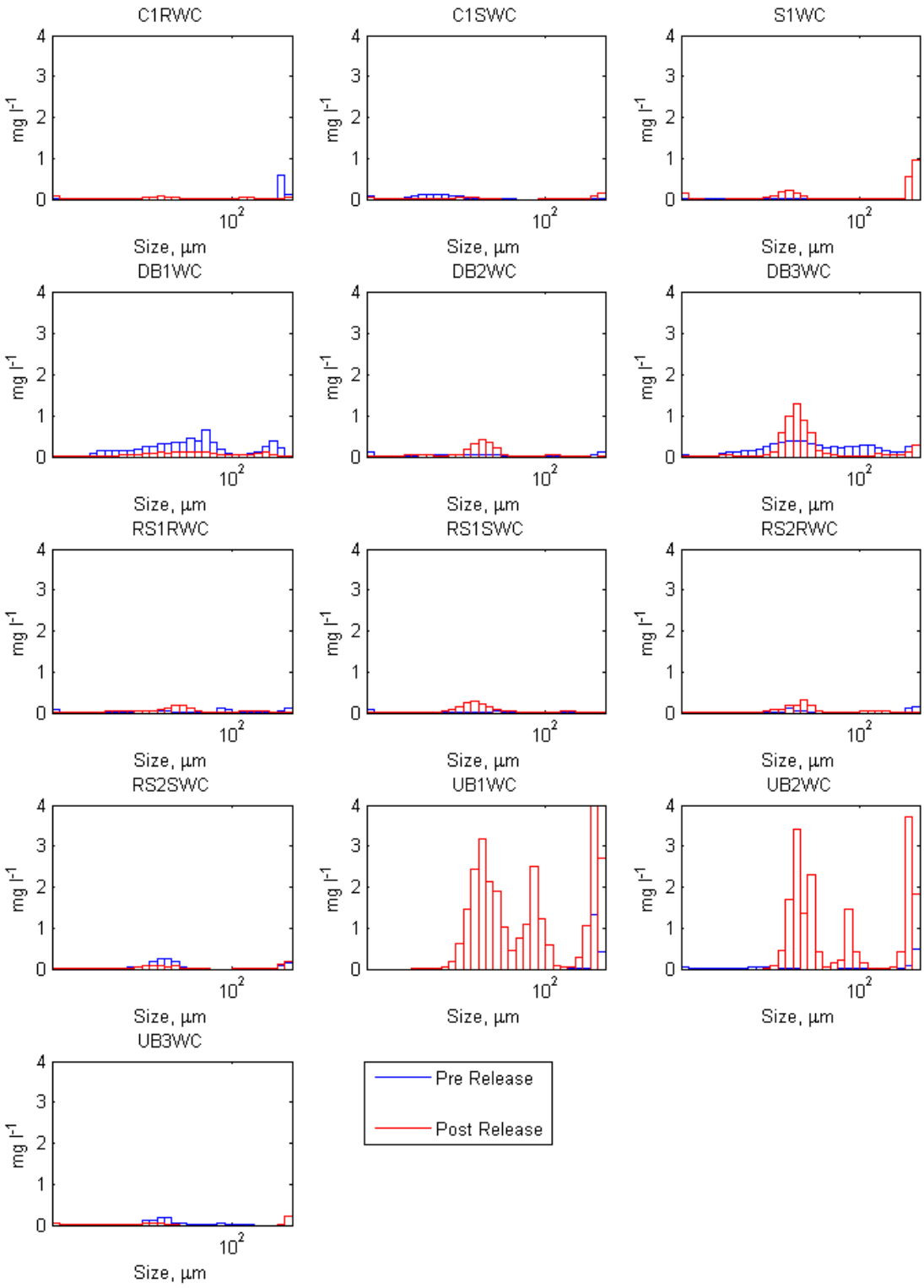

Figure PF9. Pre and post release comparison of mass weighted distributions of water column suspended particles.

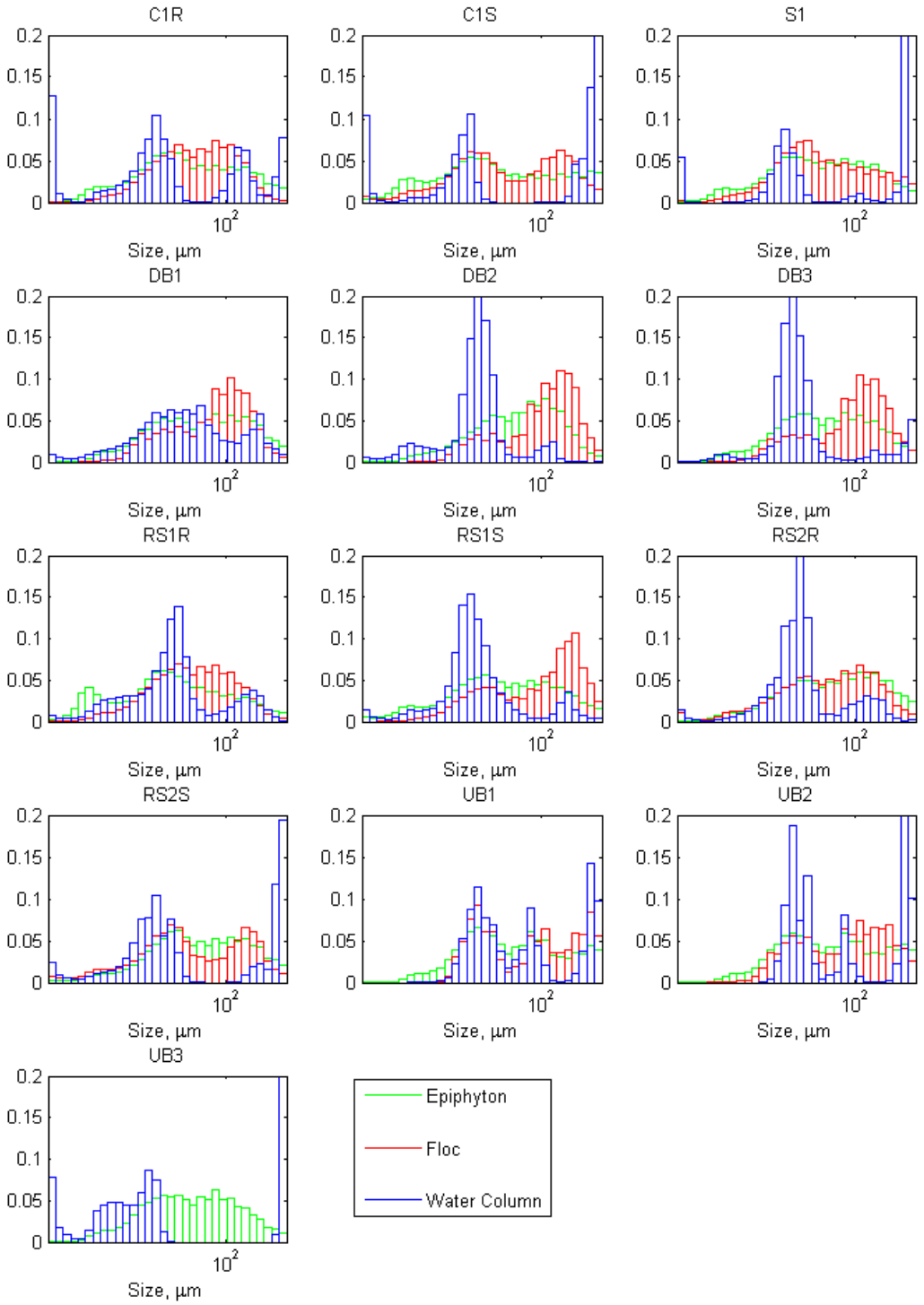

Figure PF10. Comparisons of distributions of Water Column, Floc and Epiphyton by size for samples collected November 9-10, 2013.

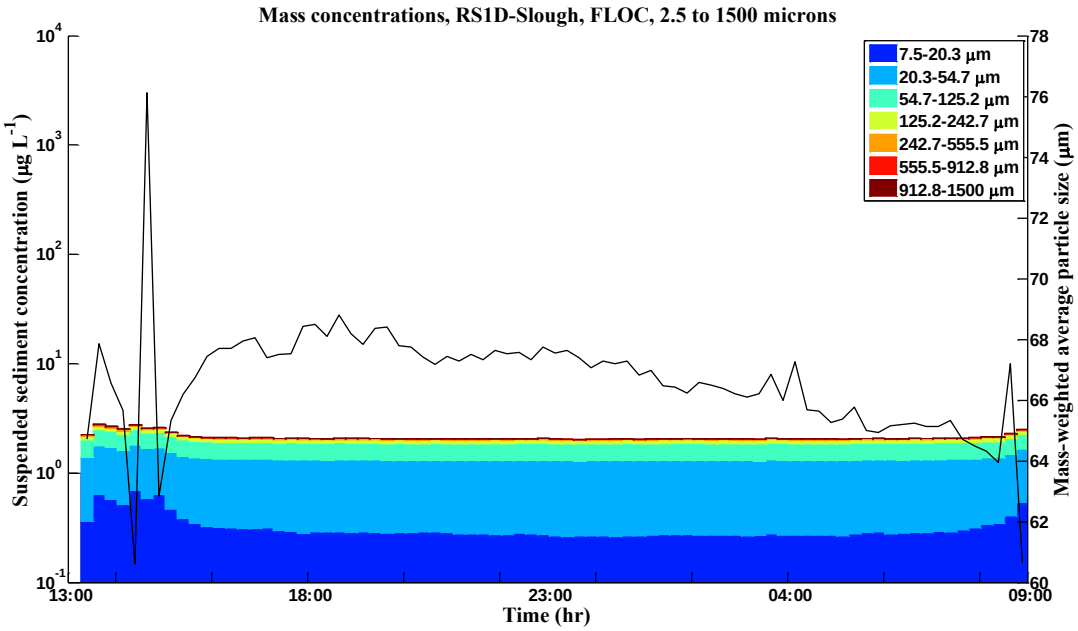

Figure PF11. Time series of particle size distribution and mass-weighted particle size distributions at RS1D site. Data was binned into 32 size categories from 7.5 to 1500 microns. Deployed period is November 4, 2013 13:30 to November 5, 2013 09:00 (Pre-Flow).

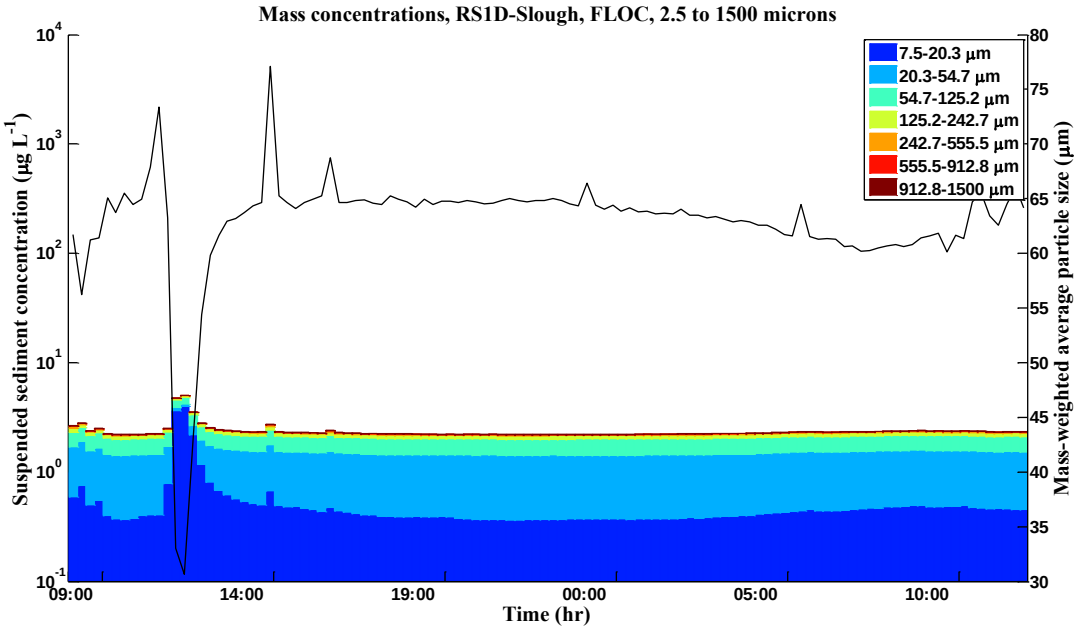

Figure PF12. Time series of particle size distribution and mass-weighted particle size distributions at RS1D site. Data was binned into 32 size categories from 7.5 to 1500 microns. Deployed period is November 5, 2013 09:00 to November 6, 2013 13:00 (Transient).

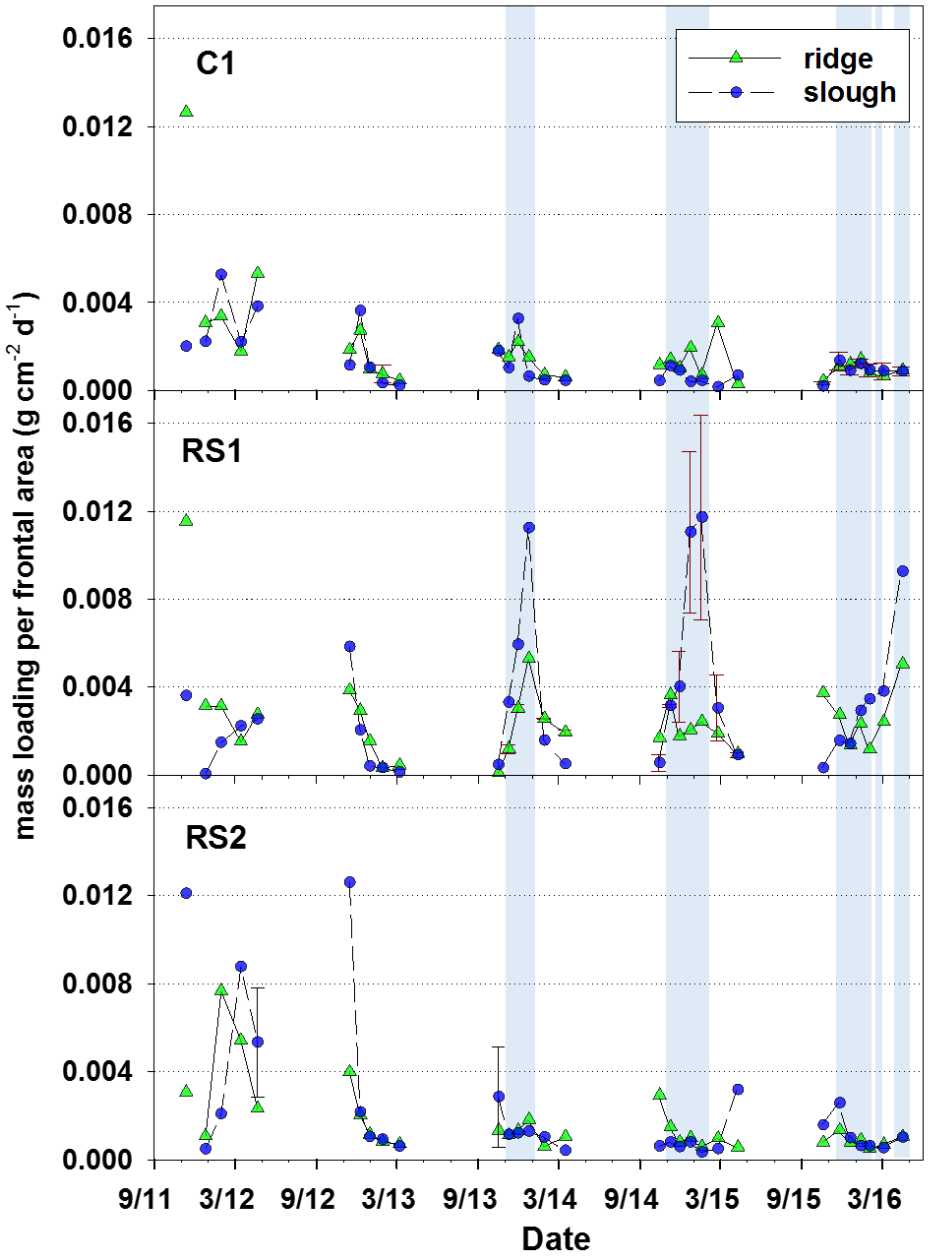

Figure PF13-A. Sediment transport estimated from horizontal trap deployments in ridge and slough habitats at the control (C1), high-flow (RS1), and low-flow (RS2) sites. Blue shading indicates the timing of flow events (S152 operations). Note that in 2016, the S152 was operated in February and March-April, beyond the normal operating window (November-January), due to a high water emergency. Error bars indicate the minimum and maximum values when duplicate traps were deployed. The study area burned in June 2011.

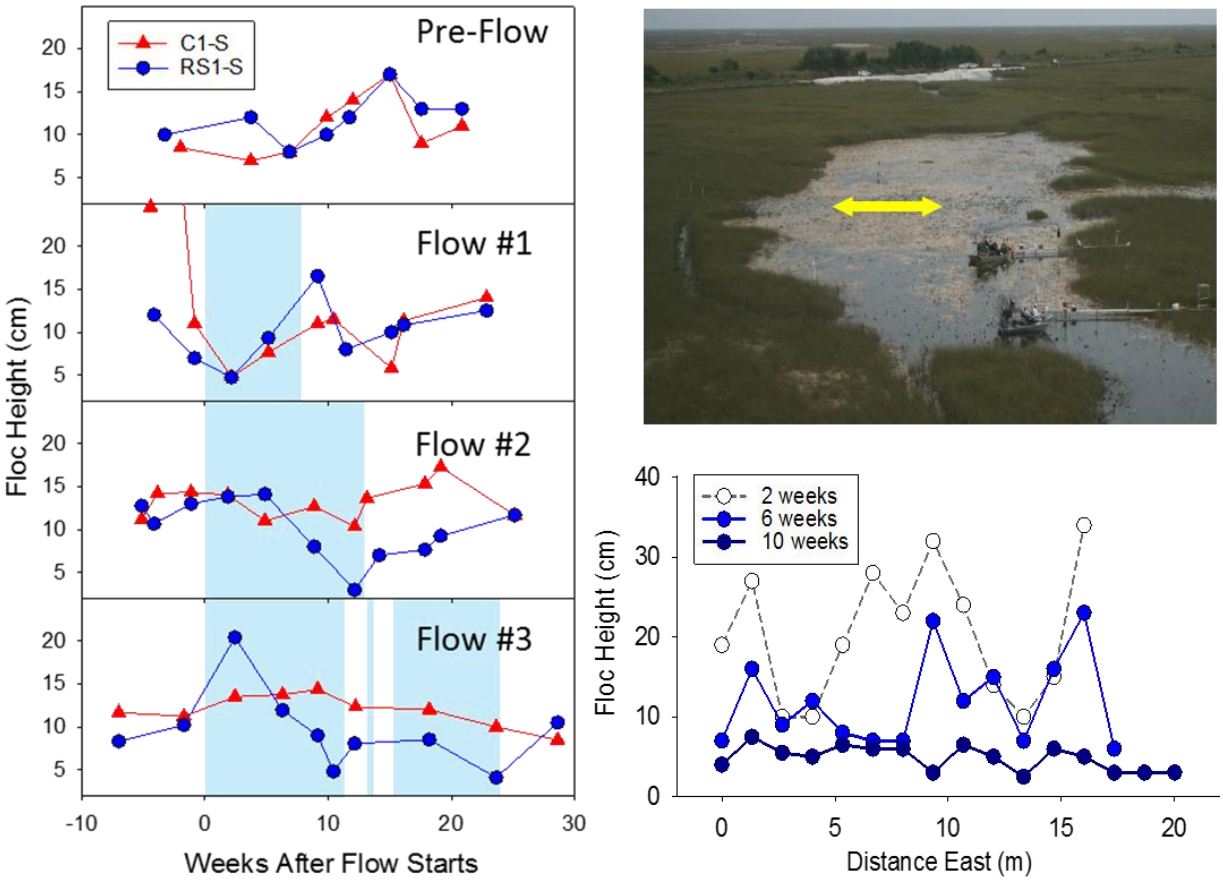

Figure PF13-B. (left panels) Floc height in the RS1 (blue circles) and C1 (red triangles) sloughs versus number of weeks after flow starts, or for the baseline period, number of weeks after November 1. Blue shading indicates timing of high flow events. (upper right) Approximate location of floc transect (yellow arrow) at RS1. (lower right) Floc height as a function of distance across the RS1 slough, at 2, 6 and 10 weeks after the start of flow on November 16, 2015.

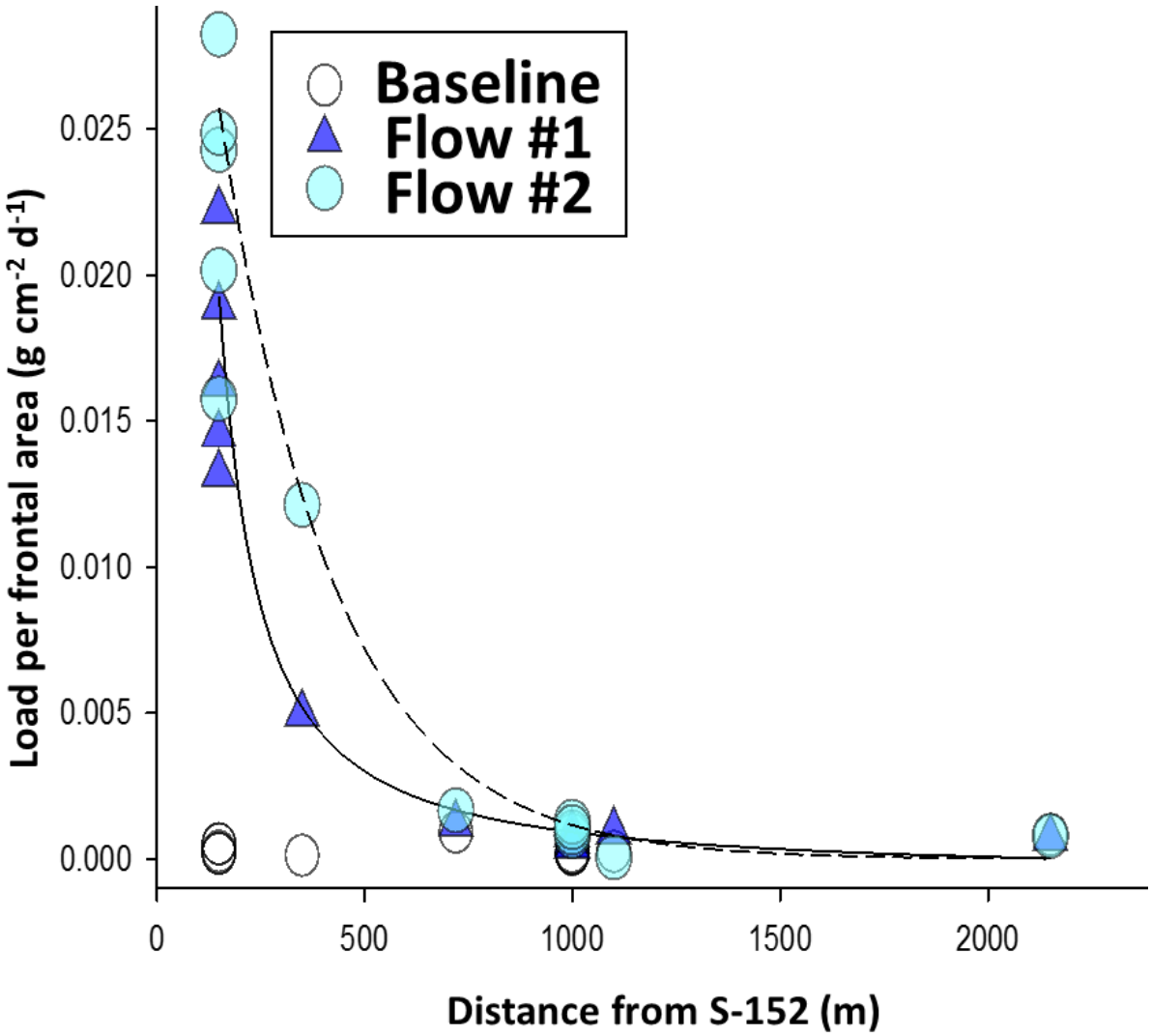

Figure PF14. Sediment transport in slough habitats as a function of distance from the S-152 in pre-flow, baseline conditions (2012) and the two high-flow events (Nov-Dec 2013 and Nov-2014 through Jan-2015). Multiple points per site and date indicate instances where multiple traps were deployed.

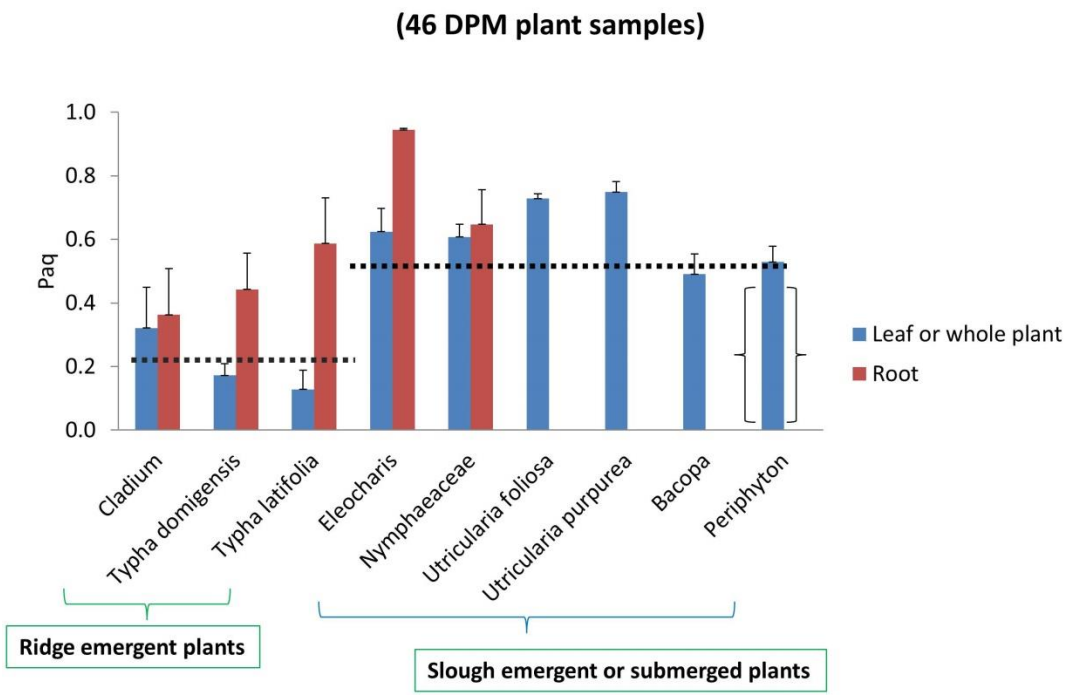

Figure PF15. Distribution of Paq values determined for selected vegetation samples. Some samples include both above- and below-ground tissues. Periphyton values in brackets since plankton does not contribute significantly to mid-to-long chain n-alkanes (see text for further details).

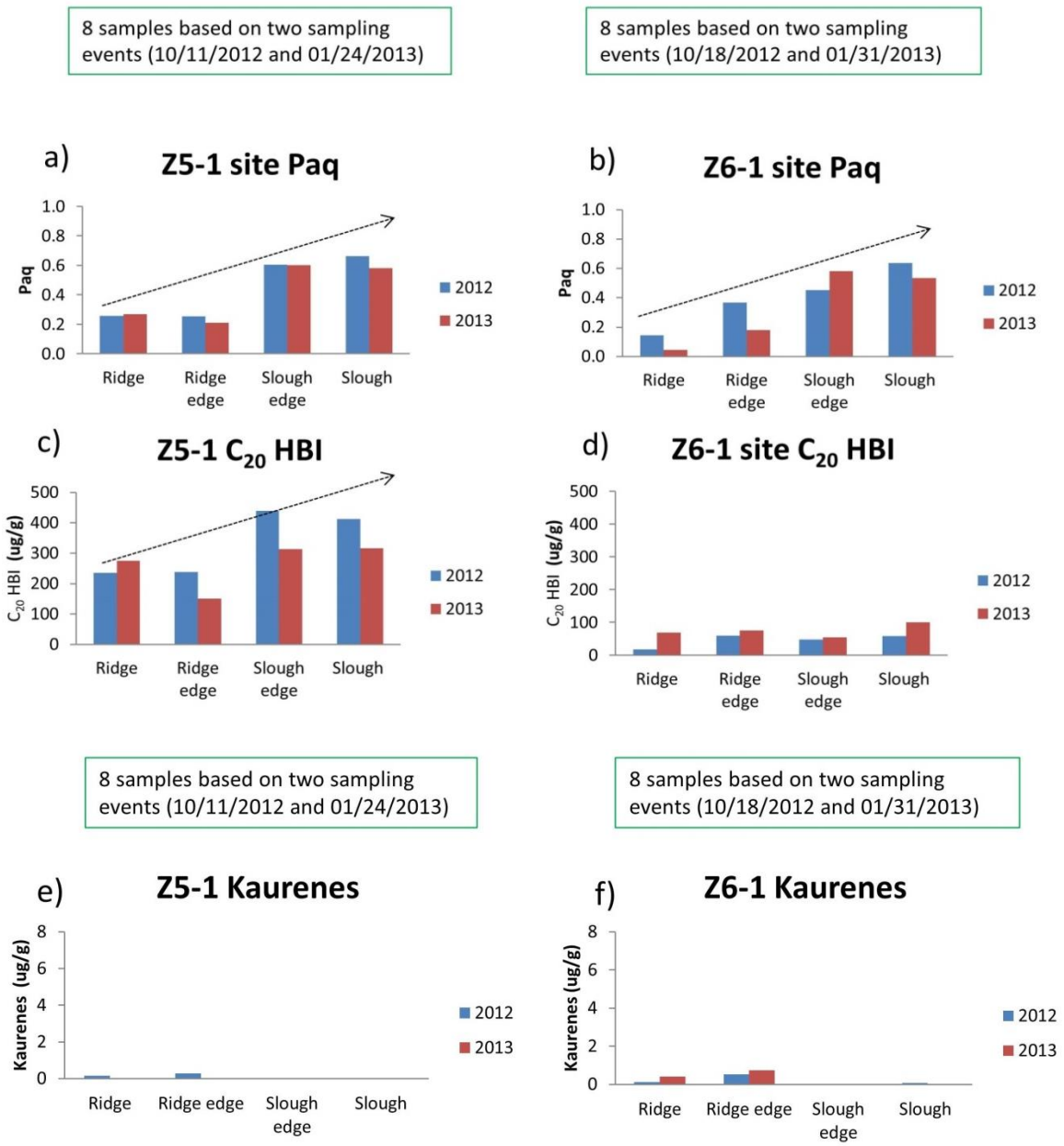

Figure PF16. Biomarker distributions along ridge-to-slough transects for two different sampling events at sites Z5-1 and Z6-1.

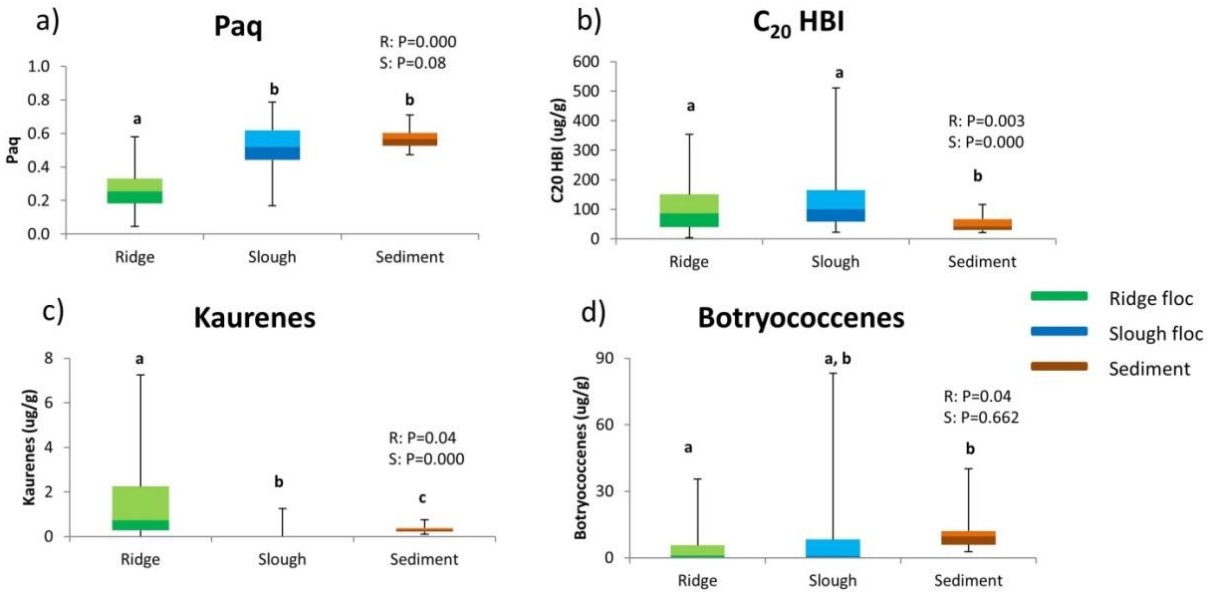

Figure PF17. Comparison between average biomarker distributions for all slough, ridge and canal sediment trap samples (107 total).

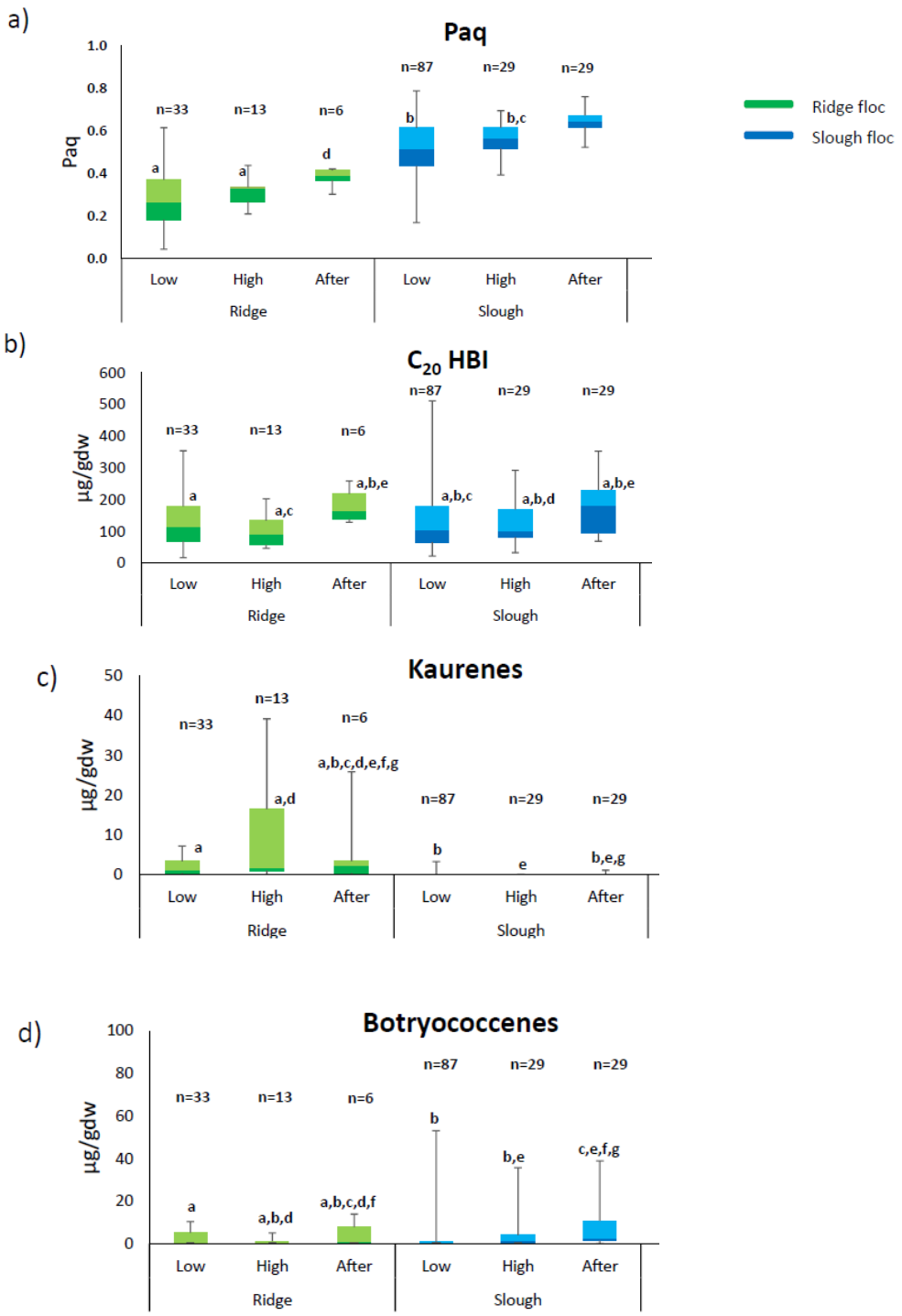

Figure PF18. Comparison of biomarkers Paq, C20 HBI, Kaurenes, and Botryococcenes in ridge and slough floc collected from BACI and spatial survey sites, in the pre-, during and post-flow sampling periods (Low, High, and After, respectively). Different letters indicate statistically different datasets; unmarked plots are statistically different from all other groups. N=197.

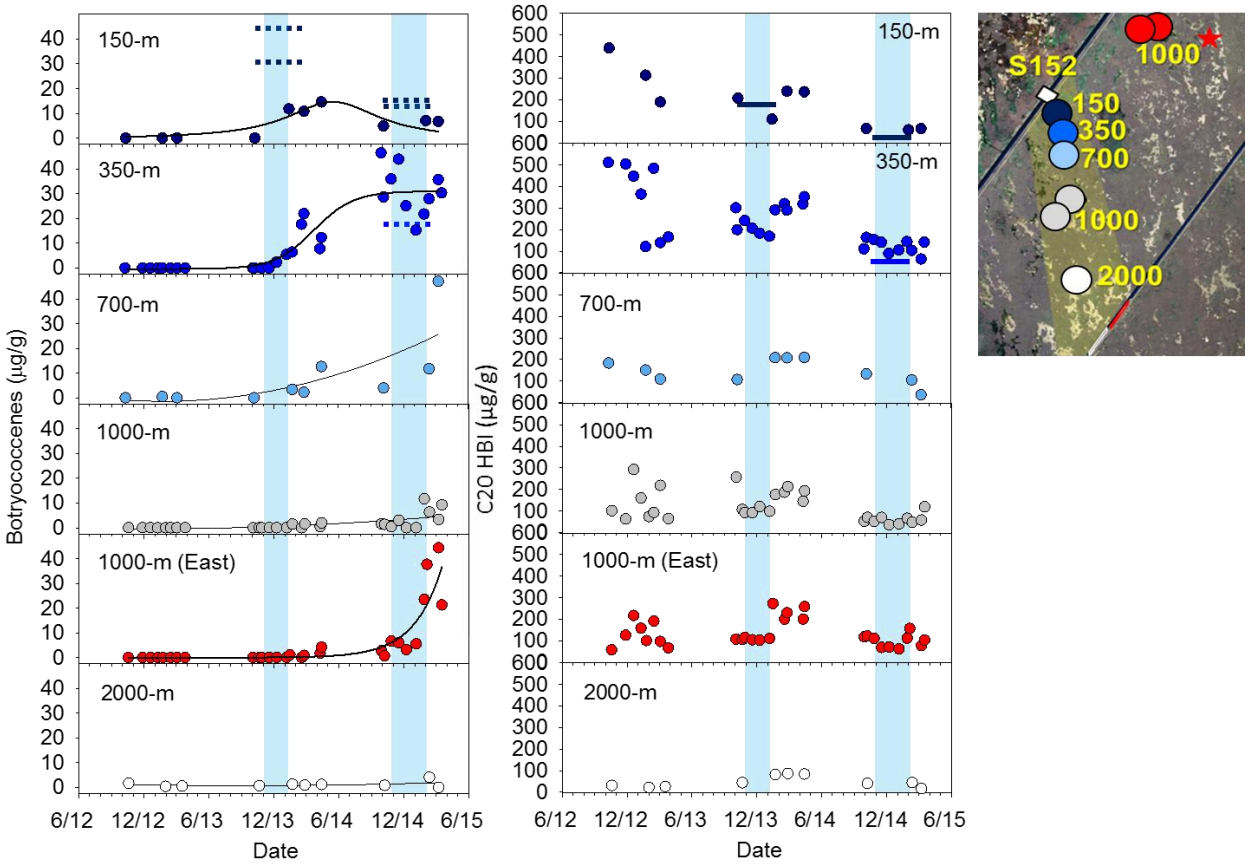

Figure PF19. Changes in floc concentrations of Botryococcenes (left) and C20 Highly Branched Isoprenoids (C20 HBI, right) collected at sloughs sites along the north-south flow path and at control site (east, in red). Blue shading indicates timing of high flow events. Dashed lines represent concentrations of biomarkers in advected sediment collected in horizontal traps.

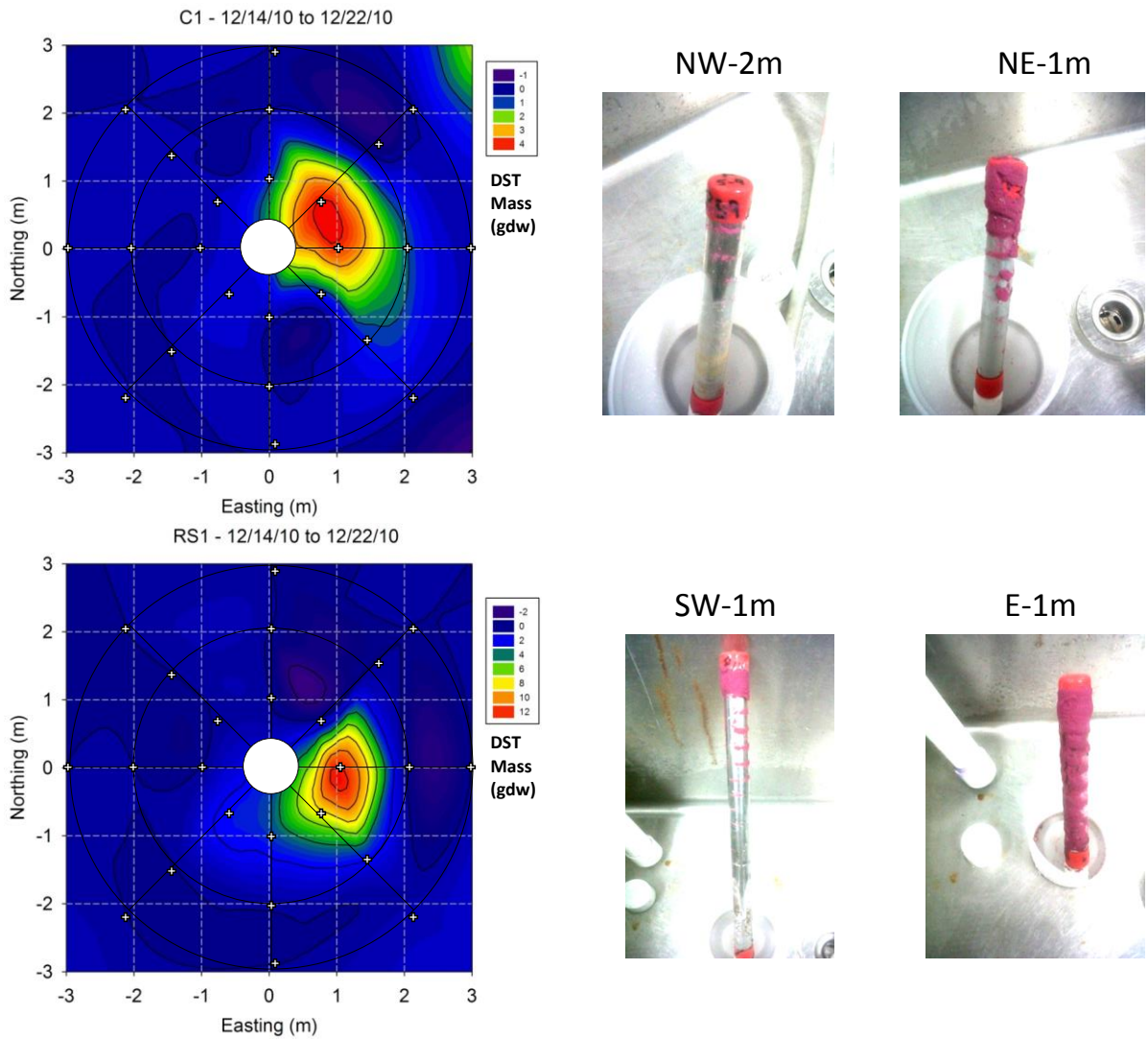

Figure PF20. Short-term movement of dual synthetic tracer (DST) at sites C1 (top) and RS1 (bottom) conducted in December 2010. Left (graphs): Contour plots of DST particles recovered from magnets (7 days after DST deployment) at each of the sampling sites arrayed at 1-m, 2-m, and 3-m from. Right (images): Examples of the range of DST collected by magnets deployed at C1 (top 2 images) and RS1 (bottom), sampling locations indicated above each image.

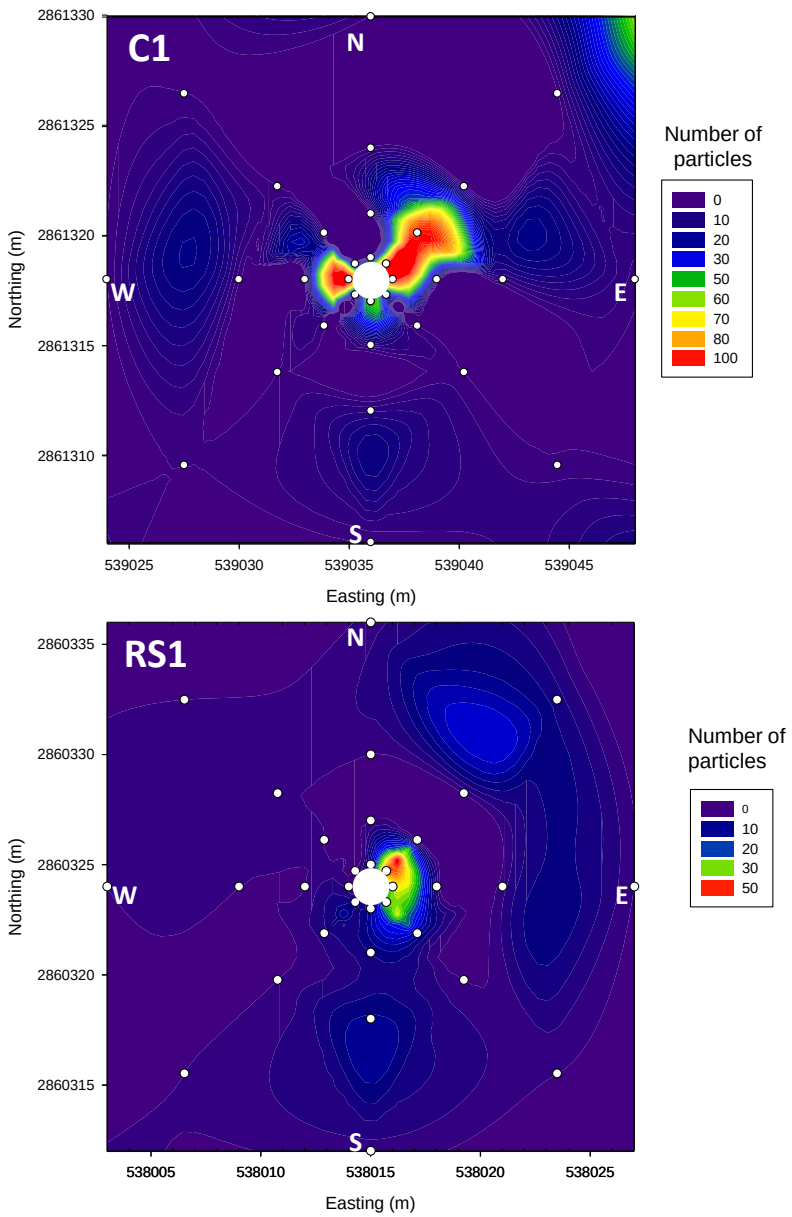

Figure PF21. Large-scale synoptic survey conducted in August 2012 at sites C1 and RS1. Colors represent number of fluorescent particles recovered from magnets at each of the sampling sites (white dots) arrayed at 1-m, 3-m, 6-m, and 12-m from the original deployment location (large white circle) in December 2010.

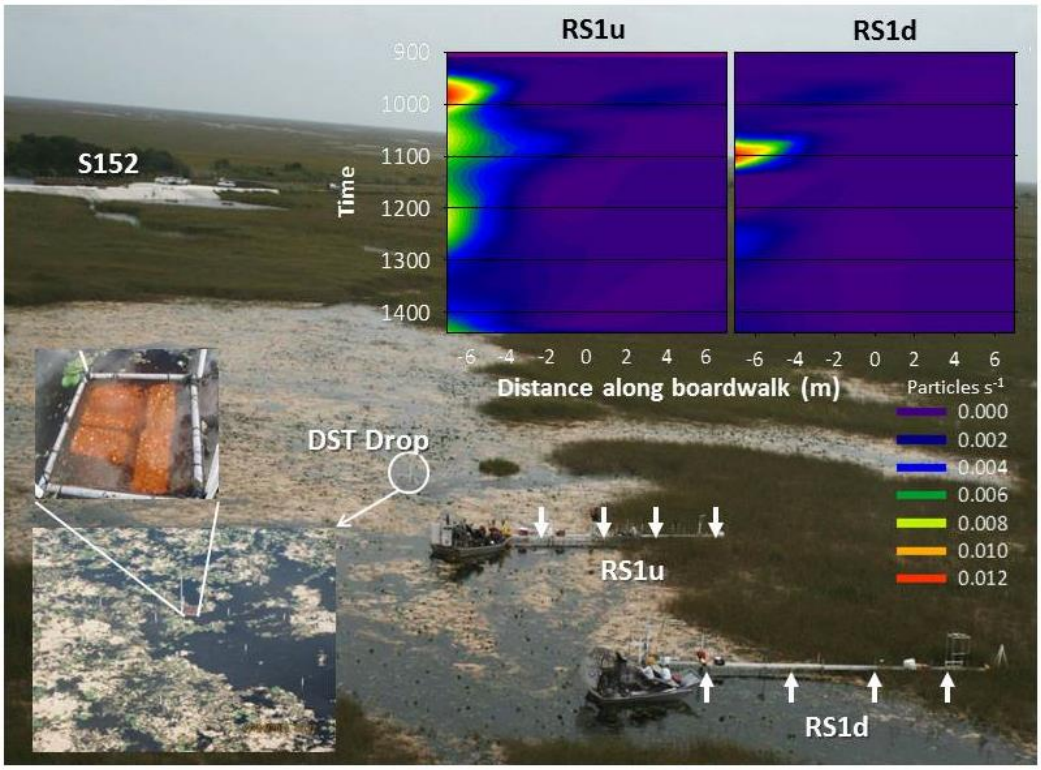

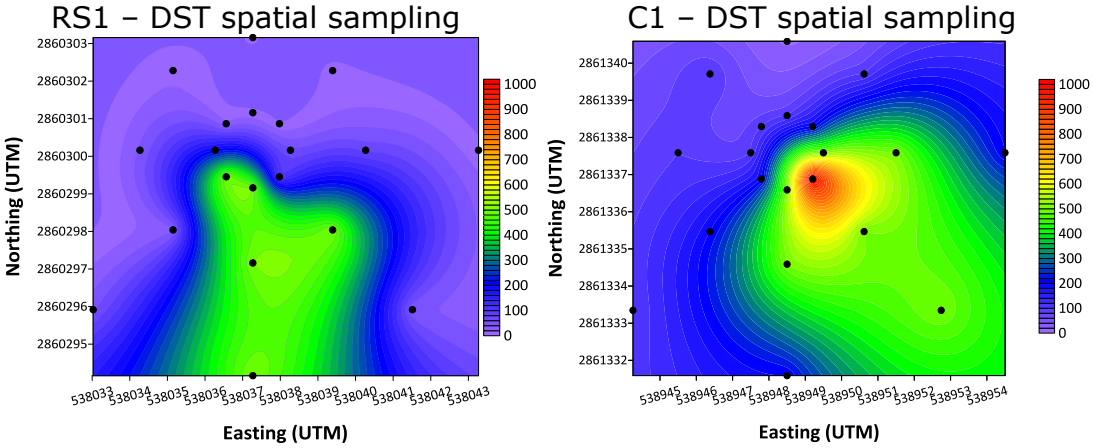

Figure PF22. **(top)** Dual synthetic tracer (DST) movement at RS1 on November 5th. Drop site indicates where floc tracer was deployed prior to flow. Contours are particle capture rates (particles s^{-1}). Arrows indicate magnet locations for capturing DST. (**bottom left**) Spatial sampling of DST at RS1 and at C1 (**bottom right**). Contours represent number of particles captured per magnet from Oct31 – Nov14 (RS1) and Nov1 – Nov15 (C1).

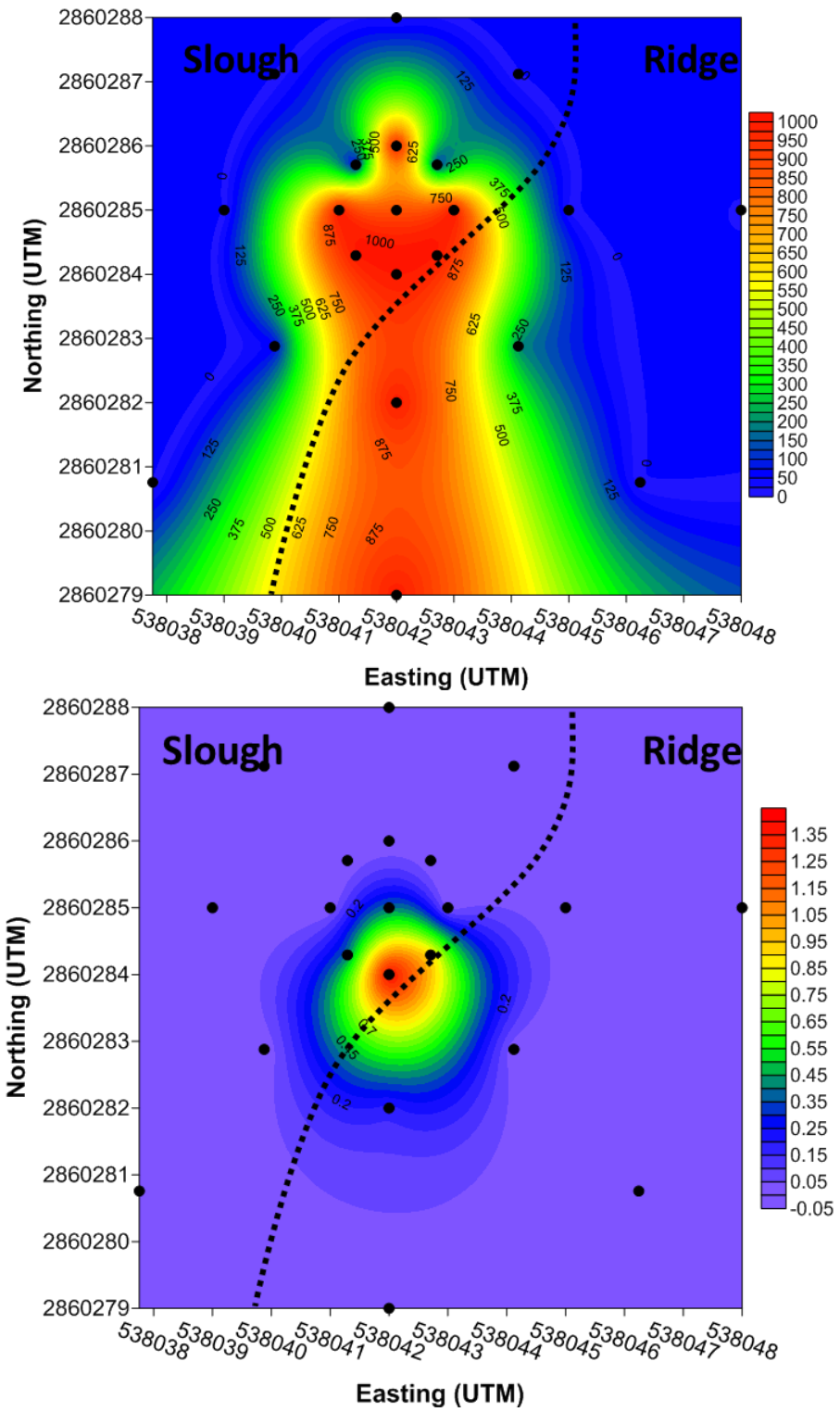

Figure PF23. Dual synthetic tracer (DST) movement at RS1. Dotted line delineates the slough-ridge edge. (top) Contour plot represents the number of particles captured per magnet from Oct30 – Nov13, 2014. (bottom) Contour plot represents the weight (g) of tracer captured per magnet for the same period.

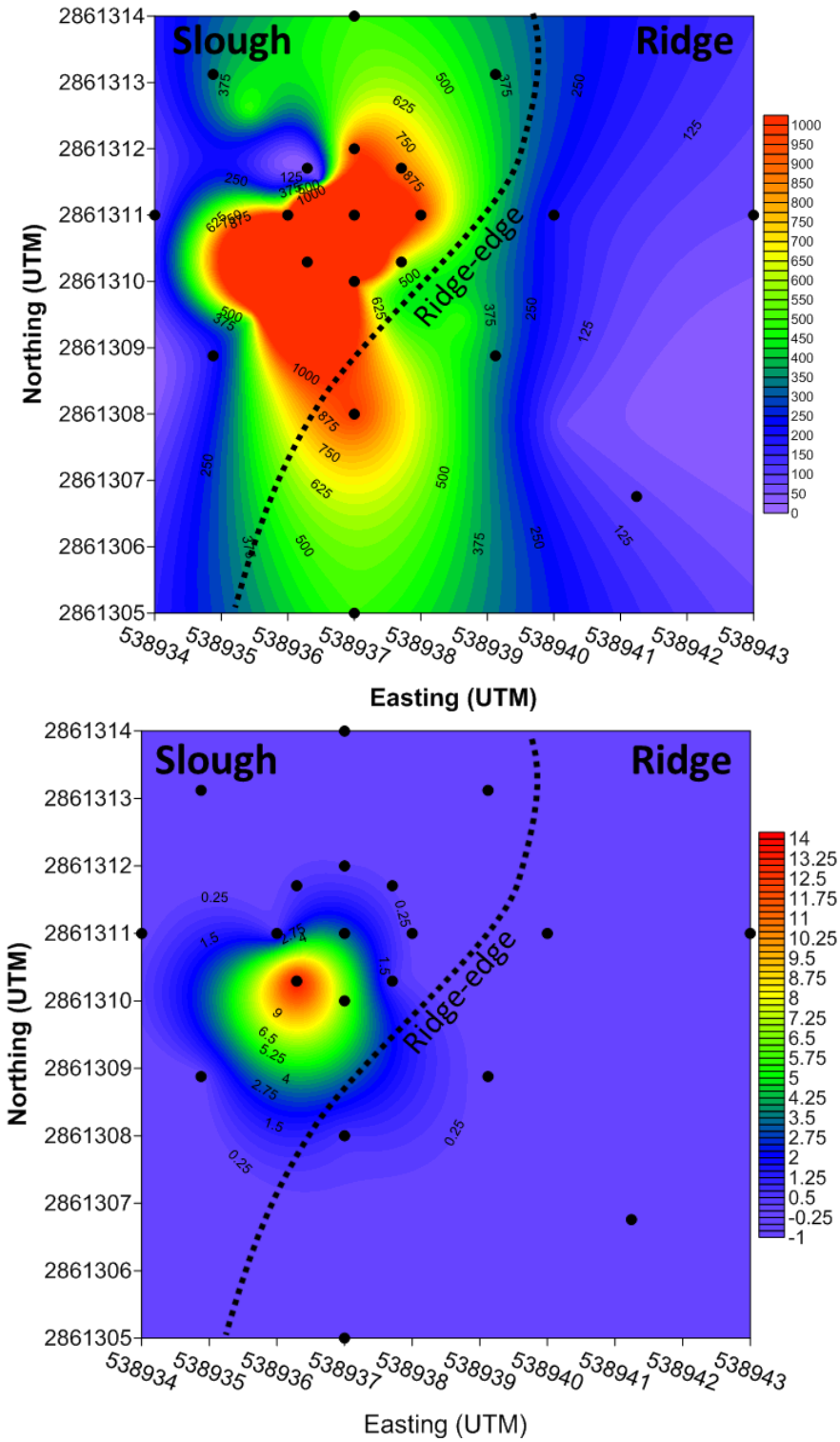

Figure PF24. Dual synthetic tracer (DST) movement at C1. Contour plot at top represents the particles captured per magnet from Oct31 – Nov14, 2014. Contour plot on bottom represents the total weight (g) of tracer captured per magnet for the same period.

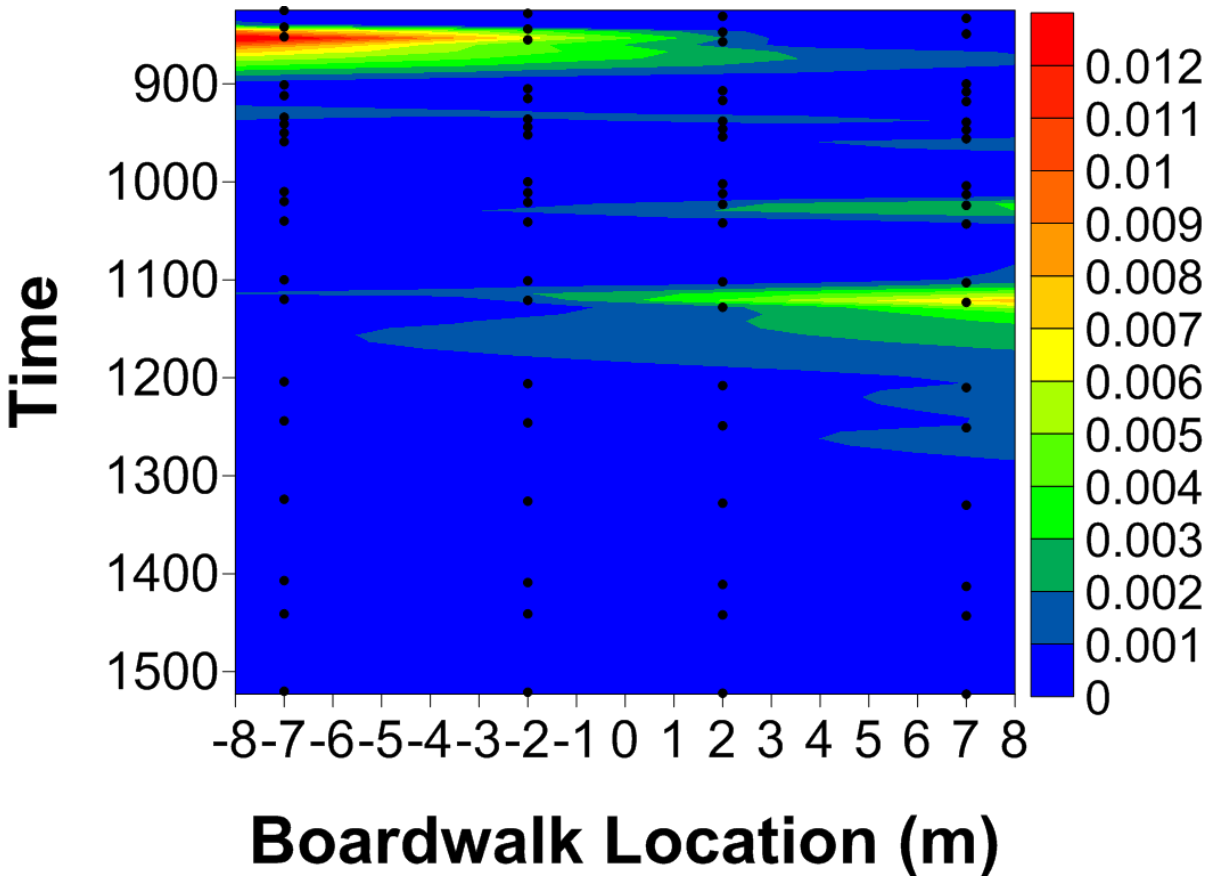

Figure PF25. Dual synthetic tracer (DST) movement at RS1u boardwalk on November 4th. Contours are particle capture rates (particles s-1). The boardwalk locations represent the gradient between slough habitat on the left (locations -8 to -1) and ridge habitat on the right (locations 1 to 8). The mid-location (0) represents the slough/ridge edge.

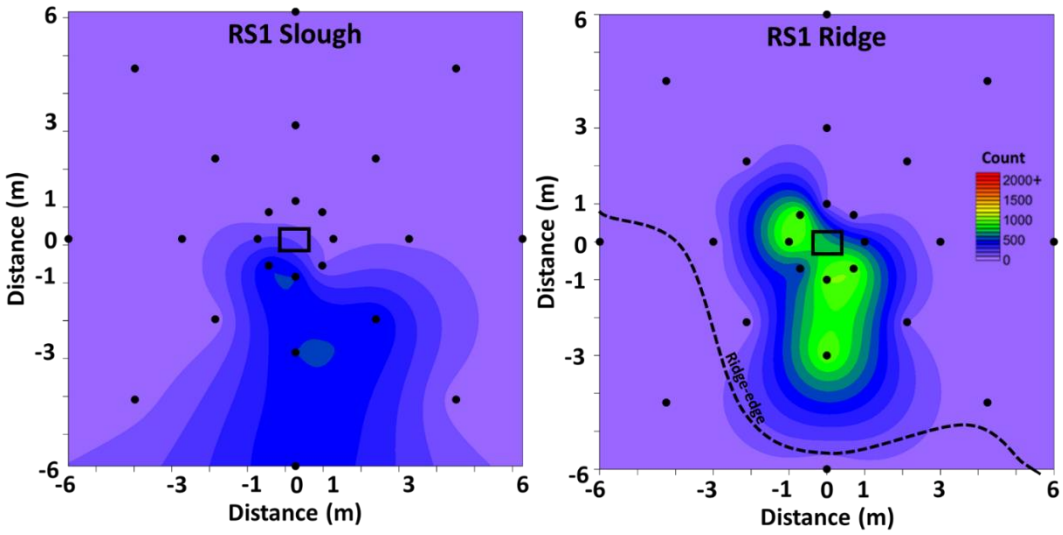

Figure PF26. Spatial distribution of dual-use, synthetic tracer (DST) collected from deployments in the slough (2013, left) and ridge (2015, right) at the RS1 site. More particulate movement was found in the slough, while in the ridges, the DST does not move past 3 meters.

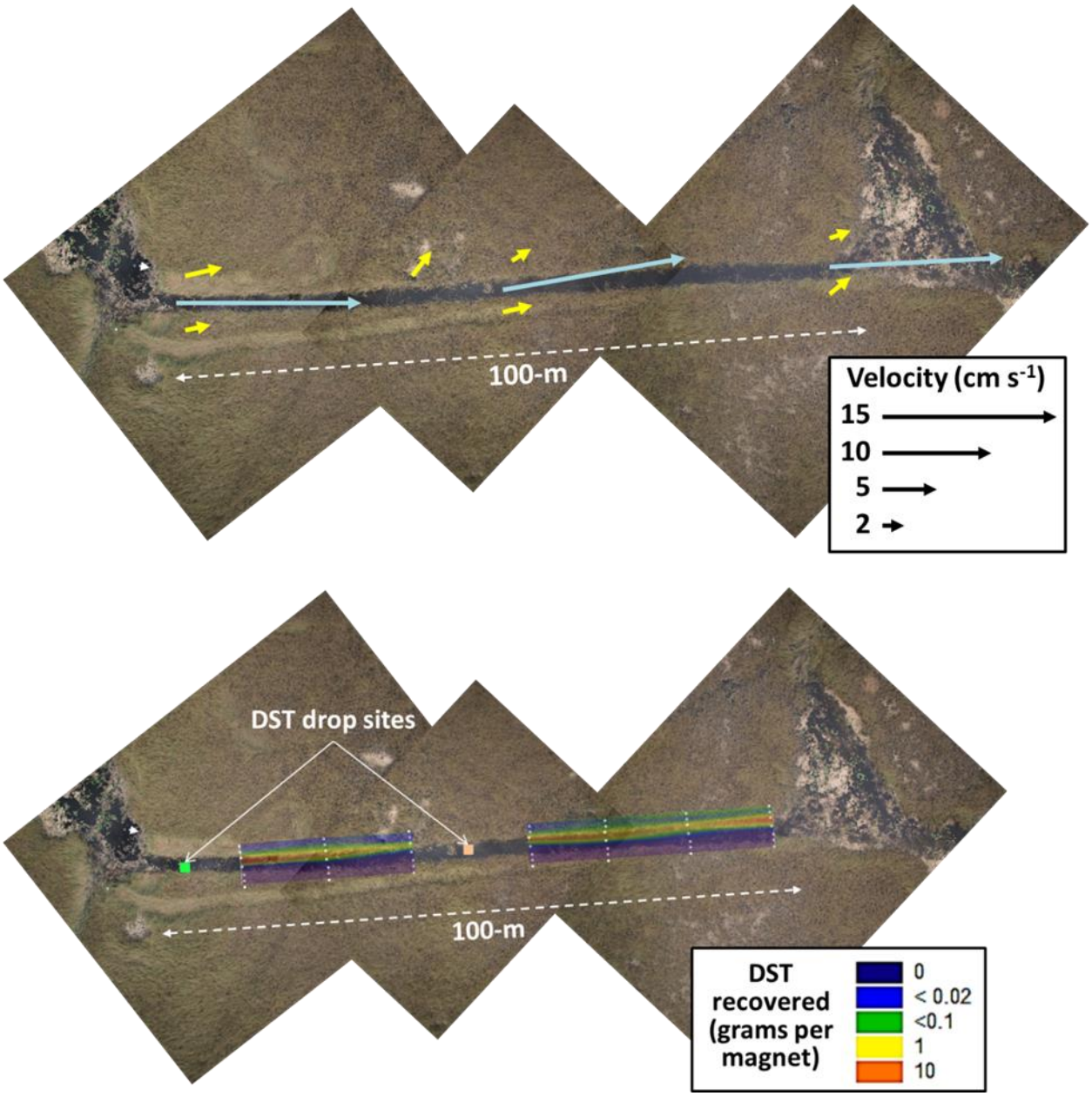

Figure PF27. **(Top)** Mid-water column flow velocities measured in the created slough and in adjacent sawgrass. Velocities were measured using a Sontek Flowtracker during high flow #2, December 30, 2014. Base of arrow represents location of measurement. **(Bottom)** DST captured on magnets along 5-m transects spanning the slough and adjacent ridges. Magnet locations are indicated by white dots. Location of DST drops at upstream and mid-slough location indicated by squares. High resolution imagery was taken from helicopter on November 4, 2014.

Figures–Biogeochemical Processes (BG1-…)

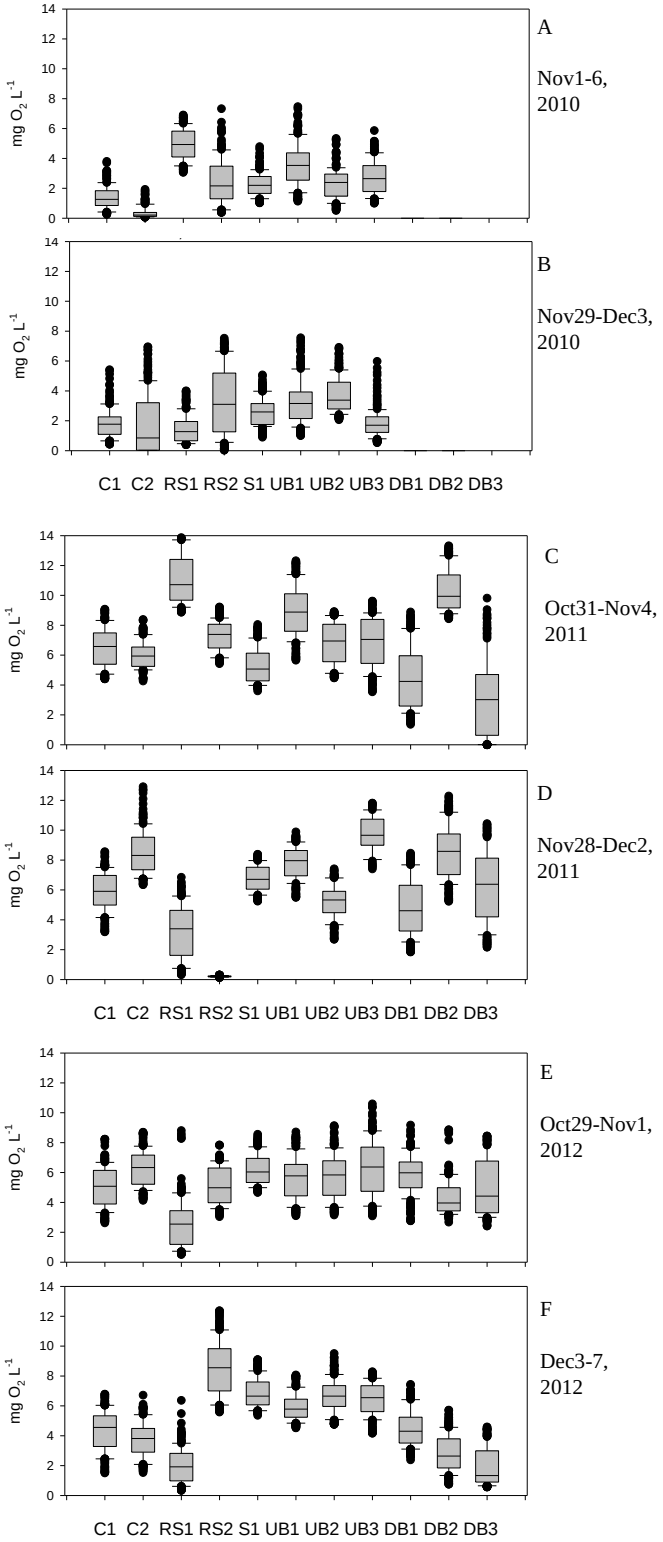

Figure BG1. Box-plot summary statistics of O_2 concentrations for 5-day deployments conducted in slough habitats at DPM sentinel sites during the Nov-Dec window of 2010, 2011 and 2012. Box represents the 75th and 25th percentiles, and the median.

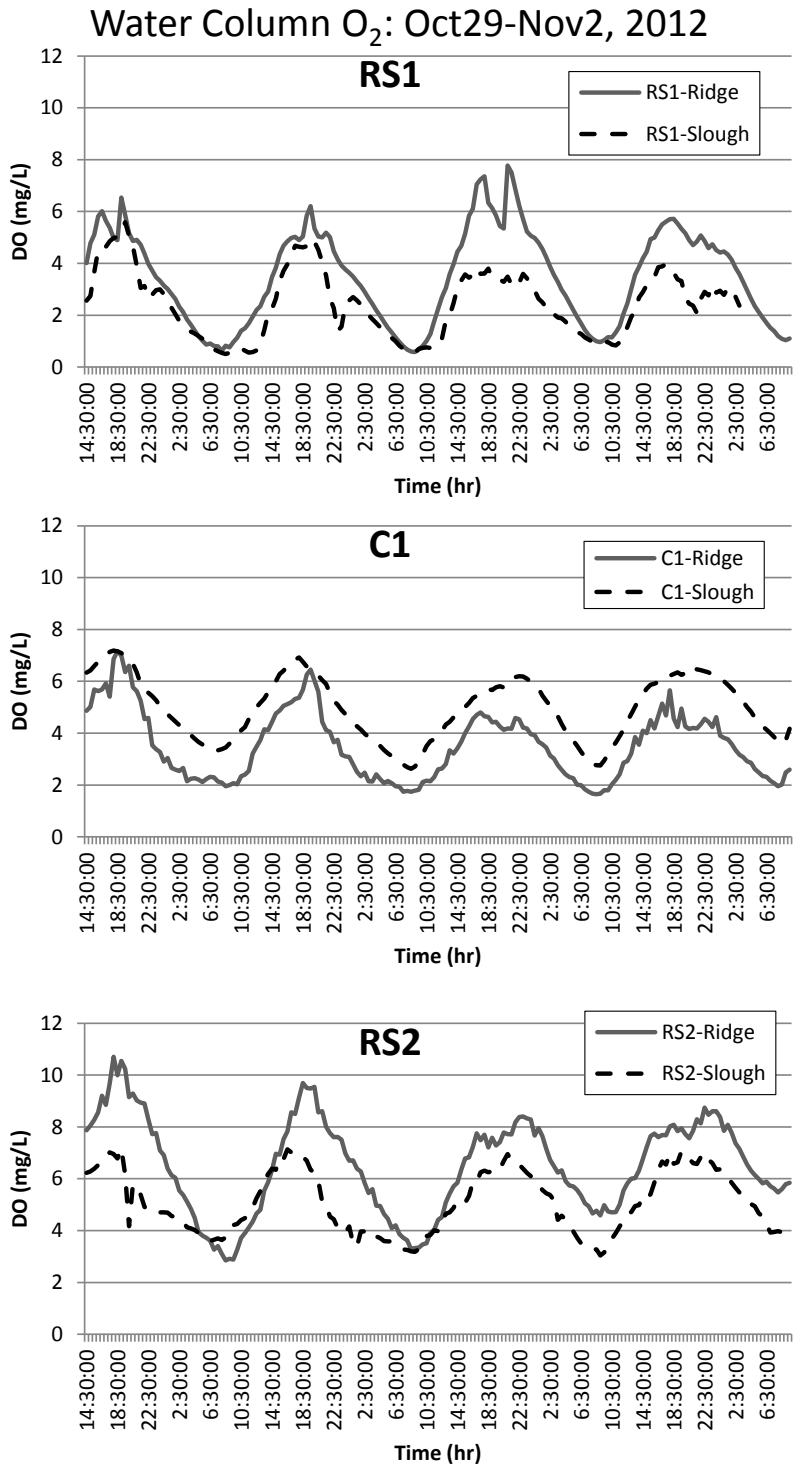

Figure BG2. Diel variation in water column O_2 concentrations for 5-day deployments in ridge and slough habitats at DPM sentinel sites RS1, C1, and RS2.

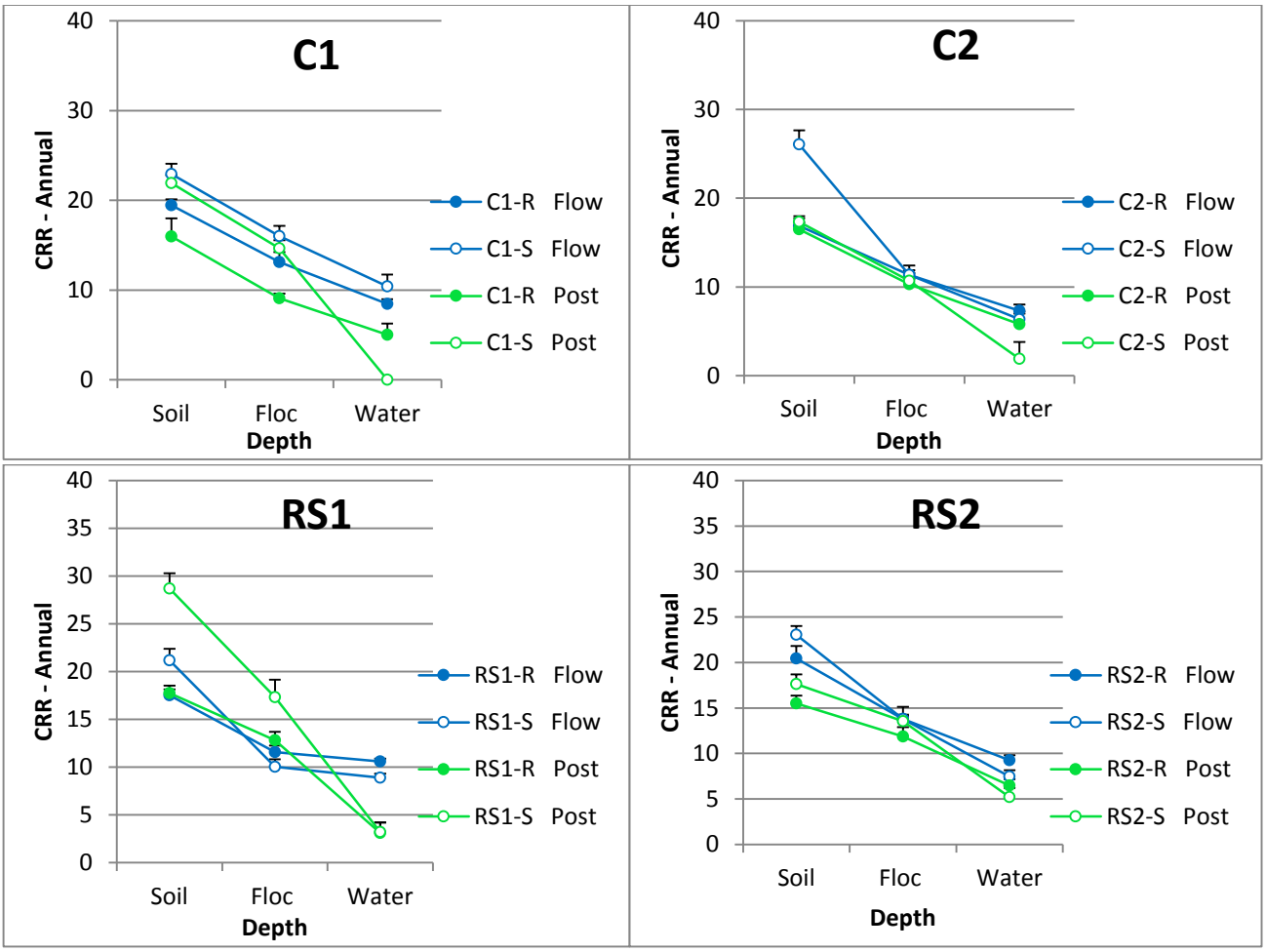

Figure BG3. Cotton Rotting Rates (CRR) at RS1, RS2, C1 and C2 in Nov-2014 Flow and post-Flow deployments.

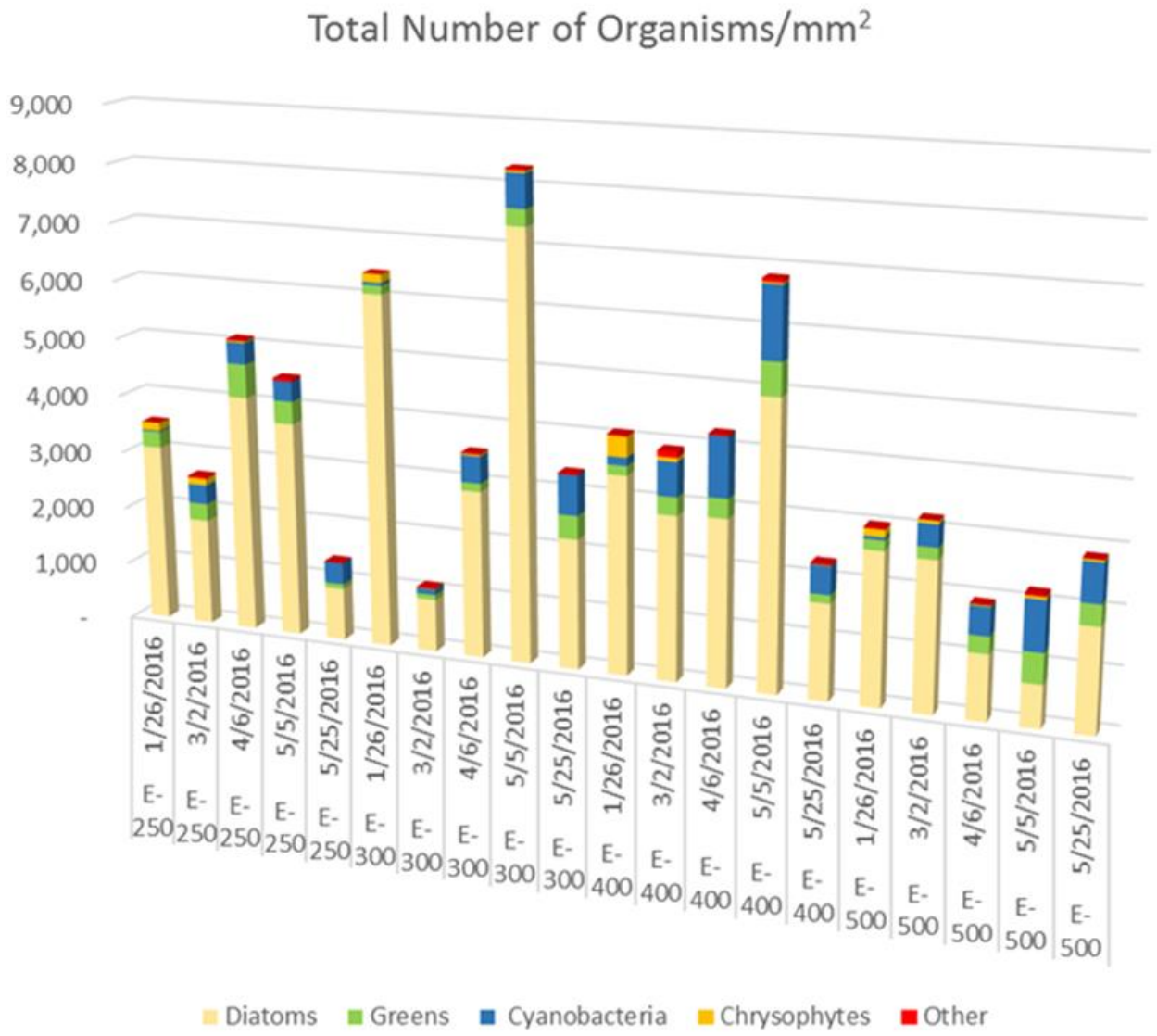

Figure BG4. Number of each taxonomic group per surface area (mm2) across site and time. Associated dates represent the collection date following a 3-week colonization period.

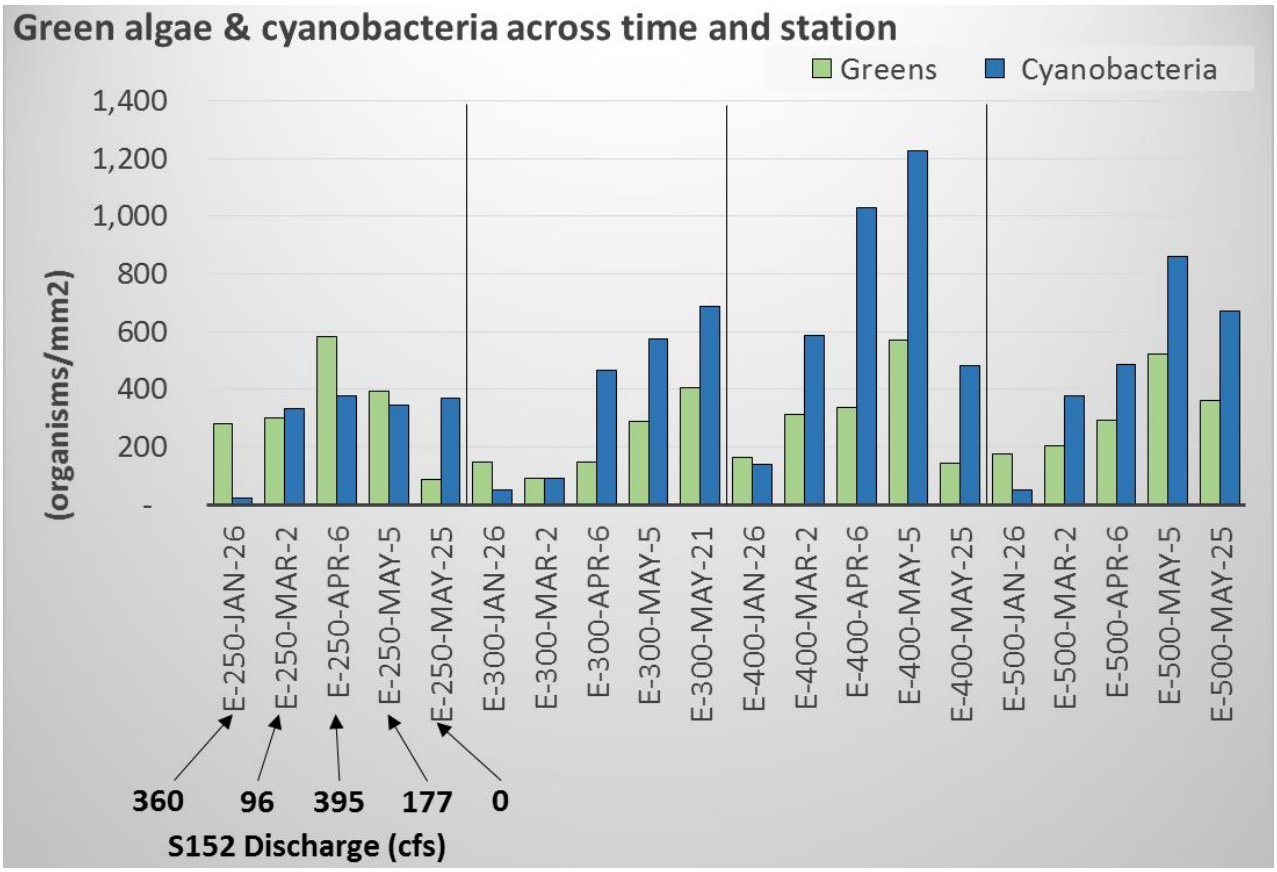

Figure BG5. Trends in green algae and cyanobacteria temporally and spatially near S152. Number of each taxonomic group per surface area (mm2) across site and time. Discharge (cfs) represents the mean daily average discharge from S152 for each colonization period.

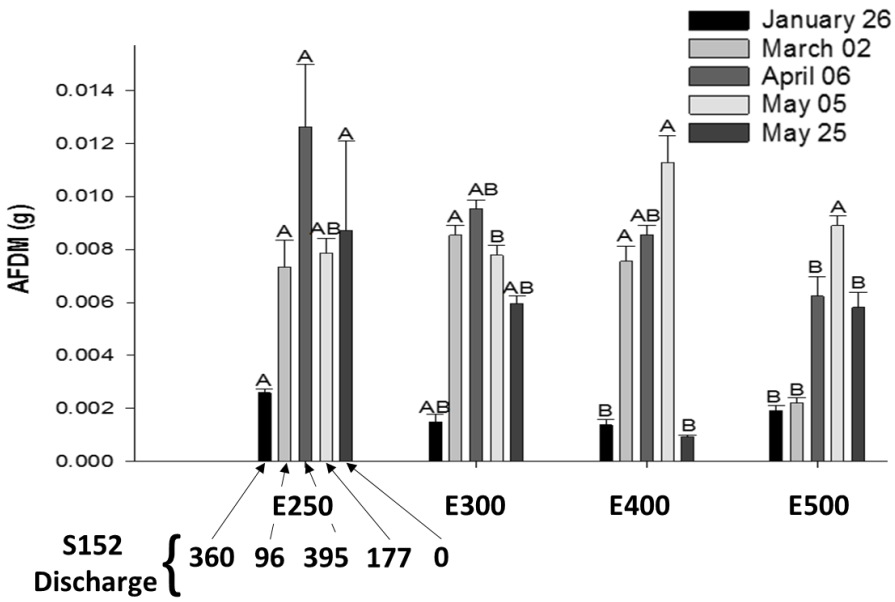

Figure BG6. Periphyton biomass on artificial dowel substrates following 3-week incubations at each site. Dates represent collection dates. Error bars represent standard error. Discharge (cfs) represents the mean daily average.

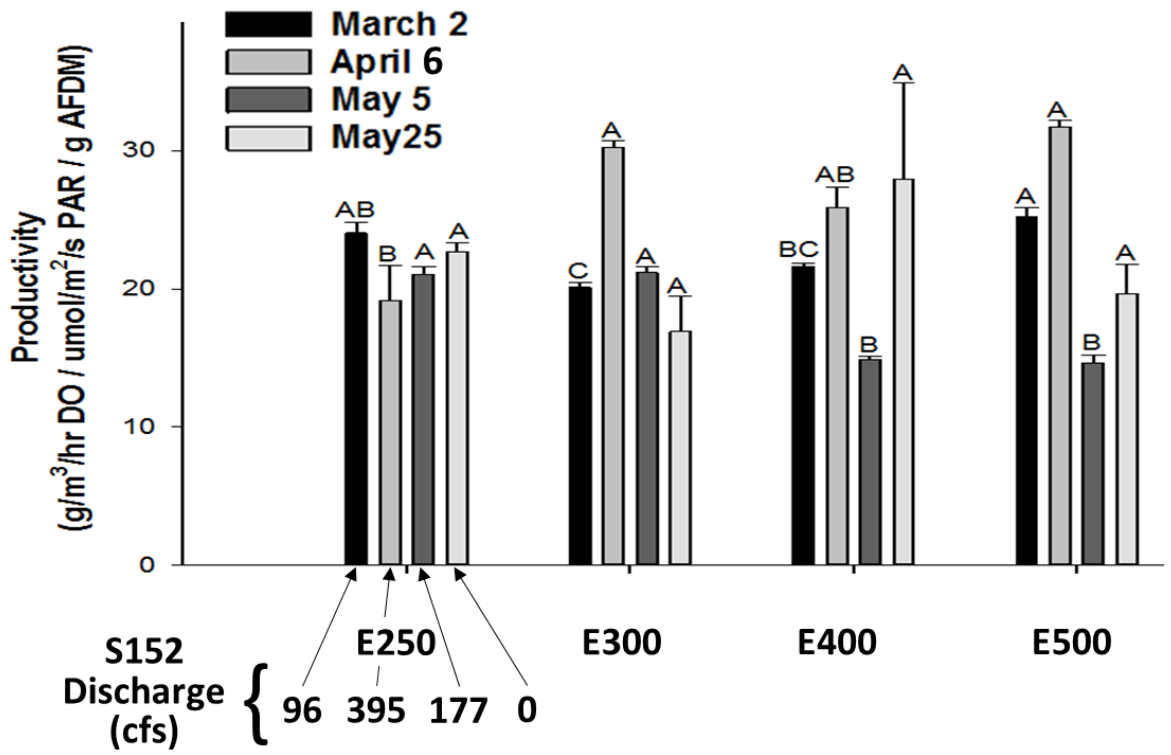

Figure BG7. Periphyton productivity expressed as gross primary productivity (GPP). Error bars represent standard error. Letters indicate significant difference between sites within a month

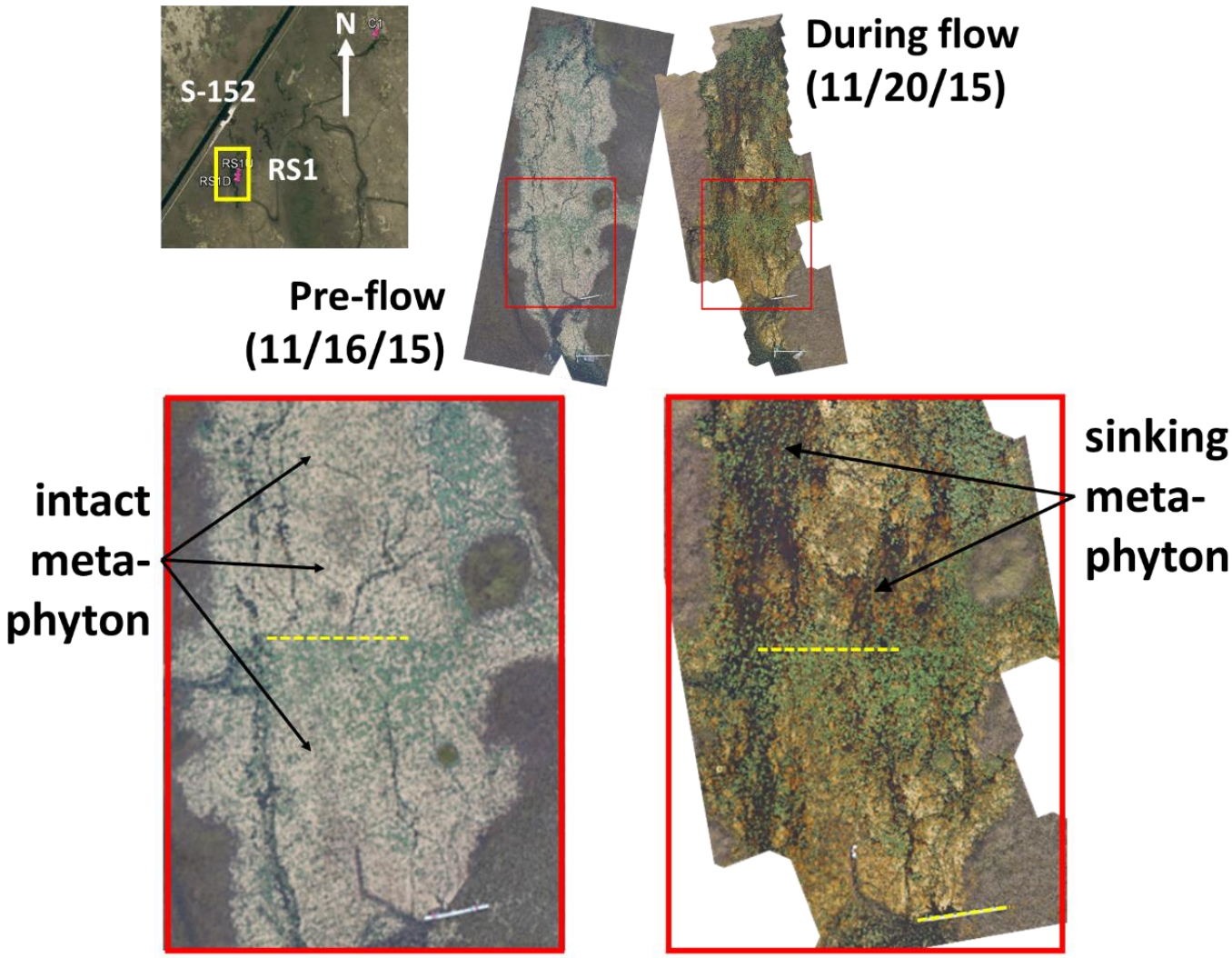

Figure BG8. High-resolution imagery of RS1 slough during pre-flow conditions (left) and 4 days after flow was initiated (right). The yellow dashed line indicates approximate location of floc height measurements along a transect across the slough. Line in bottom right portion of the images is the RS1u boardwalk (12-m length)

Figures–Biological (Fauna) Monitoring (FA1-10)

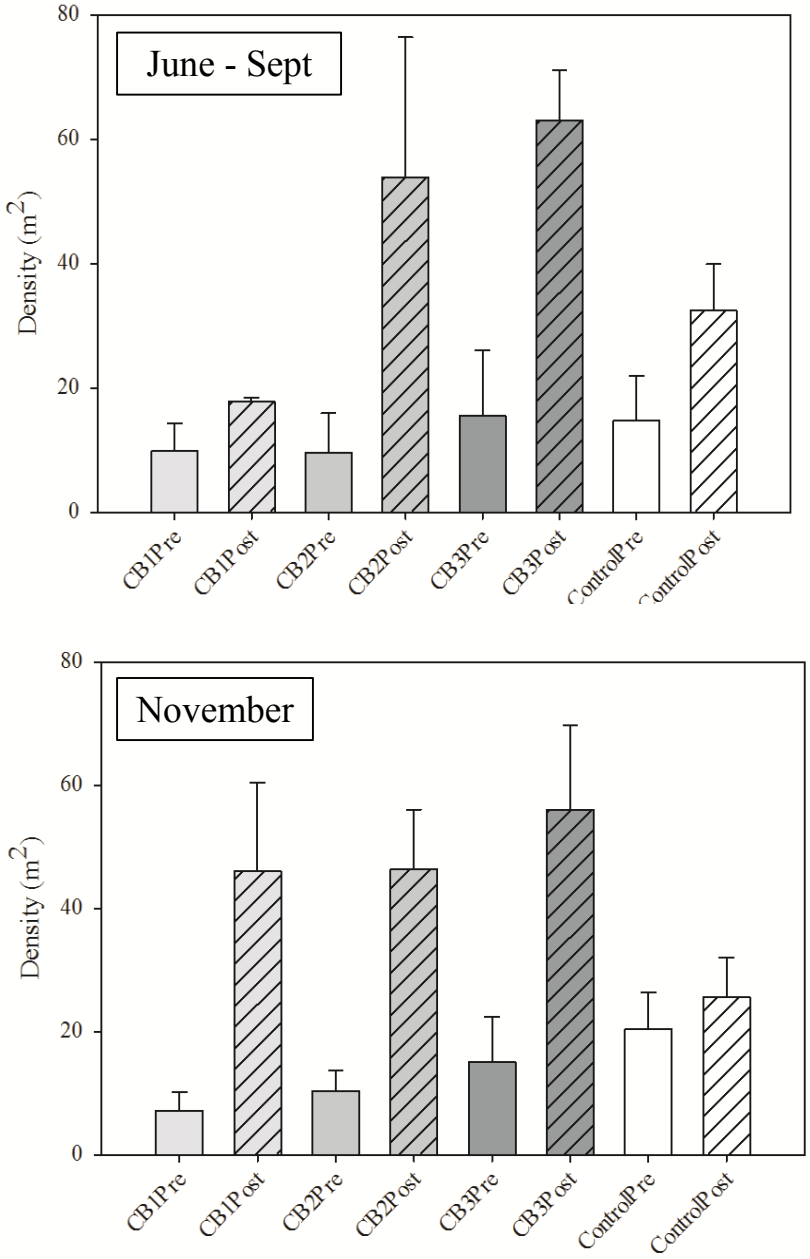

Figure FA1. Density of small fishes at the CB plots, reported by Pre (September 2010-April 2-12) and Post (January 2013-March 2015) DPM level removal. Error bars represent one standard error.

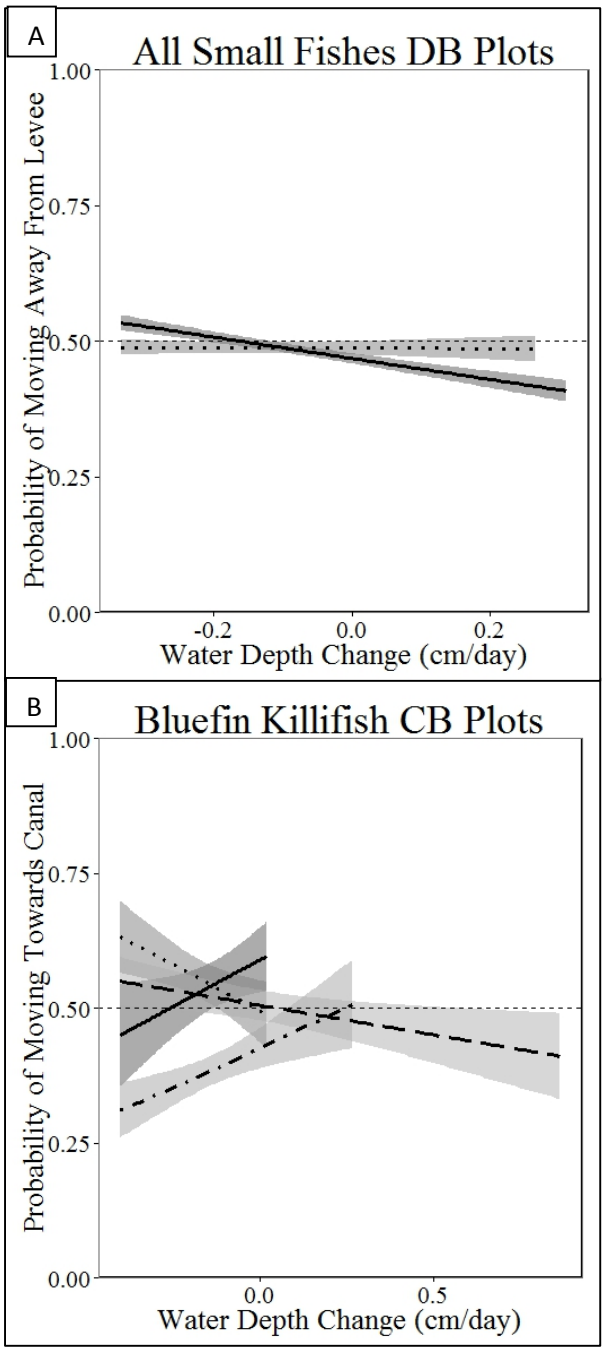

Figure FA2. A. Directionality of all small fishes at the DB sites, January, 2013 – March, 2015. Solid line represents the DB sites. Dotted line represents the DB control sites. The shaded fill around the lines represents 95% confidence intervals. **B.** Directionality of Bluefin Killifish at the CB plots, January, 2013 – March, 2015. Solid line represents CB Plot 1. Dotted line represents CB Plot 2. Dotted dashed line represents CB Plot 3. Long dashed line represents the CB control plots. The shaded fill around the lines represents 95% confidence intervals.

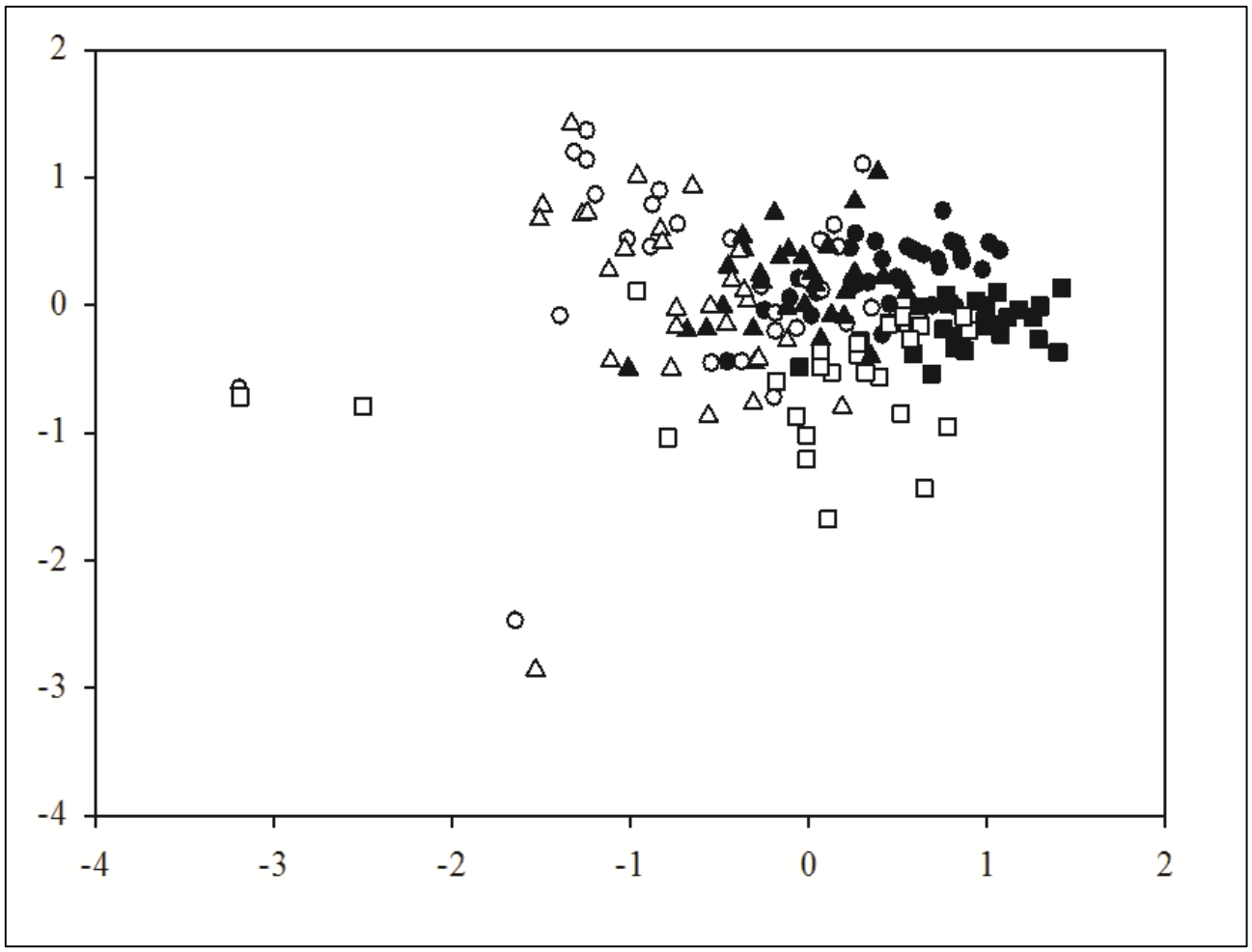

Figure FA3. NMDS plot of small fish community structure across the CB, UB, and DB plots. Data from 1-m^2 throw trap sampling. Hollow shapes are Before DPM construction. Shaded shaped are After DPM construction. Circles represent CB plots. Squares represent DB plots. Triangles represent UB plots. Stress = 0.17.

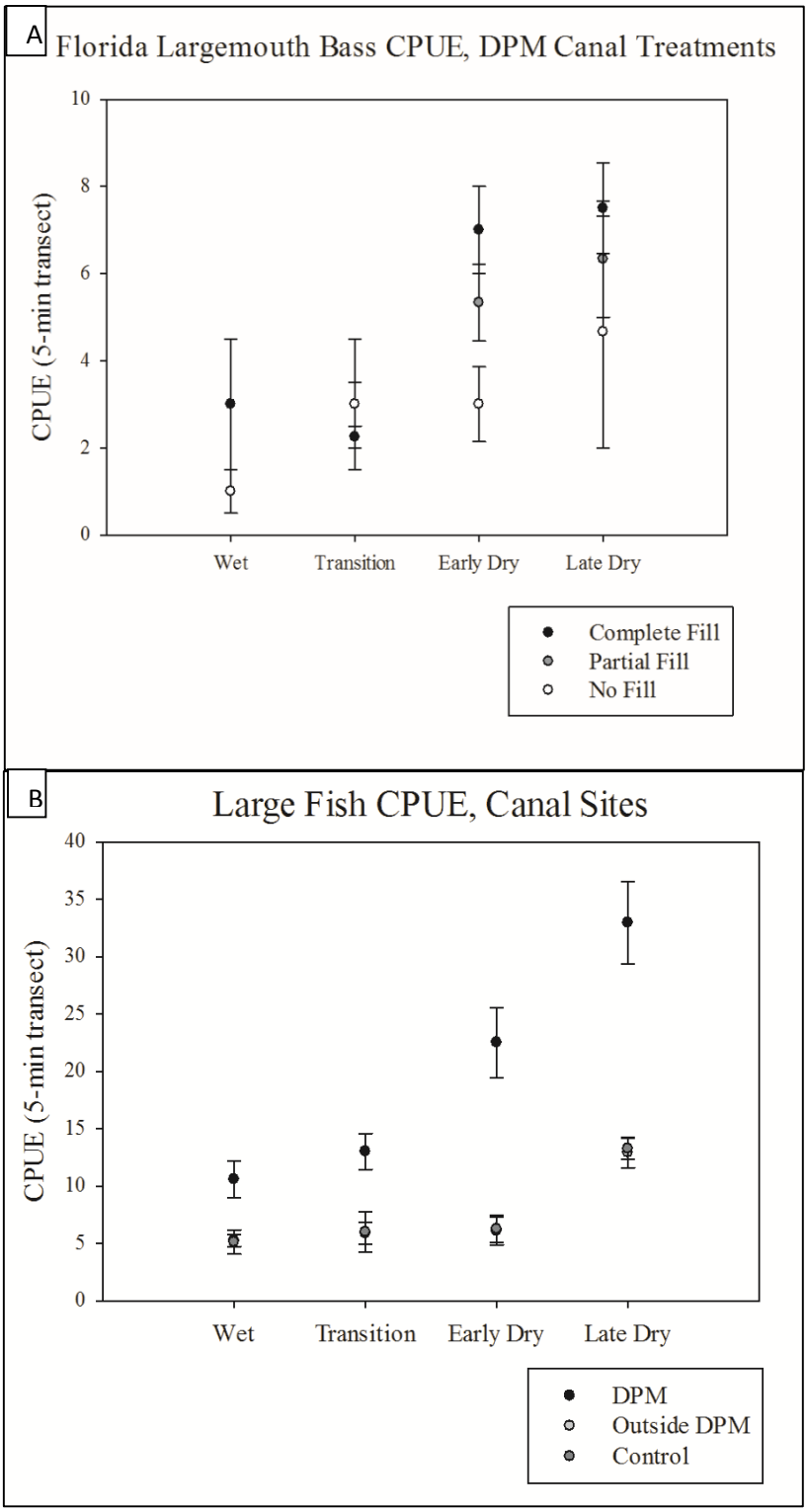

Figure FA4. A. CPUE of Florida Largemouth Bass at the DPM canal fill treatments, January, 2013 – March, 2015. Error bars represent standard error. **B.** CPUE of all large fishes and large amphibians across canal site types, January, 2013 – March, 2015. Error bars represent standard error.

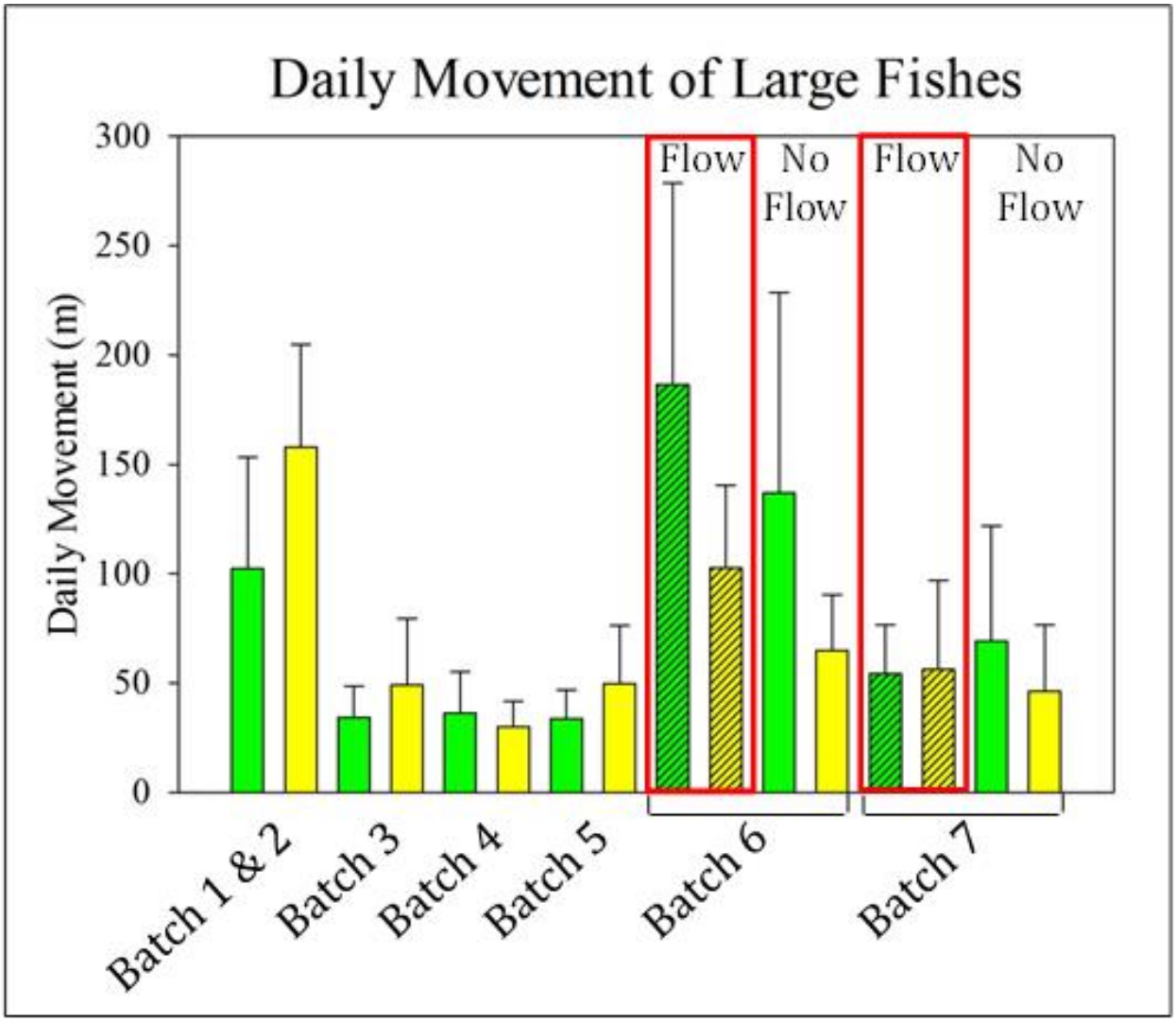

Figure FA5. Daily step length (m) of large fishes implanted with VHF radio transmitters. Green bars represent Florida Largemouth Bass. Yellow bars represent Bowfin. Batches 1 & 2 were tracked from May 2011 – November 2011. Batch 3 was tracked from January, 2012- June, 2012. Batch 4 was tracked from June 2012 – February, 2013. Batch 5 was tracked from March, 2013- September, 2013. Batch 6 was tracked from October, 2013 – May, 2014. Batch 7 was tagged in October, 2014 and is still being tracked. Error bars represent 95% confidence intervals.

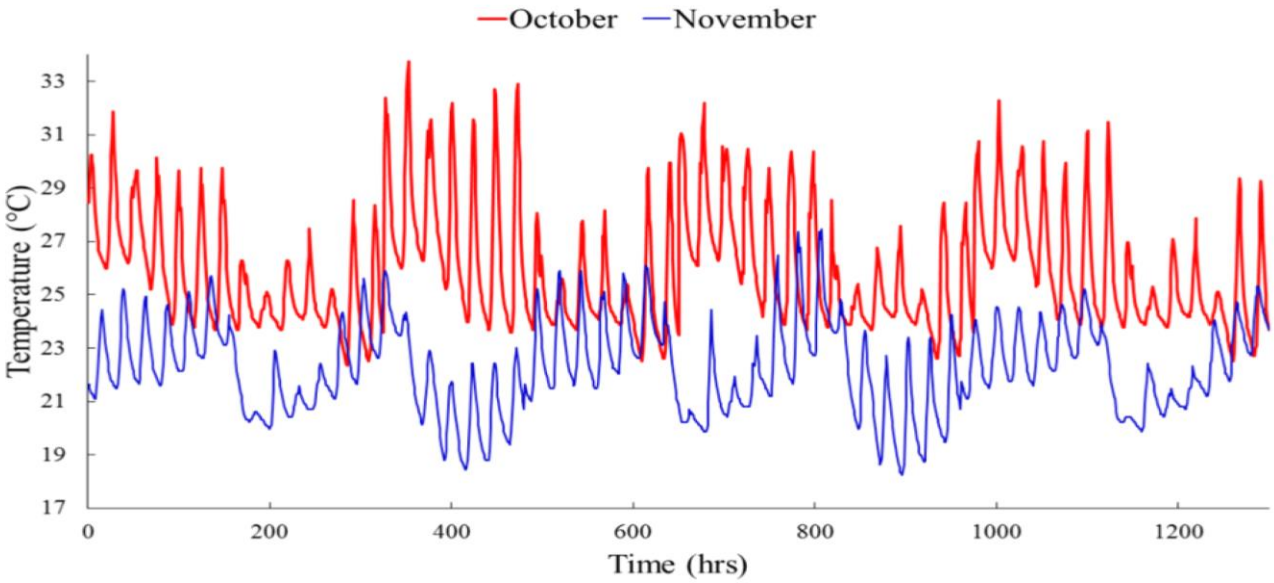

Figure FA6. Water temperature measured by continuous data recorders placed inside our experimental field cages.

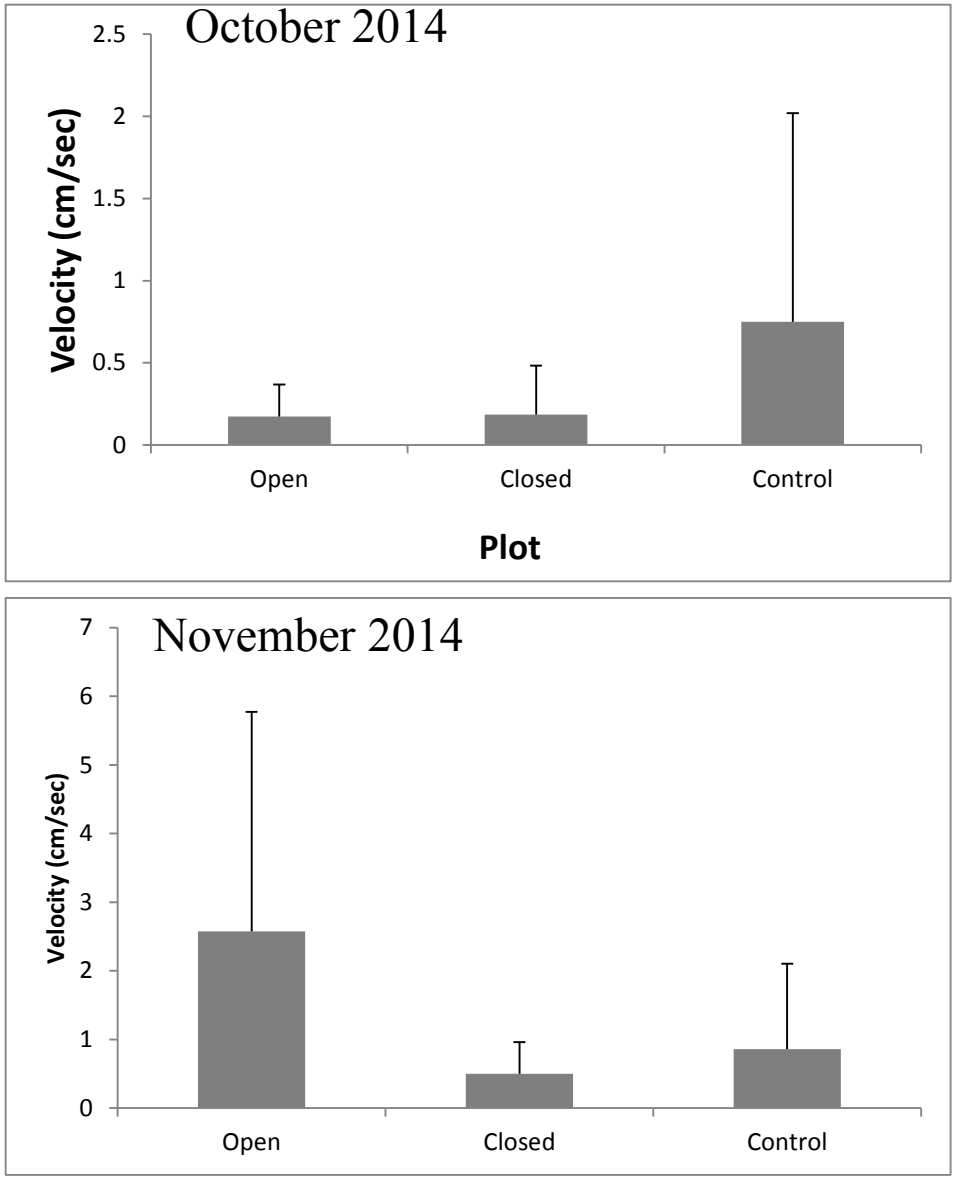

Figure FA7. Water flow velocity measured in the marsh upstream of the field cages (control), in the cages shielded from flow (closed) and in the cages with wings to enhance flow (open). Note the different scales in the two figures.

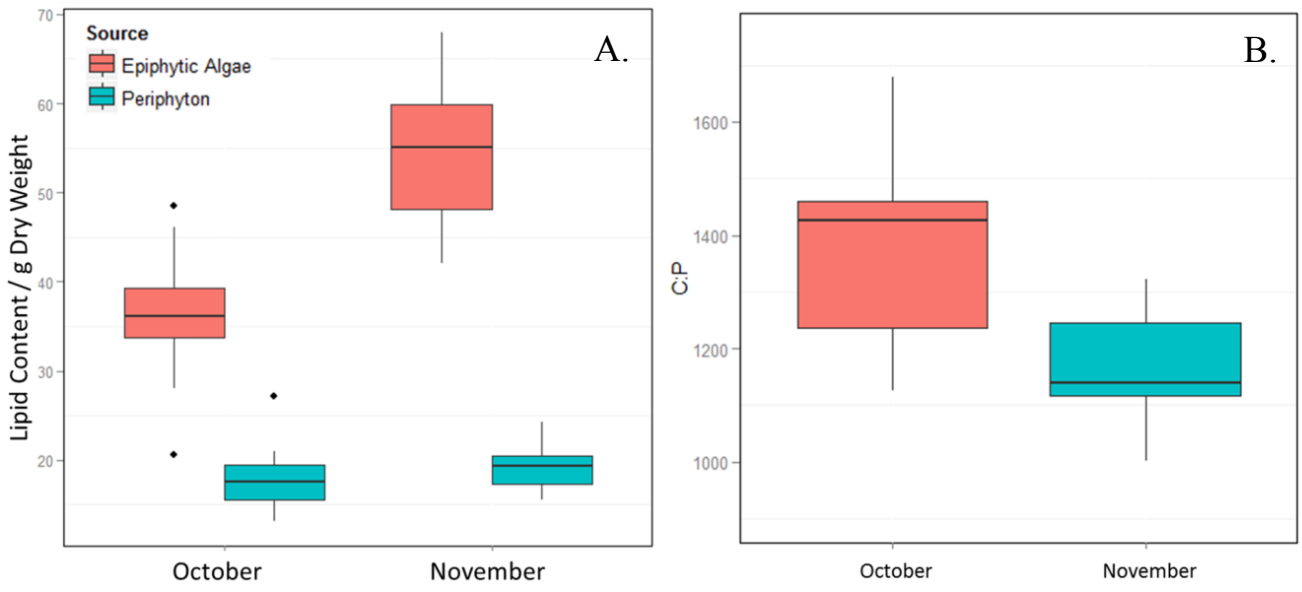

Figure FA8. **A.** Lipid content of epiphytic biofilms (algae) and periphyton mats in October and November experiments. **B.** Stoichiometric ratios (C:P) in epiphytic biofilms in October and November. Smaller values indicated higher P concentration.

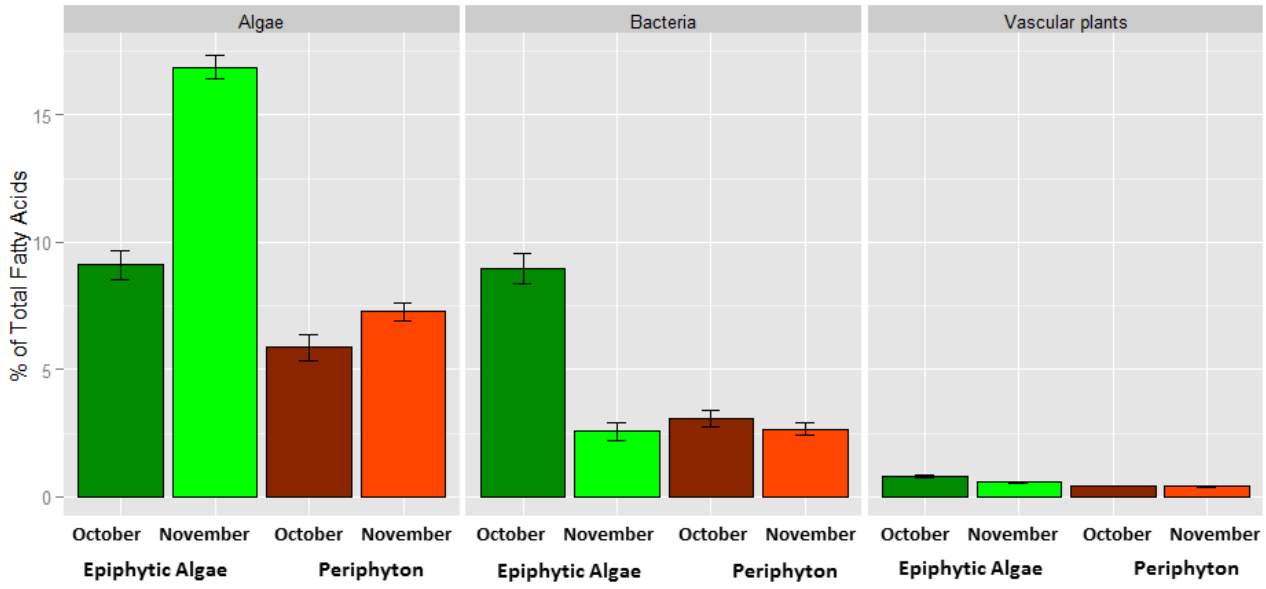

Figure FA9. Fatty acids from epiphytic biofilms and periphyton in October and November that can be uniquely attributed to algae, bacteria, or vascular plants (see Belicka et al. 2012).

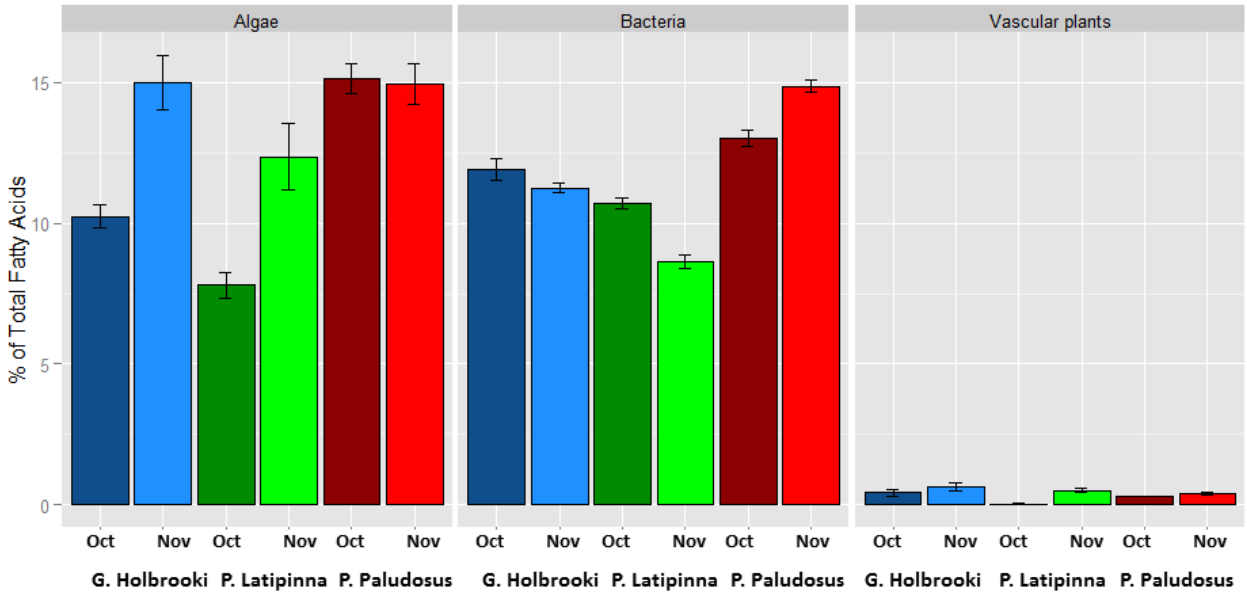

Figure F10. Fatty acids from Eastern Mosquitofish, Sailfin Mollies, and Riverine Grass Shrimp in October and November that can be uniquely attributed to algae, bacteria, or vascular plants (see Belicka et al. 2012).

Figures – Environmental Characteristics of Canal Backfill (CB1-7)

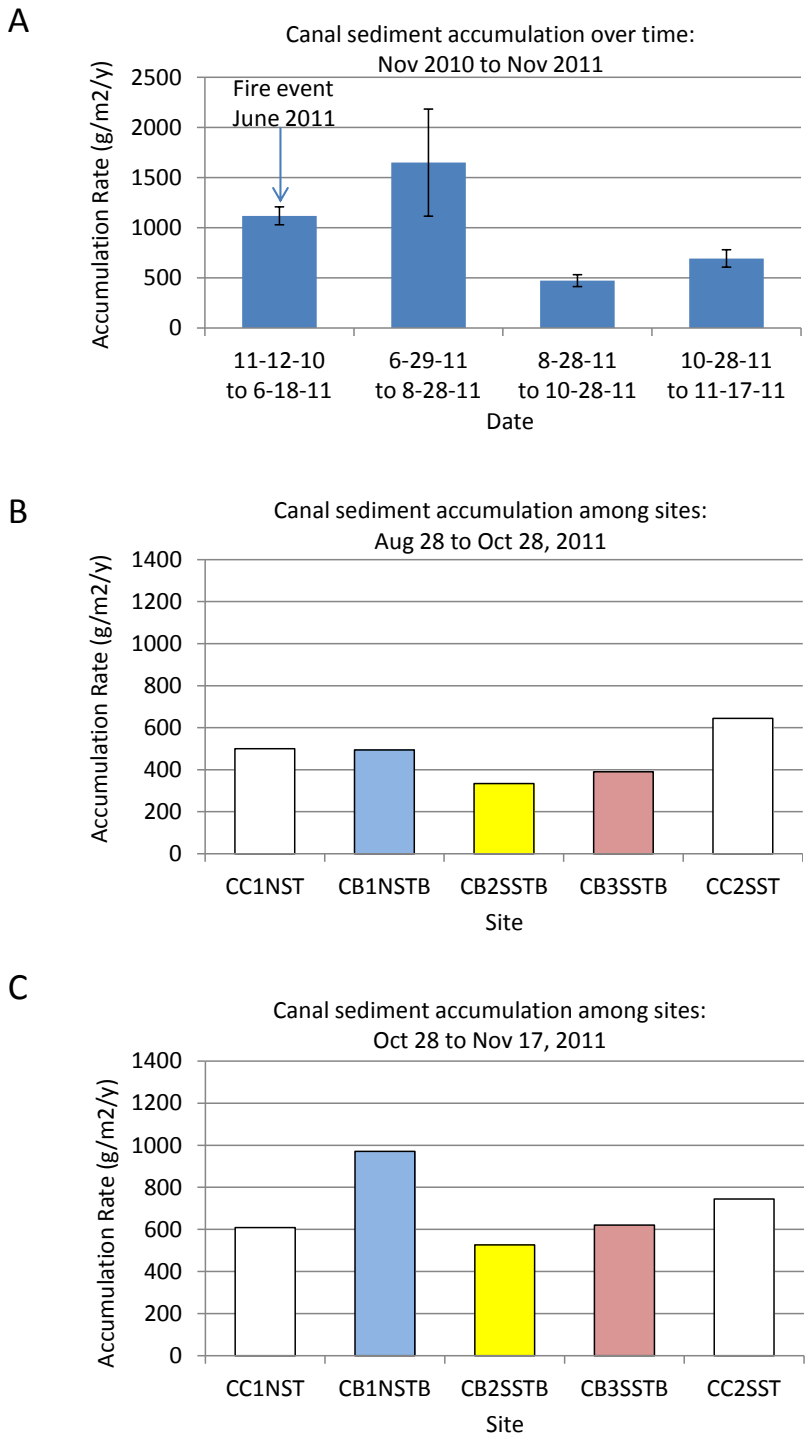

Figure CB1. Sediment mass accumulation rates in the L67C canal from November 2010 to November 2011. (A) Temporal changes in sediment accumulation (standard errors shown; sample sizes are N=5 except N=4 for the 11-12-10 to 6-18-11). Among-site variation in sediment accumulation for the August-October 2011 deployment (B) and the October-November 2011 deployment (C). Arrow in (A) indicates the occurrence of a fire that burned through most of WCA-3B including the DPM study area.

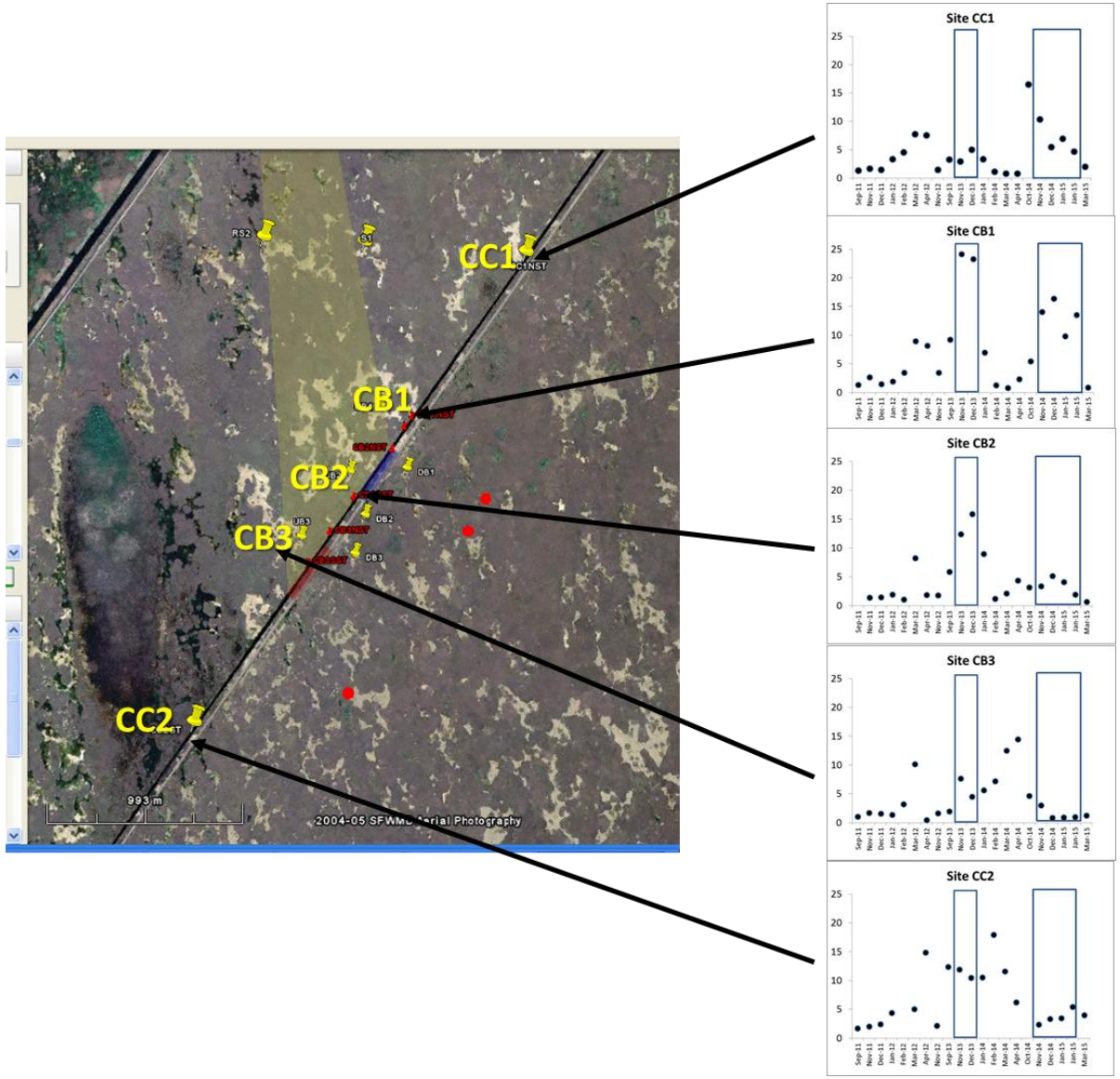

Figure CB2. Spatial and temporal pattern of sediment accumulation rates (g m^{-2} d^{-1}) along the L67C canal during and after the operational window. Blue rectangles indicate the operational periods (Nov-Dec 2013 and Nov 2014-Jan 2015).

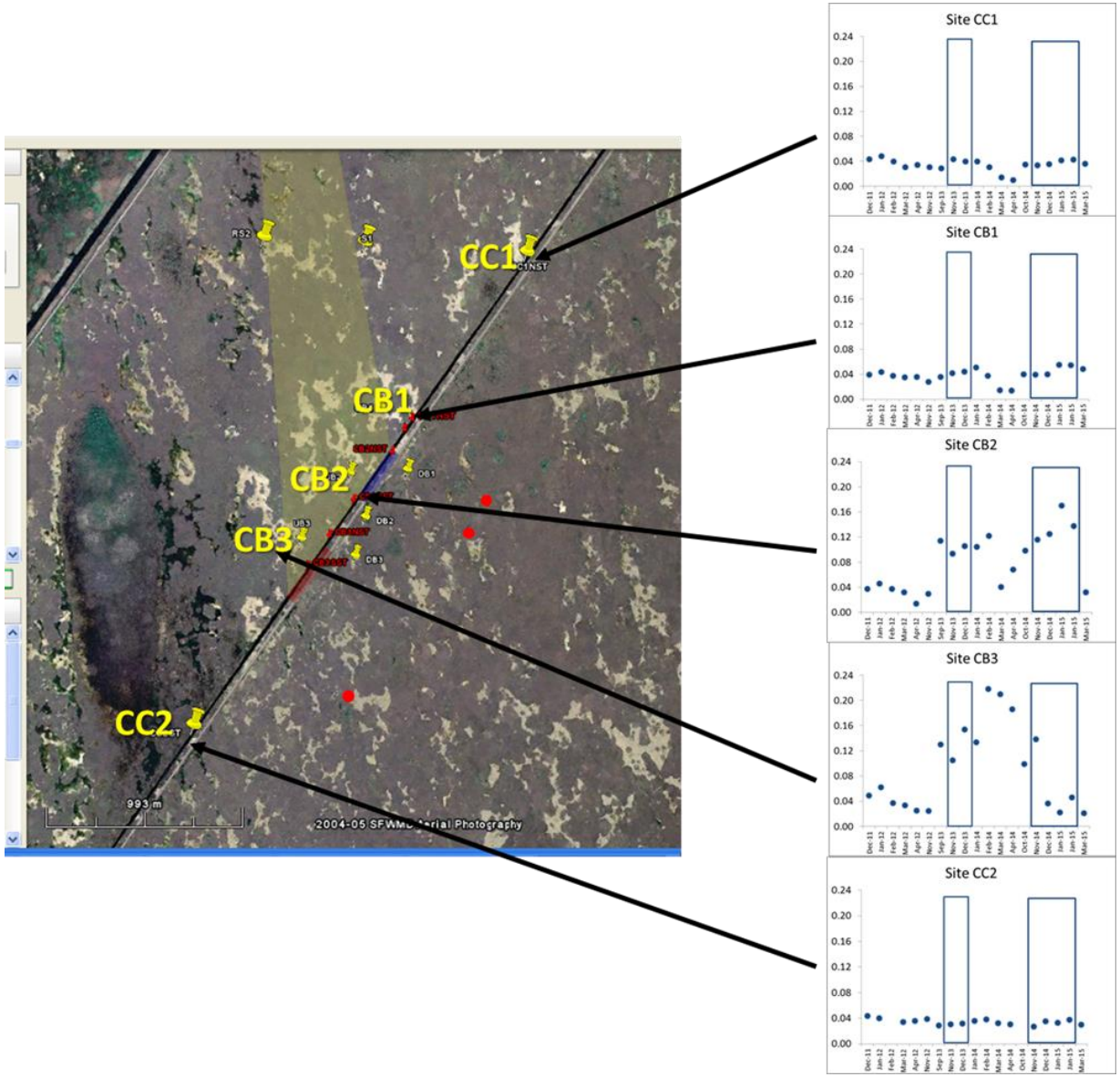

Figure CB3. Spatial and temporal pattern of particle density (g cm^{-3}) along the L67C canal during and after the operational window. Blue rectangles indicate the operational periods (Nov-Dec 2013 and Nov 2014-Jan 2015).

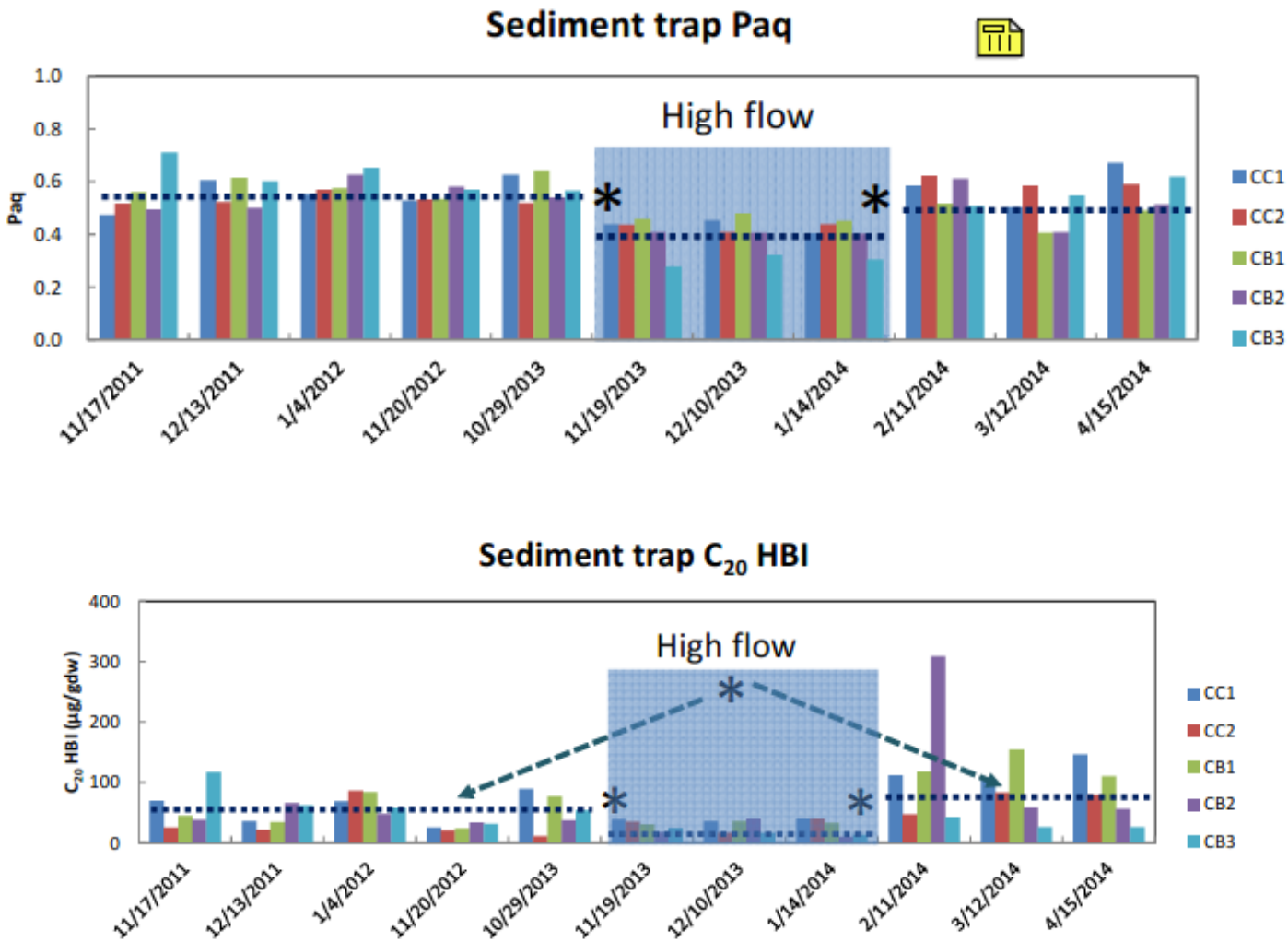

Figure CB4. Timeseries for Paq and C_{20} HBI for sediment traps during the baseline period (Nov 2011-October 2012), high flow period (Nov-Dec 2013), and post-flow period (Feb-Apr 2014)

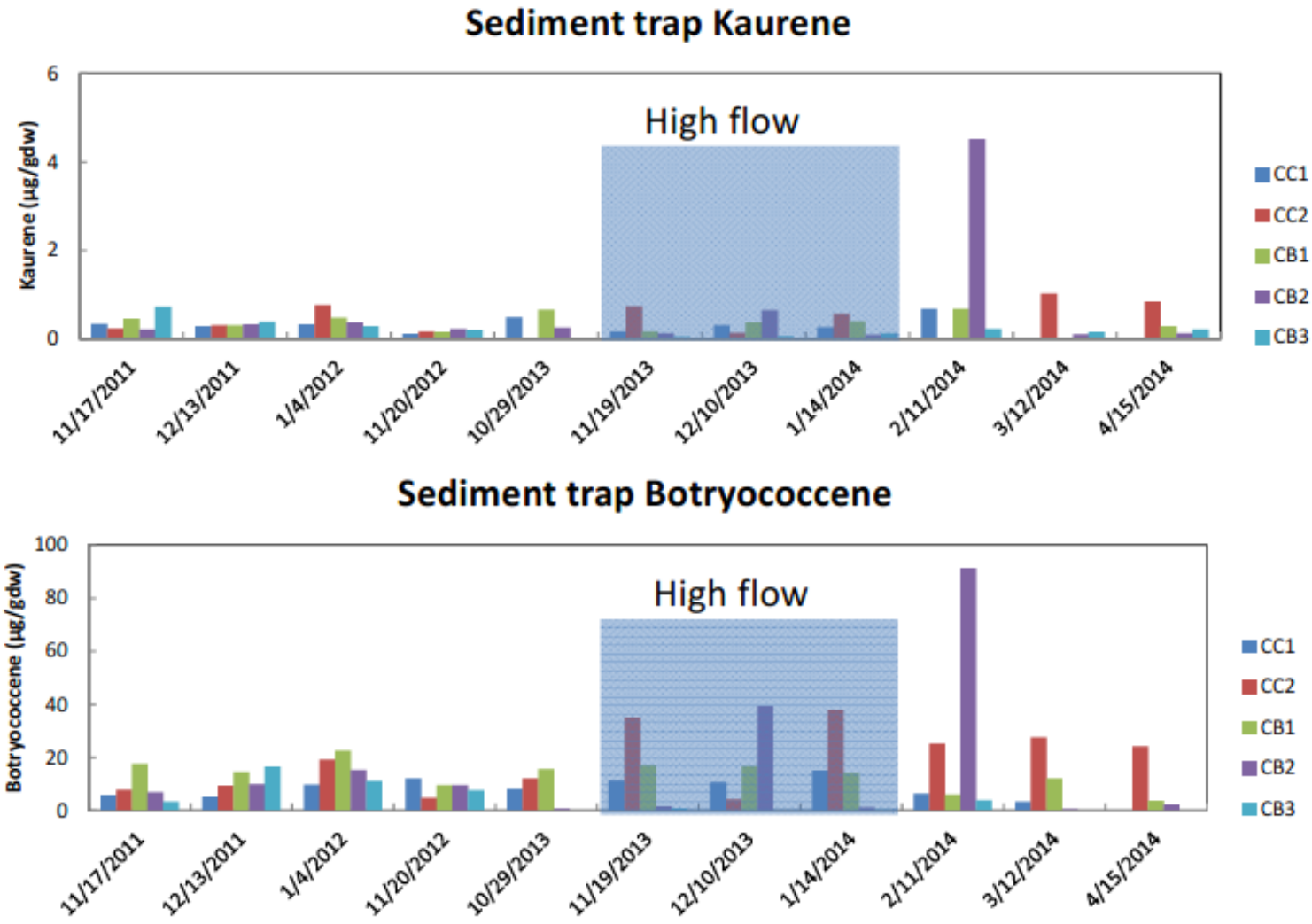

Figure CB5. Timeseries for Kaurene and Botryococcene for sediment traps during the baseline period (Nov 2011-October 2012), high flow period (Nov-Dec 2013), and post-flow period (Feb-Apr 2014).

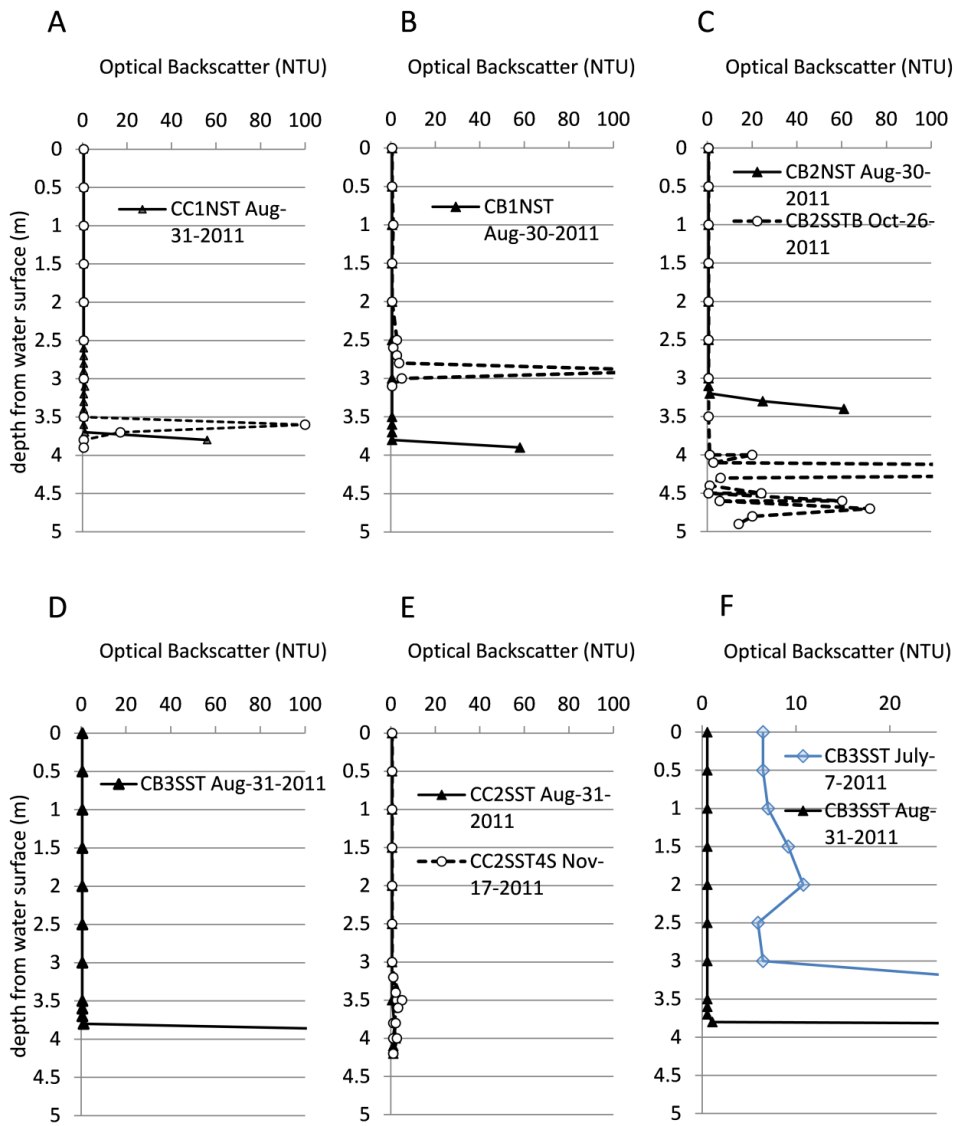

Figure CB6. Turbidity profiles in the L67C canal sites (A) CC1N, (B) CB1, (C) CB2, (D) CB3 and (E) CC2S. Step increases in turbidity at depth denote the top of the benthic floc layer. Temporal differences in floc layer height indicate changes in canal water depth or different locations between sampling events. Graph (F) shows increased turbidity that was observed in the canal in July 2011, one month after the fire that burned the DPM study area and most of WCA-3B.

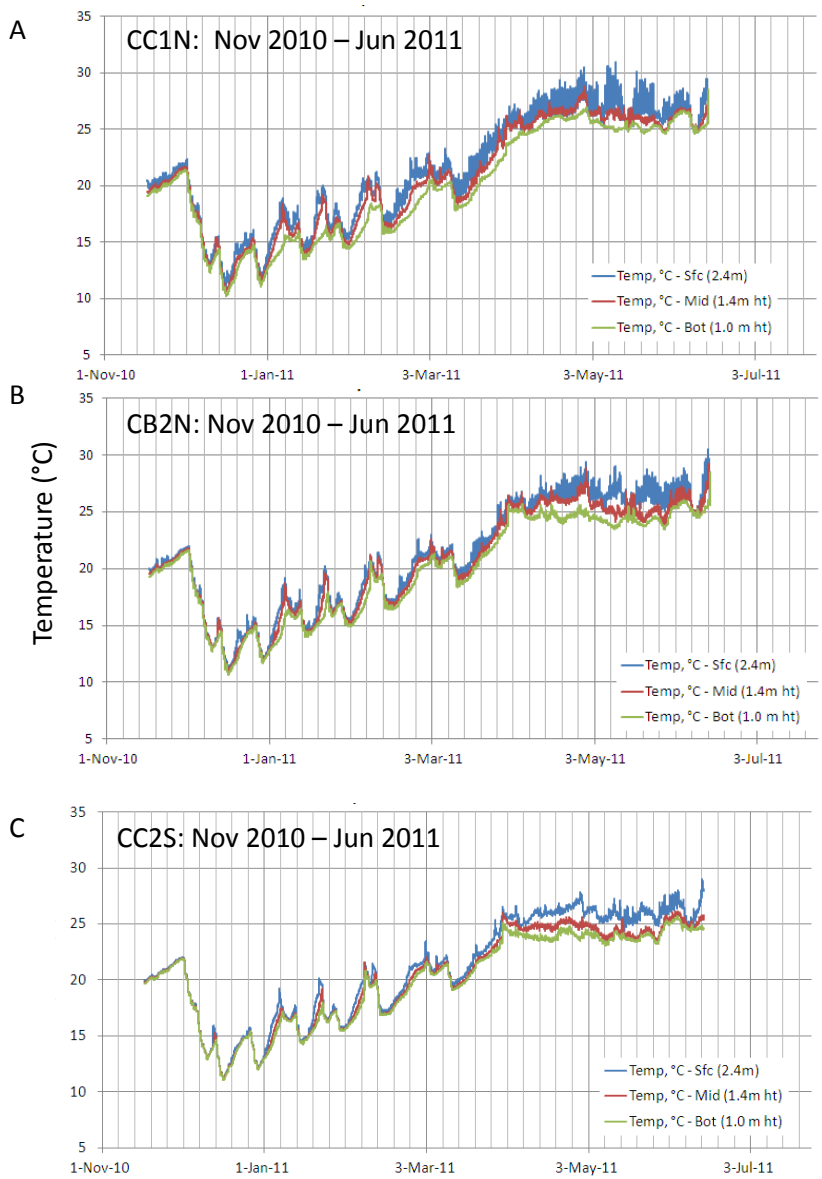

Figure CB7. Temperature profiles of L67C canal from Nov-2010 to Jun-2011, from probes attached to vertical sediment traps at (A) the north canal control site CC1N, (B) Canal Backfill site CB2, and (C) the south canal control site CC2S.

Figures–Synthesis and Modeling (SYN1-2)

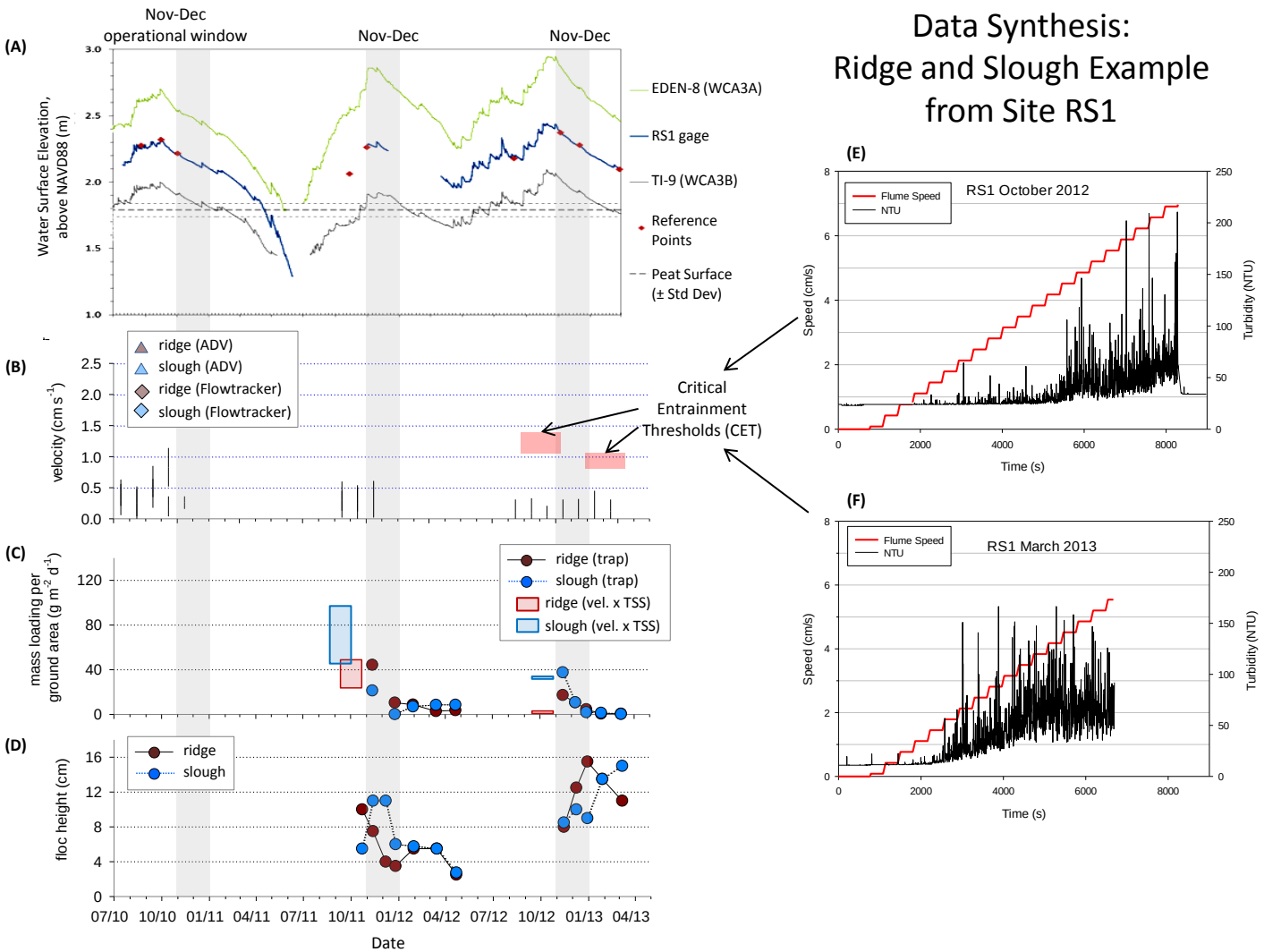

Figure SYN1/4-91. Data synthesis of hydrology and sediment dynamics Jun2010-Mar2013, exemplified by field data collected at site RS1. (a) Water stage and peat elevation, (b) flow velocities, (c) sediment transport, (d) benthic sediment (floc) height, and (e, f) sediment entrainment velocities measured within a slough at RS1 in October 2012 and March 2013. Shaded bars in (c) represent the range in transport estimated by particulate concentrations x water velocity, using SF6-based velocities and acoustic Doppler velocity (ADV)-based velocities in November. The single bar in 2012 reflects that only ADV data was available that year.

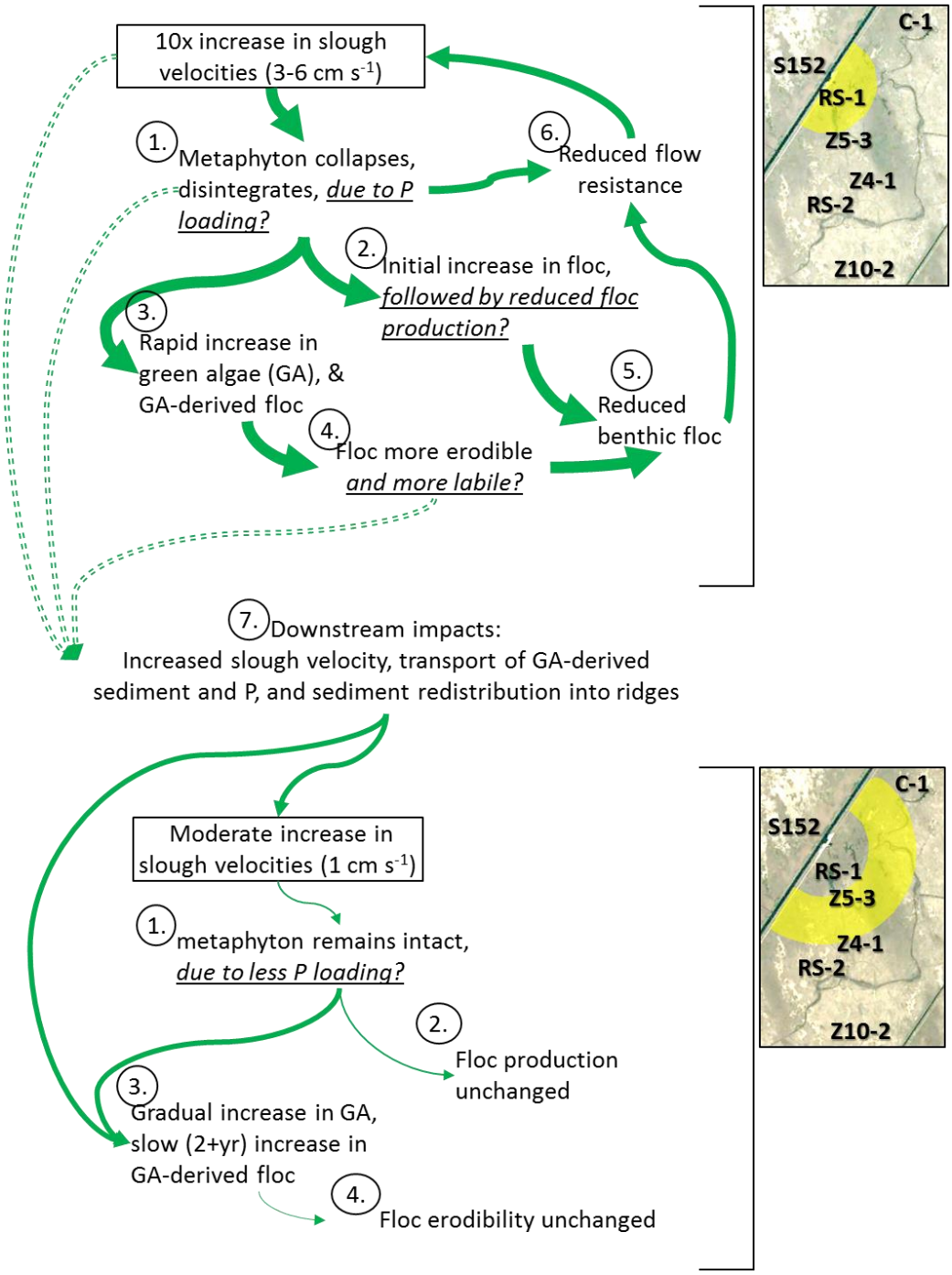

Figure SYN2. Conceptual model of flow and biogeochemical processes in the ridge and slough, based on observations within 500-m of the S152 (top), and 500-1000 m from the S152 (bottom). Remaining uncertainties (underlined and italicized) are presented as hypotheses about underlying mechanisms. Dashed lines indicate processes that affect areas downstream. Arrow thickness is related qualitatively to the magnitude of observed changes to flow.

This page deliberately left blank.

TABLES

Table 3-1. DPM Research Sites, Locations, Equipment, and Deployment Dates for Automated Hydrologic and Sediment Monitoring

Site ID	Site Type c = contin-uous d = discrete c,d = both	Latitude (WGS84)	Longitude (WGS84)	Site Description	Equipment c = continuous d = discrete c,d = both	ADV Contin-uous deploy (wet season)	ADV Discrete deployment & velocity profiles	LISST & LISST portable(p) Discrete deployment
RS1-(U)R	d	25.860436	-80.620333	Ridge; Upstream tracer site	ADV/Vectrino (d)		2010/11/09	
RS1-(U)S	d	25.860436	-80.620333	Slough; Upstream tracer site	ADV/Vectrino (d)		2010/11/09	
RS1-(D)R	c,d	25.860161	-80.620313	Ridge; upstream impact	LISST(d), ADV/Vectrino (c,d),	2010, 2011, 2012, 2013	2010/07/19, 2010/08/28, 2010/10/01, 2010/11/02, 2011/09/28, 2011/10/31, 2011/11/29, 2012/08/07, 2012/11/05, 2013/02/26, 2013/08/13, 2013/11/03, 2013/11/08, 2014/03/05	2010/11/07(Floc), 2010/11/09(100x), 2012/08/07(100x), 2012/11/05(100x), 2013/11/03(Floc), 2013/11/04(100x), 2013/11/05(100x), 2013/11/06(Floc), 2013/11/07(100x), 2013/11/09(Floc)
RS1-(D)S	c,d	25.860161	-80.620313	Slough; upstream impact	staff(c), KPSI(c), ADV/Vectrino (c,d)	2010, 2011, 2012, 2013	2010/07/17, 2010/08/24, 2010/10/01, 2010/11/02, 2011/09/28, 2011/11/01, 2011/11/29, 2012/03/22, 2012/08/07, 2012/11/05, 2013/02/26, 2013/08/13, 2013/11/03, 2013/11/08, 2014/03/05	2010/11/07(100x), 2010/11/09(Floc), 2012/08/07(Floc), 2012/11/05(Floc), 2013/08/14(Floc), 2013/11/03(100x), 2013/11/04(Floc), 2013/11/05(Floc), 2013/11/06(100x), 2013/11/07(Floc), 2013/11/09(100x)
S1	c,d	25.851202	-80.617061	Slough; Middle impact	staff(c), KPSI(c), ADV/Vectrino (c,d)	2010, 2012, 2013	2010/07/18, 2010/08/26, 2010/09/28, 2012/08/09, 2012/11/05, 2013/02/28, 2013/08/13, 2013/11/02, 2013/11/09, 2014/03/05	
RS2-R	d	25.850822	-80.622166	Ridge; middle impact	ADV/Vectrino (d)	2011	2011/11/02, 2012/11/08, 2013/09/26, 2013/11/03, 2013/11/09	

RS2-S	d	25.850822	-80.622166	Slough; middle impact	staff(c), KPSI(c), ADV/Vectrino (d)	2011	2011/11/02, 2012/03/21, 2012/11/08, 2013/09/26, 2013/11/03, 2013/11/09	
C1-R	c,d	25.869344	-80.610813	Ridge; northeast control	ADV/Vectrino (c,d)	2011	2011/11/01, 2011/11/29, 2012/11/09, 2013/09/26, 2013/11/04	
C1-S	c,d	25.869344	-80.610813	Slough; northeast control	staff(c), KPSI(c), ADV/Vectrino (c,d)	2010, 2011	2010/11/04, 2011/09/28, 2011/11/05, 2011/11/28, 2012/08/08, 2012/11/09, 2013/08/14, 2013/11/04 2013/11/08	
C2-R	d	25.832794	-80.635138	Ridge; southwest control	ADV/Vectrino (d)		2010/11/07, 2011/11/05, 2012/08/09, 2012/11/09, 2013/09/25, 2013/11/04, 2013/11/09	
C2-S	d	25.832794	-80.635138	Slough; southwest control	staff(c), KPSI(c), ADV/Vectrino (d)		2010/11/07, 2011/11/05, 2012/11/09, 2013/09/25, 2013/11/04, 2013/11/09	
UB1	c,d	25.843666	-80.615613	Slough; northeast down-stream	staff(c), KPSI(c), ADV/Vectrino (c,d)	2010, 2011, 2012, 2013	2010/11/03, 2011/11/04, 2011/11/30, 2012/08/08, 2012/11/06, 2012/12/11, 2013/02/26, 2013/08/14, 2013/11/02, 2013/11/08, 2014/03/05	2013/02/26(Floc), 2013/09/24(Floc)
UB2	c,d	25.840705	-80.617524	Slough; central down-stream	staff(c), KPSI(c), ADV/Vectrino (c,d)	2010, 2011, 2012, 2103	2010/07/19, 2010/08/25, 2010/09/27, 2010/11/03, 2011/11/02, 2012/08/09, 2012/11/09, 2012/12/11, 2013/02/27, 2013/08/14, 2013/11/02, 2013/11/08, 2014/03/05	
UB3	c,d	25.837641	-80.619905	Slough; southwest down-stream	staff(c), KPSI(c), ADV/Vectrino (c,d)	2010, 2011, 2012, 2013	2010/11/06, 2011/11/04, 2011/11/29, 2012/08/08, 2012/11/06, 2012/12/11, 2013/02/27, 2013/08/14, 2013/11/02, 2013/11/08, 2014/03/05	

MB1		25.842586	-80.614972	Canal; northeast, no backfill	Argonaut-SW(c)			
MB2		25.839978	-80.616944	Canal; central, partial backfill	KPSI(c), Argonaut-SW(c)			
MB3		25.836669	-80.619406	Canal, complete backfill	Argonaut-SW(c)			
DB1	d	25.841555	-80.613886	Canal effects, no backfill WCA-3B	ADV/Vectrino (d)		2010/11/09, 2011/11/01, 2012/12/10, 2013/08/15, 2013/11/04, 2013/11/07	
DB2	d	25.839127	-80.615697	Canal effects, partial backfill WCA-3B	staff(c), KPSI(c), ADV/Vectrino (d)		2010/11/04, 2011/11/01, 2012/12/10, 2013/08/15, 2013/11/03, 2013/11/07	
DB3	d	25.836858	-80.617422	Canal effects, complete backfill WCA-3B	ADV/Vectrino (d)		2010/11/04, 2011/11/01, 2012/12/10, 2013/08/15, 2013/11/03, 2013/11/07	

Table 4-1. Monthly Flow Velocity Statistics for continuously sampled ADV sites.

Site	Year	Month	V-X (N) (cm/s)	V-Y (W) (cm/s)	V-Z (Up) (cm/s)	I (X)	I (Y)	I (Z)	Speed (cm/s)	STD Speed	Dir.	STD Dir.	TKE	STD TKE
C1R	2011	11	-0.23	-0.31	-0.09	-1.17	-0.81	-1.54	0.4	0.25	126.2	44.4	0.08	0.08
C1S	2010	11	-0.08	-0.15	-0.18	-2.56	-1.29	-0.53	0.25	0.15	116.7	65.8	0.04	0.04
C1S	2011	9	-0.23	-0.43	-0.09	-0.87	-0.47	-2.12	0.49	0.2	118	26.5	0.06	0.06
C1S	2011	10	-0.15	-0.34	-0.05	-1.42	-0.62	-3.16	0.37	0.21	114.5	38.2	0.06	0.06
RS1DR	2010	7	-0.17	-0.26	-0.02	-1.23	-1.05	-3.8	0.31	0.25	124	55.3	0.06	0.06
RS1DR	2010	8	-0.11	-0.22	-0.01	-2.04	-1.24	-11.62	0.25	0.27	117	63.3	0.07	0.07
RS1DR	2010	9	-0.19	-0.36	-0.03	-1.07	-0.68	-2.83	0.41	0.23	117.5	33.3	0.05	0.09
RS1DR	2010	10	-0.12	-0.15	-0.01	-1.09	-1.15	-6.37	0.2	0.16	128.7	50.5	0.03	0.03
RS1DR	2010	11	-0.13	-0.19	-0.11	-0.74	-0.6	-0.21	0.26	0.1	124.7	29.9	0.01	0.01
RS1DR	2011	9	-0.16	-0.2	-0.17	-1.01	-0.8	-0.6	0.31	0.15	128.5	41.5	0.03	0.03
RS1DR	2011	10	NaN	NaN	NaN	NaN	NaN	NaN	0.25	0.15	NaN	NaN	0.04	0.04
RS1DR	2011	11	NaN	NaN	NaN	NaN	NaN	NaN	0.32	0.17	NaN	NaN	0.06	0.06
RS1DR	2012	8	-0.09	-0.01	-0.02	-2.39	-19.83	-2.98	0.1	0.21	173.7	85.35	0.05	0.05
RS1DR	2012	9	-0.09	0.01	-0.02	-2.87	21.11	-3.3	0.09	0.24	187.46	89.07	0.06	0.07
RS1DR	2012	10	-0.02	-0.02	-0.01	-7.51	-9.33	-7.19	0.03	0.18	141.48	96.76	0.03	0.05
RS1DR	2012	11	-0.01	-0.01	-0.01	-15.1	-12.01	-5.17	0.02	0.14	126.94	98.13	0.02	0.05
RS1DR	2012	12	-0.02	-0.03	-0.01	-9.07	-7.58	-5.17	0.03	0.18	129.8	96.79	0.04	0.06
RS1DR	2013	1	-0.14	-0.08	-0.02	-2.03	-3.34	-4.25	0.17	0.28	150.05	77.29	0.08	0.09
RS1DR	2013	2	-0.08	-0.08	-0.05	-2.55	-2.58	-2.1	0.12	0.19	133.7	82.32	0.05	0.06
RS1DR	2013	8	-0.23	0	-0.02	-1.04	-340.55	-5.01	0.23	0.24	179.82	61.99	0.07	0.07
RS1DR	2013	9	-0.09	0.01	-0.01	-2.97	28.61	-5.99	0.09	0.27	186.49	88.15	0.08	0.13
RS1DR	2013	10	-0.15	-0.17	-0.04	-1.7	-1.5	-3.28	0.23	0.25	130.66	65.11	0.08	0.08
RS1DR	2013	10	-0.15	-0.17	-0.04	-1.70	-1.50	-3.28	0.23	0.25	130.66	65.11	0.08	0.08
RS1DR	2013	11	-1.63	0.10	-0.33	-0.48	5.39	-0.72	1.67	0.76	183.57	30.35	0.48	0.48
RS1DR	2013	12	-1.94	0.03	-0.37	-0.33	15.37	-0.78	1.97	0.62	181.02	20.18	0.38	0.41
RS1DR	2014	1	-0.03	-0.07	-0.03	-9.46	-4.79	-3.83	0.08	0.33	115.40	92.23	0.12	0.14
RS1DR	2014	2	-0.01	-0.02	-0.01	-22.60	-14.96	-10.17	0.03	0.31	121.76	100.38	0.10	0.27
RS1DR	2014	3	-0.01	0.00	-0.01	-31.81	-73.85	-12.22	0.01	0.29	155.44	102.16	0.11	0.15
RS1DS	2010	7	-0.39	0.15	-0.04	-0.53	1.43	-2.11	0.42	0.21	201.1	32.1	0.05	0.06
RS1DS	2010	8	-0.25	-0.02	-0.04	-0.89	-9.91	-2.24	0.26	0.22	174.9	55.3	0.05	0.06
RS1DS	2010	9	-0.59	-0.1	-0.01	-0.43	-1.87	-10.3	0.6	0.25	170.1	24.7	0.06	0.06
RS1DS	2010	10	-0.83	-0.02	0	-0.38	-10.7	26.23	0.83	0.31	178.4	20.7	0.09	0.08

RS1DS	2010	11	-1.13	-0.15	-0.01	-0.31	-1.9	-10.79	1.14	0.35	172.4	17.2	0.11	0.13
RS1DS	2010	12	-1.17	-0.29	-0.08	-0.37	-1.17	-2.27	1.21	0.43	166	21.9	0.17	0.18
RS1DS	2011	9	-0.28	-0.02	-0.09	-0.61	-7.16	-0.93	0.29	0.16	175.4	40.1	0.03	0.03
RS1DS	2011	10	-0.3	-0.05	-0.09	-0.66	-3.72	-1.55	0.31	0.19	170.9	41.3	0.04	0.05
RS1DS	2011	11	-0.26	-0.17	-0.04	-1.1	-1.72	-3.25	0.31	0.29	147.2	57.3	0.09	0.12
RS1DS	2012	9	-0.42	-0.05	-0.02	-0.81	-4.58	-5.32	0.43	0.34	173.33	47.4	0.09	0.1
RS1DS	2012	10	-0.51	-0.04	-0.01	-0.51	-6.02	-8.41	0.51	0.26	175.9	31.85	0.06	0.08
RS1DS	2012	11	-0.17	-0.03	-0.06	-1.86	-9.33	-2.4	0.18	0.3	169.53	80.13	0.1	0.11
RS1DS	2012	12	-0.23	-0.02	-0.03	-1.2	-10.35	-4.32	0.24	0.28	174.4	66.12	0.07	0.08
RS1DS	2013	8	-0.49	-0.12	-0.06	-0.81	-2.96	-1.72	0.51	0.4	166.22	51.71	0.15	0.14
RS1DS	2013	9	-0.52	-0.11	-0.06	-0.79	-3.29	-1.82	0.53	0.4	168.28	49.86	0.15	0.15
RS1DS	2013	10	-0.6	-0.16	-0.06	-0.62	-2.1	-1.96	0.63	0.37	165.33	40.76	0.13	0.14
RS1DS	2013	11	-3.75	-1.27	-0.24	-0.48	-0.65	-2.62	3.96	1.72	161.22	16.72	2.15	2.21
RS1DS	2013	12	-3.29	-0.70	0.06	-0.49	-1.30	12.09	3.36	1.60	167.99	26.61	1.97	1.85
RS1DS	2014	1	-0.38	-0.18	-0.04	-1.38	-3.09	-4.00	0.42	0.53	154.87	63.42	0.30	0.69
RS1DS	2014	2	-0.54	-0.28	-0.09	-0.78	-1.28	-1.87	0.62	0.41	152.20	45.73	0.17	0.18
RS1DS	2014	3	-0.21	-0.11	-0.05	-1.78	-2.60	-2.63	0.24	0.34	151.34	77.30	0.12	0.18
S1	2010	7	-0.05	-0.15	-0.01	-4.23	-1.29	-6.6	0.16	0.19	108.02	67.25	0.04	0.05
S1	2010	8	-0.05	-0.14	-0.02	-3.81	-1.28	-3.37	0.15	0.18	108.94	66.49	0.04	0.05
S1	2010	9	-0.09	-0.19	-0.04	-2.04	-0.95	-2.1	0.21	0.18	117.1	55.48	0.04	0.04
S1	2010	10	-0.12	-0.2	-0.04	-1.4	-0.87	-2.06	0.24	0.17	121.51	49.38	0.03	0.03
S1	2010	11	0.09	-0.14	-0.05	2.21	-1.43	-1.8	0.18	0.2	56.51	68.06	0.05	0.05
S1	2010	12	0.12	-0.11	-0.04	2.04	-2.25	-2.64	0.17	0.24	42.99	73.71	0.07	0.08
S1	2012	8	-0.13	-0.16	-0.02	-1.8	-1.44	-5.16	0.21	0.24	129.23	64.9	0.06	0.07
S1	2012	9	-0.04	-0.05	-0.01	-4.83	-4.28	-7.08	0.07	0.22	131.02	90.96	0.05	0.06
S1	2012	10	-0.03	-0.01	-0.01	-7.19	-12.62	-5.54	0.03	0.18	150.39	97.02	0.04	0.06
S1	2012	11	-0.01	-0.01	0	-12.01	-13.16	-11.6	0.02	0.18	135.85	99.22	0.03	0.05
S1	2013	8	-0.22	-0.15	-0.01	-1.2	-2.01	-13.94	0.26	0.27	145.19	58.39	0.09	0.11
S1	2013	9	-0.09	-0.03	-0.02	-2.42	-7.22	-4.02	0.09	0.21	160.74	86.41	0.05	0.07
S1	2013	10	-0.02	-0.01	-0.01	-8.66	-28.31	-5.34	0.02	0.14	161.4	98.41	0.02	0.05
S1	2013	11	-0.51	-0.71	-0.08	-0.73	-0.78	-2.50	0.88	0.50	125.71	37.08	0.24	0.31
S1	2013	12	-0.66	-0.22	0.00	-0.64	-1.83	44.97	0.69	0.42	161.12	40.45	0.19	0.23
S1	2014	1	-0.21	-0.26	-0.03	-1.50	-1.43	-3.99	0.33	0.35	128.39	62.11	0.12	0.13
S1	2014	2	-0.22	-0.16	-0.06	-1.39	-2.01	-2.91	0.28	0.30	143.23	58.63	0.11	0.15
S1	2014	3	-0.05	-0.08	-0.06	-7.28	-5.65	-3.84	0.11	0.38	124.68	94.91	0.20	0.19
UB1	2010	11	-0.05	-0.08	-0.01	-6.14	-3.32	-7.52	0.1	0.28	119	87.1	0.08	0.1
UB1	2010	12	-0.04	-0.06	-0.01	-6.94	-4.42	-8.71	0.07	0.27	122.8	90.5	0.08	0.1
UB1	2011	1	-0.05	-0.05	-0.01	-5.48	-5.65	-4.87	0.07	0.27	135.6	91.3	0.08	0.1

UB1	2011	11	0.06	-0.1	-0.09	3.45	-2.07	-1.29	0.15	0.18	60.3	76.7	0.05	0.06
UB1	2012	8	-0.03	-0.12	-0.08	-5.65	-1.54	-0.91	0.15	0.17	104.25	71.33	0.04	0.05
UB1	2012	9	-0.03	-0.14	-0.08	-5.71	-1.49	-0.98	0.16	0.18	103.65	71.73	0.04	0.04
UB1	2012	10	-0.04	-0.14	-0.06	-5.55	-1.54	-1.1	0.15	0.2	104.57	72.81	0.04	0.05
UB1	2012	11	0	-0.16	-0.06	-52.46	-1.34	-1.28	0.17	0.2	91.48	69.84	0.05	0.05
UB1	2012	12	-0.08	-0.31	-0.07	-2.85	-0.89	-1.43	0.32	0.26	103.94	54.09	0.06	0.06
UB1	2013	1	-0.07	-0.33	-0.03	-2.81	-0.87	-2.26	0.34	0.28	101.85	54.77	0.06	0.05
UB1	2013	2	-0.02	-0.04	-0.01	-6.02	-4.14	-3.18	0.04	0.14	123.24	93.68	0.02	0.03
UB1	2013	8	-0.33	-0.15	-0.09	-0.78	-1.61	-1.04	0.37	0.24	155.74	46.55	0.06	0.07
UB1	2013	9	-0.13	-0.07	-0.05	-1.84	-3.22	-1.37	0.16	0.23	153.2	77.06	0.06	0.06
UB1	2013	10	-0.14	-0.05	-0.03	-1.62	-3.94	-1.94	0.15	0.22	160.62	76.15	0.05	0.06
UB1	2013	11	-0.48	-0.19	-0.10	-0.86	-2.17	-1.48	0.53	0.41	158.68	52.97	0.18	0.19
UB1	2013	12	-0.32	-0.17	-0.06	-1.37	-2.53	-2.24	0.37	0.43	152.20	67.72	0.20	0.19
UB1	2014	1	-0.25	-0.34	-0.07	-1.60	-1.19	-1.57	0.42	0.39	126.53	58.52	0.16	0.17
UB2	2010	8	0.04	0	-0.02	1.61	15.7	-1.07	0.04	0.06	354.45	74.48	0	0
UB2	2010	9	-0.01	-0.07	-0.01	-30.12	-3.23	-10.44	0.07	0.23	95.5	91.2	0.05	0.09
UB2	2010	10	-0.01	-0.09	-0.01	-22.27	-3.53	-5.94	0.09	0.32	98.5	88.8	0.1	0.13
UB2	2010	11	0.02	-0.03	-0.01	14.16	-10.45	-15.73	0.04	0.3	55.7	97.9	0.09	0.13
UB2	2011	11	-0.04	-0.09	-0.03	-6.27	-2.66	-3.31	0.11	0.24	114.5	86.4	0.07	0.07
UB2	2012	8	-0.06	-0.07	-0.04	-2.93	-2.9	-2.13	0.1	0.18	133.88	81.43	0.04	0.05
UB2	2012	9	-0.07	-0.06	-0.05	-2.7	-3.35	-1.54	0.11	0.17	141.06	79.63	0.04	0.05
UB2	2012	10	-0.01	-0.02	-0.03	-11.59	-8.83	-1.32	0.04	0.08	127.48	97.75	0.02	0.03
UB2	2012	11	-0.02	-0.02	-0.01	-7.52	-7.22	-2.19	0.03	0.1	133.72	94.4	0.01	0.04
UB2	2012	12	0.38	-0.51	-0.04	0.83	-0.62	-2.23	0.64	0.32	53.24	34.97	0.1	0.11
UB2	2013	1	0.1	-0.26	-0.01	2.81	-1.13	-9.52	0.28	0.29	68.63	61.05	0.09	0.1
UB2	2013	2	0.08	-0.21	0.01	4.1	-1.47	6.36	0.22	0.31	69.54	73.09	0.1	0.09
UB2	2013	8	-0.53	-0.35	0.08	-0.66	-0.95	2.18	0.64	0.35	146.7	37.8	0.13	0.12
UB2	2013	9	-0.61	-0.34	0.04	-0.56	-0.98	4.4	0.69	0.34	150.95	33.31	0.12	0.11
UB2	2013	10	-0.36	-0.11	0	-0.98	-2.56	-61.11	0.38	0.35	163.4	58.18	0.11	0.1
UB2	2013	11	-0.63	-0.13	0.04	-0.65	-3.03	3.89	0.65	0.41	168.37	41.84	0.18	0.18
UB2	2013	12	-0.57	-0.12	0.07	-0.78	-3.44	2.13	0.59	0.44	168.45	49.31	0.19	0.19
UB2	2014	1	-0.04	-0.18	-0.01	-8.25	-2.01	-6.67	0.18	0.35	103.71	77.97	0.13	0.15
UB2	2014	2	-0.02	-0.02	-0.01	-14.63	-11.68	-5.01	0.03	0.21	128.23	98.34	0.05	0.09
UB2	2014	3	-0.01	-0.01	-0.01	-23.58	-31.87	-6.48	0.02	0.22	143.38	100.86	0.07	0.11
UB3	2010	11	0.01	-0.06	0.01	40.82	-7.18	11.53	0.06	0.44	80.5	96.1	0.19	0.24
UB3	2010	12	0.02	-0.06	0.01	23.44	-7.78	9.89	0.06	0.45	72.8	95.6	0.21	0.25
UB3	2011	11	-0.06	-0.11	-0.03	-3.78	-2.07	-3.27	0.13	0.22	118.4	78.3	0.06	0.06
UB3	2012	8	-0.01	-0.11	-0.25	-17.27	-1.76	-0.55	0.27	0.15	94.97	74.86	0.04	0.05

UB3	2012	9	-0.02	-0.11	-0.28	-10.92	-1.82	-0.52	0.3	0.15	98.56	76.72	0.05	0.06
UB3	2012	10	0.01	-0.13	-0.3	23.18	-1.81	-0.52	0.32	0.17	85.65	78.42	0.07	0.07
UB3	2012	11	0.03	-0.06	-0.45	6.86	-3.28	-0.4	0.46	0.18	64.86	88.83	0.06	0.05
UB3	2012	12	0.02	-0.06	-0.49	10.98	-3.53	-0.29	0.5	0.15	71.88	90.8	0.05	0.06
UB3	2013	8	-0.04	-0.45	0.03	-3.98	-0.76	2.85	0.46	0.34	95.25	45	0.08	0.07
UB3	2013	9	-0.27	-0.69	0.04	-1.02	-0.82	2.27	0.74	0.53	111.24	45.09	0.2	0.14
UB3	2013	10	-0.1	-0.27	0.02	-1.84	-1.14	2.61	0.29	0.3	110.56	57.48	0.07	0.09
UB3	2013	11	-0.50	-0.73	0.06	-0.82	-0.59	2.43	0.88	0.42	124.31	31.95	0.18	0.17
UB3	2013	12	-0.09	-0.14	0.00	-2.64	-2.08	12.99	0.17	0.27	123.81	81.81	0.07	0.11
UB3	2014	1	-0.03	-0.02	-0.02	-6.70	-9.73	-2.51	0.04	0.19	145.24	96.62	0.05	0.06
UB3	2014	2	-0.06	-0.13	-0.07	-4.94	-2.32	-1.48	0.16	0.28	115.29	83.52	0.10	0.10
UB3	2014	3	-0.10	-0.03	-0.02	-2.95	-8.25	-2.61	0.11	0.28	160.58	87.88	0.08	0.08

Table 4-2. USGS monitoring stations and parameters monitored for this study.

[T, water temperature; K, water specific conductance; GH, gage height; V, water velocity; Q, discharge; Qm, measured discharge]

Basin	Station name	Parameters	USGS station number and name
WCA 3A	S-152 west	T, K, GH, V, Q, Qm	255154080371300 L-67A Canal at S-152 nr Coopertown
	Site 69 west	T, K, GH	255300080370001 Site 69 in Conservation Area 3B nr Coopertown
	EDEN 8	T, K, GH	255200080405001 EDEN 8 in Water Conservation Area 3-A
Pocket	S-152 east	T, K, GH	255154080371303 Wetland below S-152 in WCA-3 nr Coopertown
	Site 69 east	T, K, GH	255300080370001 Site 69 in Conservation Area 3B nr Coopertown

Note : The urls for accessing data are:

S-152 West: http://waterdata.usgs.gov/nwis/nwisman/?site_no=255154080371300&agency_cd=USGS
S-152 East: http://waterdata.usgs.gov/nwis/nwisman/?site_no=255154080371303&agency_cd=USGS
Site 69: http://waterdata.usgs.gov/nwis/nwisman/?site_no=255300080370001&agency_cd=USGS
EDEN 8: http://waterdata.usgs.gov/nwis/nwisman/?site_no=255200080405001&agency_cd=USGS

Table 4-3. Measured discharges through S-152 during the first and second water-release periods.

Measurement number	Date	Start time (EST)	End time (EST)	Measurement equipment	Discharge, cubic feet per second	Measurement gage height, feet
1	11/5/2013	11:55	12:47	ADV	316	8.77
2	11/5/2013	13:15	14:15	ADV	307	8.77
3	11/5/2013	15:09	16:05	ADV	303	8.78
4	11/6/2013	9:29	10:38	ADV	299	8.76
5	11/7/2013	10:00	11:47	ADV	308	8.75
6	11/12/2013	10:24	11:43	ADV	291	8.70
7	11/20/2013	10:10	11:30	ADV	260	8.62
8	11/25/2013	10:18	11:28	ADV	266	8.64
9	12/10/2013	10:46	12:01	ADV	267	8.52
10	12/27/2013	11:08	12:51	ADV	255	8.46
11	11/4/2014	11:35	12:05	ADCP	276	8.54
12	11/4/2014	12:39	13:02	ADCP	272	8.53
13	11/4/2014	12:59	14:19	ADV	275	8.52
14	11/7/2014	11:51	13:17	ADV	268	8.50
15	11/7/2014	12:13	12:40	ADCP	260	8.50
16	11/13/2014	10:54	12:04	ADCP	283	8.61
17	11/25/2014	11:02	12:04	ADCP	283	8.60
18	11/25/2014	11:18	12:43	ADV	274	8.60
19	12/8/2014	10:14	10:37	ADCP	285	8.62
20	12/22/2014	11:24	13:47	ADV	280	8.54
21	12/22/2014	11:36	12:37	ADCP	282	8.54
22	1/13/2015	10:52	11:27	ADCP	276	8.52
23	1/26/2015	11:24	13:27	ADV	245	8.38
24	1/26/2015	11:27	12:03	ADCP	237	8.38

Table 4-3-ADD. Maximum and minimum computed discharges through S-152 during the first and second water-release periods.

Flow release period	Maximum computed discharge, cubic feet per second	Date	Minimum computed discharge, cubic feet per second	Date
First	374	11/5/2013	223	11/19/2013
Second	309	12/8/2014	225	1/26/2015

Table 4-4. Maximum and minimum water temperature and specific conductance at S-152, Site 69, and EDEN 8 during the S-152 flow release period November 5 to December 30, 2013.
'HW' is headwater side of Levee 67A; 'TW' is tail-water side of Levee 67A.

		Water Temperature, °C				Specific Conductance, US/cm at 25° C			
Station	Side	Maximum	Date	Minimum	Date	Max	Date	Min	Date
S-152	HW	25.0	11/24	20.5	12/19	681	12/24	533	12/29
	TW	25.0	11/12, 11/24	20.7	12/19	668	12/24	499	12/29
Site 69	HW	25.2	11/20	21.0	12/19	702	12/25	560	12/28
	TW	25.0	11/10	19.6	11/28	779	12/29	607	12/1
EDEN 8		25.1	11/22	18.0	11/27	427	11/11	316	11/29

Table 4-5. Advection, longitudinal (K_x) and lateral (K_y) dispersion coefficients, flow direction and average water depth for EverTREx experiments 6-11. EverTREx 6 is included for comparison.

Experiment	Date	Site	Advection (cm/s)	K_x (cm^2/s)	K_y (cm^2/s)	Heading (°)	Depth (cm)
EverTREx 6	20-26 Oct 2009	RS2	0.05±0.01	323±122	1.2±1.5	141±6.2	49.6 ± 6.7
EverTREx 7	4-8 Nov 2010	RS2	0.09±0.02	177±22	1.6±0.8	123±7.6	37.0 ± 8.9
EverTREx 8	8-12 Nov 2010	C2	0.04±0.004	68±12	15±4	156±11	47.6 ± 6.6
EverTREx 9	22-27 Oct 2011	RS1	0.11 ± 0.01	998 ± 227	13.2 ± 8.6	148 ± 2.5	43 ± 6.6
EverTREx 10	27-31 Oct 2011	C1	0.15 ± 0.08	1068 ± 226	72.3 ± 33.9	109 ± 3.1	50.6 ± 7.0
EverTREx 11	31 Oct-4 Nov 2011	RS2	0.13 ± 0.03	819 ± 123	98.1 ± 20.1	106 ± 4.0	55.9 ± 5.7
EverTREx 12	7-10 Nov 2013	C1	0.29 ± 0.02			100	
EverTREx 13	12-15 Nov 2013	RS1	0.42 ± 0.02			170	

Table 4-6. Summary of water and sediment velocity measurements during high flow event. Terminology: SF_6 = Sulfur Hexafluoride; ADV = handheld Acoustic Doppler Velocimeter; DST = dual synthetic (floc) tracer. RS1u = upstream boardwalk at RS1; RS1d = downstream boardwalk at RS1

Methodology	**Date(s) sampled**	**Distance of sampling area from S152 (m)**	**Velocity (cm s^{-1})**
Water velocity			
dye front (Day 1)	11/5/13	300	5.4
dye front (Day 2)	11/6/13	300-1200	1.0
SF_6 at RS1	11/12/13 - 11/15/13	500-2000	0.42 ±0.02
SF_6 at C1	11/7/13 - 11/10/13	1200-2500	0.29 ±0.02
ADV at Z5-1	11/5/13	180	3.7
ADV at NE-S152	11/5/13	189	6.6
ADV at RS1	11/5/13	421	8.3
Sediment velocity			
turbidity peak at Z5-1	11/5/13	180	2.9
turbidity peak at NE-S152	11/5/13	189	3.0
turbidity peak at RS1	11/5/13	421	4.3
DST peak #1 - Drop site to RS1u	11/5/13	400	2.4
DST peak #1 - RS1u to RS1d	11/5/13	400	0.6
DST peak #2 - RS1u to RS1d	11/5/13	400	0.4

Table 4-7. Biogeochemistry of floc and epiphyton, November 2010.

Site	community	Mean size, um, floc	TP (mg/kg), epi	labile P (mg/kg), epi	microbial P (mg/kg), epi	TN (mg/kg), epi	Refractory P (mg/kg), epi	labile P/TP, epi
C1	RIDGE	102.71	233.00	13.80	199.20	18200.00	20.00	0.06
C1	SLOUGH	93.64	197.00	9.40	150.60	16500.00	37.00	0.05
RS1	RIDGE	66.19	287.00	13.40	218.60	24300.00	55.00	0.05
RS1	SLOUGH	119.88	265.00	26.80	134.20	19500.00	104.00	0.10
RS2	RIDGE	70.03	207.00	14.90	81.80	16800.00	110.30	0.07
RS2	SLOUGH	55.00	815.00	444.00	329.00	12700.00	42.00	0.54
S1	SLOUGH	91.52	177.00	12.30	174.70	12600.00	-10.00	0.07
UB1	SLOUGH	84.74	267.00	51.70	86.30	15900.00	129.00	0.19
UB2	SLOUGH	90.13	220.00	75.20	173.80	11600.00	-29.00	0.34
UB3	SLOUGH	85.88	230.00	36.10	159.90	13900.00	34.00	0.16
DB1	SLOUGH	114.49	902.00	14.30	233.70	33300.00	654.00	0.02
DB2	SLOUGH	142.10	685.00	18.10	269.90	35300.00	397.00	0.03
DB3	SLOUGH	82.80	266.00	27.30	121.70	21100.00	117.00	0.10

Table 4-8. Biogeochemistry of floc and epiphyton, November 2010.

Site	Community	DRYWT (g)	AFDW (%)	TP (mg/kg), floc	Labile P (mg/kg), floc	Microbial P (mg/kg), floc	TN (mg/kg), floc	Refractory P (mg/kg), floc
C1	RIDGE	4.02	87.70	450.00	23.40	193.60	37900.00	233.00
C1	SLOUGH	4.83	55.20	305.00	14.60	131.40	28700.00	159.00
RS1	RIDGE	2.68	79.20	541.00	19.90	254.10	37100.00	267.00
RS1	SLOUGH	2.93	65.20	409.00	32.60	180.40	34100.00	196.00
RS2	RIDGE	2.72	63.60	278.00	4.50	122.50	25600.00	151.00
RS2	SLOUGH	5.37	19.00	109.00	8.60	40.70	9390.00	59.70
S1	SLOUGH	8.19	23.80	101.00	2.10	41.60	10200.00	57.30
UB1	SLOUGH	10.95	28.00	270.00	27.10	79.90	15100.00	163.00
UB2	SLOUGH	12.93	27.30	195.00	11.50	67.10	13700.00	116.40
UB3	SLOUGH	2.66	41.90	248.00	7.90	160.10	20800.00	80.00
DB1	SLOUGH	2.56	74.00	1085.00	22.90	523.10	39450.00	539.00
DB2	SLOUGH	1.87	82.60	976.00	7.85	520.65	42200.00	447.50
DB3	SLOUGH	7.37	18.60	230.00	17.00	104.00	14600.00	109.00

Table 4-9. CPUE of dominant species collected in the Canal and Marsh habitats. All sampling periods were grouped together. Canal sites include all canal treatments. Marsh sites include both canal margin marsh sites and marsh sites. We pooled the latter because they were relatively similar in species composition.

Species	Canal Abundance	Marsh Abundance
Largemouth Bass	3.95	0.48
Bluegill Sunfish	1.43	0.31
Warmouth	1.34	0.91
Florida Gar	1.16	0.07
Lake Chubsucker	1.07	0.48
Bowfin	0.93	0.57
Redear Sunfish	0.75	0.30
Yellow Bullhead	0.18	0.11

This page deliberately left blank.